Atomic-Level Dynamical, Structural and Functional Investigation of a Membrane Protein Complex through Nuclear Magnetic Resonance Spectroscopy

by

Kazutoshi Yamamoto

A dissertation submitted in partial fulfillment
of the requirements for the degree of
Doctor of Philosophy
(Chemistry)
In The University of Michigan, Ann Arbor
2011

Doctoral Committee:

Professor Ayyalusamy Ramamoorthy
Professor Hashim Al-Hashimi
Professor Lucy Waskel
Assistant Professor Kevin J. Kubarych

DEDICATION

To the things and people who continue to open my eyes, and inspire me.

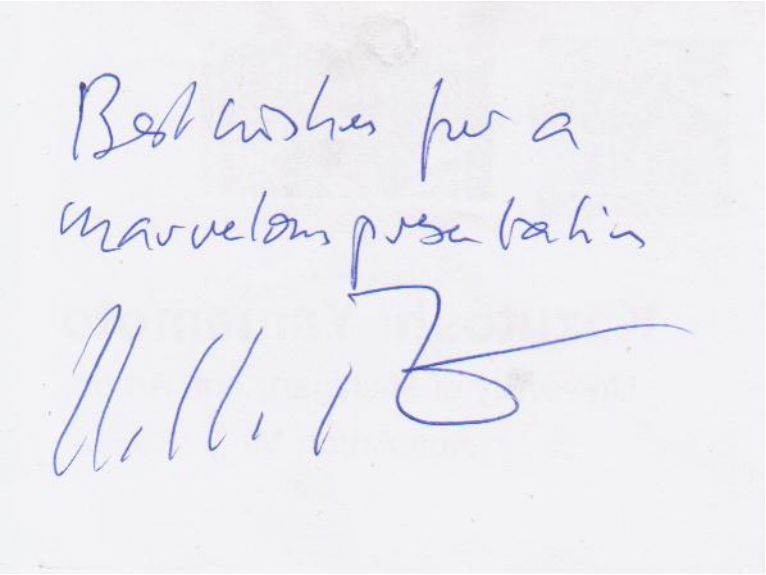

Nobel Laureate Prof. Richard R. Ernst (Swiss Federal Institute of Technology in Zürich)

Remarks on my Ritchey Award presentation at the 52nd Experimental Nuclear Magnetic Resonance Conference in Pacific Grove, California on April 10, 2011.

ACKNOWLEDGEMENTS

I would like to acknowledge my advisor, Professor Ayyalusamy Ramamoorthy, for guiding me throughout my stay in Michigan, providing me with an intellectual environment that encouraged independent research and professional growth. His quest for high quality research has been a major source of inspiration and for my high productivity as a graduate student in his laboratory.

I would like to thank all the co-authors of the publications for their tremendous help in completing the project and with the preparation of manuscripts. I would also like to thank the other members of the *Rams* lab who have helped and taught me an immeasurable amount. Thanks to Dr. Dong-Kuk Lee, Dr. Sergey V. Dvinskikh, Dr. Jiadi Xu and Dr. Vivekanandan Subramanian for teaching me about the NMR spectrometer, and maintaining the spectrometer so that all our experiments ran smoothly.

I would like to thank my parents and family who have always supported me. I would like to thank friends who make my life interesting and inspire me. Finally, thank you to Prof. Hazime Saito for not only encouraged me to study in the United States, but also has always been supportive in my scientific career.

This research was supported by funds from National Science Foundation (CAREER award) and National Institute of Health (AI054515, DK078885, GM084018, RR023597) to Dr. A. Ramamoorthy.

TABLE OF CONTENTS

LIST OF FIGURES

LIST OF TABLES

ABSTRACT

Biological cell membranes are vital boundaries that separate the intracellular elements from the extracellular environments, and they are fundamental regulators of a number of cellular and physiological phenomena. In fact, these biological processes are essentially based on biomolecular interactions within and between cells. A significant number of biologically important protein-protein and protein-lipid interactions in life science, for instance, signal transductions (an essential molecular machinery for sensory systems), electron transport chains (an essential scheme for respiration systems) and photosynthesis (one of our primary sources of energy), all take place at the membrane interface of cells. Furthermore, more than 30% of the human genome and 50% of known drug targets are membrane-associated proteins. Therefore, it is critical to establish techniques that will allow us to investigate these kinds of membrane complex systems and gain insights into biological phenomena for scientific and biomedical purposes. Despite their importance there are very few reports on the atomic-level structure and dynamics investigations of the combinatorial complexes composed of protein-protein interactions and protein-lipid interactions within bilayers. The lack of success in this area of research is largely attributed to the challenges imposed by membrane proteins when examined with the most commonly used biophysical techniques such as X-ray crystallography, electron microscopy and Nuclear Magnetic Resonance (NMR) spectroscopy. My dissertation concentrates on three novel components that will accelerate the understanding of these important and challenging systems. The first element is to gain atomic-level structure and dynamics determination of biologically important systems by developing new solid-state and solution NMR approaches that enhance resolution and the sensitivity of spectra, allowing for the robust NMR experiments for samples that have higher molecular weight. The second

component pertains to the preparation of stable and well-behaved biologically relevant samples. The third is to retain the biological functions of membrane complex systems in order to investigate dynamical structure of membrane complexes. The combination of these three approaches has already led, for the first time, to the determination of structural and dynamical interactions in an intact mammalian membrane protein complex, rabbit Cytochrome-b_5, and Cytochrome-P450, which metabolizes more than 50% of the pharmaceuticals in clinical use today.

Chapter I

Introduction

I-1. Goals

The goal of this project was to develop new Nuclear Magnetic Resonance spectroscopy methodologies to investigate structures, dynamics and functions of membrane bilayers, membrane-associated proteins, membrane-protein interactions and membrane protein-protein interactions. The results demonstrate three novel concepts that will accelerate the understanding of these important and challenging systems. The first element is to gain atomic-level structure and dynamics determination of biologically important systems by developing new solid-state and solution NMR approaches that enhance resolution and the sensitivity of spectra, allowing for the robust NMR experiments of samples that have a higher molecular weight. The second component pertains to the preparation of stable and well-behaved biologically relevant samples. The third is to retain the biological functions of membrane complex systems in order to investigate dynamical structure of membrane complexes. The combination of these three approaches has already led, for the first time, to the determination of structural and dynamical interactions in an intact mammalian membrane protein complex, rabbit Cytochrome b_5, and Cytochrome P450, which metabolizes more than 50% of the pharmaceuticals in clinical use today.

I-2. Membrane Biology

Biological cell membranes are vital boundaries that separate the intracellular elements from the extracellular environments, and they are fundamental regulators of a number of cellular and physiological phenomena. In fact, these biological processes are essentially based on biomolecular interactions within and between cells. A significant number of biologically important protein-protein and protein-lipid interactions in life science, for instance, signal transductions (an essential molecular machinery for sensory systems), electron transport chains (an essential scheme for respiration systems) and photosynthesis (one of our primary sources of energy), take place on the membrane interface of cells. Furthermore, more than 30% of the human genome and 50% of known drug targets are membrane-associated proteins. Therefore, it is critical to establish techniques that will allow us to investigate these kinds of membrane complex systems and gain insights into biological phenomena for scientific and biomedical purposes. Despite their importance, there are very few reports on the atomic-level structure and dynamics investigations of the combinatorial complexes composed of protein-protein interactions and protein-lipid interactions within bilayers.[1] The lack of success in this area of research is largely attributed to the challenges imposed by membrane proteins when examined with the most commonly used biophysical techniques such as X-ray crystallography, electron microscopy and Nuclear Magnetic Resonance (NMR) spectroscopy. While obtaining well-behaved biologically relevant samples of these systems is a main major bottle-neck for high-resolution structural studies, recent solid-state NMR studies have demonstrated the feasibility of obtaining high quality structural information to understand the function of membrane proteins.[2] In this thesis, I will demonstrate that solid-state NMR is capable of characterizing protein-protein interactions in lipid bilayers at a very high-resolution and for the first time, structural and dynamical interactions in an intact mammalian membrane protein complex, rabbit cytochrome b_5 (Cyt b_5) and cytochrome P450 2B4 (Cyt P450), which is a medically and pharmaceutically interesting biomolecule, in a membrane bilayer were revealed.

Specifically, this dissertation concentrates on three novel components that will accelerate the understanding of these important and challenging systems. (1) The first

element is to gain atomic-level structure and dynamics determination of biologically important systems by developing new solid-state and solution NMR approaches that enhance resolution and the sensitivity of spectra, allowing for the achievement of robust NMR experiments for complex biomolecules and samples that have higher molecular weight (Chapter II). (2) The second component pertains to the preparation of stable and well-behaved biologically relevant samples of lipid bilayers (Chapter III). (3) The third is to retain the biological functions of membrane complex systems during experiments in order to investigate dynamical structure of membrane complexes in a biologically relevant form (Chapter IV). The combination of these three approaches has already led, for the first time, to the determination of structural and dynamical interactions in an intact mammalian membrane protein complex, rabbit Cytochrome b_5 (Cyt b_5), and Cytochrome P450 (Cyt P450), which metabolizes more than 50% of the pharmaceuticals in clinical use today and is an extremely challenging system for NMR spectroscopy because of its huge overall molecular weight (more than 200 kDa). Additionally, these NMR methodological developments allowed us to gain novel insights into various different biological molecules and materials, such as cell membrane permeable pharmaceutical nanoparticles, liquid crystals, membrane associated proteins/peptides and lipid membranes. The experimental details, significance, and future directions are discussed in this dissertation.

The vast majority of pharmaceutical compounds in use today are hydrophobic compounds that are broken down in the body to water soluble, extractable compounds by a superfamily of enzymes known as the Cyt P450.[3,4] A single member of this family, Cyt P450 3A4, was found to metabolize more than 50% of current-day drugs.[3] Other members metabolize a broad range of xeno- as well as endobiotic substrates. Cyt b_5 is a membrane-bound protein which modifies the metabolism of selected drugs by Cyt P450.[3] The electron transfer scheme in Figure I-1 shows the binding of Cyt P450 and Cyt b_5 changes the efficiency of Cyt P450's enzymatic activity.[5] Remarkably, Cyt b_5 enhances (or is even essential to) some catalytic reactions, but does not affect, or in some cases even inhibits, others. Its suggested functions include direct donation of an electron to Cyt P450, fine-tuning of kinetic parameters by relaying electrons, or an allosteric effector function on Cyt P450.[7] In order to understand the molecular mechanism by which Cyt b_5

influences the oxidation by Cyt P450 *in vivo*, one must understand the structural details of the interaction between Cyt b_5 and Cyt P450.

A model constructed from the solution NMR structure of the soluble domain of rabbit Cyt b_5 is given in Figure I-2A.[6] The 16.7kDa Cyt b_5 contains 3 structurally distinct domains: a ~95 amino acid amino-terminal catalytic heme-containing soluble domain, a ~25 amino acid carboxyl-terminal membrane-anchor domain and a ~14 residue linker region which connects the two. The carboxyl domain is assumed to be a helix which spans the membrane. When Cyt b_5 is treated with proteases, the heme domain is released as a soluble protein which can no longer interact with Cyt P450, but still can react with the soluble protein, Cyt c.[8] Our interest is in trying to understand why the membrane-spanning domain is required for the interaction between Cyt b_5 and Cyt P450.

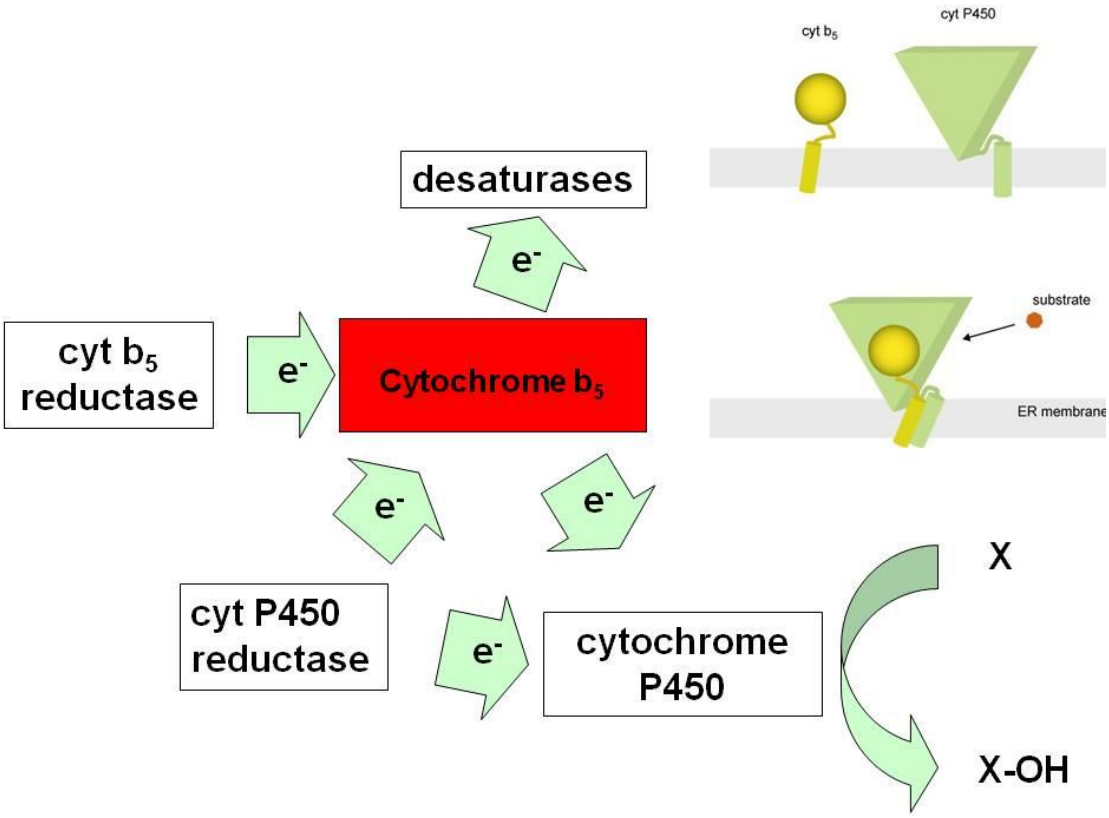

Figure I-1. **The electron transfer scheme and a molecular model of the Cyt b_5, Cyt P450 and Cyt b_5- Cyt P450 complex.** [9]

(A)

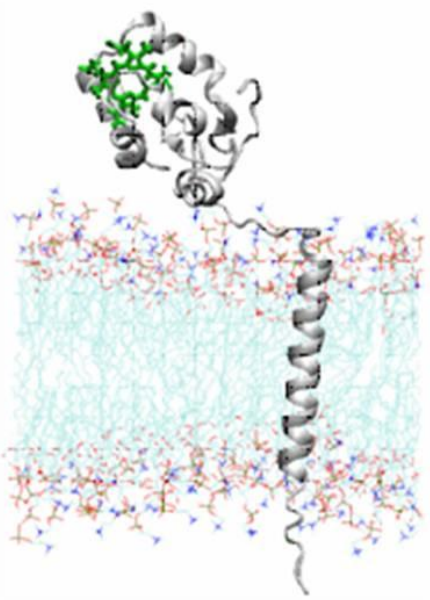

(B)

MAAQSDKDVK$_{10}$-YYTLEEIKKH$_{20}$-NHSKSTWLIL$_{30}$-HHKVYDLTKF$_{40}$-
LEEHPGGEEV$_{50}$-LREQAGGDAT$_{60}$-ENFEDVGHST70-DARELSKTFI$_{80}$-
IGELHPDDRS$_{90}$-KLSKPMETLI$_{100}$-TTVDSNSSWW$_{110}$-TNWVIPAISA$_{120}$-
LIVALMYRLY$_{130}$-MADD

Figure I-2. (A) **Molecular model showing Cyt b_5 in the context of a DMPC bilayer**; the transmembrane, linker, and heme-carrying soluble domains are evident. (B) **Amino acid sequence of rabbit Cyt b_5.** The amino acid residues in the predicted transmembrane region of the protein are underlined.[14]

Since the full-length Cyt b_5 and Cyt P450 are not amenable for structural studies using most common biophysical techniques, only the structures of the soluble domains these proteins have been solved using X-ray and solution NMR techniques. However, Cyt b_5 lacking the transmembrane (TM) domain, neither interacts with nor influences the function of Cyt P450. Therefore, while solving the high-resolution structure of the Cyt b_5-Cyt P450 complex is very important, it has been proven challenging and impossible using common biophysical approaches. On the other hand, it could be a suitable problem using solid-state NMR spectroscopy which has no fundamental restriction on the molecular size and phase of the sample. Here, for the first time, the solid-state NMR investigation of membrane topology and dynamics of a Cyt b_5-Cyt P450 complex in lipid bilayers was conducted. Magnetically aligned bicelles are used in solid-state NMR experiments under static experimental conditions.

I-3. NMR Spectroscopy Methodology Developments for Membrane Biology

Structural biology of membrane proteins has rapidly evolved into a new frontier of science. Although solving the structure of a membrane protein with atomic-level resolution is still a major challenge, Separated-Local-Field (SLF) NMR spectroscopy has become an invaluable tool in obtaining structural images of membrane proteins under physiological conditions. Among SLF experiments, PISEMA (Polarization Inversion and Spin Exchange at Magic Angle) pulse sequence is commonly used. The advantages of PISEMA experiments are high resolution spectra in the dipolar coupling dimension, high scaling of dipolar couplings (scaling factor 0.816) and tolerance to RF field inhomogeneity.[17] However, the major disadvantage of PISEMA is its ^{1}H carrier frequency offset dependence because of the off-resonance spin-locking of proton magnetization during t_1 dimension.[17] In fact, this carrier offset gives artifacts in the PISEMA spectra. For example, with an increase of the ^{1}H carrier frequency offset value, the signal-to-noise ratio of the dipolar coupling spectra gets worse and the scaling factor increases. These problems are severe when the dipolar couplings are

smaller and for studies at higher magnetic fields. Dipolar couplings are smaller when studying the nucleus is more mobile, so this is a particular problem in studying the soluble domain of Cyt b_5. Since a uniformly labeled protein can have an amide-^{1}H chemical shift span of about 15 ppm, this offset dependency of the sequence could provide inaccurate dipolar coupling values. Since PISEMA is one of the powerful sequences in the structural studies of aligned samples, it would be significant to find countermeasure to this problem. To overcome this difficulty, I have designed a broadband-PISEMA sequence in Prof. Ramamoorthy's lab using the average Hamiltonian theory.[18] We have demonstrated that the newly developed sequence maintains the high-resolution nature of the on-resonance PISEMA sequence and at the same time overcomes the off-resonance effects.[18]

We have further developed alternate pulse sequences that avoid the off-resonance pulses utilized in PISEMA. As a result, we proposed a family of pulse sequences called HIMSELF (Heteronuclear Isotropic Mixing leading to Spin Exchange via the Local Field) as shown in Figure I-3.[19] The unique feature of the HIMSELF sequences is that they utilize on-resonance spin-lock multiple pulse sequences to suppress ^{1}H-^{1}H dipolar coupling and chemical shift interactions. Advantages of HIMSELF sequences are following; (i) because the pulses are applied on-resonance, the RF power required in HIMSELF is relatively low compared to PISEMA experiments using off-resonance pulses which require significant RF power in the low γ nuclear channel for efficient spin exchange. (ii) Resonance offset effects on both nuclei are suppressed. (iii) Unlike PISEMA, HIMSELF sequences do not require fast frequency switching and therefore can be implemented in most commercial NMR spectrometers. One of the HIMSELF sequences, based on a supercycle of WIM (Windowless Isotropic Mixing)[19] pulse blocks, is intrinsically broadband and does not require 180° pulses to suppress offset effects. This is an advantage because 180° pulsesrequire high RF power. Based on experiments on a NAVL (N-acetyl-L-^{15}N-valyl-L-^{15}N-leucine dipeptide) test sample and simulations, this sequence is superior to all other sequences designed so far in these respects (Chapter II).

For NMR spectroscopy of membrane biophysics, the sensitivity enhancements are an important subject as well as resolution enhancements. In spite of recent technological advances in NMR spectroscopy, its poor sensitivity continues to be a major limitation,

particularly for the structural studies of membrane proteins. In the last part of Chapter II, we demonstrate the feasibility of very fast acquisition of two-dimensional spectra of antimicrobial peptides embedded in lipid bilayers. A copper-chelated lipid embedded in bicelles is used to speed-up the spin-lattice relaxation of protons without affecting the spectral resolution and thus enabling fast data collection. Our results suggest that this approach is effective on solid-state as well as solution NMR spectroscopy, using a very small amount (~3 mM) of copper-chelated lipid. These results demonstrate that it is possible to use this approach in the structural studies of membrane proteins with *nano*-mole concentrations of labeled proteins using solid-state NMR spectroscopy and without the need for isotopic enrichment using solution NMR spectroscopy as shown in Figure I-4.

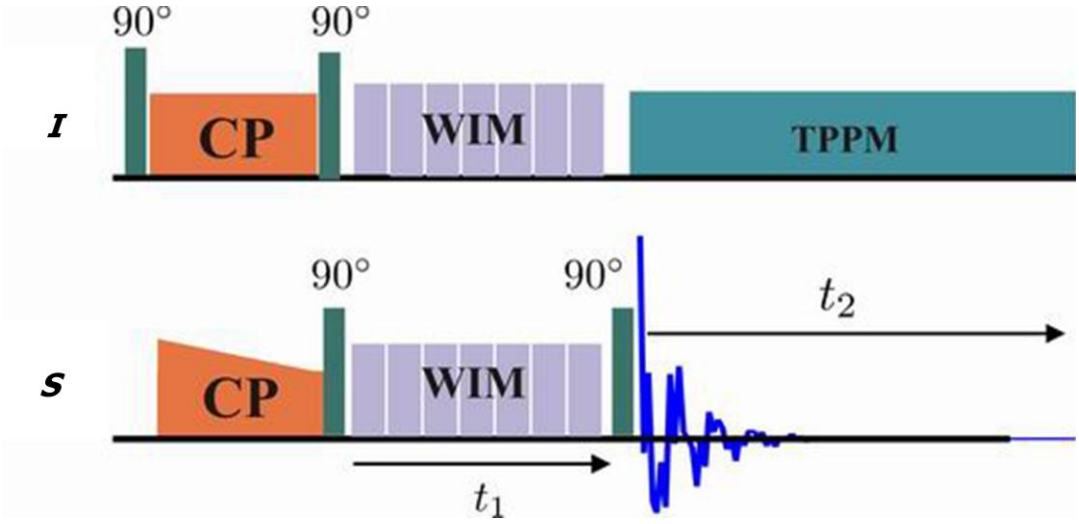

Figure I-3. **2D HIMSELF sequence**. Phase and flip-angle of the flip-back pulse depends on the the spin-lock sequence used in t_1.[19] Use of WIM and a selection of the *z*-magnetization for t_1 evolution gave excellent results.

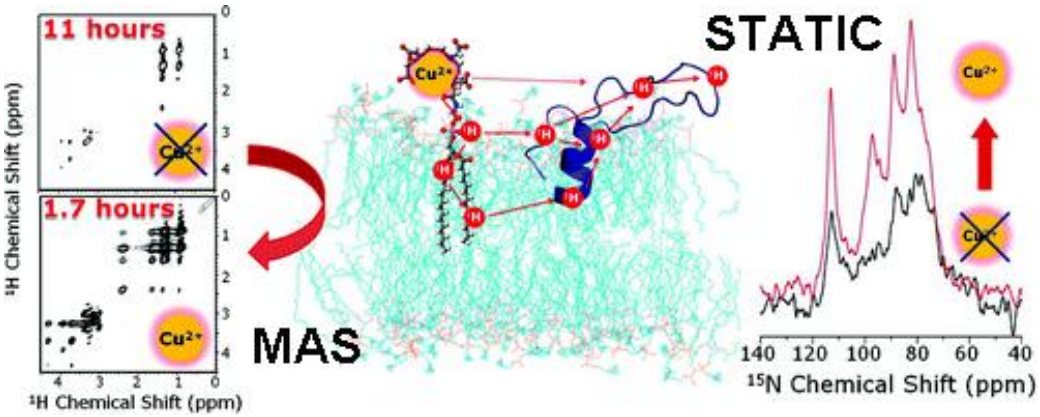

Figure I-4. **A Copper-ChelatedLipid Speeds Up NMR Measurements from Membrane Proteins.** A 6.2-fold speed increase (left) and a 2.7-fold improvement in signal-to-noise ratio (right) for solid-state NMR experiments under magic-angle spinning and static conditions. 2D $^{1}H/^{1}H$ chemical shift correlation spectra of bicelles without [top] and with [bottom] a copper-chelated lipid obtained under MAS using a homonuclear dipolar recoupling sequence. (left). ^{15}N chemical shift spectra of magnetically aligned bicelles containing a 10% of uniformly-^{15}N-labeled (only 70 nmoles) subtilosin A and with (red) and without (black) the copper-chelated-lipid (right).

I-4. NMR Spectroscopy on Membrane Bilayers

Lipids, when combined with detergents in specific ratios, form elongated, disc shaped or planar structures called bicelles (shown in Figure I-5). Bicelles spontaneously align in certain temperature ranges with an external magnetic field due to their elongated shape and the magnetic susceptibility of the phosphorous nuclei. Magnetically aligned bicelles are becoming attractive model membranes to investigate the structure, dynamics, geometry, and interaction of membrane-associated peptides and proteins using solution- and solid-state NMR experiments. Recent studies have shown that bicelles are more suitable than mechanically aligned bilayers for multidimensional solid-state NMR experiments. In solid-state NMR studies, magnetically aligned bicelles have been previously used as model membranes and in solution NMR studies as an alignment medium to measure residual dipolar couplings in the structural studies of water-soluble proteins.[10] Bicelles, composed of different types of combinations of lipids and a detergent, have been well characterized using ^{31}P, ^{2}H, ^{13}C and 2D SLF experiments.[11] 2D HIMSELF and 2D SAMY spectra correlating the ^{13}C chemical shifts and ^{1}H-^{13}C dipolar couplings of the components of bicelles demonstrated the feasibility of high-resolution experiments at a physiologically-relevant temperature without having to enrich with ^{13}C isotopes.[12] This remarkable advantage was later utilized to study the drug-membrane interactions using solid-state NMR spectroscopy (Chapter III). The physicochemical properties and the size of bicelles have also been well documented in literature.[13] Magic angle spinning solid-state NMR experiments have also utilized bilcelles to obtain spectra of uniformly labeled proteins with a resolution approaching solution NMR.[9] Recent solid-state NMR studies have shown that it is also possible to obtain high-resolution spectra from peptides and proteins labeled with ^{15}N isotope under static experimental conditions which allow the topology of the protein relative to the membrane to be determined. We have used bicelles to align Cyt b_5 and a complex of two different membrane proteins to study the structural interactions between them.

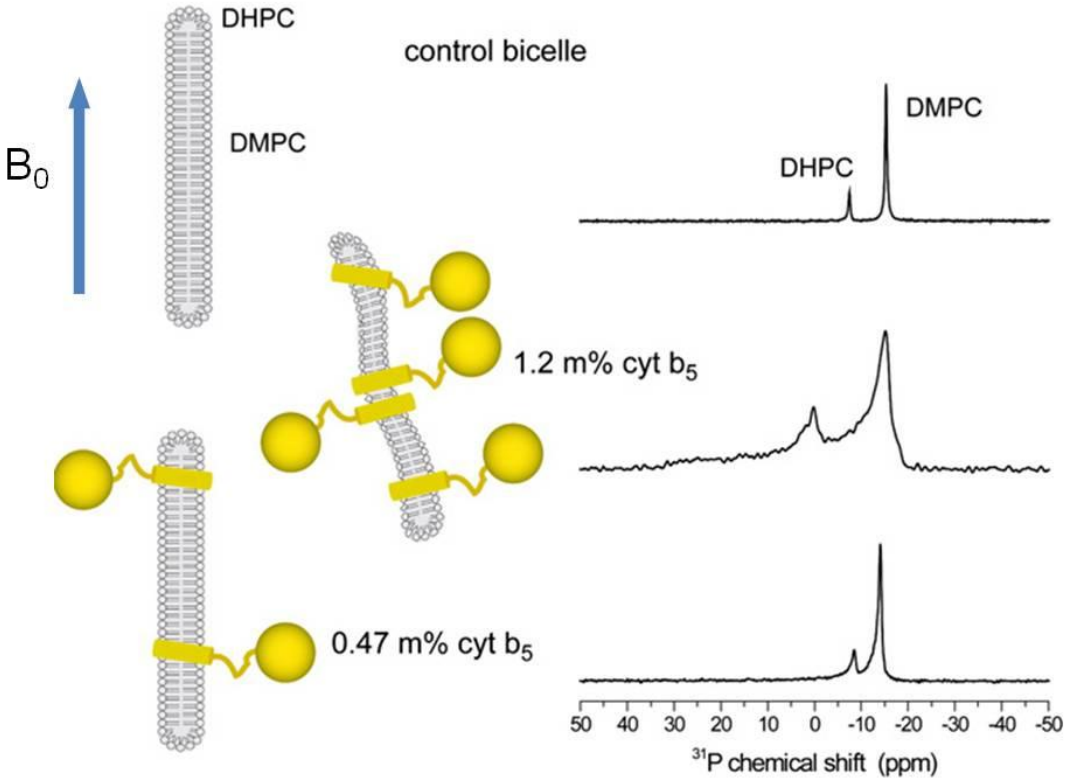

Figure I-5. **A pictorial model of Cyt b_5 in bicelles and ^{31}P NMR spectra at different protein:lipid ratios.** Bicelles without protein show two sharp lines in a static sample, one from the DHPC and the other from DMPC.[9] At high concentrations of Cyt b_5 the lines broaden as the phosphorous molecule are no longer appointing all in the same direction. An optimum concentration considering the degree of alignment vs.the signal to noise ratio was found at 0.47% Cyt b_5.

I-5. NMR Spectroscopy on Membrane Proteins

Determination of the structure, dynamics and orientation of Cyt b_5 in lipid bilayers

In order to determine the structure, membrane-orientation, and dynamics of rabbit Cyt b_5 in phospholipid bilayers, solid-state NMR static (under aligned sample conditions) experiments as well as MAS experiments on bicelles and also on unaligned multilamellar vesicles were performed. To achieve this goal it was necessary to overcome the difficulties related to sample preparations, sensitivity and resolution of NMR experiments and resonance frequency offset effects.

In Professor A. Ramamoorthy's Lab, we have been using aligned bicelles for structural studies on membrane proteins under static conditions which have the advantage of preserving anisotropic spin interactions that can be used for structural information. There are several advantages of using bicelles. Bicelles are fully hydrated with excess water and remain stable for long time. Solution conditions, such as the buffer and pH used, can be adjusted. Unlike detergent micelles commonly used for solution NMR, the curvature and other physical properties of bicelles are relatively close to cell membranes. Therefore, physiologically relevant conditions for structural studies of membrane associated proteins can be achieved in bicelles. Recent studies from our lab as well as others have shown that bicelles are suitable for multidimensional solid-state NMR experiments essential to solve the structure of membrane proteins.

After the sample conditions of magnetically aligned bicelles containing membrane proteins using ^{31}P and ^{15}N NMR experiments have been optimized, 2D Separate Local Field (SLF) experiments correlating the ^{15}N chemical shift with the ^{1}H-^{15}N dipolar couplings of each amide site can be performed. SLF spectra can be interpreted in terms of the molecular geometry or image.[14, 16] For example, the SLF spectrum of a transmembrane helical protein can be used to interpret the tilt of the helix relative to the bilayer normal (Figure I-6).[14-16] This method has previously been used to determine several membrane proteins and peptides structures.[14,15] However, in case of cytochromes, the size of Cyt b_5-Cyt 450 system and presents substantial difficulties in assignment. Furthermore, the soluble region of the protein is expected have high flexibility while the transmembrane region is expected to high low

flexibility. A protein that differs in flexibility like this is difficult for solid-state NMR because the pulse sequences used are frequently sensitive to the timescale of the motion of the nucleus. In order to solve the structure of Cyt b_5 it will be helpful to make advances in the application of solid-state NMR to the study of membrane proteins with a soluble domain (Chapter IV).

While the membrane orientation of TM domains of Cyt b_5 can directly be measured from the 2D HIMSELF spectra, assignment of resonances to amino acid residues would be useful to elucidate the role of individual residues on the interaction with Cyt P450 and their dynamics.

(a) Resonance Assignments

The assignment of resonances in the 2D HIMSELF spectrum from a uniformly ^{15}N-labeled Cyt b_5 is an important step to understand Cyt b_5 structure and function relationships (Figure I-7). However, the resonance assignment using the 'shotgun' approach[20] might be difficult because the Pro residue in the transmembrane region could distort the helix.[9, 14] In order to overcome this difficulty, a combination of the following approaches can be used.

(i) H/D exchange to suppress amide-^{15}N resonances from the soluble domain.

Due to the H/D exchange process, the use of D_2O in the sample will convert amide-^{1}H to amide-^{2}H. Therefore, the resonances from amide-^{15}N-^{1}H of the soluble domain, which are exposed to the water phase in bicelles in the 2D HIMSELF spectrum can be suppressed and this procedure would leave the resonances from the TM domain of the uniformly ^{15}N-labeled protein.

(ii) Selective ^{1}H magnetization transfer to ^{15}N nuclei in the transmembrane domain.

The TM region of Cyt b_5 is relatively more rigid than the soluble/linker region of Cyt b_5. Therefore, it is possible to selectively prepare the transverse magnetization of ^{15}N nuclei present in the transmembrane region. We concluded that ^{1}H-^{15}N pairs in the rigid part of the molecule require a short contact time while those ^{1}H-^{15}N pairs in the water-soluble, less-rigid, domain requires a long contact time to prepare ^{15}N magnetization.[14] Therefore, we are able to selectively acquire the ^{15}N peaks arising from the TM region by using a short contact time.

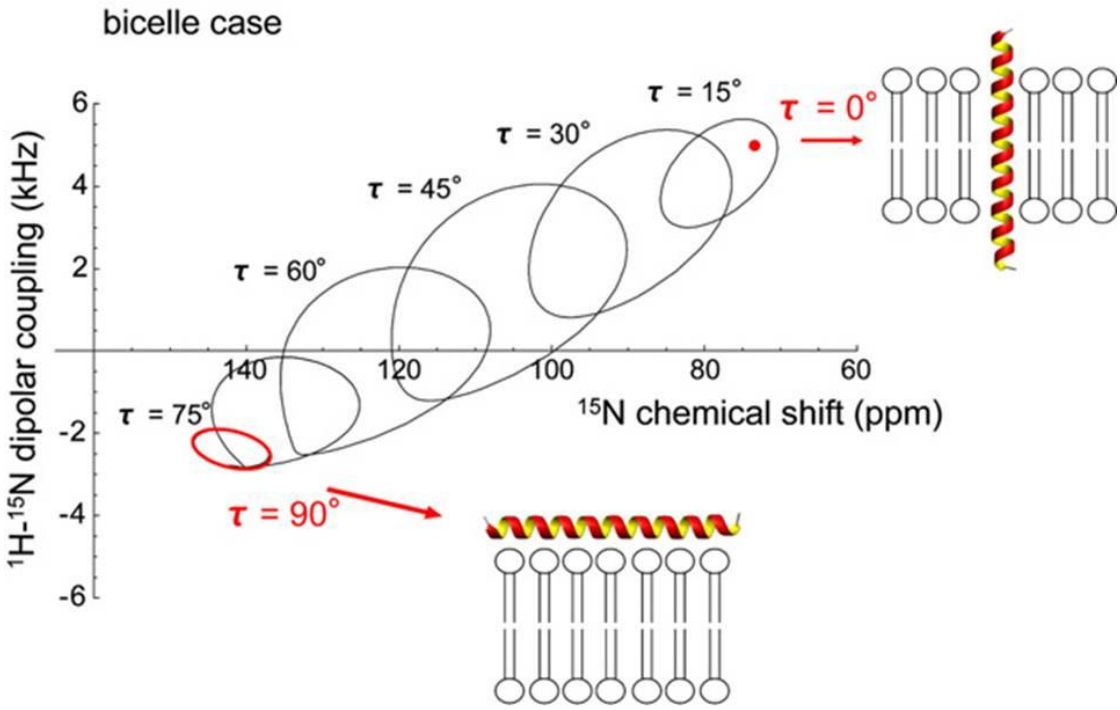

Figure I-6. **PISA wheels are spectral patterns found in SLF spectra that correlate ^{15}N chemical shift and ^{1}H–^{15}N dipolar coupling.** PISA wheels are observed for uniformly ^{15}N-labeled segments with α-helical secondary structure. From comparisons of simulated spectra vs. the experimental spectrum the tilt angle τ of a membrane-bound α-helix with respect to the membrane normal can be determined.[9]

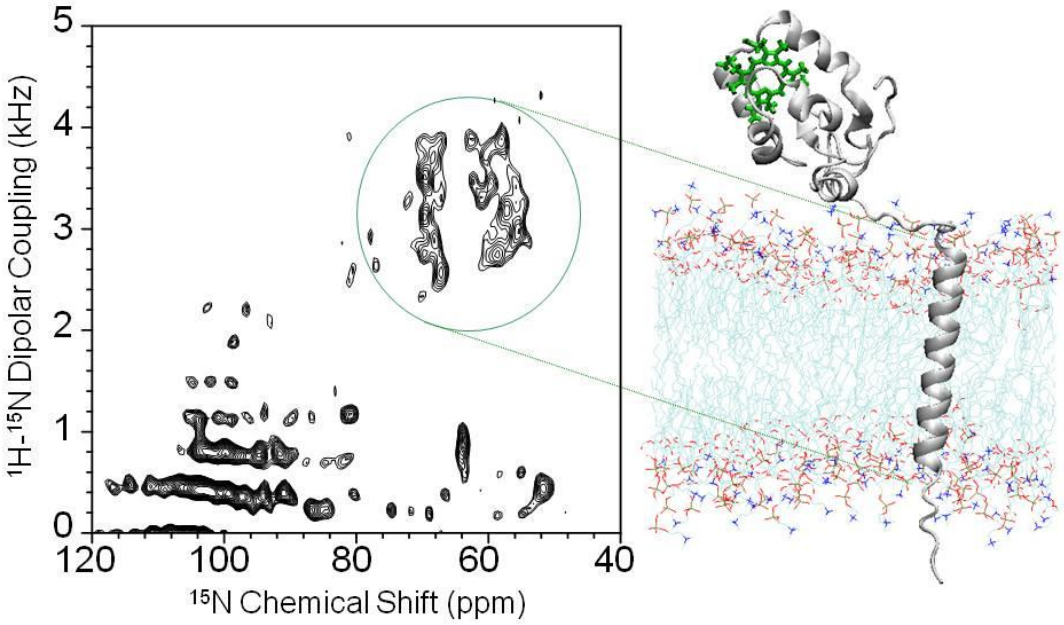

Figure I-7. **Two-dimensional ^{1}H-^{15}NHIMSELF spectrum of uniformly ^{15}N-labeled Cyt b_5 in DMPC:DHPC bicelles.** The spectrum shows well-resolved resonances and a clearly discernible PISA wheel pattern. The transmembrane α-helix is tilted 15° (±3°) withrespect to the bilayer normal, but indicates that it deviates from perfect α-helical geometry.

These spectral editing techniques will be extended to obtain 2D HIMSELF experiments to obtain the PISA wheel-type resonances arising from the transmembrane region (or soluble/linker region) of the uniformly ^{15}N-labeled Cyt b_5.

(iii) Use of selectively labeled Cyt b_5.

Cyt b_5 with only certain amino acids labeled with the ^{15}N isotope such as ^{15}N-Ala (there are 9 Ala residues: 3 of them are expected to be in the TM region) or ^{15}N-Trp (4 Trp residues: 3 of them are expected to be in the TM region) can be overexpressed and HIMSELF experiments on those samples can be conducted. The methods which I mentioned above in (i) and/or (ii), distinguish Ala or Trp residues in the TM region of Cyt b_5 from in the soluble/linker region.

There are a number of approaches to overcome the difficulties in assigning resonances from the TM region of Cyt b_5. Resonance assignments will also enable us to understand the role of the TM region of Cyt b_5 in the catalytic function of Cyt P450.

Characterization of the structure and dynamics of membrane-bound Cyt b_5 in a complex with Cyt P450

Previously, high-resolution information on ligand binding to Cyt P450 BM-3 has been reported by means of solid-state NMR.[21] Water-soluble truncated Cyt b_5, which lacks the transmembrane domain, does not activate Cyt P450. However, it does bind to Cyt $_C$. While structural studies on the Cyt b_5-Cyt c complex have been done, there is no structural data on the Cyt b_5-Cyt P450 complex, due to the difficulties in studying the complex by X-ray crystallography or solution NMR spectroscopy. Solid-state NMR experiments on the Cyt b_5-Cyt P450 complex can be performed in order to obtain the first structural data on the Cyt b_5-Cyt P450 complex. Experiments using published procedures[5,7] suggest that the Cyt b_5- Cyt P450 complex can be form on NMR samples (Figure I-8).

The ultimate goal is to complete characterization of the structure, membrane-topology and dynamics of the Cyt b_5-Cyt P450 complex and correlate the structural information with the functional data.

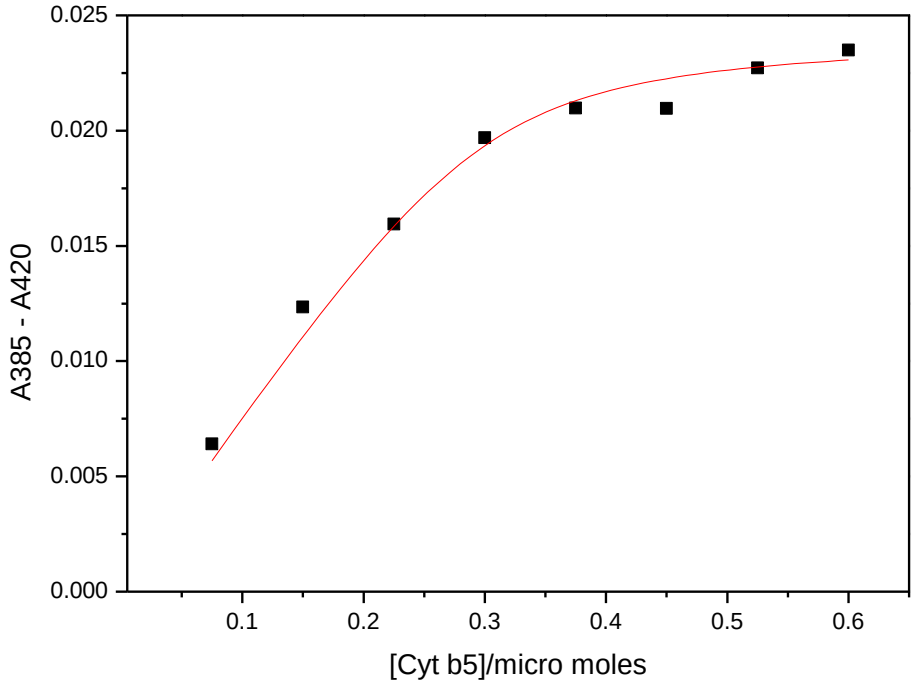

Figure I-8. **Measurement of Complex formation between between Cyt P450 2B4 and Cyt b_5 as measured by a change in absorbance at 385 and 420 nm.** Published experimental procedures were used in these measurements.[5,7]

I-6. References

1 (a) Arakawa, T.; Shimono, K.; Yamaguchi, S.; Tuzi, S.; Sudo, Y.; Kamo, N.; Saitô, H. *FEBS Lett*. **2003**, 536, 237-240. (b) Luca, S.; White, J. F.; Sohal, A. K.; Filippov, D. V.; van Boom, J. H.; Grisshammer, R.; Baldus, M. *Proc. Natl. Acad. Sci. USA*. **2003**, 100, 10706-10711. (c) Sato, T.; Pallavi, P.; Golebiewska, U.; McLaughlin, S.; Smith, S. O. *Biochemistry*, **2006**, 45, 12704-12714.

2 (a) Andronesi, O.C.; Becker, S.; Seidel, K.; Heise, H.; Young, H.S.; Baldus, M. *J. Am. Chem. Soc.*, **2005**, 127, 12965-12974. (b) Opella, S. J.; Zeri, A.C.; Park, S.H. *Annu. Rev. Phys. Chem.*, **2008**, 59, 635-657.

3 Zhang, H.; Myshkin, E.; Waskell, L. *Biochem. Biophys. Res. Commun.* **2005**, *338*, 499-506.

4 (a) Vergéres, G.; Waskell, L. *Biochimie* **1995**, *77*, 604-620. (b) Schenkman, J. B.; Jansson, I. *Pharmacol. Ther.* **2003**, *97*, 139-152.

5 Clarke, T. A.; Im, S.-C.; Bidwai, A.; Waskell, L. *J. Biol. Chem.* **2004**, *279*, 36809-36818.

6 Banci, L.; Bertini, I.; Rosato, A.; Scacchieri, S. *Eur. J. Biochem.* **2000**, 267, 755-766.

7 (a)Vergères, G.; Waskell, L. *J. Biol. Chem.*, **1992**, 267, 12583-12591. (b) Chiang J.Y., *Arch. Biochem. Biophys.* **1981**, 211, 662-673.

8 Shao, W.; Im, S-C.; Zuiderweg, E.R.; Waskell, L. *Biochemistry.* **2003**, 42, 14774-14784.

9 Dürr, U.H.; Waskell, L.; Ramamoorthy, A. *Biochim. Biophys. Acta.* **2007**, 1768, 3235-3259.

10 (a) Prestegard, J.H.; Al-Hashimi, H.M.; Tolman, J.R. *Q. Rev. Biophys.* **2000**, 33, 371-424. (b) Tjandra, N.; Bax, A. *Science* **1997**, 278, 1111-1114.

11 (a) Prosser, R.S.; Evanics, F.; Kitevski, J.L.; Al-Abdul-Wahid, M.S. *Biochemistry* **2006**, 45, 8453–8465. (b) Sanders, C.R.; Prosser, R.S. *Structure* **1998**, 6, 1227–1234.

12 (a) Dvinskikh, S.V.; Dürr, U.H.N.; Yamamoto, K.; Ramamoorthy, A. *J. Am. Chem. Soc.* **2007**, 129, 794-802 (b) Dvinskikh, S.V.; Dürr, U.H.N.; Yamamoto, K.; Ramamoorthy, A. *J. Am. Chem. Soc.* **2006**, 128, 6326-6327 (c) Dvinskikh, S.V.; Yamamoto, K.; Dürr, U.H.N.; Ramamoorthy, A. *J. Magn. Reson.*, **2007**, 184, 228–235. (d) Lu, J.-X.; Damodaran, K.; Lorigan, G.A., *J. Magn. Reson.* **2006**, 178, 283–287.

13 (a) Triba, M.N.; Warschawski, D.E.; Devaux, P.F. *Biophys. J.* **2005**, 88, 1887–1901

14 Dürr, U.H.N.; Yamamoto, K.; Im, S.-C.; Waskell, L.; Ramamoorthy, A. *J. Am. Chem. Soc.* **2007**, 129, 6670-6671.

15 (a) Opella, S. J. *Nat. Struct. Biol.* **1997**, *4*, 845. (b) Opella, S. J.; Marassi, F. M. *Chem. Re*v. **2004**, *104*, 3587-3606. (c) Ketchem, R. R.; Hu, W.; Cross, T. A. *Science* **1993**, *261*, 1457-1460. (d) Kovacs, F.; Quine, J.; Cross, T. A. *Proc. Natl. Acad. Sci. U.S.A.* **1999**, *96*, 7910-7915.

16 (a) Denny, J.K.; Wang, J.; Cross, T.A.; Quine, J.R. *J. Magn. Reson.* **2001**, 152, 217-226. (b) Marassi, F.M.; Opella, S.J. *J. Magn. Reson.* **2000**, 144, 150–155.

17 (a) Wu, C.H.; Ramamoorthy, A.; Opella, S.J. *J. Magn. Reson. Ser. A* **2003**, 109, 207–272. (b) Ramamoorthy, A.; Wei, Y.; Lee, D.-K. *Annu. Rep. NMR Spectrosc.* **2004**, 52, 1–52. (c) Ramamoorthy, A.; Yamamoto, K. A familiy of PISEMA experiments for structural studies of biological solids, in: G.A. Webb (Ed.), *Modern Magnetic Resonance*, Springer, 2006, pp. 699–705. (d) Gan, Z. *J. Magn. Reson.* **2000**, 143, 136–143.

18 Yamamoto, K.; Lee, D.K.; Ramamoorthy A. *Chem. Phys. Lett.* **2005**, 407, 289–293

19 (a) Yamamoto, K.; Dvinskih, S.V.; Ramamoorthy, A. *Chem. Phys. Lett*. **2006**, 419, 533-536. (b) Dvinskikh, S.V.; Yamamoto, K.; Ramamoorthy, A. *Chem. Phys. Lett*. **2006**, 419, 168-173. (c) Dvinskikh, S.V.; Yamamoto, K.; Ramamoorthy, A. *J. Chem. Phys.* **2006**, 125, 034507.

20 Marassi, F.M.; Opella, S.J. *Protein Sci.* **2003**, 12, 403–411.

21 (a) Jovanovic, T.; McDermott, A.E. *J. Am. Chem. Soc.* **2005**, 127, 13816-13821. (b) Jovanovic, T.; Farid, R.; Friesner, R.A.; McDermott, A.E. *J. Am. Chem. Soc.* **2005**, 127, 13548-13552.

Chapter II

Nuclear Magnetic Resonance Spectroscopy Method Developments for Membrane Biology*

II-1. Summary

Narrowest heteronuclear dipolar coupling spectral lines provided by the two-dimensional polarization inversion spin exchange at the magic angle (PISEMA) technique lead to the development and application of a series of multidimensional solid-state NMR methods for the structural studies of biological solids. Studies have shown that the measurement of structural and orientational constraints from uniformly labeled proteins using PISEMA is crucial, particularly in the structure determination of membrane-associated proteins. Excellent line-narrowing efficiency, high scaling factor, and performance at various magic angle spinning (MAS) speeds and radio frequency (RF) power are the main advantages of PISEMA. However, high RF power requirement and offset effects are the major limitations of this technique. In this chapter, these difficulties and methods to overcome them are discussed for both static and MAS experimental conditions. Experimental and simulated data to demonstrate the efficacy of newly developed PISEMA-type pulse sequences are also discussed.

The resolution of NMR spectra and sensitivity of NMR spectroscopy have been always important area of study. In later part of this chapter, we described methodological

* This chapter is a version of manuscripts published in *Handbook of Modern Magnetic Resonance* (Chemistry section) edit by Graham Webb, Part 1, (2006)703-709., *Chem. Phys. Lett*., 407 (2005) 289-293., *J. Am. Chem. Soc.*, 127(2005)6958-6959., *Chem. Phys. Lett*. 408 (2005)118-122., *Chem. Phys. Lett*., 419(2006)167-173., *Chem. Phys. Lett*., 419(2006)533-536., *J. Chem. Phys.*, 125(2006) 034507., *J. Magn. Reson.*, 184(2007)228-235. and *J. Am. Chem. Soc.*, 132(2010)6929-6931. This study was supported by the funds from NIH and NSF.

developments and experimental aspects of sensitivity and resolution enhancement of membrane lipid bilayers and membrane-associate peptides and proteins on NMR spectroscopy. In particular, approaches to enhance the sensitivity and resolution and to quantify radio frequency heating effects on the natural abundance ^{13}C and ^{14}N NMR of DMPC/DHPC bicelles are discussed. Sensitivity of ^{13}C detection using the single pulse excitation, conventional cross-polarization (CP), ramp-CP, and NOE techniques are compared. Our results suggest that the proton decoupling efficiency of the FLOPSY pulse sequence is better than that of continuous wave decoupling, TPPM, SPINAL, and WALTZ sequences for the studies of magnetically aligned bicelles. A simple method of monitoring the water proton chemical shift is demonstrated for the measurement of sample temperature and calibration of the radio-frequency-induced heating in the lipid bilayer samples. The possibility of using ^{14}N experiments on bicelles is also discussed.

In spite of recent technological advances in NMR spectroscopy, its poor sensitivity continues to be a major limitation particularly for the structural studies of membrane proteins. In the last part of this chapter, we demonstrated the feasibility of very fast acquiring multidimensional NMR spectra of an antimicrobial peptide (subtilosin A and MSI-78) embedded into bicelles. A copper-chelated lipid embedded in bicelles is used to speed-up the spin-lattice relaxation of protons without affecting the spectral resolution and thus enabling fast data collection. Our results suggest that for solid-state NMR spectroscopy experiments a 6.2-fold speed increase and a 2.7-fold improvement in signal-to-noise ratio under magic-angle spinning and static conditions, respectively, on the other hand, for solution NMR spectroscopy experiments even a 2D SOFAST-HMQC spectrum can be obtained four times faster using a very small amount (~3 mM) of copper-chelated lipid using natural-abundance ^{15}N nuclei on solution NMR spectroscopy. These results demonstrate that it is possible to use this approach in the structural studies of membrane proteins using NMR spectroscopy. Furthermore, NMR measurements are shown to be feasible even for *nano*-mole concentrations of a membrane-associated peptide.

II-2. A Family of Separated-Local Field Experiments for Structural Studies of Biological Solids

Accurate measurement of heteronuclear dipolar couplings is very important to determine the high-resolution structure, dynamics, and orientation of molecules using solid-state NMR spectroscopy.[1] A variety of multiple pulse sequences have been used to suppress homonuclear ^{1}H spin–spin interactions in a two-dimensional (2D) Separated-Local-Field (SLF) experiment, which provides narrow heteronuclear dipolar coupling lines.[1] The best sequence should satisfy following seven qualities: (i) completely suppress dipole-dipole interactions among *I* (usually high γ and/or highly abundant nuclei such as ^{1}H and ^{19}F) spins, (ii) have a large scaling factor (scaling factor = 1.0 represents 0% reduction in the measured *I*-*S* dipolar coupling values) in order to measure small heteronuclear dipolar couplings as well as to resolve resonances from uniformly labeled proteins, (iii) have a short duration that can provide a large spectral width, (iv) be tolerant to pulse imperfections such as offset and RF field inhomogeneity, (v) require a low RF power to avoid sample heating, (vi) avoid rotor synchronization and be independent of the spinning speed of the sample for studies under MAS, and (vii) be easy to set up in most commercially available solid-state NMR spectrometers. Among all the reported SLF sequences, polarization inversion spin exchange at the magic angle (PISEMA) (Figure II-1A and B) satisfies most of these requirements.[1-4] An Flip-flop Lee-Goldburg (FFLG)-[5-8] or Phase-Modulated Lee-Goldburg (PMLG)-[9] based PISEMA sequence efficiently suppresses ^{1}H–^{1}H dipolar couplings with a scaling factor of 0.816 and a short cycle time (16.33μs for a 50 kHz rf field strength), tolerant to most of the experimental errors, easy to set up, and can easily be modified to work efficiently under various spinning speeds without the need for rotor synchronization.[1,3] In addition, the sensitivity enhancement offered by the polarization inversion, and the reduction of relaxation rates and suppression of *I* and *S* spin chemical shifts by the spin-locks during SEMA are other intrinsic benefits of the sequence.[1,2] Therefore, the pulse sequence has been widely used for studies both under static (Figure II-1A)[1,10-15] and MAS (Figure II-1B)[1,4,16] experimental conditions. The SEMA sequence has also been utilized to develop several new solid-state NMR methods to study biological solids[17-23]. Studies have shown that

replacing FFLG in SEMA with the Lee-Goldburg magic angle irradiation (LG), such as LG-PISEMA, LG-SEMA, or LG-CP, also provides heteronuclear dipolar coupling spectra with an identical scaling factor.[1,3,4,24] In fact, LG-SEMA is routinely used to set up 2D PISEMA experiments[3] and selective transfer of ^{1}H magnetization to its dipolarcoupled heteronuclei such as ^{13}C or ^{15}N.[22,23,25] The main advantages of LG-SEMA are its short cycle time and the absence of phase transients.[1,3] However, the extent of ^{1}H homonuclear decoupling and tolerance toward RF field mismatch and RF field inhomogeneity by FFLGSEMA is far better than that of LG-SEMA.[3,24]

II-2-1. Radio Frequency Resonance Offset Effect of SLF pulse sequences

There are some disadvantages that limit the application of PISEMA to investigate certain systems. Studies have shown that the SEMA sequence is highly sensitive to *I* spin offset.[1] Our simulations (data not shown) on a dipolar-coupled two-spin (*I* and *S*) system show that the offset dependency is identical for LG-SEMA and FFLGSEMA sequences as there is no homonuclear ^{1}H dipolar couplings are included in the calculations. Since the effective field direction of LG or FFLG is dependent on the offset value, the line-narrowing efficiency decreases and the observed dipolar splitting increases with offset (Figure II-2A, plot A). In addition, a strong zero-frequency peak appears as the off-magic angle spin-lock of *I* spins eliminates the spin exchange among *I* and *S* nuclei (Figure II-3). These effects are severe when a low RF power is used and also for experiments conducted at high magnetic fields. For example, a span of ~12 ppm for amide ^{1}H chemical shift resonances makes it very difficult to satisfy the LG condition for all amide sites of a uniformly labeled protein/peptide. As a result, the intensity, scaling factor, and line width are not uniform in a 2D PISEMA spectrum of a uniformly ^{15}N-labeled protein embedded in aligned lipid bilayers. The offset effects are stronger for small ^{1}H-^{15}N dipolar couplings. Thus it is difficult to accurately measure the ^{1}H-^{15}N dipolar couplings for the structural studies of membrane proteins. Therefore, it is of considerable importance to develop new PISEMA-type pulse sequences that can overcome the above-mentioned offset effects.

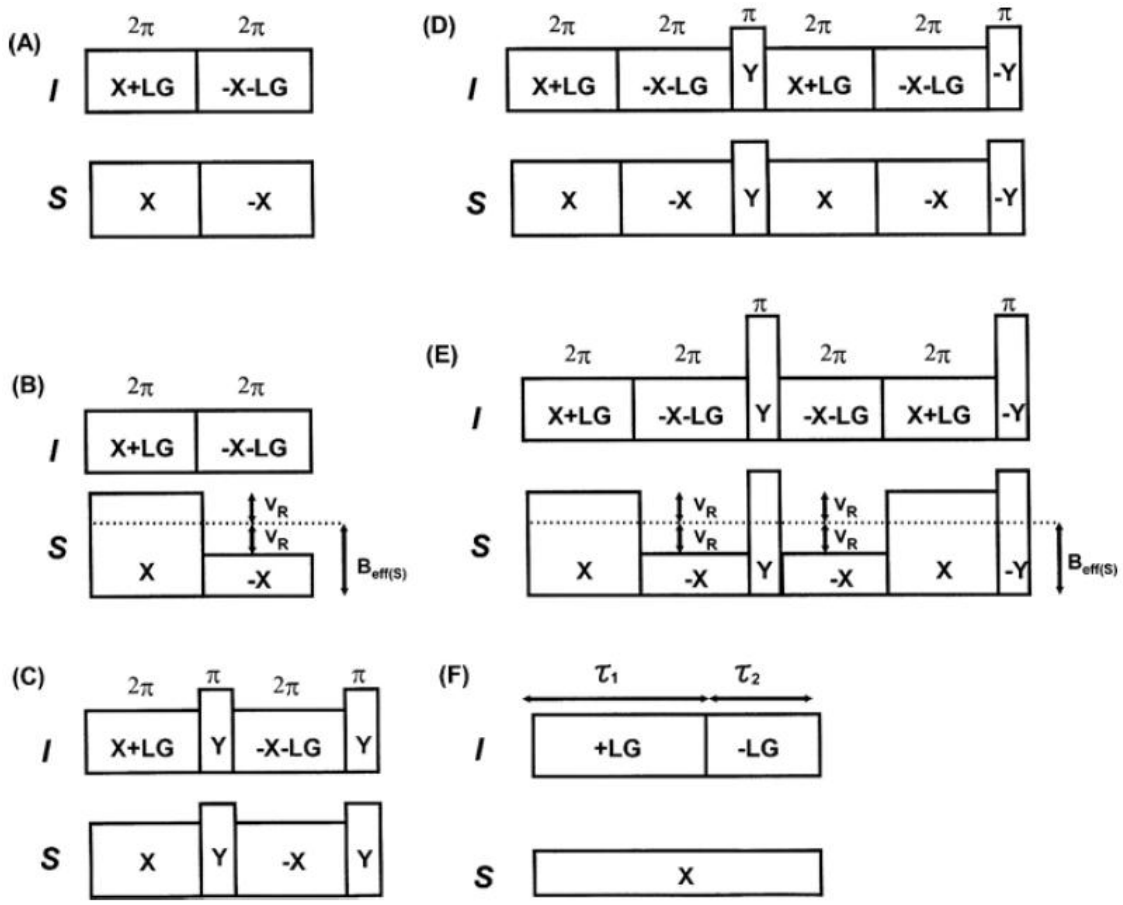

Figure II-1. **Timing diagrams for a family of SEMA sequences that can be used in the t_1 period of 2D PISEMA**: (A) SEMA, (B) SEMAMAS, (C) BB-SEMA-1, (D) BB-SEMA-2, (E) BB-SEMA-MAS, and (F) TANSEMA. LG stands for the Lee–Goldburg magic angle irradiation.

II-2-2. Broad-Band PISEMA Solid-state NMR Spectroscopy

Studies have shown that the use of ramped spin-lock pulses[26] during SEMA in the *S* spin channel or the newly developed SAMMY[27] sequence reduces offset effects. However, the extent of line narrowing of the SAMMY sequence are smaller than that of the PISEMA sequence. We recently proposed a modified PISEMA sequence (called BB-PISEMA (Figure II-1C–E) that compensates the effects of offset.[28] Introduction of simultaneous π pulses in the SEMA sequence suppresses the evolution of the magnetization under offset in the SEMA period of PISMEA. This is reflected in the results shown in Figures II-2A (plots B and C) and II-3. While the offset compensation is better for BB-SEMA-1 than BB-SEMA-2, line-narrowing efficiency may depend on the π pulse width. The number of FFLG cycles in between the π pulses can be varied depending on the required dwell time. The efficacy of SEMA (Figure II-1A) and BB-SEMA (Figure II-1D) sequence was examined using 2D experiments on a single crystal (Figure II-2A) and simulations (Figure II-2B) using SIMPSON.[29] Experimentally obtained dipolar coupling slices are given in Figure II-4. Both the experimental and simulated data demonstrate that heteronuclear dipolar coupling spectra obtained using BB-PISEMA are less sensitive to *I* spin offset than those obtained with the regular PISEMA pulse sequence.

This is a significant improvement and therefore the BB-PISEMA sequence can be used in the structural studies of membrane proteins at high magnetic fields where there is a range of ^{1}H chemical shifts.

Simulations suggest that the use of ideal π pulses provides a scaling factor of 0.816 and the deviation from ideality reduces the scaling factor of BB-SEMA (Figure II-1C). Nevertheless, our experimental results demonstrate that the scaling factor of BB-PISEMA is 0.73 even for a π pulse width of 8.16 μs. In theory, the scaling factor of BB-PISEMA ($SF_{BB\text{-}PISEMA}$) is given in a following equation:

$$SF_{BB\text{-}PISEMA} = \sin\theta_m \cdot (1-\tau_\pi/\tau_c)$$
$$= 0.816 \cdot (1-\tau_\pi/\tau_c)$$

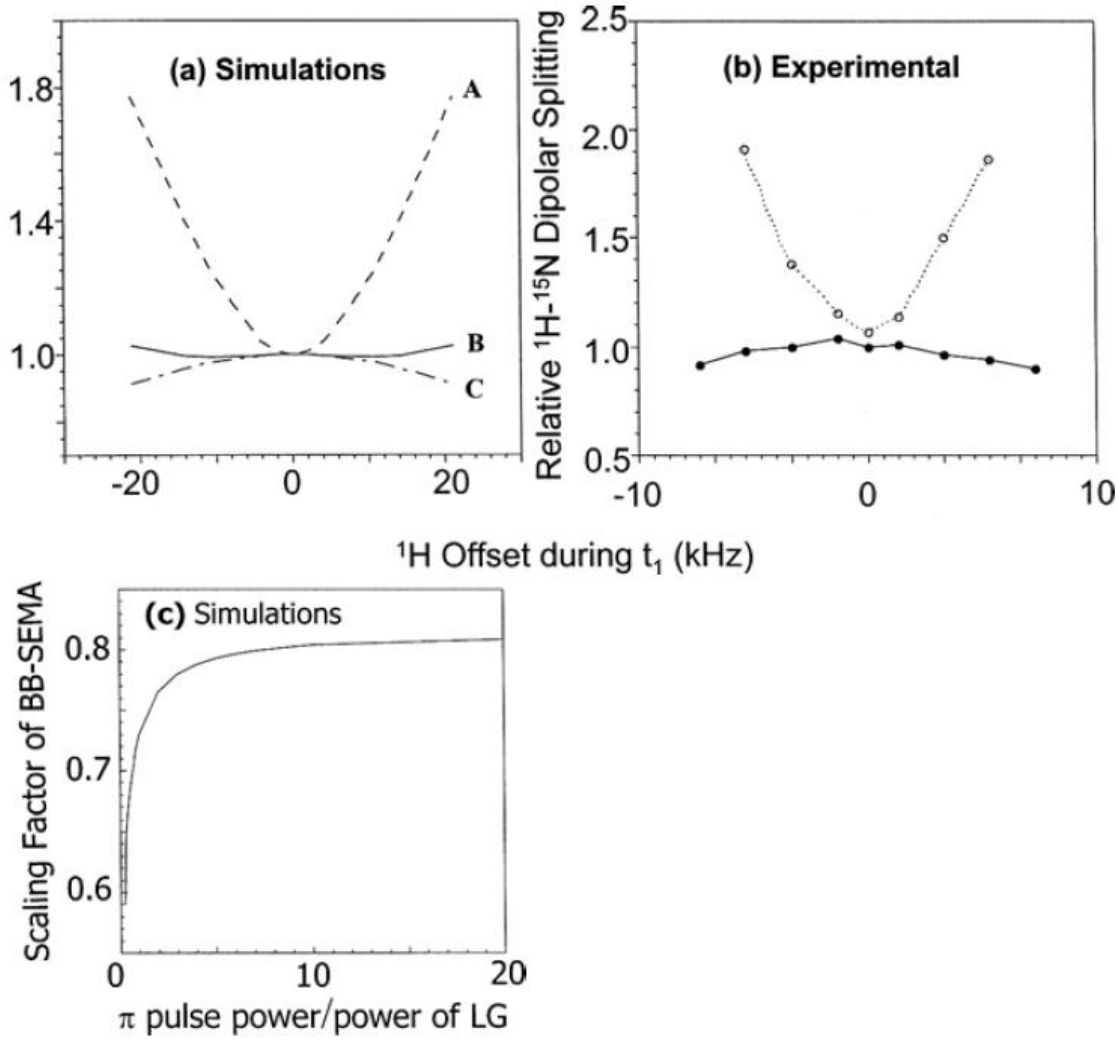

Figure II-2. **Dependence of the simulated (a) and experimentally (b) measured heteronuclear dipolar couplings on the *I* spin carrier offset.** Experimental data were measured from 2D PISEMA and BB-PISEMA spectra (data not shown) of *n*-acetyl-l-^{15}N-valyl-l-^{15}N-leucine single crystal under the same experimental conditions. The simulated data in (a), (b), and (c) were obtained using the PISEMA, BB-SEMA-1, and BB-SEMA-2 sequences, respectively. (c) Variation of the scaling factor with the ratio of the RF power used for the π and LG pulses in the BB-PISEMA. In all the simulations, 100 kHz RF field was used for LG and the π pulse in BB-SEMA-2. The πgulse power was varied in (c).

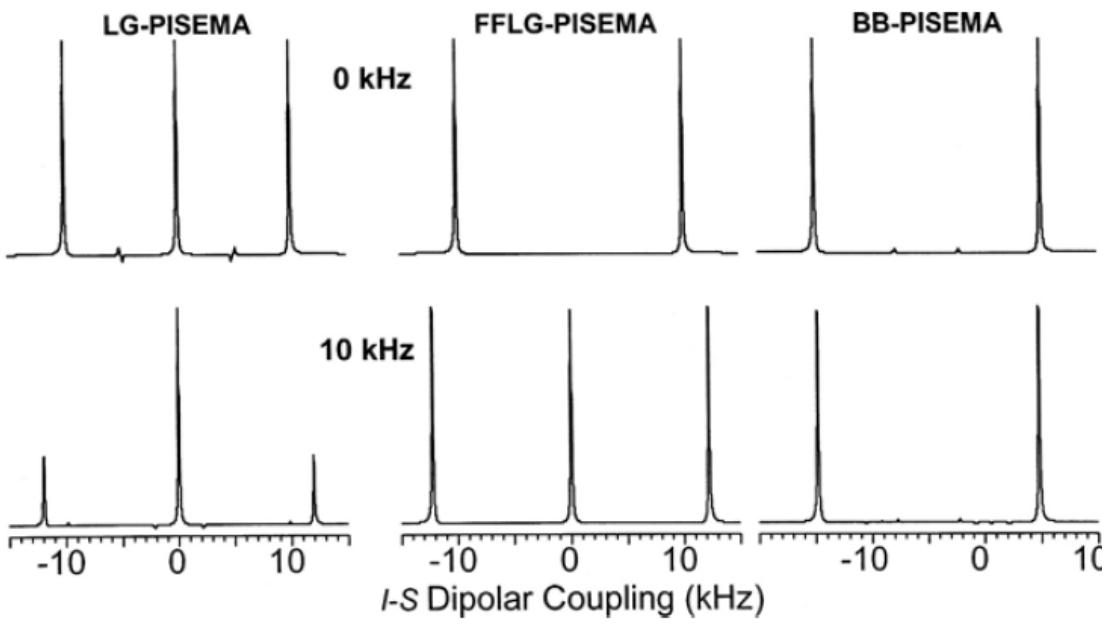

Figure II-3. **Simulated *I* –*S* dipolar coupling spectra of an aligned two-spin system** with a dipolar coupling constant of 10 kHz at *I* spin carrier offset frequencies of 0 and 10 kHz. Note the appearance of the zero-frequency peak and the increase in the dipolar splitting in LG- and FFLG-based PISEMA sequences. Offset effects are stronger when the *I* –*S* dipolar coupling is small. On the other hand, BB-PISEMA spectra are independent of the *I* spin carrier frequency.

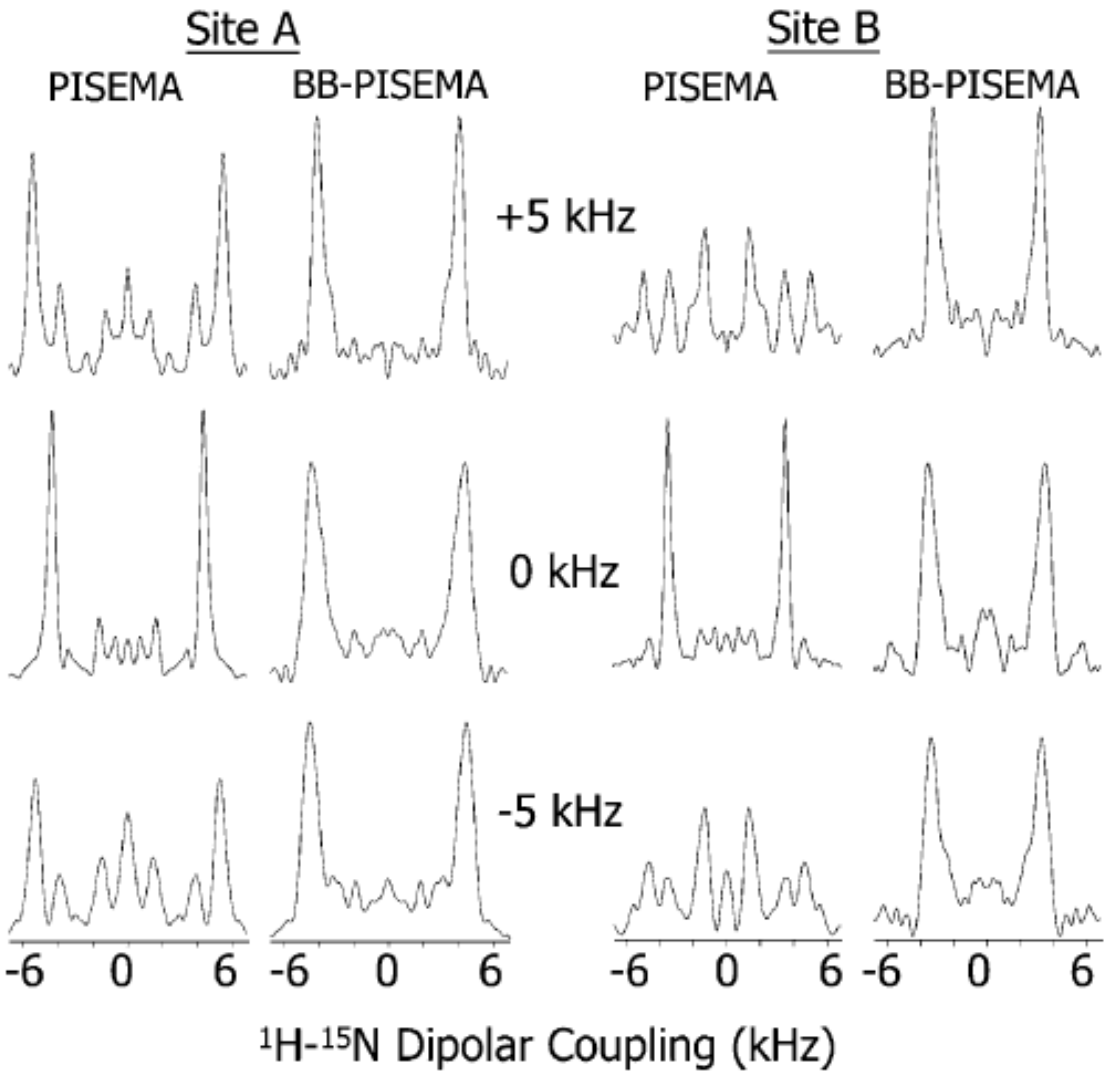

Figure II-4. **^{1}H–^{15}N dipolar coupling spectra obtained at different ^{1}H offset values from PISEMA (A) and BB-PISEMA (B).** Sites A and B correspond to a ^{15}N chemical shift value of 83.7 and 102.2 ppm, respectively. In addition to the increase in the observed dipolar coupling values, S/N is significantly decreases with the offset value in PISEMA spectra. On the other hand, BB-PISEMA spectra are to a large extent independent of the offset values.

where θ_m is magic angle, τ_π is π pulse width and τ_c is the SEMA block, RF cycle time (τ_c = SEMA time + 2 τ_π). Simulated results from an unoriented dipolar-coupled two-spin system are given in Figure II-5. Recently published CSA values were used in the simulations[30-36]. FFLG-PISEMA provides better power line shapes than the LG-PISMEA sequence. However, the line shapes from both LG- and FFLG-based PISEMA sequences are dominated by the zero-frequency peak due to *I* spin offset effects. On the other hand, BB-PISEMA significantly suppresses the offset effects (Figure II-5). Offset effects of SEMA-MAS (Figure II-1B) can also be compensated using a pair of π pulses as shown in Figure II-1E (data not shown). While the BB-SEMA-based sequences are efficient in compensating the *I* spin offset effects even when low power π pulses were used, the performances of these sequences are dependent on the *S* spin offset values as shown in Figure II-6 (plot B). As shown in Figure II-6 (plot C), this effect can be overcome by using high power π pulses in BB-SEMA sequences. The spin dynamics and the performance of this new pulse sequence can be analyzed using average Hamiltonian and density matrix approaches. Several such studies reported the theoretical details of the offset effects under heteronuclear spin exchange process under static and MAS conditions.[24,37-39]

The on-resonance performance of the PISEMA sequence is impressive even when low power is used for the FFLG sequence.[1,27,28] For example, as low as a 40-kHz RF field in the ^{1}H channel can be used at 400 MHz to obtain high-resolution ^{1}H-^{15}N dipolar spectral lines for a peptide embedded in bilayers.[28] However, the requirement of RF power in the *S* spin channel is quite demanding as it has to match the effective field in the ^{1}H channel for static conditions: $B_{rf,S} = (B^2_{rf,S} + B^2_{off,I})^{1/2}$. In addition, under MAS, the power requirement is increased by the spinning speed (Figure II-1B and E); this means for experiments under fast MAS and/or at high magnetic fields, this requirement will be quite challenging to satisfy. This problem is also significant for wet biological solids such as lipid bilayers as these samples are power loss and are highly sensitive to RF heat.[40-42] For example, even in the above-mentioned peptide example, ~1 kW RF power is required in the ^{15}N RF channel.[40] Therefore, it is essential to overcome these difficulties in order to use PISEMA-type experiments on membrane proteins.

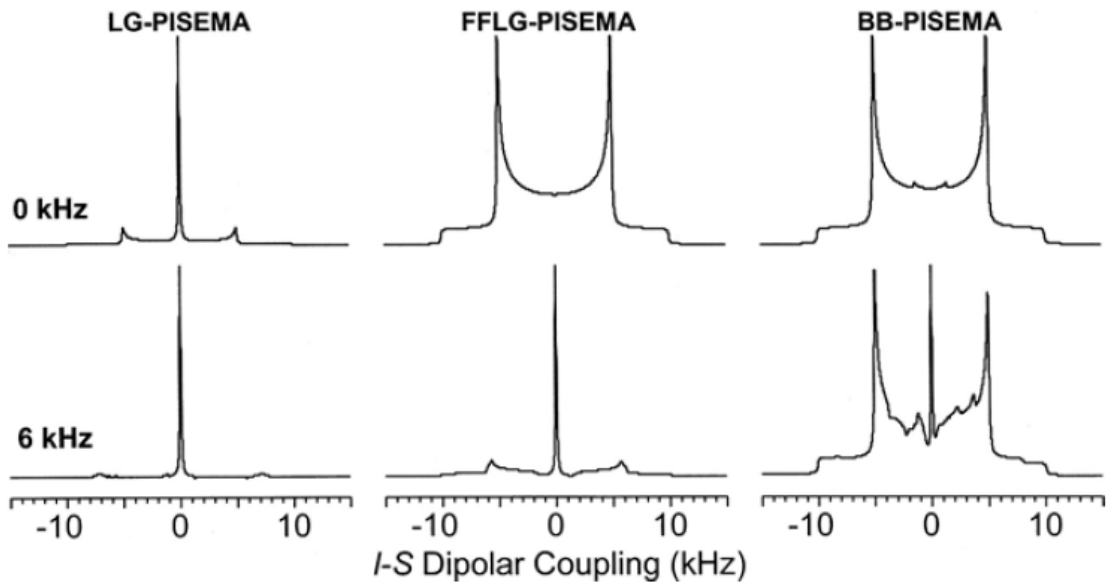

Figure II-5. **Simulated *I* –*S* dipolar coupling spectra of an unoriented two-spin system** with a dipolar coupling constant of 10 kHz at 0 and 6 kHz *I* spin carrier offset values. The strong zero-frequency peak in LG-PISEMA (both on- and off-resonances of *I* spin) and FFLG-PISEMA makes it difficult to measure the powder lineshape, whereas BB-PISEMA is tolerant to offset effects. The intensity of the zero-frequency peak depends on the span of the CSA values used in simulations.

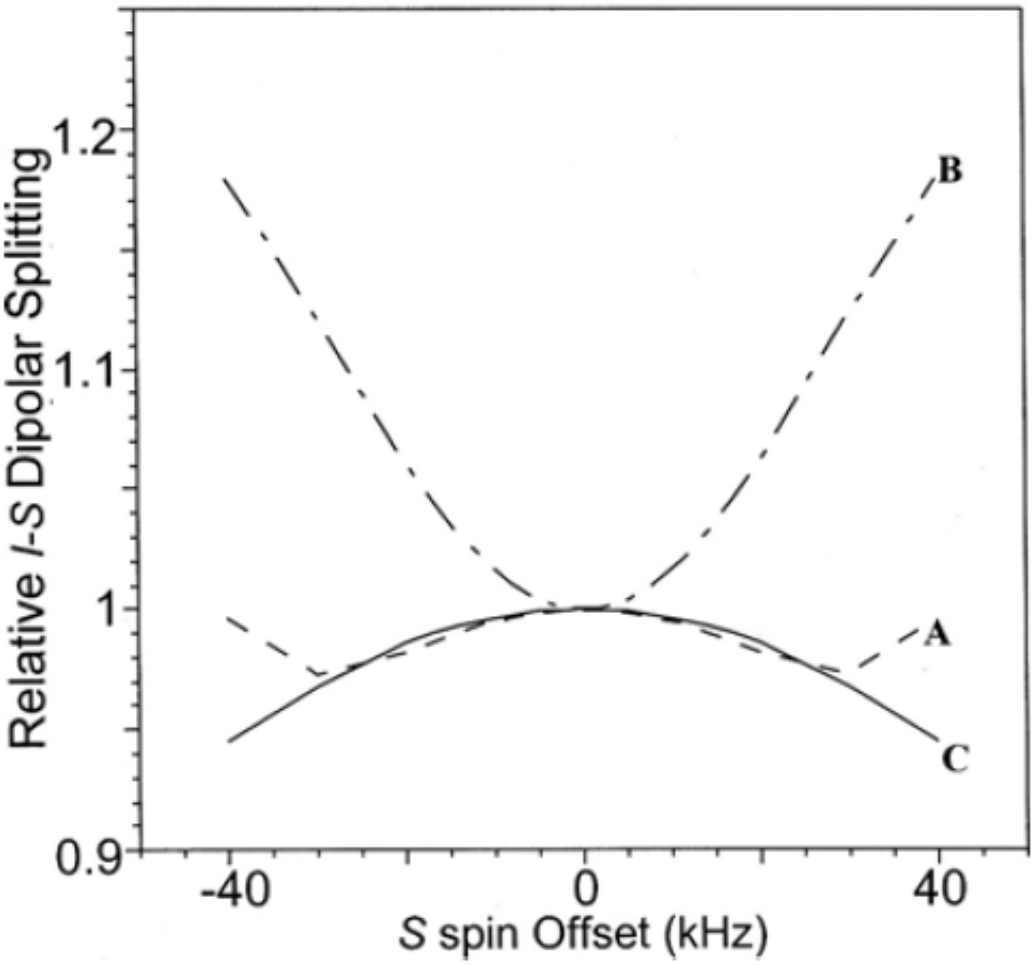

Figure II-6. **Variation of simulated $^{1}H–^{15}N$ dipolar coupling values as a function of ^{15}N offset in PISEMA (A) and BB-PISEMA sequences (B and C)**. A 100 kHz rf field was used for LG in all cases, while the πpulse power was 100 kHz for (B) and 500 kHz for (C).

II-2-3. PITANSEMA Pulse Sequence for Low Power Solid-state NMR Spectroscopy

In order to overcome the high RF heating effect on solid-state NMR, we demonstrated the utility of time averaged nutation (TAN)[43] concept for the reduction of RF power in SEMA experiments. The TANSEMA[44] pulse sequence shown in Figure II-1F drastically reduces the RF power required in the *S* spin channel. The values of t_1 and t_2 can be varied to obtain the desired effective nutation field in the ^{1}H channel. For example, PITANSEMA experiments even with a 11-fold reduction in the ^{15}N RF power, as compared to the regular PISEMA experiment, on a single crystal sample resulted in 2D spectra with line widths as good as that of PISEMA.[44] Use of supercycles and ramped spin-locks further improved the efficacy of the PITANSEMA sequence. This sequence has also shown to be effective for liquid crystalline samples.[44,45] Figure II-7. However, our simulations show that the measured dipolar splitting is offset dependent as shown in Figure II-8. Simulated *I-S* dipolar coupling PITANSEMA spectra of an aligned two-spin system for various *I* spin carrier offset values showed increase in the zero-frequency peak and the dipolar splitting like the PISEMA sequence. Research in Professor A. Ramamoorthy laboratory to improve the efficacy of PITANSEMA is in progress.

II-2-4. PITANSEMA-MAS Pulse Sequence for Low Power Solid-state NMR Spectroscopy

The time average nutation (TAN) concept can be applicable for solid-state NMR experiments under magic angle spinning as well. This technique, polarization inversion spin exchange at the magic angle-magic angle spinning (PITANSEMA-MAS), combines the advantages of time averaged nutation (TAN) and SEMA concepts.[44,45] The efficiency of the sequence is examined numerically and experimentally on several solids. Our results suggested that the proposed PITANSEMAMAS technique requires an order of magnitude less RF power to spin-lock the low γ nuclei than the standard PISEMA experiment. RF pulse sequences for the spin exchange (or polarization transfer) via the heteronuclear (*I* and *S*) dipolar coupling are sketched in Figure II-9. The spin-locks suppress the chemical shift interactions of both nuclei, FFLG sequence suppresses the *I-I* dipolar interaction,[5-8] and when the effective field strength of the spin-locks match (for

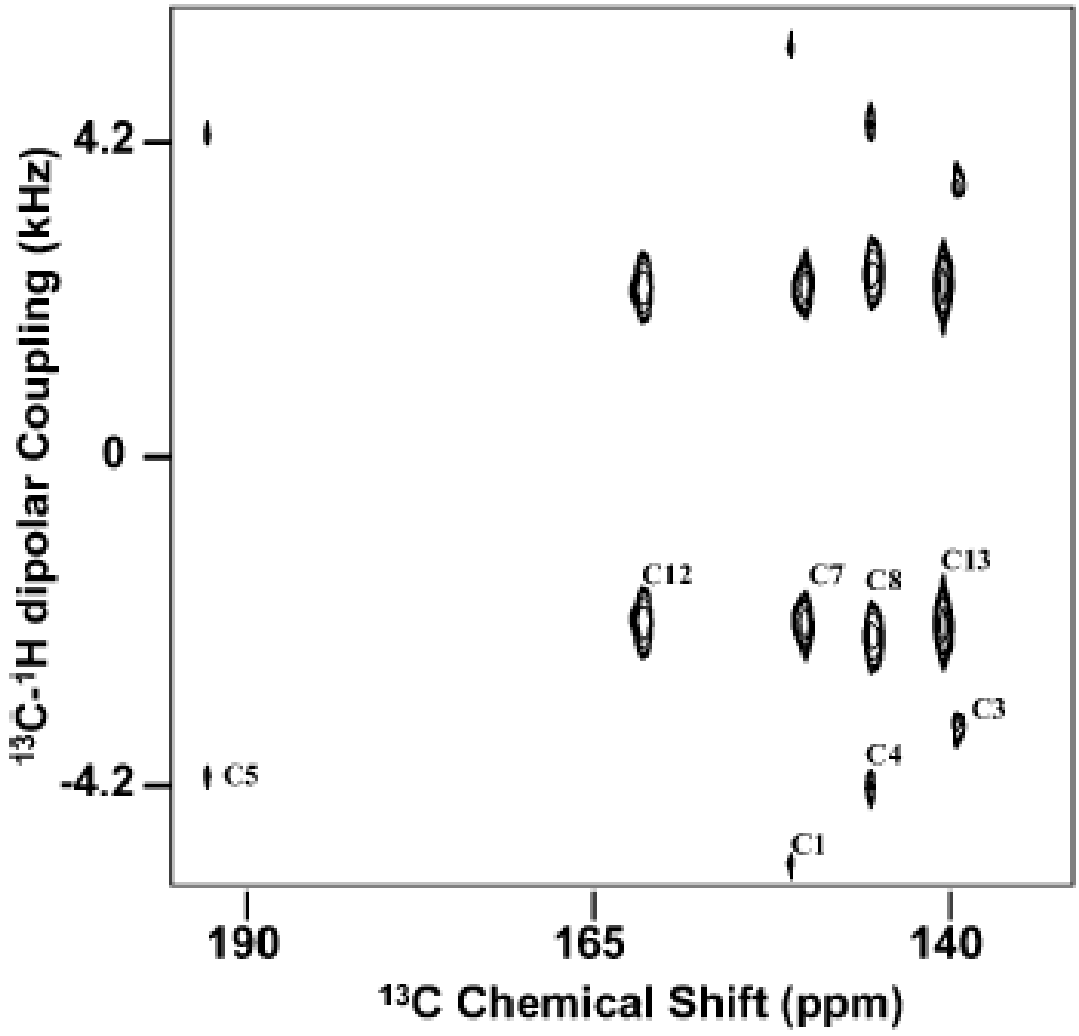

Figure II-7. **2D PITANSEMA spectrum of TMAPB at 130 °C.** An experimentally measured scaling factor of 0.6 was used. τ_1 = 10 μs, τ_1 = 15 μs, 128 t_1 increments, 16 scans, and a 3 s recycle delay were used.

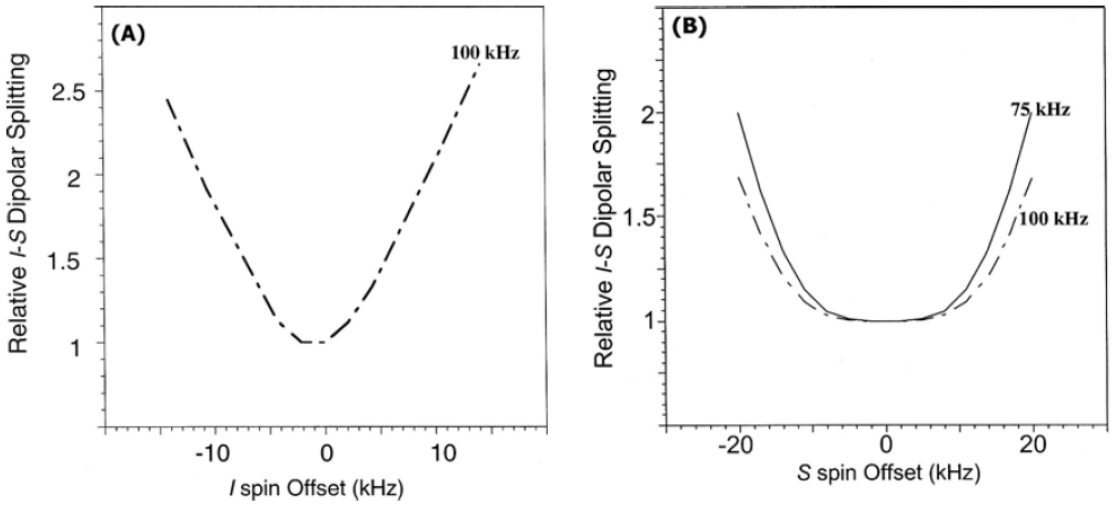

Figure II-8. **Variation of simulated *I* –*S* dipolar splitting as a function of *I* (A) and *S* (B) spin carrier offset frequency in PITANSEMA** with $\theta_1 = \pi$ and $\theta_2 = \pi/2$; where θ_1 and θ_2 are the effective nutation angles during the 1st and 2nd halves of the TANSEMA sequence, respectively (Figure II-1E). Note that these angles are equal (i.e. $\theta_1 = \theta_2$) in PISEMA and therefore the time average nutation for SEMA is zero.

example in the SEMA sequence given in Figure II-9A), spin exchange between the strongly coupled *I* and *S* nuclei are enabled. These sequences significantly suppress weak heteronuclear interactions and lead to a high-resolution dipolar coupling spectrum.[1,3,46] In a 2D experiment like PISEMA, following the initial preparation of magnetization (i.e., cross polarization with -x phase spin-locks from *I* to *S* and a 35.3_y^o pulse to flip back the I_x magnetization to the magic angle), these sequences in Figure II-9 are employed in the t_1 period. SEMA sequences for static and MAS conditions are given in Figure II-9A,B, respectively. To avoid the averaging of the heteronuclear dipolar interactions under fast MAS, in SEMA-MAS (Figure II-9B), the difference in the two spin-lock field strengths is matched to the spinning sidebands: $B_{eff,I} - B_{rf,S} = n\nu_r$; where $B_{eff,I}$ is the effective spin-lock field strength, $(B_{rf,I}^2 + B_{off}^2)^{1/2}$, in the *I* channel, B_{off} is the offset frequency, $B_{rf,S}$ is the RF field strength in the *S* channel, and ν_r is the spinning speed. The extent of recovered *I*-*S* dipolar coupling is higher when $n = \pm 1$ sideband than $n = \pm 2$ or ± 3. The splitting between the two singularities in a dipolar-coupled spectrum obtained using SEMA-MAS is $D_{IS}\cos\theta_m$, where D_{IS} is the *I*-*S* dipolar coupling and θ_m is the magic angle.

To reduce the required RF field strength in the *S* spin channel, the TAN and SEMA concepts were used to obtain the TANSEMA[44,45] sequence (Figure II-9C). In this sequence, the unequal τ_1 and τ_2 durations generate an effective nutation field (B_{TAN}) in the *I* channel that is matched with the *S* spin-lock field strength: $B_{rf,S} = \{(\tau_1 - \tau_2)/(\tau_1 + \tau_2)\}B_{eff,I}$. This TANSEMA sequence for static experiments is modified for studies under MAS (TANSEMA-MAS) as shown in Figure II-9D. In TANSEMA-MAS, the matching condition for an effective spin exchange is given as $\{(\tau_1 - \tau_2)/(\tau_1 + \tau_2)\}B_{eff,I} - B_{rf,S} = n\nu_r$ with $n = \pm 1$. The values of τ_1 and τ_2 can be chosen to alter the scaling factor of the pulse sequence as shown in Figure II-9E. Supercycles can also be constructed to overcome some of the experimental problems, such as RF field inhomogeneity or offset, and to match the desired extent of recovered *I* and *S* dipolar coupling as explained for the static case.[44] This TANSEMA-MAS sequence (Figure II-9D) drastically reduces the required RF power as compared to the sequence given in Figure II-9B.

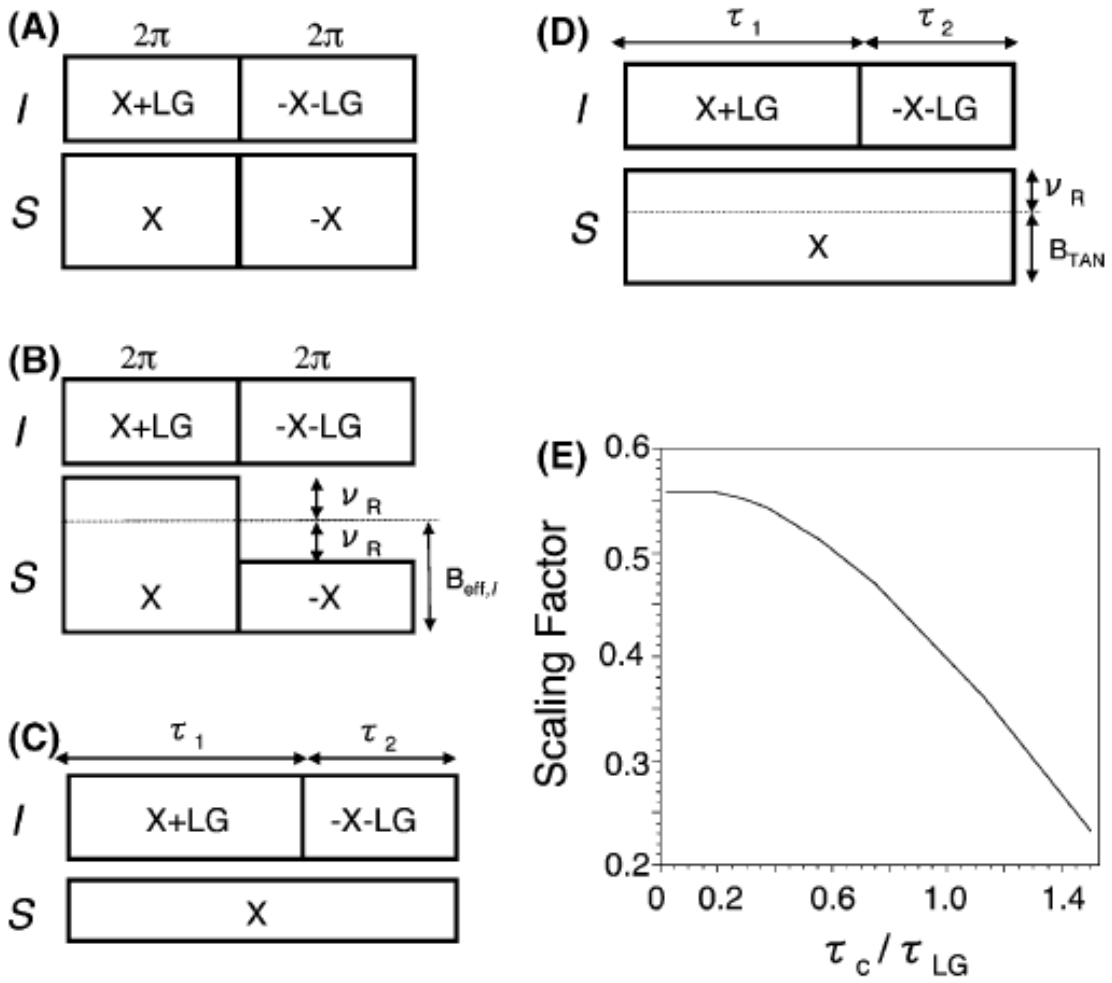

Figure II-9. **RF pulse sequences for the spin exchange at magic angle (SEMA) via the heteronuclear (*I* and *S*) dipolar coupling.** (A) SEMA, (B) SEMA-MAS, (C) TANSEMA and (D) TANSEMA-MAS pulse sequences. (E) Variation of the scaling factor of the PITANSEMAMAS as a function of τ_c/τ_{LG} for a time averaged factor, (τ_1 - τ_2)/τ_c, of 1/3; τ_c is a cycle time of TANSEMA-MAS and τ_{LG} is the 2π duration of the LG sequence. An RF field strength of 62.5 kHz for FFLG and an NH dipolar coupling of 10 kHz were used in the simulation. B_{TAN} is the effective nutation field, ν_r is the spinning speed, and LG stands for Lee–Goldburg.

All experiments were carried out on a Chemagnetics/Varian Infinity 400 MHz and a Varian INOVA 800 MHz spectrometers at room temperature. A 5 mm HXY and a 2.5 mm HCN triple resonance probes were used in 400 and 800 MHz, respectively. Powder samples of *n*-acetyl-D,L-^{15}N-valine (NAV), natural abundance D,L-alanine and 2-^{13}C-leucine were used. All the experimental conditions are given in the figure caption. All simulations were carried out using SIMPSON[29] on a PC. Two spins (^{1}H and ^{15}N with a dipolar coupling constant of 9.8 kHz or ^{1}H and ^{13}C with a dipolar coupling constant of 20 kHz) and 376 crystallite orientations were considered in the simulations. All other parameters were as used in the experiments. Simulated ^{1}H–^{13}C dipolar coupling spectra obtained using the PITANSEMAMAS sequence are given in Figure II-11 for various spinning speeds and for matching with the first ($n = \pm1$) and second ($n = \pm2$) sidebands. While the scaling factor of the sequence is independent of the spinning speed, it decreases with the increasing |n| value with an optimum line shape for the $n = \pm1$ condition. Sidebands can be seen for slow spinning speeds.

2D PITANSEMA-MAS experiments with various values of the scaling factor were carried out at many different spinning speeds. While the pulse sequence recovered ^{1}H–^{15}N dipolar coupling under various spinning speeds, the magnitude of the recovered interaction depended on the τ_i values (Figure II-9E). Sample spectra obtained from the NAV powder sample are compared with simulations in Figure II-11. These results indicate that the experimental and simulated results are in good agreement. Experimentally measured dipolar splittings for various experimental conditions (such as τ_i values, RF power and spinning speed) are identical. The spinning sidebands can be seen for spectra obtained with a large scaling factor. As shown in Figure II-11B, the resolution can be enhanced using a super cycle. Except for the scaling factor, the line shape obtained from a PITANSEMAMAS experiment was similar to that obtained using PISEMA-MAS. However, it is important to note that the RF power used in a PITANSEMA-MAS experiment (at a 7 kHz spinning speed) was ~11 times less than that of PISEMAMAS. This factor increased when the spinning speed increased, as a high RF power is essential to match the +1 spinning side band. Use of +2 sidebands not only decreased the extent of recovered dipolar coupling but also increased the RF power needed in the experiment.

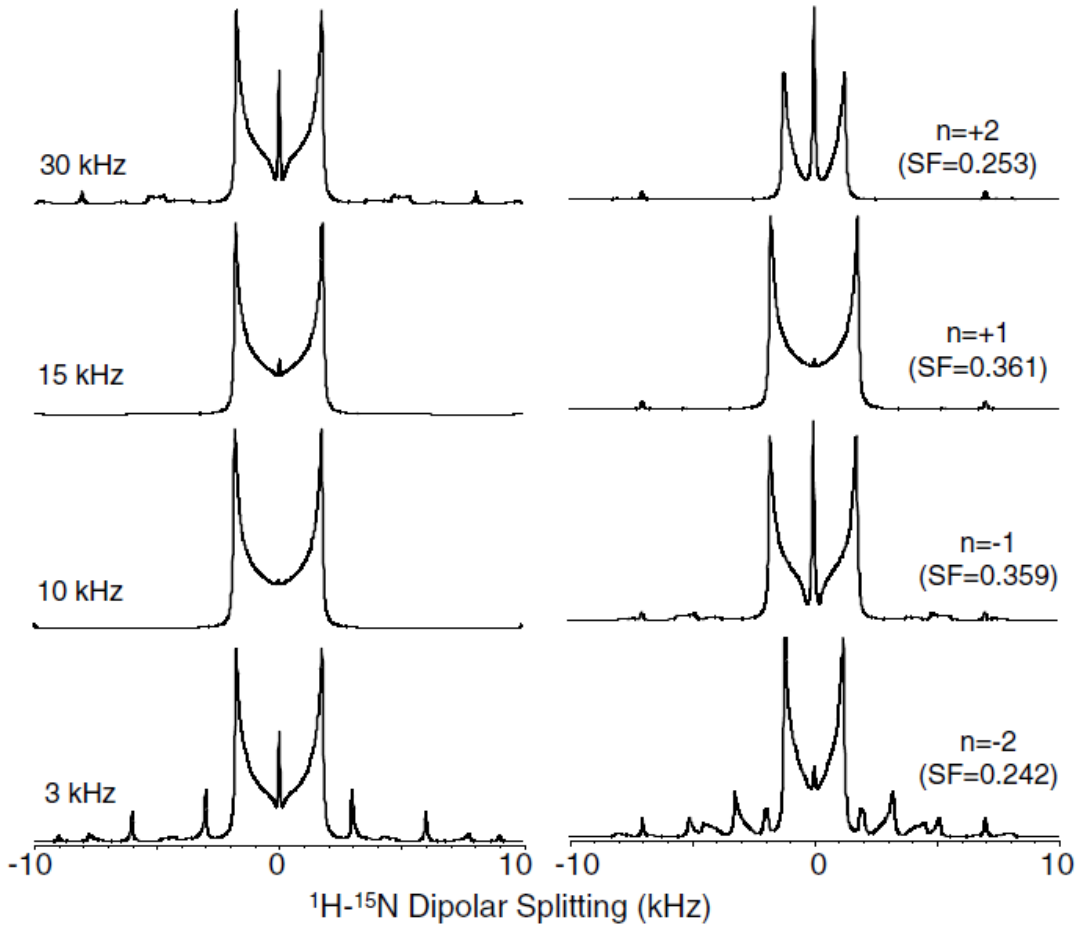

Figure II-10. **Simulated PITANSEMA-MAS spectra for various spinning speeds and spinning sideband-matching condition.** Nutation angles of 1.5π and 0.75π with an $^{15}N^{1}H$ dipolar coupling of 9.8 kHz were used. Scaling factor (SF) for each condition is given.

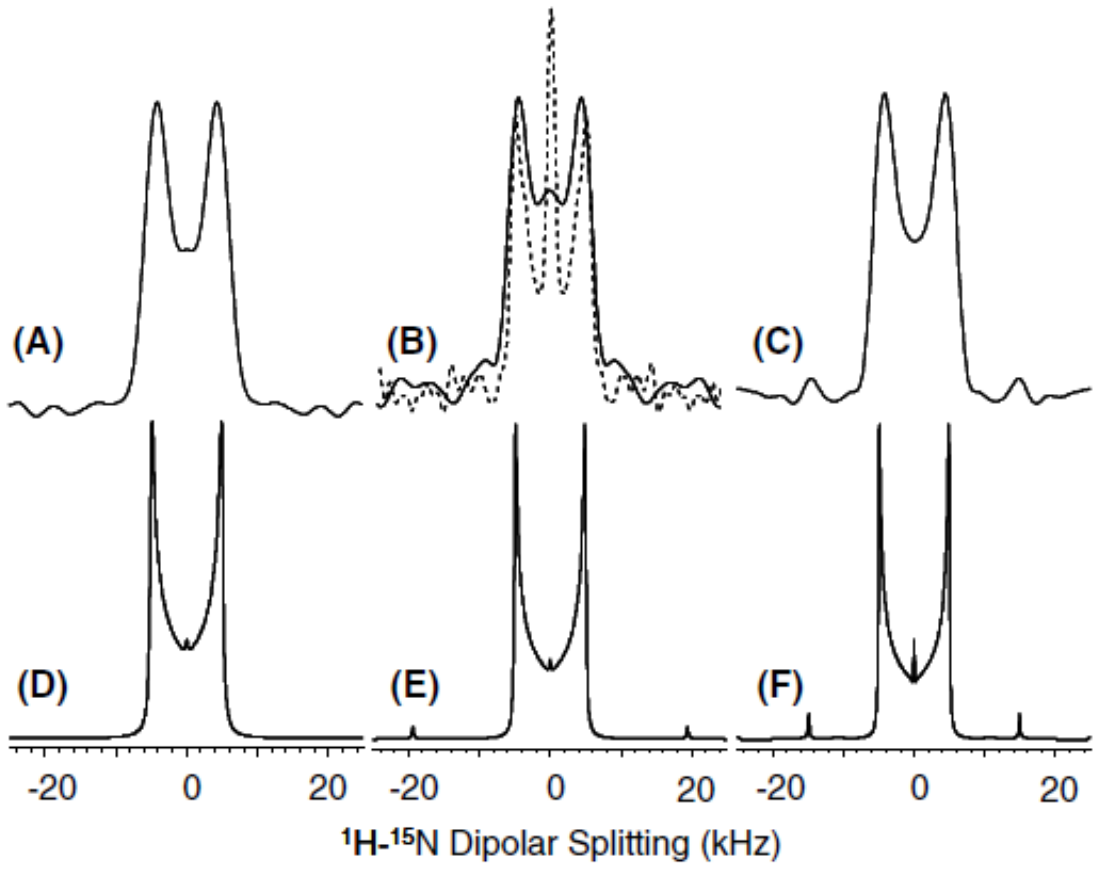

Figure II-11. **Experimental (A, B and C) and simulated (D, E and F) $^{1}H–^{15}N$ dipolar coupling spectral lines obtained using the 2D PITANSEMAMAS sequence (Figure II-9D) under 7 kHz MAS.** Experimental spectra were obtained from an *n*-acetyl-D,L-^{15}N-valine powder sample. A 50 kHz RF field for the preparation period, a 62.5 kHz RF field with an offset of 44.19 kHz for FFLG in the t_1 period, and a 62.5 kHz TPPM decoupling of protons during the ^{15}N signal acquisition were used. Other experimental parameters include a 0.5 ms cross-polarization time, 64 t_1 experiments, 4 scans and a 4 s recycle delay. (τ_1, τ_2) Values of (30.76 μs, 15.38 μs), (23.08 μs, 11.54 μs) and (15.38 μs, 7.69 μs) were used to obtain spectra (A and D), (B and E) and (C and F), respectively. Scaling factors of 0.232, 0.361 and 0.470 were used for (A and D), (B and E) and (C and F), respectively. The dashed line spectrum in B was obtained using 3-cycles while all other spectra (solid line) were obtained using 1-cycle of TANSEMA-MAS.

Similar experiments were also carried out on natural abundance alanine and 2-^{13}C-leucine powder samples. A 2D PITANSEMA-MAS spectrum of alanine along with the dipolar coupling slices is given in Figure II-12. The dipolar coupling is measurable for both the sites even though a zero-frequency peak is present. The measured C_α-H dipolar coupling provides an accurate measurement of the bond length. The zero-frequency peak could be attributed to the ^{13}C magnetization that does not participate in the spin exchange process during the t_1 period of the sequence in addition to the contribution from the isotropic peak. The results obtained from alanine suggested that the sequence is efficient and can be used to measure inter-nuclear distances in natural abundance samples. Therefore, this sequence can be applied to study biological and liquid crystalline materials that are sensitive to RF heat without the need for isotope enrichment.

Experiments and simulations were performed on a 2-^{13}C-leucine powder sample to examine the effects of offset frequencies of ^{1}H and ^{13}C resonances and the results are given in Fig. 5. The results suggest that the scaling factor of the sequence depends on the proton offset frequency while it is relatively less sensitive to ^{13}C offset. The dependence on the ^{1}H offset is not surprising as off resonance irradiation is used to suppress the ^{1}H-^{1}H dipolar couplings in the FFLG sequence. On the other hand, it is interesting to note the tolerance of the sequence towards ^{13}C offset even though very low RF power was used in the PITANSEMA experiment. However, PISEMA-MAS is relatively less sensitive to offset effects than PITANSEMA-MAS (Figs. 5B,D). These effects can be understood using the theoretical analysis of the spin dynamics related to an off resonance heteronuclear coherence transfer process.[24,45,38,39]

Since the heteronuclear dipolar coupling Hamiltonians for SI_i and SI_j in an SI_n system do not commute, the smaller couplings are suppressed by SEMA.[1,45] This is an advantage in the structural studies of proteins as one interested in measuring the dipolar coupling between the directly bonded amide ^{1}H and ^{15}N spin pairs by suppressing the coupling between remote protons and ^{15}N. However, in several other systems such as liquid crystalline materials, measurement of small dipolar couplings is important. Recent studies have showed that it is difficult to measure small dipolar couplings in the presence of large dipolar couplings.[46,47] For this kind of systems, which contain smaller dipolar

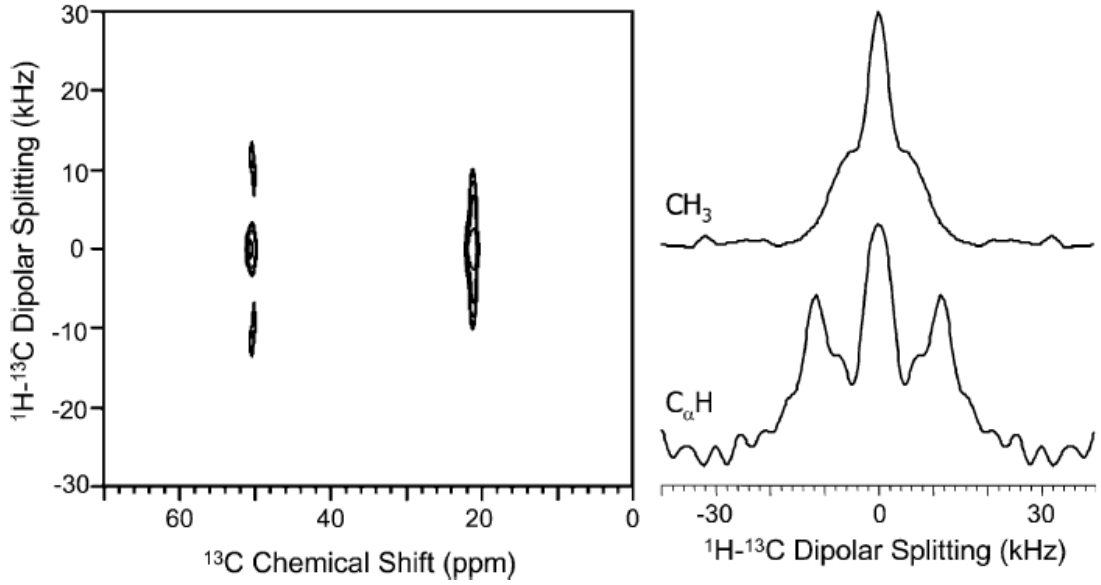

Figure II-12. **2D Experimental PITANSEMA-MAS spectrum that correlates the ^{13}C isotropic chemical shift and ^{1}H–^{13}C dipolar coupling of natural abundance D,L-alanine powder sample.** The ^{1}H–^{13}C dipolar coupling slices extracted from the 2D spectrum are given for the methyl (21.4 ppm) and alpha (50.5 ppm) carbons. (τ_1, τ_2) Values of (23.08 μs, 11.54 μs) with a scaling factor of 0.36 were used. All other experimental conditions were as given in Figure II-11.

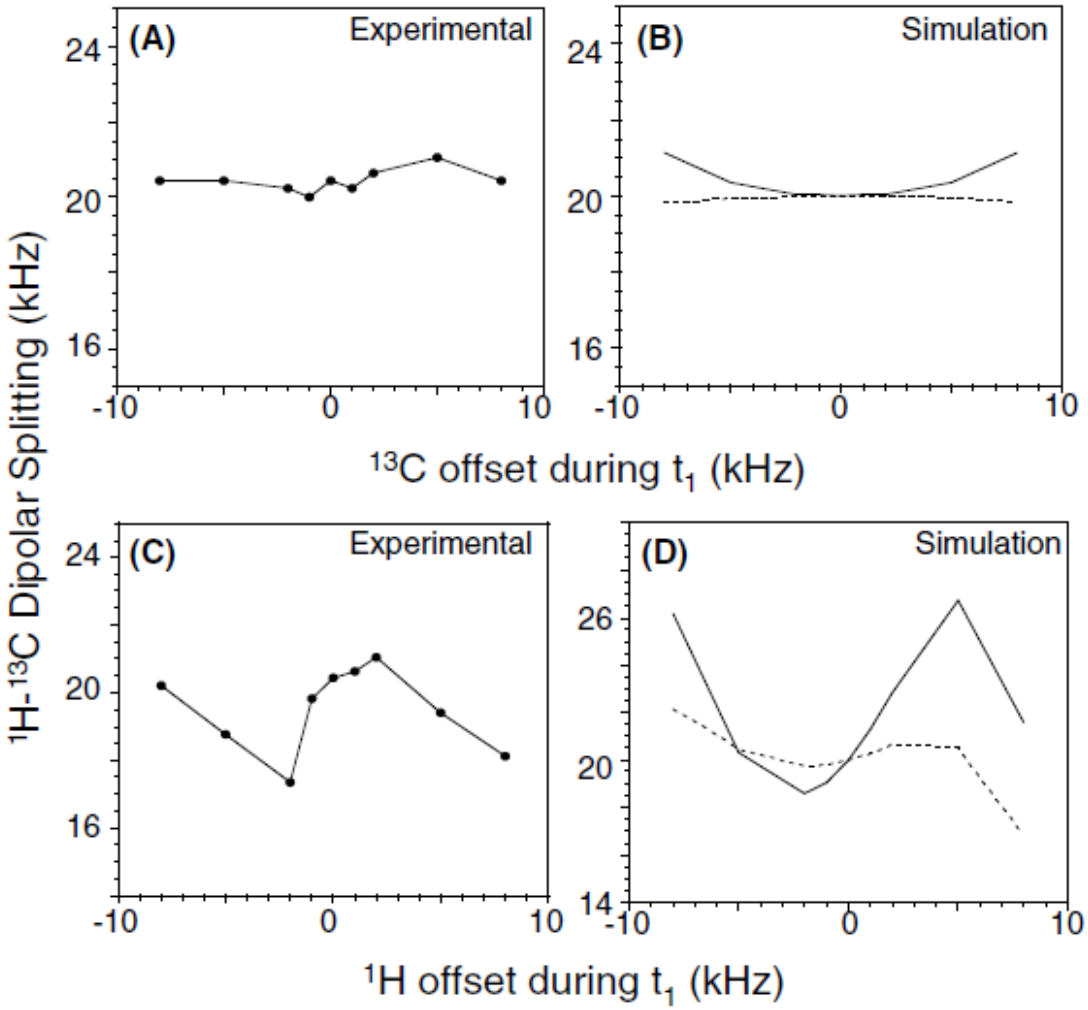

Figure II-13. **Experimental (A and C) and simulated (B and D) values of the ^{1}H–^{13}C dipolar coupling as a function of offset frequencies of ^{13}C (A and B) and ^{1}H (C and D) resonances.** Solid and dashed lines are for PITANSEMA-MAS and PISEMAMAS, respectively. All other experimental conditions were as given in Figure II-12. In the simulations, an RF field strength of 62.5 kHz for FFLG and a dipolar coupling of 20 kHz were used.

couplings, we developed new approach. This approach is discussed in details in Chapter III and IV.

II-2-5. Heteronulcar Isotropic Mixing Separated-Local-Field NMR Spectroscopy

The structural and dynamics investigations of rigid solids and anisotropic liquids have been greatly advanced by solid-state NMR techniques probing heteronuclear dipolar spin interactions such as ^{1}H-^{13}C dipolar couplings.[1-4] Highly resolved ^{13}C spectra can be recorded at natural abundance and are assigned by routine NMR methods. The problem of signal overlap in dipolar spectra of complex chemical systems is solved by using two-dimensional (2D) Separated-Local-Field (SLF) spectroscopy.[5] SLF methods based on the heteronuclear spin exchange in the rotating frame,[6-12] SELF (*S*pin *E*xchange via the *L*ocal *F*ield), have been applied to the studies of thermotropic liquid crystals,[9,10,13-15] lipid bilayers,[16,17] and biological membranes.[1,3] Typically, in SELF, the dipolar couplings are monitored through the oscillations of spin-locked components of the magnetizations taking place when two radio-frequency (RF) fields are matched at the Hartman-Hahn (HH) conditions.[18] In stationary samples, the superior dipolar resolution is achieved when SELF is combined with the efficient homonuclear proton decoupling. Most popular technique of this kind, polarization inversion spin exchange at the magic angle (PISEMA) experiment,[7] employs off-resonance flip-flop, frequency- and phase-switched Lee-Goldburg homonuclear decoupling.[19,20] However, this approach is highly sensitive to the interfering effect of the ^{1}H chemical shift term.[21] The problem can be partly solved by intercalating the original sequence with the repetitive refocusing 180^{o} pulses, which however requires high power pulses and the spin dynamics is complicated due to effect of the finite pulse width.[22,23] In other approach, the technique has been suggested which uses on-resonance magic sandwiches at the proton frequency and HH-matched irradiation in carbon channel.[11] While the technique is robust towards to chemical shift and frequency offset terms, the dipolar resolution suffers.

In this part of the chapter, we propose an alternative SELF approach to measure the dipolar couplings in anisotropic oriented media. It is based on the windowless isotropic mixing (WIM) sequences[24] and employs the heteronuclear polarization exchange between z-components of the ^{1}H and ^{13}C magnetizations. In contrast to Hartmann–Hahn

cross polarization (HH-CP), where only spinlocked component of the spin-magnetization is transferred, isotropic mixing sequences allow for the transfer of any magnetization component of one nucleus to the corresponding component of its dipolar coupled partner. Heteronuclear isotropic mixing leading to spin exchange via the local field (HIMSELF) provides the dipolar resolution comparable to that of other advanced SELF methods, but preserves high robustness towards chemical shifts and frequency offsets. The method is especially competitive for accurate measurements of motionally reduced dipolar couplings.

The 2D WIM-z SELF sequence is shown in Figure II-14a. During the variable evolution period t_1, WIM24 sequence, which consists of on-resonance 90^o backto-back pulses in ±x, ±y directions of the rotating frame,[24] is applied simultaneously to proton (*I* spins) and carbon-13 (*S* spins) nuclei. This results in coherent polarization transfer between z-components of *I* and *S* spin magnetization with the oscillation frequency determined by the heteronuclear spin coupling. The homonuclear dipolar spin interaction and chemical shift evolution are suppressed during WIM24 irradiation.[24] Following the 90^o pulse, the ^{13}C signal is acquired in the presence of TPPM proton heteronuclear decoupling.[25] Alternatively, the evolution of the proton magnetization during t_1 can be encoded in the detected ^{13}C signal using the ^{1}H-^{13}C HH-CP as shown in Figure II-14b. In the sequence of Figure II-14c, the initial *I* and *S* spin polarizations are prepared to be aligned in opposite directions to achieve polarization inversion (PI) that would enhance the sensitivity. The WIM24-based spin exchange experiments can also be performed in a more conventional way by employing the polarization exchange in the transverse plane as shown in Figure II-14d.

WIM24 cycle eliminates the homonuclear dipolar interactions and suppresses the chemical shift evolution.[24] When WIM24 sequence is applied to I_i-*S* spin system synchronously in two frequency channels, the spin evolution is, in the lowest order average Hamiltonian theory,[26,27] governed by the isotropic mixing Hamiltonian of the form

$$H^M = \sum_i \frac{2}{3}\omega_{IS}^i \mathbf{I}^i \cdot \mathbf{S} \qquad (1)$$

where $\omega_{IS}^{i} = 2\pi(d_{IS}^{i} + J_{IS}^{i}/2)$, and d_{IS}^{i} and J_{IS}^{i} are the direct dipolar and scalar coupling constants, respectively. This Hamiltonian allows for coherent polarization transfer between the corresponding spin components I_α and S_α (α,β,γ = x,y,z). For the ^{1}H-^{13}C spin pair, the signal $s(t_1,t_2 = 0)$ detected in the sequence of Figure II-14a as a function of the mixing time is given by

$$s_{\mathrm{CH}}(t_1,0) \sim \mathrm{Tr}\left\{S_x e^{-i\frac{\pi}{2}S_y} e^{-iH^M t_1} I_z e^{iH^M t_1} e^{i\frac{\pi}{2}S_y}\right\} \sim \frac{1}{2}\left[1 - \cos\frac{1}{3}\omega_{IS}t_1\right]. \quad (2)$$

After Fourier transform in the t_1 dimension, the doublet with a dipolar splitting of $2\omega_{IS}/3$ is resulted. The zero frequency component can be eliminated by adjusting the initial conditions. Using the z-polarization inversion step, accomplished as in the sequence of Figure II-14c, the density matrix at the beginning of the evolution period is $\sigma(0,0) = -I_z + S_z$ and the signal is given by

$$s_{\mathrm{CH}}(t_1,0) \sim \cos\frac{1}{3}\omega_{IS}t_1. \quad (3)$$

Thus, non-oscillating part is removed and the amplitude of the informative oscillating term is doubled.

For the fast rotating CH_2 methylene group with the equivalent couplings, it has been shown[28] that under WIM24 irradiation the time-dependent term of the signal is given by

$$s_{\mathrm{CH_2}}(t_1,0) \sim \frac{4}{9}\cos\frac{1}{2}\omega_{IS}t_1 \quad (4)$$

which leads to a dipolar doublet with the splitting of ω_{IS}.

In Figures II-15a and b the SIMPSON[29] numerical simulations of the frequency offset effect on the dipolar splitting in the ^{13}C-^{1}H spin pair are compared for WIM24, PISEMA and the BB-PISEMA (offset refocused PISEMA) sequences. Both for the smaller, d_{CH} = 2 kHz, and larger, 10 kHz, dipolar coupling constants the offset is best suppressed by the WIM24 sequence. In the conventional PISEMA, strong offset effect is resulted from the lowest (first) order contribution of the chemical shift term in the average Hamiltonian[21,22] and is essentially independent of the B_1 field amplitude. In WIM and BB-PISEMA

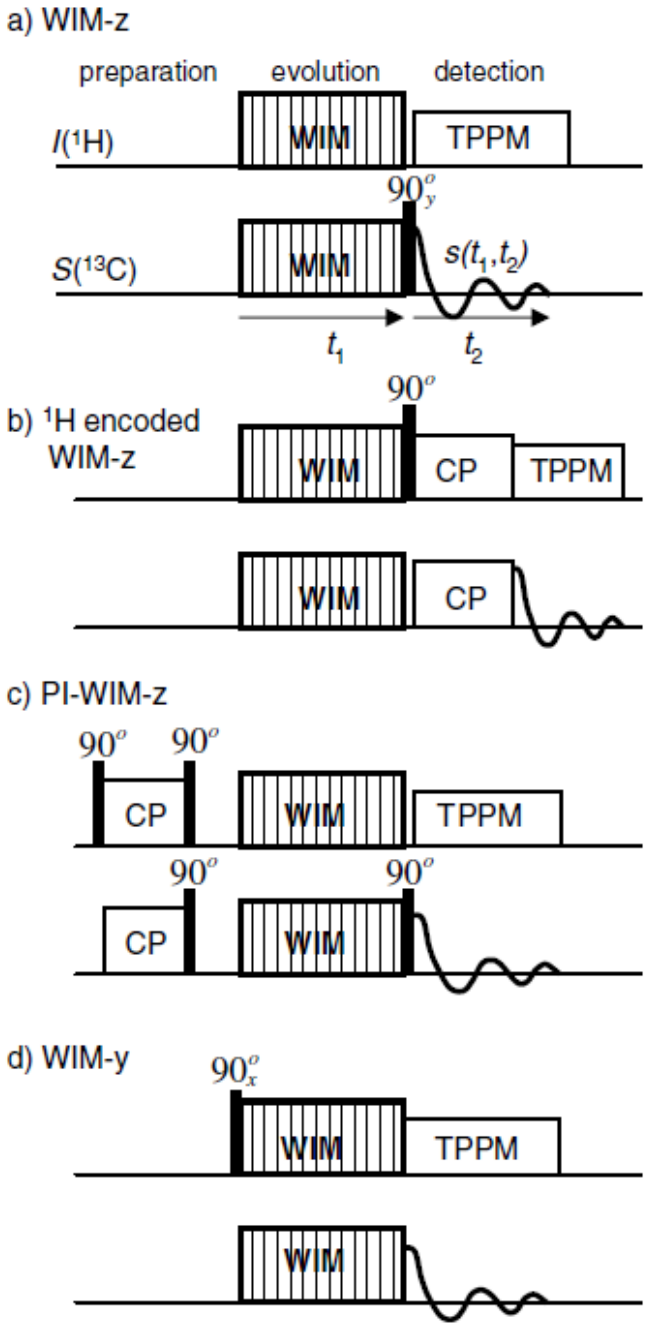

Figure II-14. **Radio-frequency pulse sequences for the spin exchange via the local field using the homonuclear decoupling windowless isotropic mixing sequences (HIMSELF).** In WIM-z experiment, the spin exchange during WIM24 irradiation (t_1 period) takes place between the z-components of the spin magnetization. The z-magnetization of either *S* or *I* spin is encoded in the detected signal, as shown in the schemes (a) and (b), respectively. In the PIWIM-z experiment (c), the polarization inversion is used to prepare the two magnetizations in opposite directions in order to enhance the sensitivity of the experiment. In the scheme (d), the experiment involving the transverse magnetizations (along y-axis) during SELF is shown.

sequences, the chemical shift contribution is the second order effect $\sim(\delta \times \tau_c)^2$, where τ_c is the RF cycle time and δ is the chemical shift, and it can be further reduced by increasing the RF field strength.

The simulated dipolar spectral shapes for fast rotating methylene group CH_2 obtained with the WIM sequence are shown in Figure II-15c. Spectra calculated without (top spectrum) and with accounting for the homonuclear proton coupling and chemical shift (bottom spectrum) exhibit essentially the same dipolar splittings.

The performance of the new technique was experimentally demonstrated on a sample of the thermotropic discotic liquid crystal hexahexyloxy-triphenylene (THE6); see the molecular structure in Figure II-16. THE6 forms a hexagonal columnar mesophase in the temperature range from 64 to 97 ^{o}C, where the molecules arranged in the columns undergo fast rotation around the molecular symmetry axis.[30] Experiments were performed on a stationary sample at the temperature of 85 ^{o}C. The mesophase sample was prepared by slow cooling from the isotropic phase in the presence of the strong magnetic field of the spectrometer. This procedure resulted in the macroscopically oriented sample with the columnar axes distributed in a plane perpendicular to the field direction.[30]

NMR experiments were carried out at a magnetic field of 9.4 T on a Chemagnetics Infinity-400 spectrometer equipped with 6 mm double-resonance magic-angle spinning probe used in a static sample mode. Length of 90^{o} radio frequency pulses during WIM irradiation was adjusted to 4.0 μs. The RF field strength was set to $\gamma B_1/2\pi \sim 50$ kHz for proton-carbon HH-CP and proton heteronuclear decoupling.

Spin exchange during a variable contact time of WIM irradiation results in a time domain spin magnetization that oscillates with a frequency determined by the heteronuclear coupling constant. In the experimental results shown in Figure II-16, left column, the carbon-13 z-magnetization was followed by employing the pulse sequence given in Figure II-14a. The time domain signals can be monitored separately for each in-equivalent site in the THE6 molecule because the ^{13}C chemical shift lines are well resolved as shown in Figure II-17. In this experiment the equilibrium carbon magnetization has been suppressed by a train of saturation pulses, therefore the initial signal intensity is essentially zero. After several milliseconds of contact time the thermal

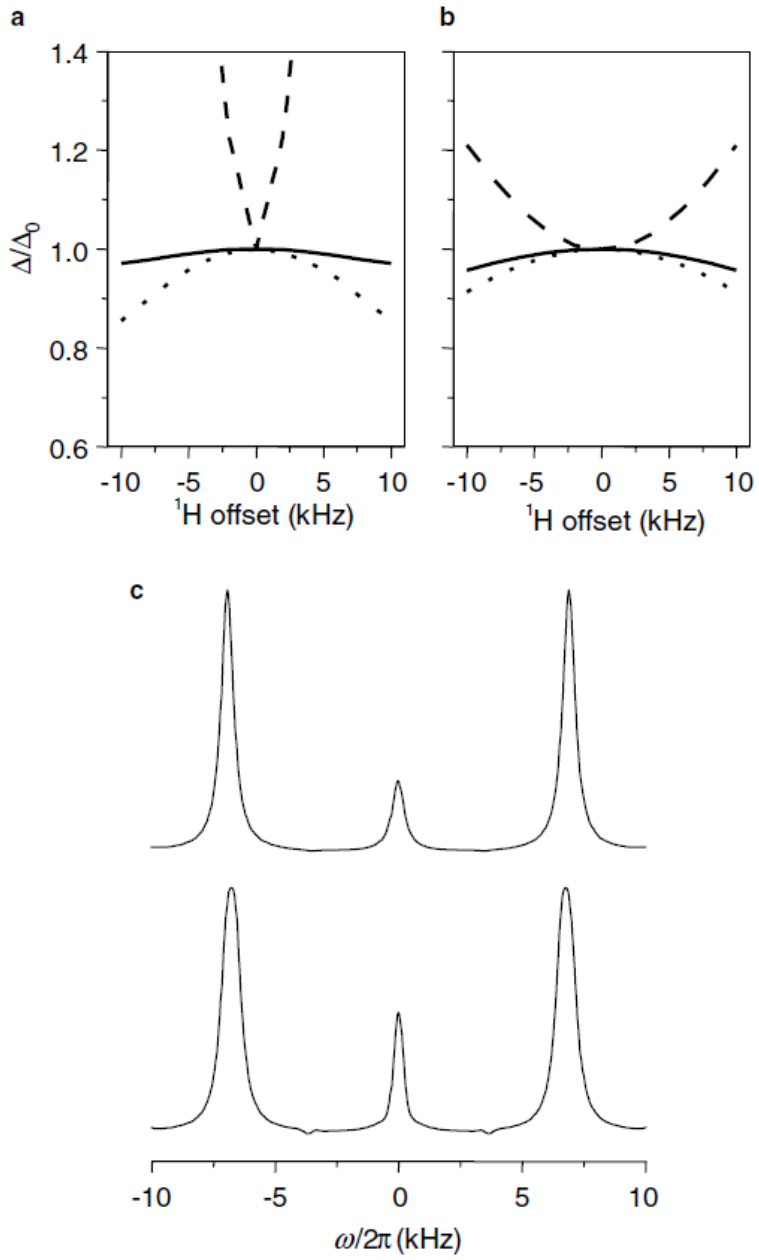

Figure II-15. **Simulated frequency offset dependences of the normalized dipolar splitting Δ/Δ_0, where Δ_0 is the splitting at zero offset, for PISEMA (dashed line), Broad-band PISEMA (dotted line), and PIWIM-z (solid lines) experiments.** (a) Coupling constant d_{CH} = 2 kHz, (b) d_{CH} = 10 kHz. RF field $\gamma B_1/2\pi$ = 62.5 kHz. In the refocused PISEMA, the 180^o pulses were inserted after every second SEMA block in (a) and after each SEMA block in (b). In (c), the simulated CH_2 WIM-z spectra are shown for $d_{CH(1)} = d_{CH(2)}$ = 7 kHz, d_{HH} and frequency offsets are zero for the spectrum on the top while d_{HH} = 10 kHz and ^{1}H offsets $d_{H(1,2)}$ = 4 kHz for the bottom spectrum.

equilibrium between *I* and *S* spin systems is reached, resulting in a constant magnetization level.

With the polarization inversion step prior to the WIM-z irradiation, as implemented in the sequence of Figure II-14c, the evolution starts from the maximum ^{13}C magnetization, the amplitude of the dipolar oscillation is effectively doubled, and the equilibrium state is close to zero. This experiment is demonstrated in the right column of Figure 16. The signals in both columns in Figure 16 for each individual carbon site are plotted on the same vertical scale, thus allowing for the comparison of the signal intensities obtained in two experiments.

Similar time domain signals were also obtained in the experiment with the transverse spin magnetizations exchange using the sequences of Figure II-14d. However, the decay times were shorter which resulted in a lower dipolar resolution in the Fourier transformed signals. Moreover, the 2D Fourier transform spectra displayed phase distortions and artifact peaks.

In contrast, highly resolved dipolar doublets with pure absorption line shapes were obtained in the experiments with the exchanging z-magnetizations. In Figure II-17, the contour plot of the 2D local field spectrum, acquired using the sequence of Figure II-14c, is shown with the cross sections along the dipolar dimension plotted to the right.

In the columnar phase of the THE6 sample, as a result of the molecular rotation around the molecular symmetry axis and the orientation of the director perpendicular to the external magnetic field, the dipolar couplings are reduced by about factor of 4 as compared to that of the rigid C-H bond aligned along the magnetic field. Therefore, the t_1 increment time corresponding to complete WIM24 RF cycle provides the spectral window sufficient to record the dipolar spectra without aliasing. The two-fold increase of the spectral window can be obtained by setting the t_1 increment to half of the WIM24 cycle. Essentially the same dipolar spectral shapes in the THE6 sample were resulted from the experiments with full and half of WIM24 cycle increment.

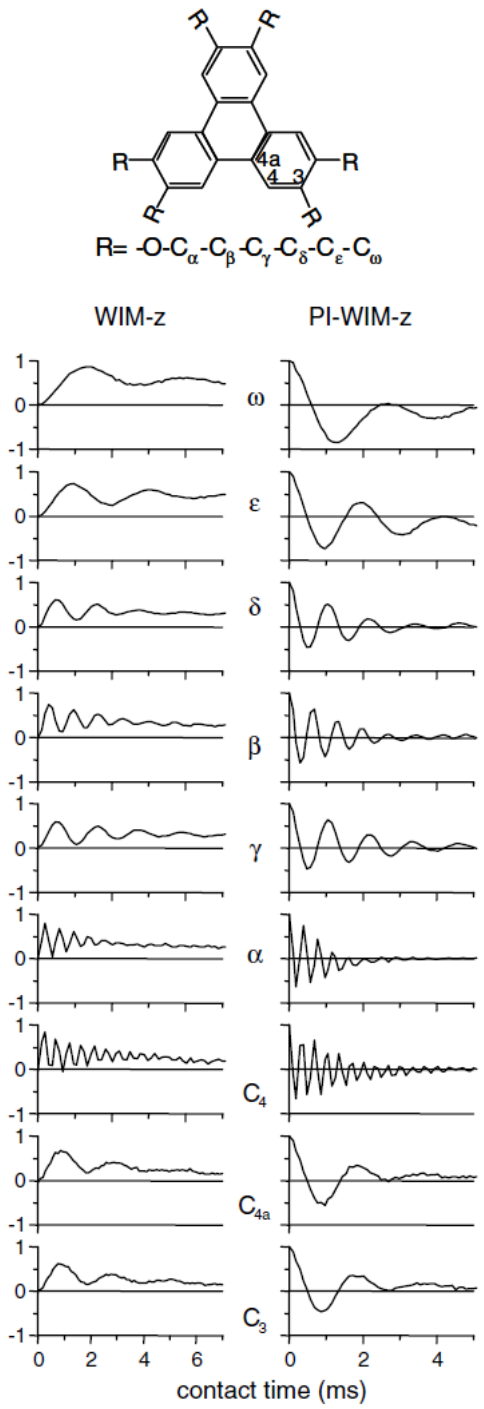

Figure II-16. **The time evolution of the carbon-13 z-magnetization as obtained with WIM-z (left column) and PIWIM-z (right column) experiments in the THE6 sample in the columnar mesophase at 85 ^{o}C.** The decays for in-equivalent carbon sites are shown. The zero-time signals in the right column were normalized to one and the corresponding signals in the left column are plotted on the same vertical scale. The molecular structure of the THE6 is shown on the top.

The experimental frequency offset dependencies of the spectral splittings are shown in Figure II-18. Clearly, in the broad offset range of ±8 kHz the effect is small in agreement with the simulation results. The deviation from the theoretically predicted symmetric dependence about zero offset is due to experimental RF pulse imperfections.

In addition to efficient suppression of the chemical shift and the frequency offset terms, WIM24 has the practical advantage of easy set up. There is no requirement for the fast frequency switching capability of the spectrometer hardware and extra delays between pulses are avoided, in contrast to PISEMA-type sequences. Scaling factor of 2/3 (~ 0.67) is comparable to that in the BB-PISEMA technique (e.g., scaling factor is 0.73 for sequence with the 180^{o} pulse after each SEMA block).

Super-cycling of the basic WIM sequence is possible to further suppress the effects of the pulse imperfections. For example, we found empirically, that the transverse ^{13}C magnetization created during WIM-z irradiation due to RF non-idealities is compensated by overall 180^{o} shifts of the ^{13}C field or both, ^{1}H and ^{13}C fields, in alternated scans.

The potential disadvantage of WIM-based SELF technique is that the truncation of weak remote dipolar interactions by the strong ones is not that efficient as in the HH-CP type methods. However, this effect was not observed in our experiments on liquid crystal with motionally reduced dipolar spin couplings. Also, in preliminary experiment performed on a single crystal sample of *n*-acetyl-L-^{15}N-valyl-L-^{15}N-leucine the resolution of the ^{15}N–^{1}H dipolar couplings was very similar to that in PISEMA experiment.

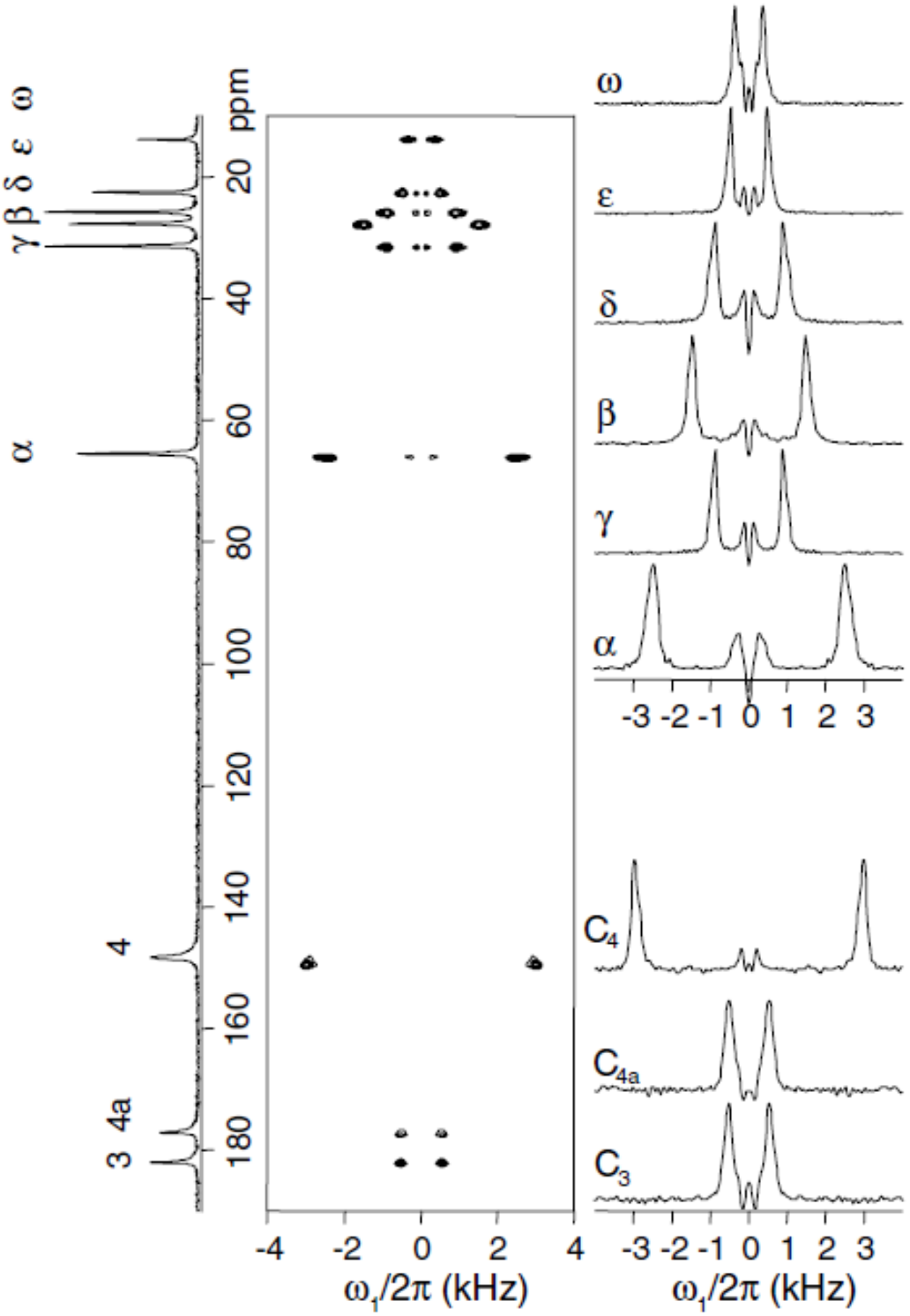

Figure II-17. **Contour plot of the 2D separated local field spectrum, acquired in the THE6 sample in the columnar mesophase at 85°C using the PIWIM- z sequence** of Figure II-14c. Cross sections along the dipolar dimension are shown to the right and the chemical shift spectrum is on the left.

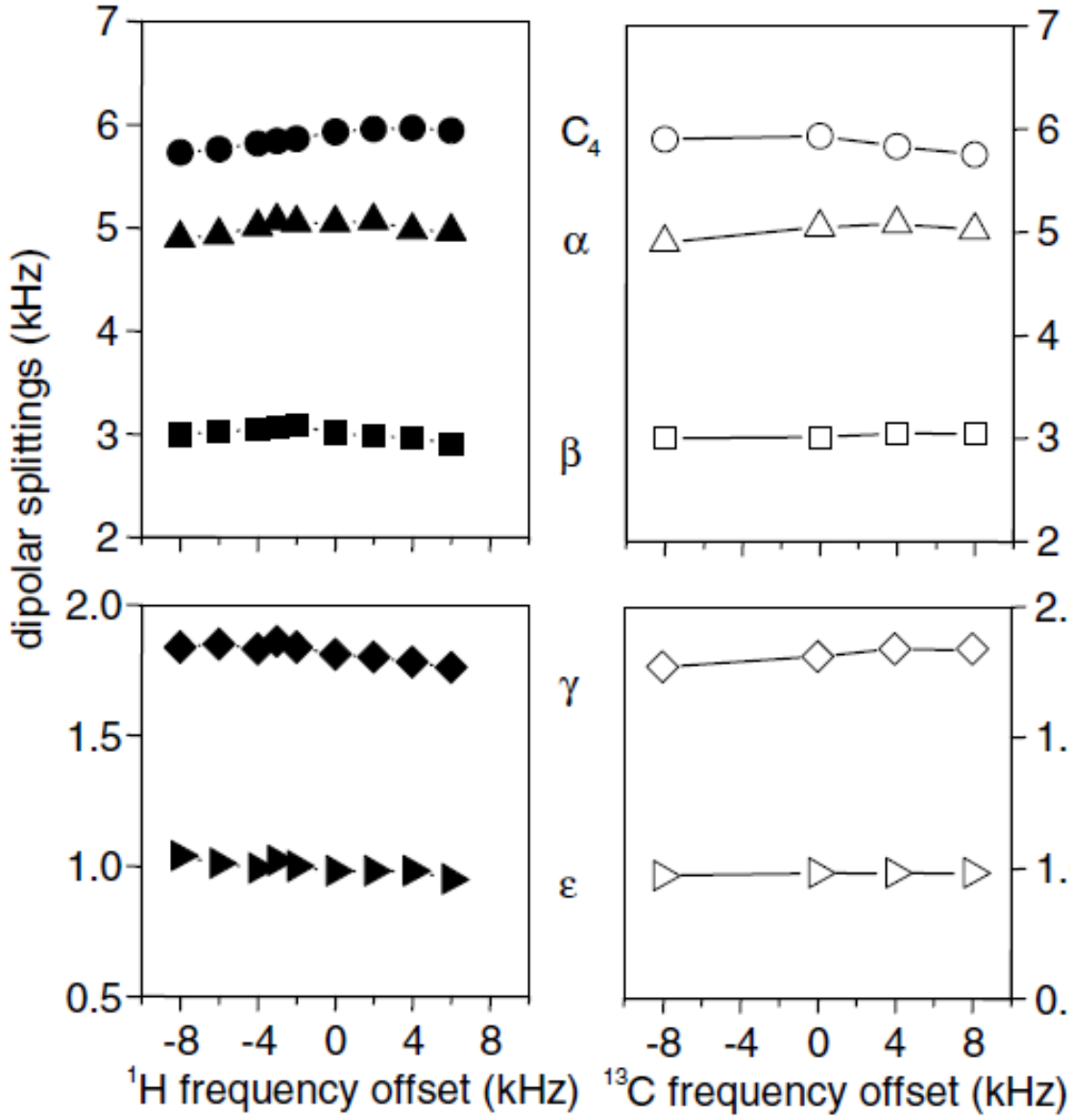

Figure II-18. **Experimental ^{13}C and ^{1}H frequency offset dependences of the ^{13}C–^{1}H dipolar splittings in the THE6 sample obtained in PIWIM-z experiments.**

II-3. Sensitivity and Resolution Enhancement in Solid-state Spectroscopy of Bicelles

The molecular aggregates formed by phospholipids in aqueous solution, which usually exist as bilayers in the form of vesicles, gels, or lamellae, are often used as models for cell membranes. Although the disordered multilamellar vesicles have extensively been used in NMR studies, the

macroscopically oriented phases have the advantage of preserving anisotropic spin interactions that offer a wealth of information about the molecular geometry and dynamics.[1] Therefore, considerable efforts have been devoted to develop magnetically oriented phospholipid bilayers.[2-9] While several studies have reported on the preparation, characterization, and applications of bicelles,[4-6,8] a systematic optimization of solid-state NMR experiments on bicelles is lacking.

Since molecules embedded in bicelles are dynamic, the molecular motion could degrade the efficiency of solid-state NMR pulse sequences. For example, it is difficult to establish an experimental condition that efficiently transfers magnetization from protons to carbons (or other low sensitive nuclei) at all sites of a molecule, and also for all molecules, in a bicelle sample. A short contact time crosspolarization (CP)[10] sequence is more efficient for rigid parts of a molecule than for mobile regions, as heteronuclear dipolar couplings in the latter case are averaged by the motion.[11,12] On the other hand, a long contact time or the NOE (nuclear Overhauser effect)-type magnetization transfer may be better for mobile sites of a molecule.[13] In this section, we have compared the efficiencies of different methods to enhance the sensitivity of ^{13}C signal from bicelles.

The use of high RF (radio frequency) decoupling field strengths is necessary to achieve line-narrowing in most solid-state NMR applications.[14, 15] Proton decoupling in the form of multiple pulse sequences is commonly used to record signals of less sensitive nuclei (such as ^{13}C and ^{15}N). An actual RF power required to accomplish an efficient proton decoupling depends on the design of a decoupling pulse sequence. The use of high RF field strengths, which becomes important for experiments at high magnetic fields, however, generates sample heating because of the RF power dissipation within the sample. A majority of biological samples are very susceptible to RF-induced heating,

because of the interaction of fast oscillating fields with ions in salty samples and/or the electric dipolar moment of the molecules in dielectrics.[16-19] These effects are a major concern in the application of multidimensional SLF (Separated-Local-Field)[20,21] experiments to static samples such as bicelles. Since most physicochemical properties of biological molecules depend on the sample temperature, an adequate temperature control during NMR experiments is, therefore, important. The RF heating effects are not typically measurable from the readings of a variable-temperature control unit of an NMR spectrometer, and therefore they must be properly calibrated and corrected prior to an experiment. In this section, we propose a simple method to measure the sample temperature during solid-state NMR experiments on bicelles. The efficiency of various proton-decoupling sequences and the requirement of the RF field strength are also analyzed in this study.

II-3-1. Experimental Procedure

Materials.

1,2-Dimyristoyl-sn-glycero-3-phosphatidylcholine (DMPC) and 1,2-dihexanoyl-sn-glycero-3-phosphatidylcholine (DHPC) were purchased from Avanti Polar Lipids, Inc. (Alabaster, AL). DMPC and DHPC with a molar ratio (q = DMPC:DHPC) of 3.5:1 was dissolved in chloroform. The solvent was slowly evaporated under a stream of nitrogen gas at room temperature and completely removed by overnight lyophilization. A 100 mM Hepes buffer at pH 7.0 was added to obtain a concentration of 37.5% (w/w) phospholipids to solution. Peptide was cosolubilized in chloroform along with the lipids at the desired molar ratios, while an appropriate amount of $YbCl_3$ salt was added to the HEPES buffer to yield 'flipped' bicelles.[66,67] The sample was vortexed until all of the lipids were solubilized in the HEPES buffer. The solubilized sample was gently sonicated in an ice-cold water bath. The final sample was obtained by several freeze and thaw cycles until a clear transparent solution was formed.

NMR measurements.

All NMR experiments were carried out on a Chemagnetics/Varian Infinity-400 MHz solid-state NMR spectrometer using a 5 mm custom-modified doubleresonance magic-angle spinning probe under static sample conditions. About 100 mg of sample was

loaded in a 5 mm NMR glass tube of 4 cm length and was closed tightly with a Teflon tape and a cap. The sample was equilibrated prior to the measurement for about 1 h in the magnet at 37 ^{o}C. All experiments were performed at 37 ^{o}C. Phosporus-31 chemical shift spectra were recorded to test the magnetic alignment of bicelles. A ramped-CP[44] sequence with a contact time of 5 ms was used to record the 1D ^{13}C chemical shift spectra under proton decoupling using various decoupling sequences for a comparative study. A 5 μs ^{1}H 90^{o} pulse, a recycling delay of 7 s, a 25 kHz spectral width, and an acquisition time of 41 ms were used. Data were processed without any line broadening. For the NOE enhancement, protons were irradiated using a 1 kHz RF field during the recycling delay.

To record signals of ^{14}N NMR spectra the quadrupole echo sequence[68] was used with the pulse length of 4.4 μs and an echo-delay of 1 ms. With this long delay the interference effect of the probe acoustic ringing, which is severe at the ^{14}N resonance frequency of 29 MHz, was negligible. No influence of the proton decoupling on the ^{14}N spectral shape was observed. Hence, spectra presented here were acquired without the proton decoupling. Up to 4000 scans were accumulated with a repetition delay of 0.2 s.

II-3-2. Sample Heating due to RF Irradiation

To assess the sample heating induced by the high frequency ^{1}H decoupling ($\geq$ 100 MHz), we used the high sensitivity of the water proton chemical shift to the sample temperature.[22,23] Figure II-19(a) shows the temperature dependence of the water proton chemical shift. The slope is 0.010 ± 0.001 ppm/^{o}C (or 4.0 ± 0.4 Hz/^{o}C at a magnetic field of 9.4 T), which is similar to the value reported for the pure water.[22] The experimental setup used in this study resulted in a line width of 23 Hz, thus providing an accuracy of about 0.6 ^{o}C in the sample temperature measurement. To measure the RF-induced sample heating, an RF irradiation emulating the heteronuclear decoupling sequence was applied at the proton resonance frequency and, after a short magnetization recovery period, the proton FID signal was recorded following a $\pi/2$ pulse. A 40 ms RF irradiation time corresponding to the ^{1}H decoupling time in ^{13}C experiments was used. A delay of 200 ms after the decoupling pulse required for the magnetization recovery was chosen sufficiently short to avoid significant heat dissipation in the sample before acquiring the

spectrum. For each measurement, 16 transients with a delay of 5 s were accumulated preceded by 16 dummy scans to ensure a steady state sample temperature. The heating effect in the bicelle sample versus the RF field strength is presented in Figure II-19(b). In agreement with theory,[24,25] a second power dependence of the heating effect on the RF power was observed. The temperature gradient in the sample volume induced by the RF irradiation was estimated from the increase in the linewidth of the $^{1}H_2O$ peak. The results are also included in Figure II-19(b). In principle, the average temperature shift can be corrected by adjusting the setting on the temperature control unit. On the other hand, the temperature gradient within the sample and the heating during the decoupling pulse cannot be dealt with in that way.

In the ^{13}C experiments presented below, a 20 kHz proton- decoupling field was typically used. This resulted in an increase of the average sample temperature by about 2 ^{o}C. A comparable effect is also expected due to the RF irradiation of protons during the indirect period (t_1) of a 2D experiment. For example, the popular PISEMA (polarization inversion spin exchange at the magic angle) experiment[13,26-28] and other rotating-frame SLF experiments[29-35] for the measurement of the heteronuclear dipolar coupling utilize a high RF power in the t_1 period. On the other hand, the effect of the RF irradiation on the ^{13}C channel (for example, as applied in a cross-polarization sequence, and also during the evolution period of rotating-frame experiments) was found to be negligible. This stems from less power losses at a lower RF frequency[24]. Generally, experiments at a higher magnetic field lead to more significant sample heating due to a higher resonance frequency[24] and also due to wider signal dispersion by the chemical shift which requires a stronger RF field for effective decoupling of protons. The amount of heating may also depend on the sample size and geometry,[36,37] sample composition,[17,19,38] RF coil design,[37,39,40] and the flow-rate of the heating/cooling gas.[24] Therefore, the calibration of the RF heating effect on each sample is required for an experimental set-up. Finally, we note that the recent developments in the probe and coil design minimizing the electric field inside the sample provide a significant reduction of sample heating.[40]

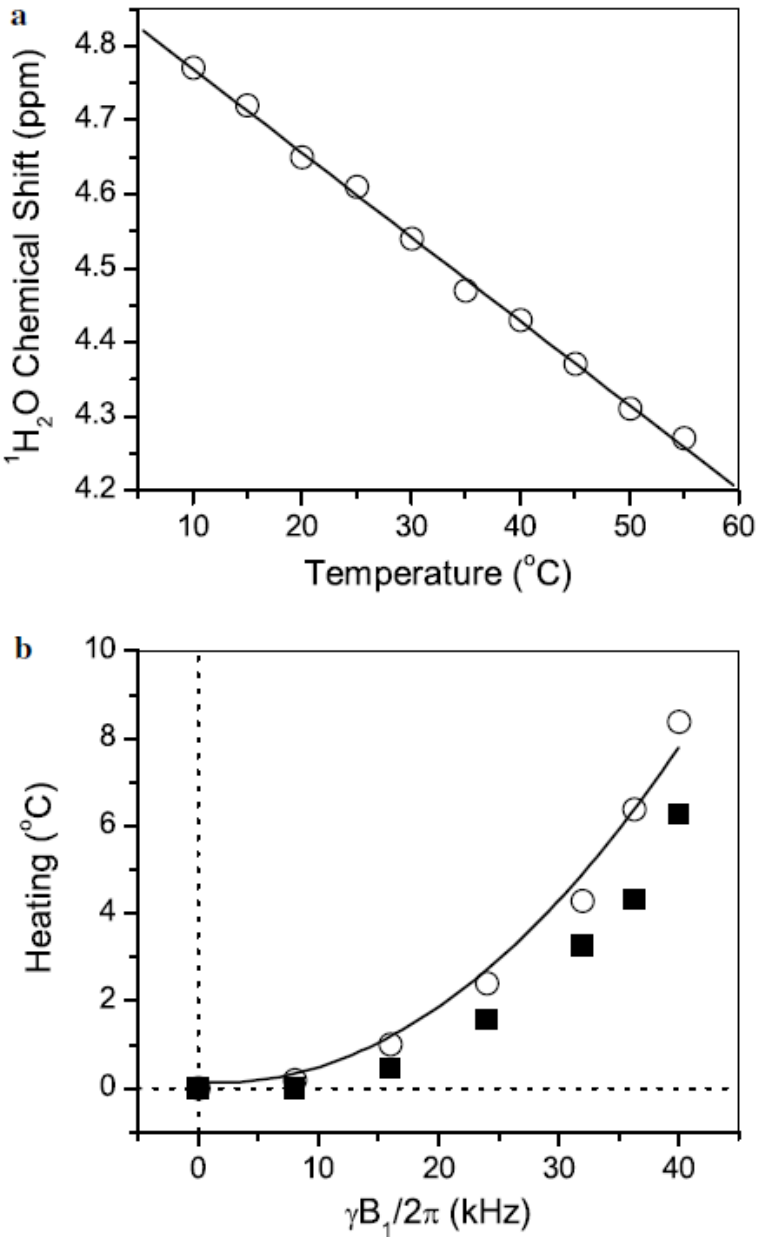

Figure II-19. **The heating evaluation due to R.F. induced heating.** (a) Variation of the chemical shift of water protons in a bicelle sample with the temperature. The proton chemical shift of water was set at 4.6 ppm at 25 ^{o}C. (b) Open symbols represent the heating effect versus the R.F. field strength. The line is the fit to a second power dependence. Solid symbols represent the temperature gradient in the sample volume induced by the R.F. irradiation.

II-3-3. Signal Enhancement

In NMR spectroscopy of low-gamma nuclei in liquids, the common approaches for sensitivity enhancement are *J*-coupling mediated polarization transfer using the INEPT (insensitive nuclei enhanced by polarization transfer) sequence[41] and heteronuclear cross-relaxation under the condition of saturating ^{1}H RF field using NOE.[42] In solids, on the other hand, CP in the rotating frame[10] is the most popular technique, which is also frequently used in anisotropic biological samples. However, the motional averaging in bicelles reduces C-H dipolar couplings, as compared to rigid solids, and results in an increased sensitivity to the Hartmann–Hahn mismatch[43] of RF fields during CP. Hence, a ramp-CP sequence[44] is advantageous to overcome the Hartmann–Hahn mismatch.[10,43] On the other hand, high molecular mobility may favor the NOE approach,[45] which becomes efficient when the correlation time of the motion is small compared to the inverse of resonance frequency. The INEPT transfer is not practical in static anisotropic samples, since the J_{CH} couplings are unresolved in the presence of strong residual heteronuclear dipolar interactions. (INEPT, however, has been employed in lipid bilayer samples under the MAS condition, when dipolar couplings are suppressed by the sample spinning.[45])

In Figure II-20, ^{13}C chemical shift spectra obtained by single pulse excitation (SPE), conventional CP,[10] ramp-CP,[44] and NOE[45] techniques are compared. Overall, the ramp-CP[44] provides the largest enhancement factor (of about three with respect to SPE) in our sample for most of the sites. The optimal contact time in CP strongly differs for various sites in the molecule resulting in a non-uniform enhancement. NOE is superior only for the most mobile groups, the c and C_{14} sites of a lipid molecule.

II-3-4. Heteronuclear Decoupling

Since RF heating is a problem for NMR studies on bicelles, it is important to effectively utilize the RF power of pulse sequences. A long data acquisition under proton decoupling, needed to obtain a high-resolution ^{13}C chemical shift spectrum of bicelles, is an obvious heat-generating part of an experiment and therefore needs to be optimized. It is known that the RF power needed to achieve efficient heteronuclear spin decoupling depends on the design of a decoupling sequence.[46] A careful choice of the decoupling

scheme is, therefore, important to obtain highly resolved ^{13}C spectra at a limited RF power level. We examined the performances of decoupling sequences that are frequently used in studies on biological samples and liquid crystals. In particular, we investigated the efficiencies of TPPM (two pulse phase-modulation),[47] SPINAL-64 (small phase incremental alternation),[48] WALTZ-16 (wideband alternating phase low-power technique for zero residue splitting)[49] and FLOPSY-8 (flip-flop spectroscopy)[50] schemes, and compared them to a conventional continuous wave (CW) decoupling. The ^{13}C chemical shift spectra acquired using different decoupling schemes are presented in Figure II-21. The ^{1}H RF field strength was 20 kHz and the decoupler frequency was set to obtain the best resolution in the most crowded ^{13}C spectral region, 30– 36 ppm, by applying a CW irradiation. For the acyl chain ^{13}C signals, the performances of TPPM, SPINAL-64, and FLOPSY-8 decoupling sequences are comparable and significantly better than CW and WALTZ sequences. Excellent resolution was achieved using the FLOPSY-8 pulse sequence scheme, which was originally designed for the broadband homonuclear cross-polarization in liquids,[50] but was also used for heteronuclear decoupling in lyotropic liquid crystalline systems.[51] Compared to the SPINAL-64 decoupling, use of the FLOPSY-8 sequence improved the spectral resolution for the head group and glycerol carbons; in particular for g2, g3, and b sites (Figure II-21). In addition the FLOPSY sequence is relatively easy to set up since it requires only adjusting the single parameter, the 180^{o} pulse length, and is very tolerant to the miscalibration of the pulse length.

Figure II-22 compares the ^{13}C chemical shift spectra of a bicellar sample obtained at different RF power levels using the FLOPSY-8 decoupling. Notably, an RF field strength as low as 16 kHz is sufficient to achieve adequate resolution comparable to that obtained using other sequences at much higher fields. It is interesting to note that very strong decoupling fields, up to 80 kHz, were commonly employed in similar systems.[45] It should be pointed out that a previous study on magnetically aligned bicelles containing a peptide suggested that a SPINAL-16[48] decoupling sequence provided a better decoupling performance than other decoupling sequences analyzed,[52] however, the performance of the FLOPSY sequence was not examined in that study. Our results suggest that broadband sequences like FLOPSY can provide significant advantage in bicellar systems.

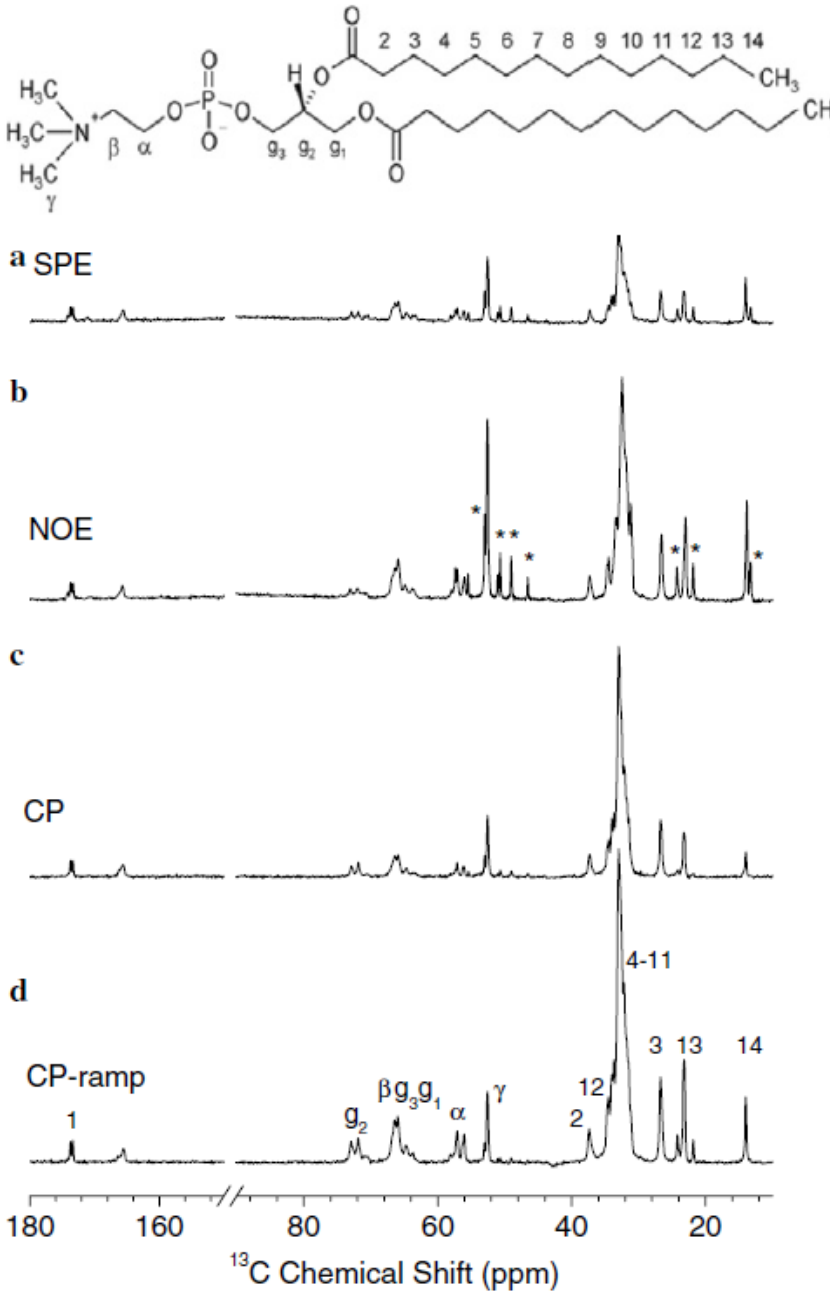

Figure II-20. **Comparison of the ^{13}C spectra of DMPC/DHPC bicelles at 37°C measured with different sensitivity enhancement techniques**: (a) 90° single pulse excitation (SPE), (b) NOE, (c) constant amplitude CP, and (d) ramped amplitude CP. Signals from DHPC detergent, observed most clearly in NOE and SPE spectra, are indicated by asterisks. The molecular structure of DMPC is shown at the top.

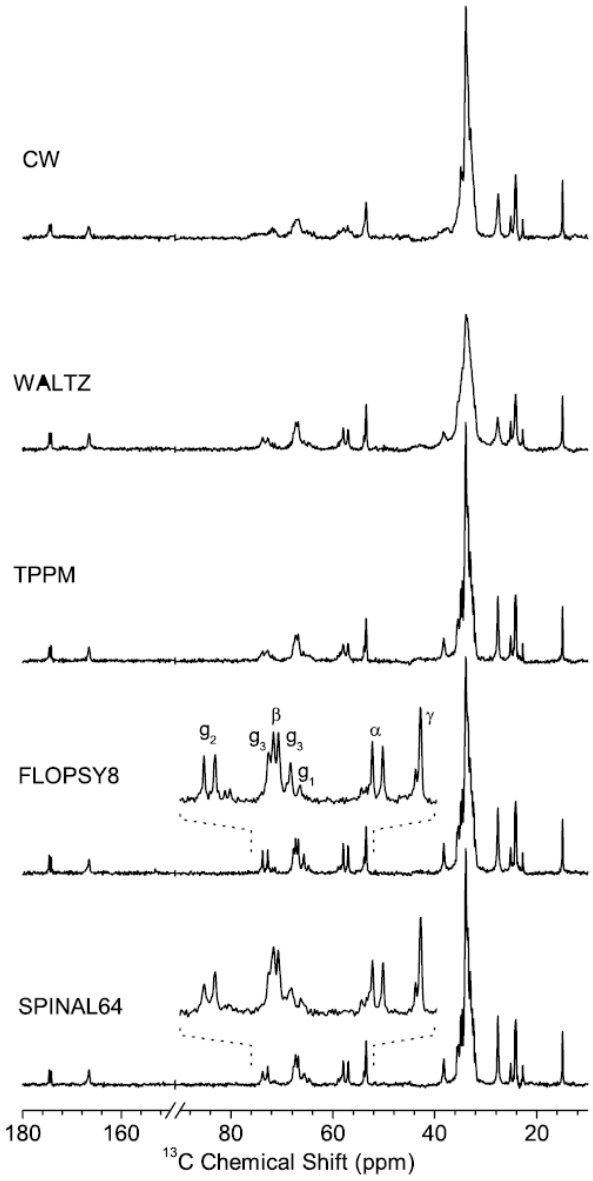

Figure II-21. **^{13}C spectra of DMPC/DHPC bicelles at 37^{o}C measured with different heteronuclear decoupling sequences.** The proton decoupler RF field strength was set at 20 kHz. The RF decoupler frequency was set to a value that resulted in an optimal resolution for the crowded chain-carbon region when CW irradiation was used. The pulse durations were optimized for WALTZ-16 and FLOPSY-8 sequences, while both pulse durations and RF phase shifts were optimized for TPPM and SPINAL-64 schemes. The spectral region containing signals from the lipid head group and glycerol sites is expanded for an easy comparison of spectra obtained using the FLOPSY and SPINAL decoupling sequences.

II-3-5. Nitrogen-14 NMR Spectra of Bicelles.

The electric field gradient around the ^{14}N nucleus, and hence the quadrupole coupling, is considerably reduced due to the near-tetrahedral symmetry of the choline groups of DMPC and DHPC molecules.[53-57] The dynamics of the lipid head group further reduces the quadrupole coupling to about 20 kHz. Therefore, the detection of ^{14}N in bicelles requires neither extremely short pulses nor a wide spectral window.

Nitrogen-14 spectra of aligned bicelles are given in Figure II-23. Two sets of narrow doublet peaks are observed in the spectra. The doublet with a larger quadrupole splitting arises from DMPC as it is similar to the spectra obtained from mechanically aligned DMPC or POPC bilayers,[54] while the doublet with a smaller splitting corresponds to the DHPC molecule. Flipped bicelles[58] are characterized by the orientation of the bilayer normal along the external magnetic field. As demonstrated in Figure II-23b, in a flipped bicelle sample the quadrupolar splittings are nearly doubled compared to that of unflipped bicelles in correspondence with the direction of the alignment.

As seen from spectra of bicelles containing ligands, ^{14}N is very sensitive to the ligand–lipid interactions that alter the electric field gradient surrounding the ^{14}N nucleus. For example, the presence of an amphipathic, a-helical antimicrobial peptide, MSI-78,[59] significantly reduces the quadrupole splitting of DMPC (Figure II-23d and e). Since MSI-78 is cationic with a net charge of +9 and interacts with the lipid headgroups, it could interfere with the cross-linking of lipids. This would enhance the symmetry of the positively charged choline group and therefore reduce the quadrupole splitting. Similar effects have been utilized in probing the interaction of antidepressants with membranes in mechanically aligned bilayers. A sample spectrum of bicelles containing an antidepressant, desipramine, is given in Figure II-23c, which shows the expected reduction in the ^{14}N quadrupole splitting.[54] Interestingly, the presence of an anionic lipid, DMPG, slightly increases the quadrupole coupling of DMPC as well as DHPC while the line width depends on the concentration of salt in the sample (Figure II-23f and g). While more experimental analyses are needed to understand the observed changes in the ^{14}N quadrupole coupling, these results suggest that ^{14}N NMR spectroscopy of magnetically aligned bicelles can be used as a 'voltmeter' to measure the interaction of ligands with membranes. It should be mentioned here that the measurement of the ^{14}N

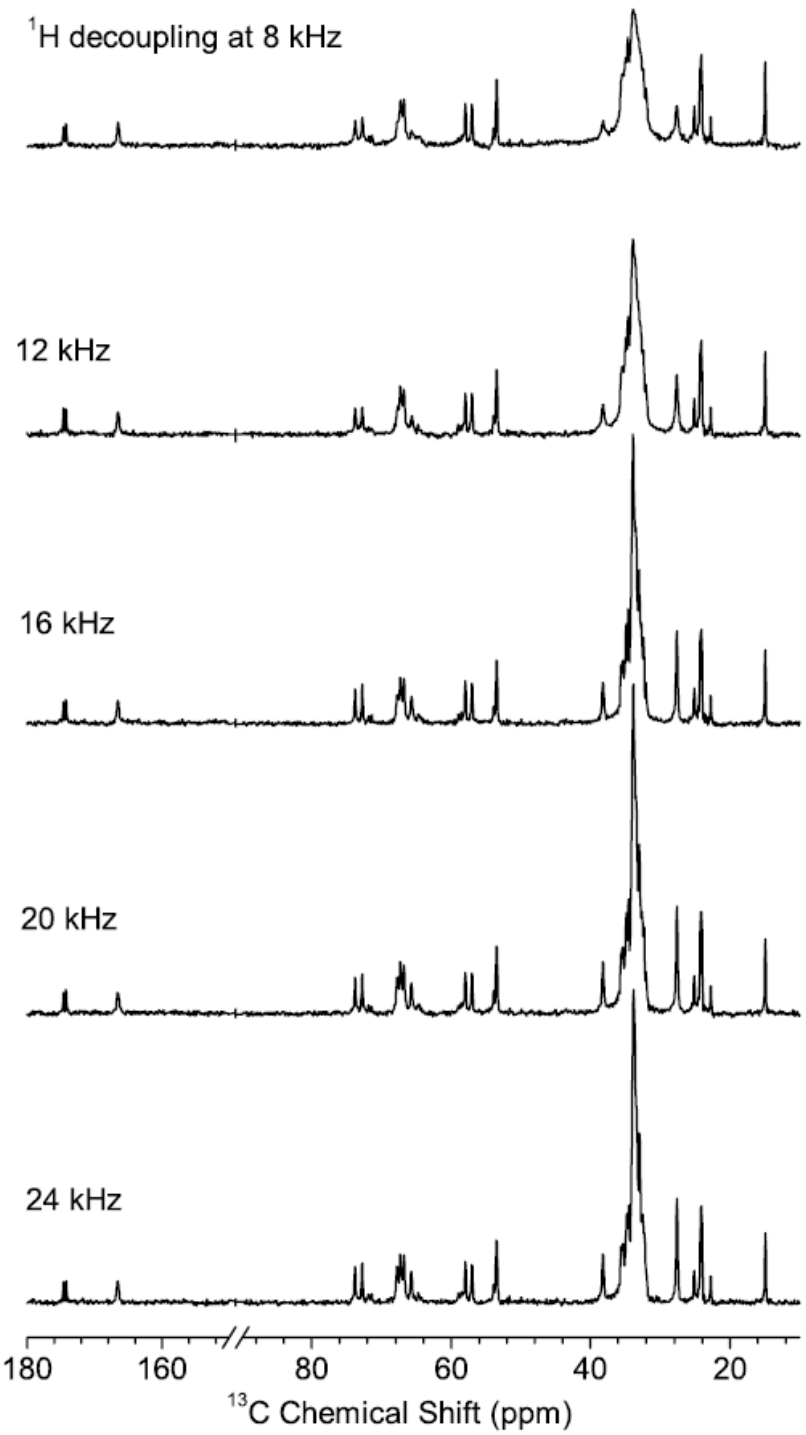

Figure II-22. **^{13}C spectra of DMPC/DHPC bicelles at 37^{o}C obtained using the FLOPSY-8 proton-decoupling sequence at different decoupling power levels.**

quadrupole coupling of the choline group was recently utilized to understand the membrane-interaction of charged molecules such as antimicrobial peptides in mechanically aligned bilayers and also in multilamellar vesicles under static and MAS conditions.[60-62]

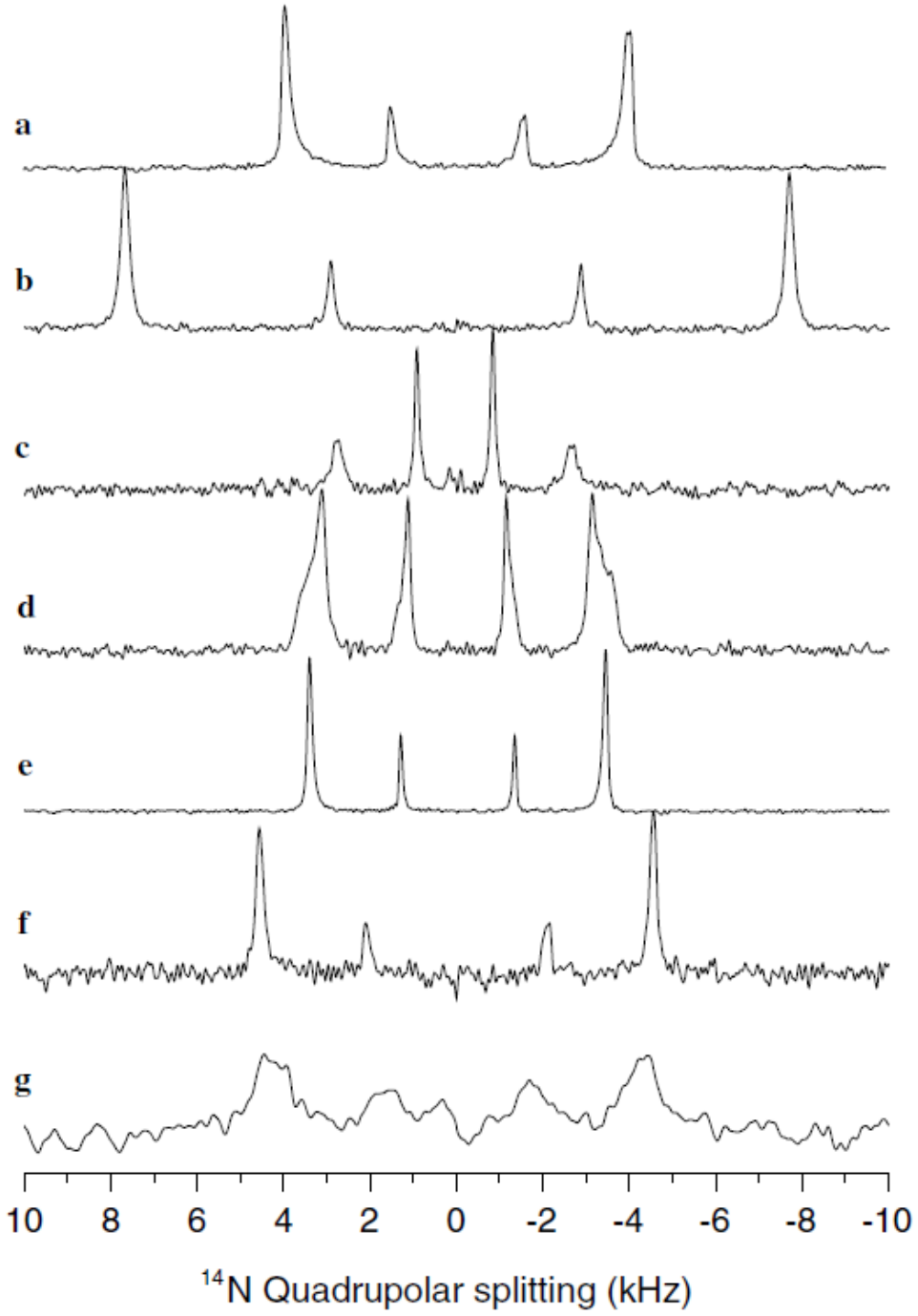

Figure II-23. **^{14}N quadrupole coupling spectra of magnetically aligned DMPC:DHPC bicelles, *q* = 3.5, showing the influence of admixing different substances**: (a) Pure DMPC:DHPC bicelles; (b) in the presence of Yb^{3+} ions, resulting in 'flipped' bicelles; (c) 2.0 mol% desipramine; (d) 2.0 mol% MSI-78; (e) 0.5 mol% MSI-78; (f) 20.0 mol% negatively charged lipid DMPG in the presence and (g) absence of 150 mM NaCl.

II-4. Use of a Copper-Chelated Lipid Speeds Up NMR Measurements from Membrane Proteins

II-4-1. Use of Copper-Chelated Lipids on Solid-state NMR Spectroscopy

Atomic-level structure and dynamics are essential for understanding the function of membrane proteins and their roles in biological processes and for the development of compounds to treat related diseases. While these are challenging tasks for most techniques, recent studies have demonstrated that solid-state NMR spectroscopy is promising, as it neither requires a single crystal nor imposes a restriction on the molecular size to be investigated. Membrane proteins reconstituted in lipid bilayers are commonly used in solid-state NMR studies.[1] The key difficulties that limit the high-throughput application of solid-state NMR spectroscopy are (1) the requirement of a large amount of sample and/or a long data collection time to enhance the signal-to-noise ratio (S/N), (2) radio frequency (RF)-induced sample heating (due mainly to the long measurement time) that may denature expensive membrane proteins labeled with isotopes, (3) the need for stable NMR probes and electronics, and (4) the demand for the continuous availability of a spectrometer. Therefore, the development of new approaches to speed up solid-state NMR measurements is essential. Previous studies successfully utilized copper salts and Cu-EDTA in crystalline samples at lower temperature[2] and Gd-DTPA in glycosphingolipid bilayer samples.[3] However, the presence of excess water and molecular mobilities in fluid lamellar-phase membranes complicates the direct utilization of paramagnetic ions. In this study, we overcome this limitation by using a copper-chelated lipid to significantly enhance the sensitivity of an NMR experiment on lipid bilayers under either aligned static or unaligned magic-angle spinning (MAS) conditions.

II-4-2. Experimental Procedure

Protein Expression Protocol.

In this study, we used an antimicrobial peptide subtilosin A embedded in bicelles as a test sample to demonstrate the efficiency of paramagnetic-doping to speed up solid-state NMR measurements. Subtilosin A is a 35-residues (a molecular weight of 3398.9 Da)

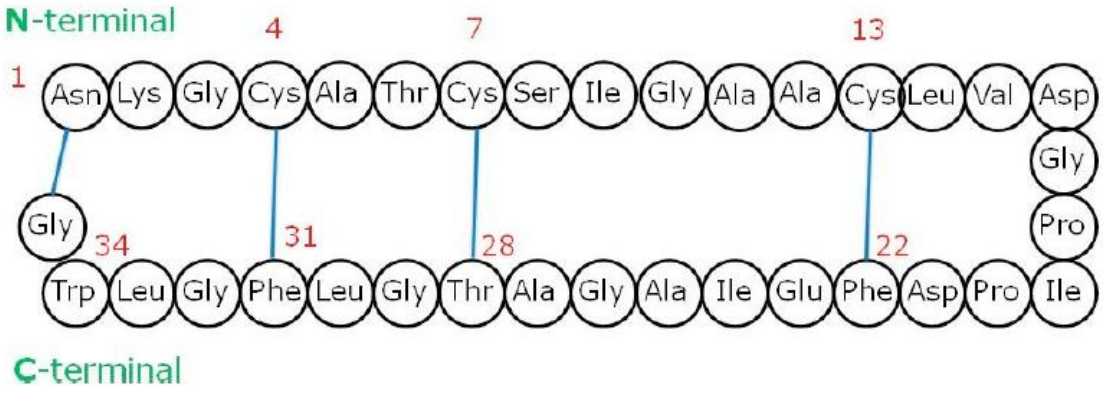

Figure II-24. **An amino acid sequence of a cyclic antimicrobial peptide, subtilosin A.**

cyclic antimicrobial peptide produced by Bacillus subtilis bacteria. As shown in Figure II-24, this cyclic peptide has 3 unusual chemical bonds (three cross-links between sulphurs of cysteine and the a-positions of amino acids are linked by a chemical bond between residues (bonds in blue color): Cys-4 and Phe-31, Cys-7 and Thr-28, and Cys-13 and Phe-22) that render rigidity to the structure of the peptide. Our previous solid-state NMR studies have reported the mechanism of action of subtilosin A.[4]

For this study, 12 to 14 % ^{15}N isotope labeled Subtilosin A was produced from fermentations of *Bacillus subtilis*, isolated and purified as reported elsewhere.[4] A filtersterilized 10 mL of 0.15 M [^{15}N] NH_4NO_3 in 10 mL water and 0.5 mL of 1 M $CaCl_2 \cdot H_2O$ were used instead of 0.5 mL of 1 M $Ca(NO_3)_2 \cdot 4H_2O$ in the original procedure. MALDI TOF mass spectroscopy was applied to analyze the percentage of ^{15}N incorporation in subtilosin A as described previously.[4] Labeled [^{15}N] NH_4NO_3 was purchased from Cambridge Isotope Laboratories (Andover, MA).

Preparation of Bicelles for Solid-state NMR Experiments.

In this study, to demonstrate the efficiency of paramagnetic effects in reducing the spin-lattice relaxation (T_1) of protons, we used magnetically-aligned bicelles as a model membrane. As mentioned in the main text of the manuscript, the use of copper-EDTA resulted in sample heating that interfered with the alignment of bicells as observed from the broadening of ^{31}P spectral lines. Therefore, we decided to develop alternate approaches to optimize the sample preparation conditions that suit for solid-state NMR measurements. We found that the use of a copper-chelated phospholipid (DMPE-DTPA : 1,2-ditetradecanoyl-*sn*-glycero-3- phosphoethanolamine-N-diethylenetriaminepentaacetic acid) in magnetically-aligned bicelles (Figures II-25 and II-26) offer several advantages: (a) since copper is chelated to a lipid (Figure II-25) that mixes well with other components of bicelles without altering the properties of bicelles, about 10 times lower concentration of copper was sufficient for our studies; (b) devoid of free copper ions in the sample considerably reduced sample heating and enabled fast data collection from aligned bicelles. Bicelles composed of a phospholipid (DMPC : 1,2- dimyristoyl-*sn*-glycero-3-phosphocholine) and a detergent (DHPC : 1,2-diheptanoyl-*sn*glycero- 3-phosphocholine) with and without a chelated lipid were prepared as outlined below.

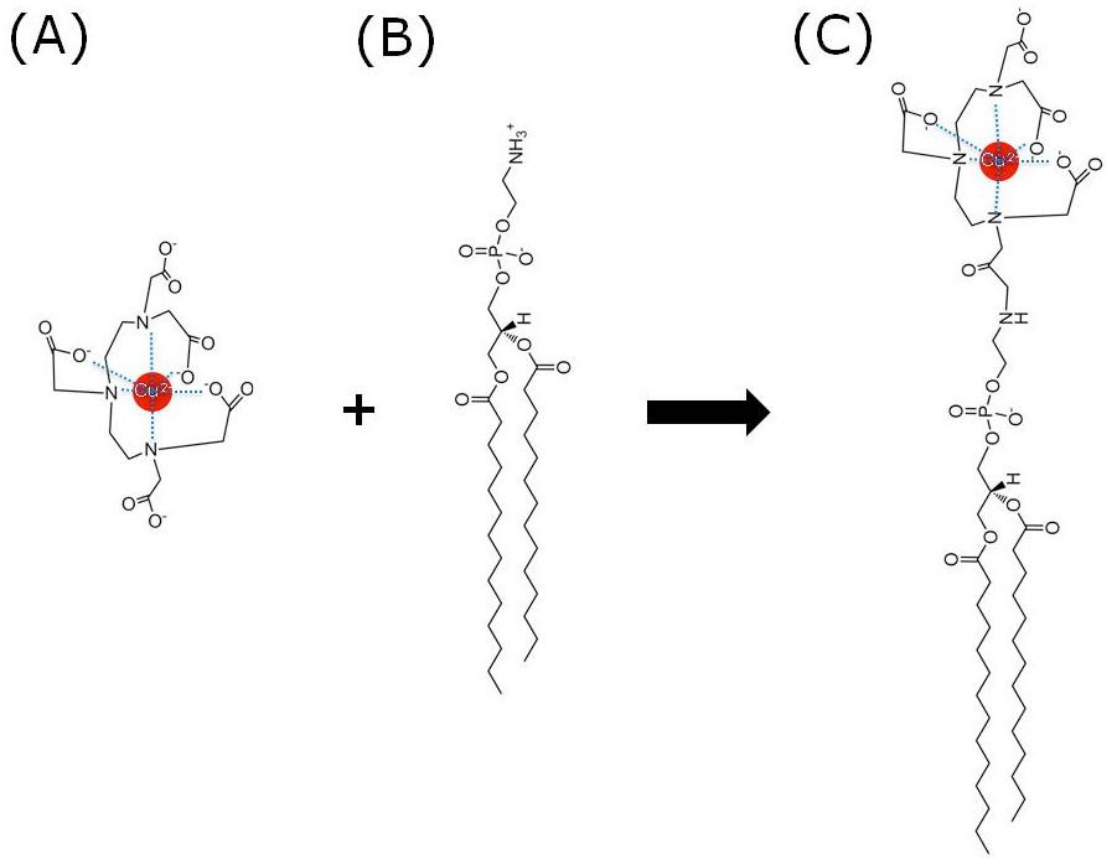

Figure II-25. **The structure of a copper-chelated lipid** (A) The structure of DTPA that is commonly used as chelating metal ions. (B) The structure of DMPE (1,2-ditetradecanoyl-*sn*-glycero-3-phosphoethanolamine) lipid. (C) The structure of DMPE-DTPA, which is the combination of DMPE and DTPA.

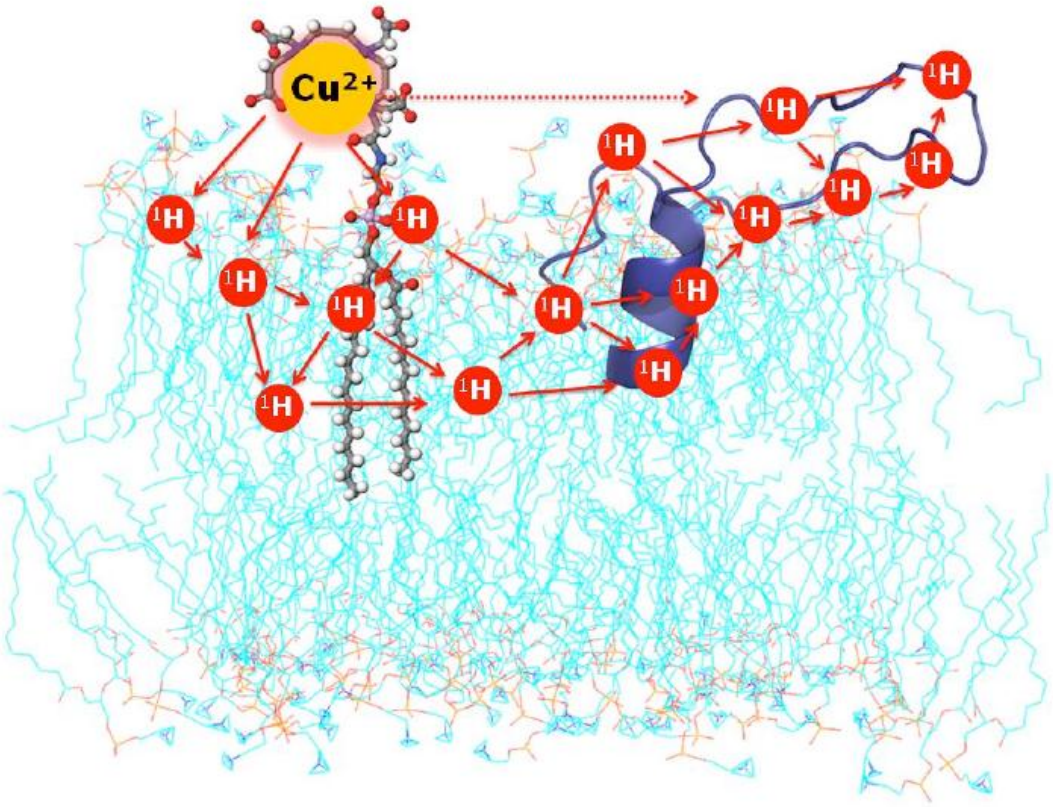

Figure II-26. **A model depicting lipid bilayers with copper-chelated DMPE-DTPA and a cyclic antimicrobial peptide Subtilosin A.**

DMPC, DHPC and DMPE-DTPA were purchased from Avanti Polar Lipids, Inc. (Alabaster, AL). All other chemicals are purchased from Sigma-Aldrich (St. Louis, MO).

DMPC/DHPC bicelles were prepared as follows (Figure II-27). 40 mg DMPC and 7.6 mg DHPC corresponding to a q ratio, q = [DMPC]/[DHPC] = 3.5 were cosolubilized in chloroform. Chloroform was removed under a stream of N_2 gas to form a lipid film on the walls of a glass tube, which was kept under vacuum overnight to remove all residual solvent. In the glass tube, 111.9 µl of 100 mM HEPES buffer, pH 7.0 was added to the lipids. The resulting viscous mixture was homogenized by gently sonication in an ice bath for 30 minutes, and >4 freeze/heat cycles between liquid nitrogen and 40 °C of water. The resulting turbid gel is still viscous, but the viscosity was slightly reduced at 5 °C. Once a satisfactory mixing of the components was reached, the sample was transferred to a 5 mm NMR glass tube. It was sealed using a Teflon tape and was capped. The degree of alignment was measured using ^{31}P-NMR and the alignment was found to be stable after 1 h of equilibration. A previous study showed that a ytterbium-chelated phospholipid (DMPE-DTPA:Yb^{3+}) can be incorporated into DMPC/DHPC bicelles and aligned under an external magnetic field such that the average bilayer normal is parallel to the magnetic field due to the magnetic susceptibility of the chelated lanthanide ions.[6] In this study on bicelles with copper-chelated phospholipids, the spontaneous magnetic alignment was achieved at 37 ^{o}C and the average bilayer normal of bicelles is perpendicular to the magnetic field.

Bicelles containing ^{15}N-labeled Subtilosin A were prepared by mixing 48 mg of lipids (0.316 mg of DMPE-DTPA, 40 mg of DMPC and 7.65 mg of DHPC) with 2 mg of 12-14% ^{15}N-labeled Subtilosin A. The bicelles/peptide mixture sample making procedure was the same as that of pure bicelles except that 0.136 mg of $Cu(NO_5)_2$ was added in the bicelle/peptide mixture before adding 100 mM HEPES buffer (pH 7.0) as shown in Figure II-27. DMPC/DHPC bicelles with 30 mM Cu-EDTA samples were prepared in the same manner except that Cu-EDTA was added to DMPC/DHPC bicelles before adding 100 mM HEPES buffer, pH 7.0.

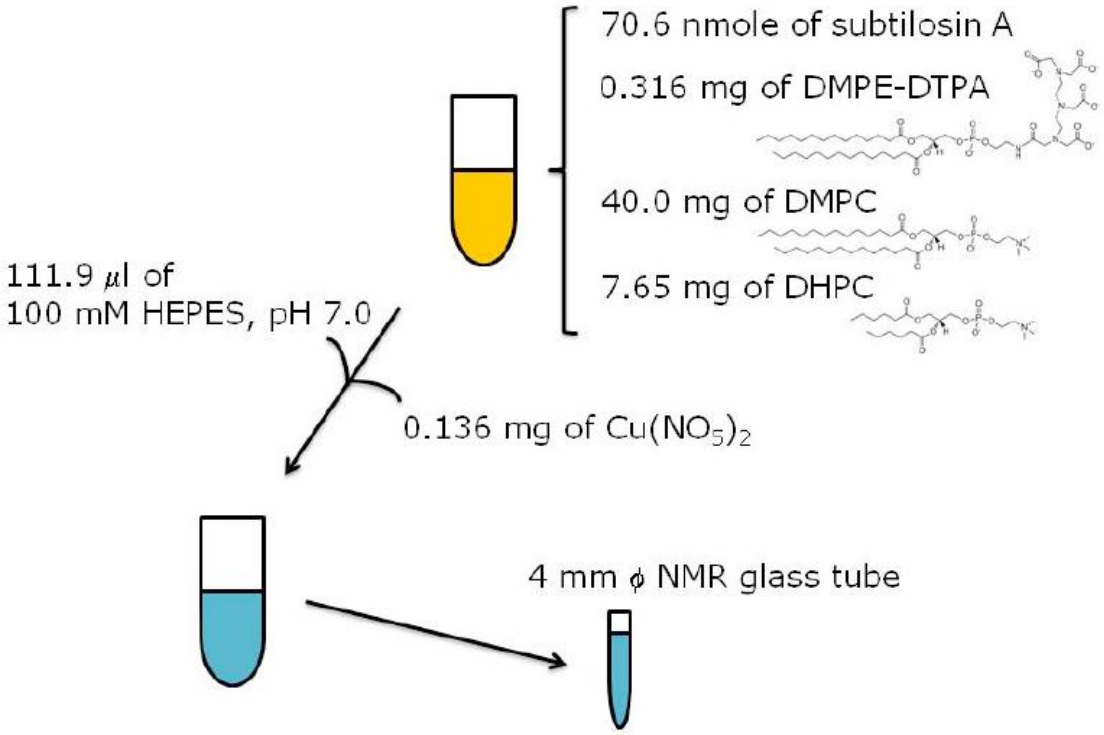

Figure II-27. **Preparation of DMPC:DHPC bicelles containing ^{15}N-labeled Subtilosin A and copper-chelated lipids for solid-state NMR experiments.**

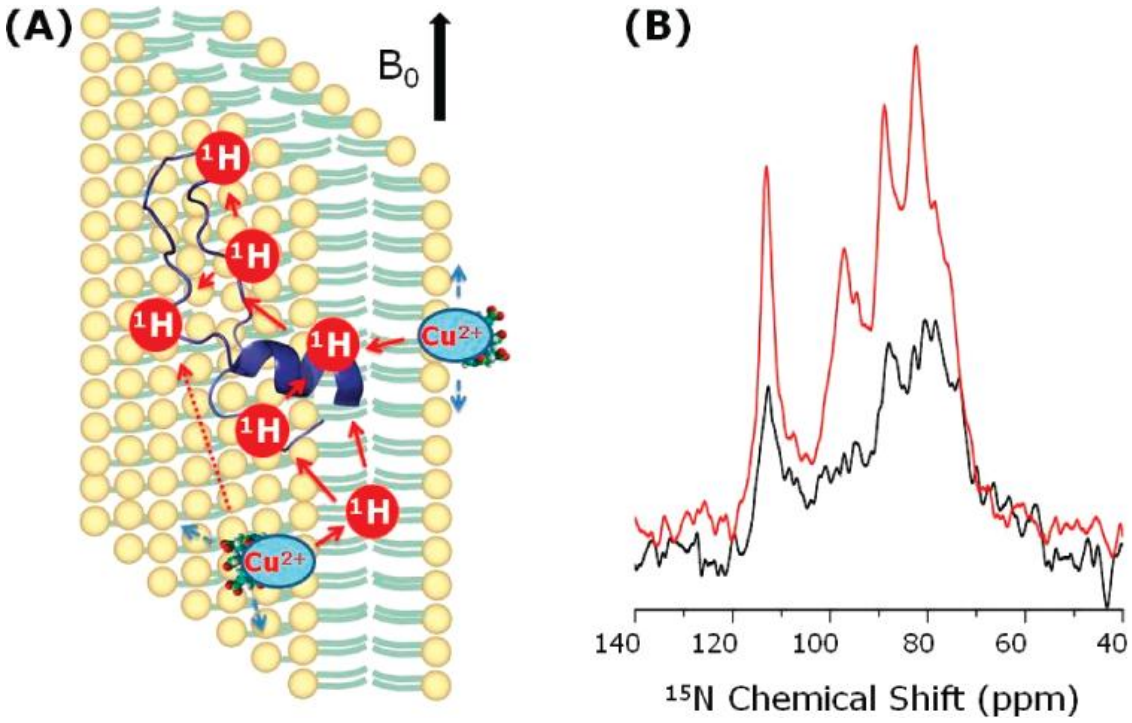

Figure II-28. **A coppor-chelated lipid enhances S/N of ssNMR spectra.**
(A) Representation of lipid bilayers containing a paramagnetic copper-chelated lipid and subtilosin A. Subtilosin A is a 35-residue cyclic antimicrobial peptide (Figure II-24) that has been shown to interact with lipid bilayers with the membrane orientation depicted in (A).4 (B) ^{15}N spectra of aligned 7:3 DMPC/DHPC bicelles containing 12-14% uniformly ^{15}Nlabeled (only 70-82 nmol) subtilosin A (red) with and (black) without the 2.56 mM copper-chelated lipid. The spectra were obtained on a 400 MHz Varian NMR spectrometer using a ramped-amplitude cross polarization (ramp-CP) sequence[5] with a contact time of 0.8 ms under static conditions at 37 °C. The S/N dependence on the contact time and the recycle delay were optimized (Figures II-30 and II-31). While the total data collection time was 8 h for both spectra, the recycle delay was different for samples without (2 s) and with (1 s) the copper-chelated lipid. The transfer of the paramagnetic effect in T_1 reduction for nuclei in the membrane via proton spin diffusion is also indicated in (A).

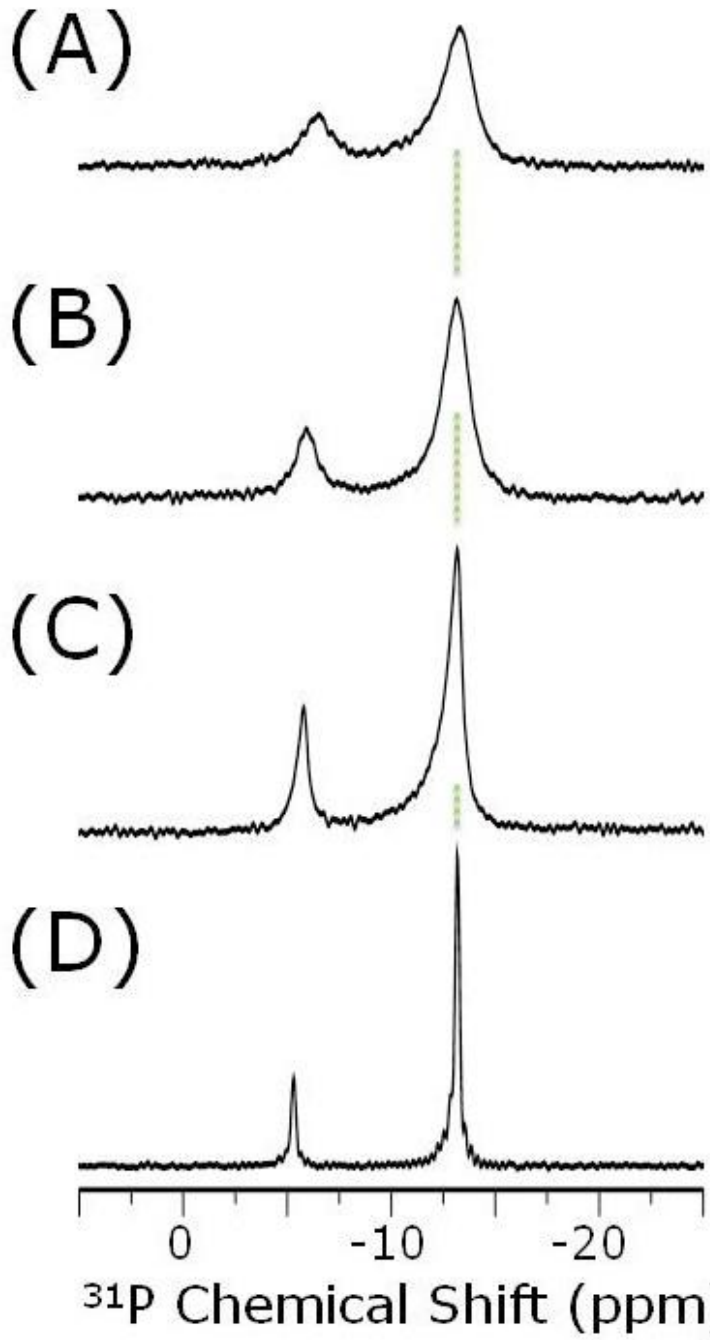

Figure II-29. **^{31}P NMR spectra of *q* = 3.5 DMPC/DHPC bicelles with (A) 3.85 mM Cu DMPE-DTPA, (B) 2.56 mM Cu DMPE-DTPA, and (C) 1.92 mM Cu DMPE-DTPA**. (D) Copper free DMPC/DHPC bicelles. ^{31}P spectra were acquired after a 90^{o} RF pulse by decoupling protons using TPPM pulse sequence under static condition at 37 ^{o}C.

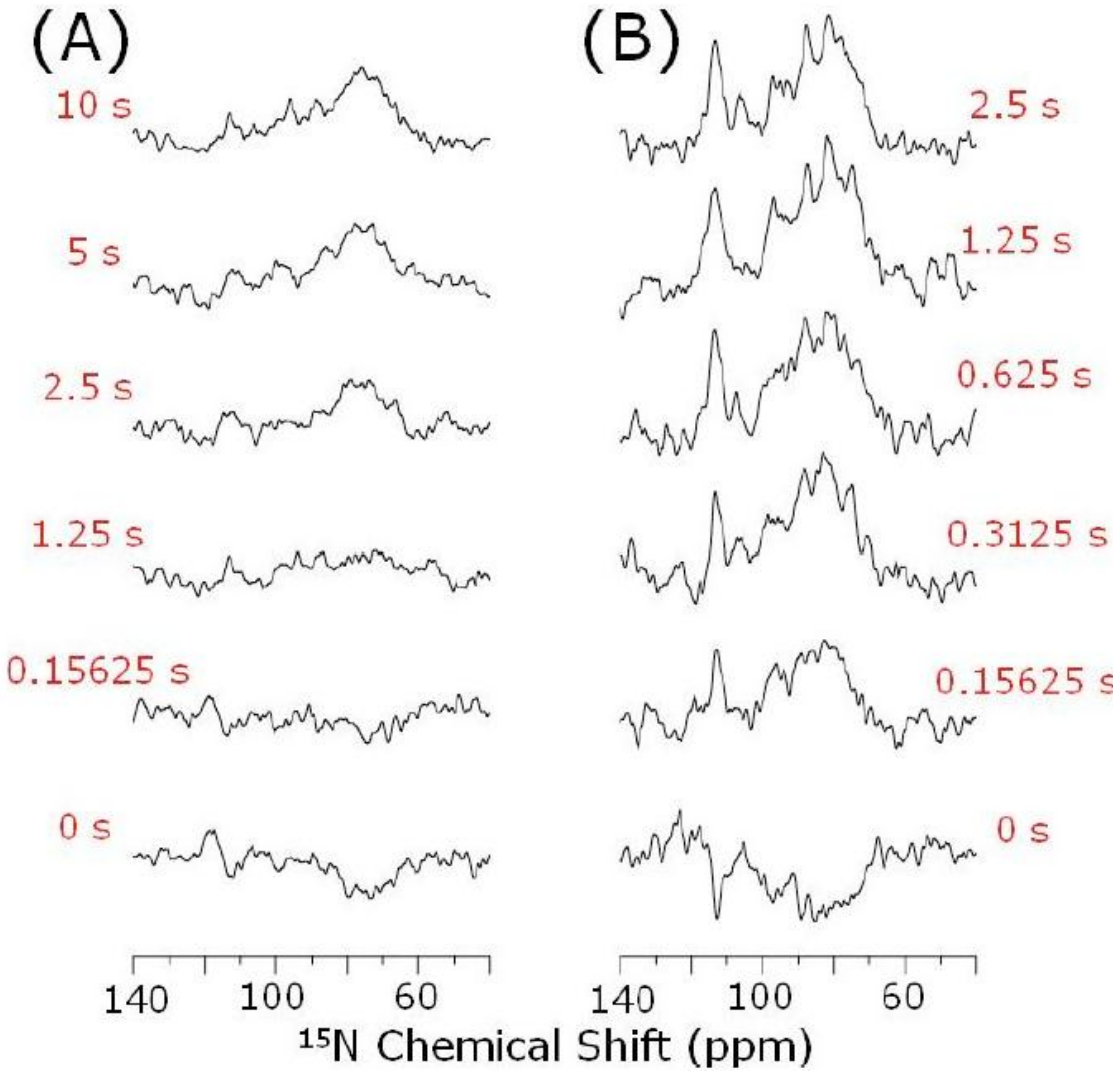

Figure II-30. **^{1}H inversion recovery experiments of ^{15}N-labeled Subtilosin A in *q* = 3.5 DMPC/DHPC bicelles**: (A) without and (B) with 2.56 mM Cu DMPE-DTPA at 37 ^{o}C. Inversion recovery times are indicated for each spectrum.

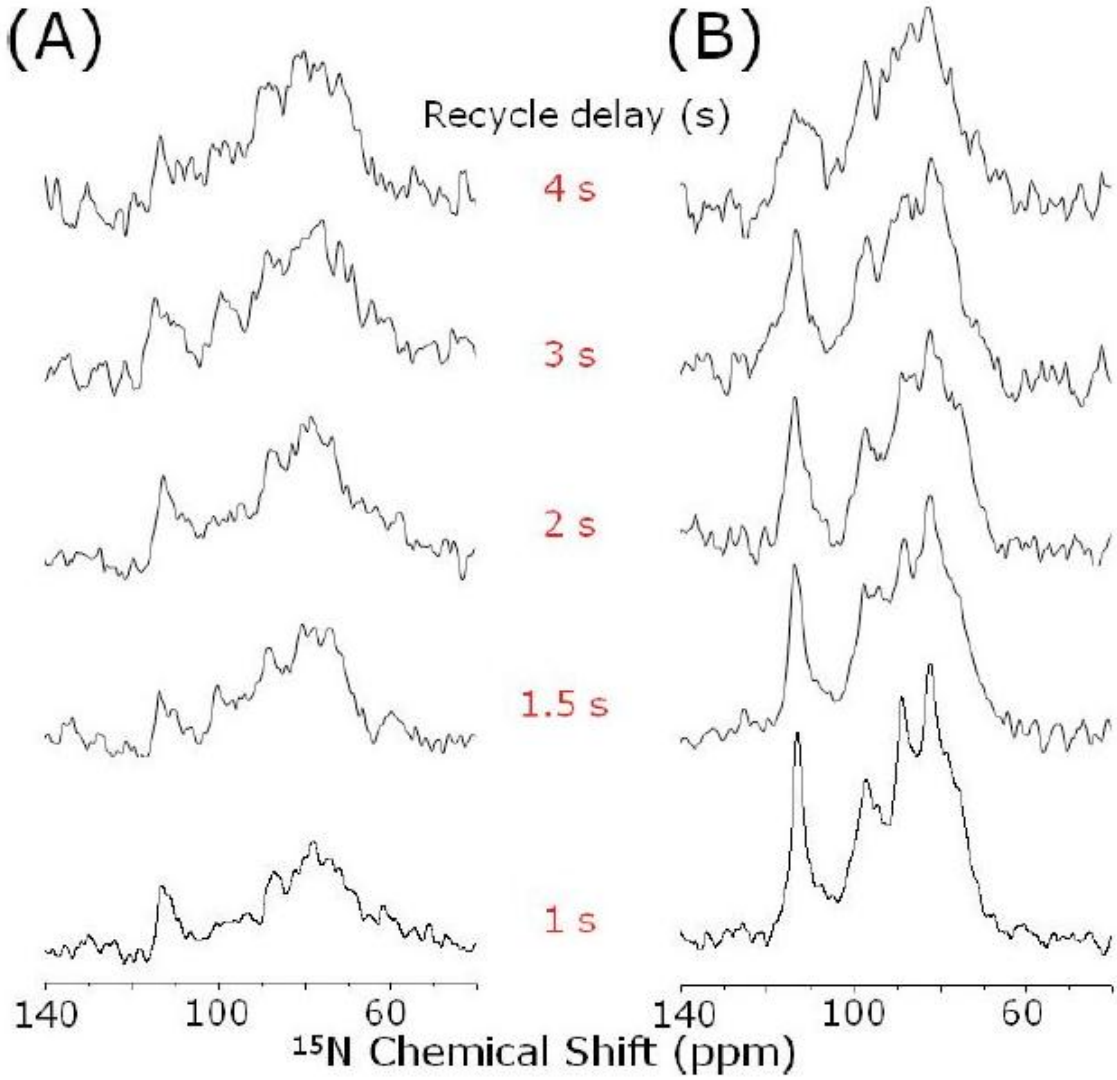

Figure II-31. **The recycle delay dependence of U-^{15}N Subtilosin A in *q* = 3.5 the DMPC/DHPC bicelles (A) without and (B) with 2.56 mM Cu DMPE-DTPA at 37 ^{o}C**. The recycle delay times in the experiments are indicated in the figure. The total experimental time for each spectrum was 8 hours.

II-4-3. Solid-state NMR Results

Magnetically aligned bicelles6 composed of a lipid [1,2-dimyristoyl-sn-glycero-3-phosphocholine (DMPC)], a detergent [1,2-dihexanoyl-sn-glycero-3-phosphocholine (DHPC)], and subtilosin A[4] (Figure II-24) were used to demonstrate the paramagnetic effect of Cu^{2+} in reducing the spin-lattice relaxation time (T_1) and the recycle delay of NMR experiments in membranes. Cu^{2+} ions were introduced in bicelles either by adding Cu-EDTA or a copper-chelated lipid (Figure II-28A and Figures II-25 – II-27). ^{31}P NMR experiments were performed to optimize the alignment of the bicelles (Figure II-29). ^{15}N spectra of uniformly ^{15}Nlabeled subtilosin A embedded in bicelles are shown in Figure II-28B. T_1 values of ^{1}H and ^{13}C nuclei in DMPC and ^{15}N nuclei in subtilosin A were also measured (Figure II-32). These results suggested that a 2 s recycle delay provided the maximum S/N for the sample in the absence of Cu^{2+}. On the other hand, the presence of 2.56 mM copper-chelated lipid in bicelles reduced the T_1 of protons by a factor of 10, and therefore, ~0.2 s recycle delay would have been sufficient. However, RF heating and dehydration or denaturing effects (including degradation of the magnetic alignment and protein stability) due to a very short recycle delay forced us to use a longer recycle delay. Nevertheless, it was found that a 1 s delay was sufficient to avoid RF heating, thus allowing 2-fold faster data collection. The experimental results given in Figure II-28B suggest a ~2.7-fold increase in the S/N due to the use of the copper-chelated lipid in bicelles.

Our results suggest that while the use of Cu-EDTA also decreased the T_1 values effectively (as shown in Figure II-32B), it was ineffective in enhancing the S/N in comparison with the immobilized Cu-chelated DMPE lipid (Figure II-32F-H) and also resulted in more RF heating (Figure II-32E) due to the presence of mobile Cu^{2+} ions; the heating effects were also observed in the ^{31}P spectra (Figures II-33 and II-34). The use of ~15-fold less [Cu^{2+}] in the chelated form is of considerable advantage for NMR studies.

Since magnetic alignment of the bicelles is not needed and the sample temperature can be lowered in MAS experiments, the use of Cu-DMPE-DTPA-containing bicelles can be extended for MAS experiments. Two-dimensional (2D) MAS experiments were performed on such bicelles (Figure II-35). An RF-driven dipolar recoupling (RFDR)

technique was used during the mixing period to recouple the ^{1}H-^{1}H dipolar couplings.[7] Cross-peaks connecting dipolar coupled protons can be seen in the spectra. While the spectra of bicelles without (Figure II-35A) and with (Figure II-35B) the copper-chelated lipids have similar overall S/N, the intensities of some of the peaks are different. The proximity of the Cu^{2+} ion broadens peaks associated with the lipid headgroup, whereas the intensities of peaks from the hydrophobic acyl chains are enhanced. Since no decoupling was used in these experiments, the much reduced RF induced heating of the bicelles enabled a further reduction in the recycle delay period to 0.2 s, unlike in the static experiment of Figure II-28. Therefore, a 6.2-fold overall reduction in the 2D experiment time was achieved.

In this study, we have shown that the inclusion of Cu^{2+} ions in bicelles results in a 10-fold T_1 reduction. It has also been demonstrated that the challenges posed by the molecular mobilities and presence of bulk water can be overcome by using a copper-chelated lipid. About 2.7-fold increase in S/N of spectra for static experiments and 6.2-fold decrease in MAS experimental time were achieved. While this enhancement is not as dramatic as that reported for crystalline solids,[2] given the tremendous challenges in the investigation of fluid membranes, this S/N enhancement is significant and will be of considerable use in structural studies of membrane proteins. For example, satisfactory completion of a typical 2D experiment used to study aligned lipid bilayers containing an ^{15}N-labeled membrane protein takes ~3 days time. The use of Cu-DMPE, on the other hand, could enable the completion of such experiments in <1.5 days. There are a number of membrane disrupting/permeating systems (such as antimicrobial peptides, toxins, amyloid peptides, and fusion peptides) whose concentration cannot be increased, as they result in nonlamellar conditions; such systems tremendously benefit from the use of the approach proposed in this study to reduce the amount of peptide/protein used in the experiment. Interestingly, further reduction in the measurement time would be possible in the following cases: (a) lowering the sample temperature to avoid heating, as in MAS experiments on frozen samples; (b) use of efficient electric-field-free probes;[8] (c) use of bicelles that align at low temperatures (as shown in Figure II-36); and (d) use of cryoprotectants. Therefore, we believe that the approach presented in this study will have a broad impact on structural studies of a variety of membrane-associated peptides and

proteins that are scarcely available, quite unstable, and/or for which production could be very expensive.

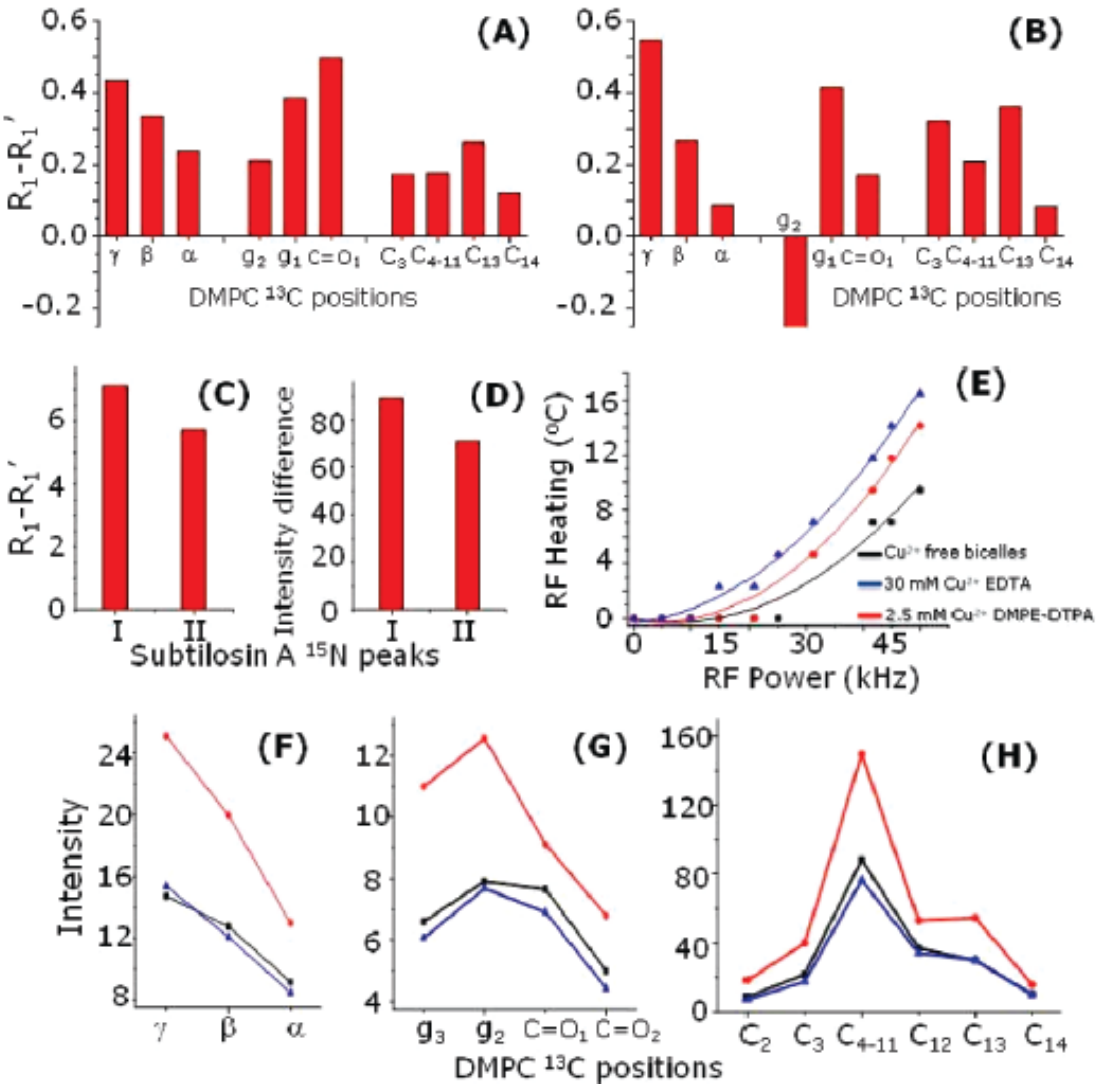

Figure II-32. **NMR relaxation measurements on bicelles and ^{15}N-labeled subtilosin A for the evaluation of the paramagnetic doping effect** with (A) 2.56 mM copper-chelated lipid and (B) 30 mM Cu-EDTA. (C) Difference in spin-lattice relaxation rates with (R_1) and without (R_1') copper-chelated lipid. Labels I and II correspond to ^{15}N signals from the rigid transmembrane (78.3 ppm) and flexible membrane-surface (112.6 ppm) regions, respectively. (D) Difference in signal intensities obtained from bicelles with and without copper-chelated lipid. (E) Data showing RF-induced heating of bicelles measured as explained in Figure II-33. (F-H) Comparison of ^{13}C CP signal intensities measured for bicelles with (E) no copper, (blue) 30 mM Cu-EDTA, and (red) 2.5 mM Cu-DMPE-DTPA.

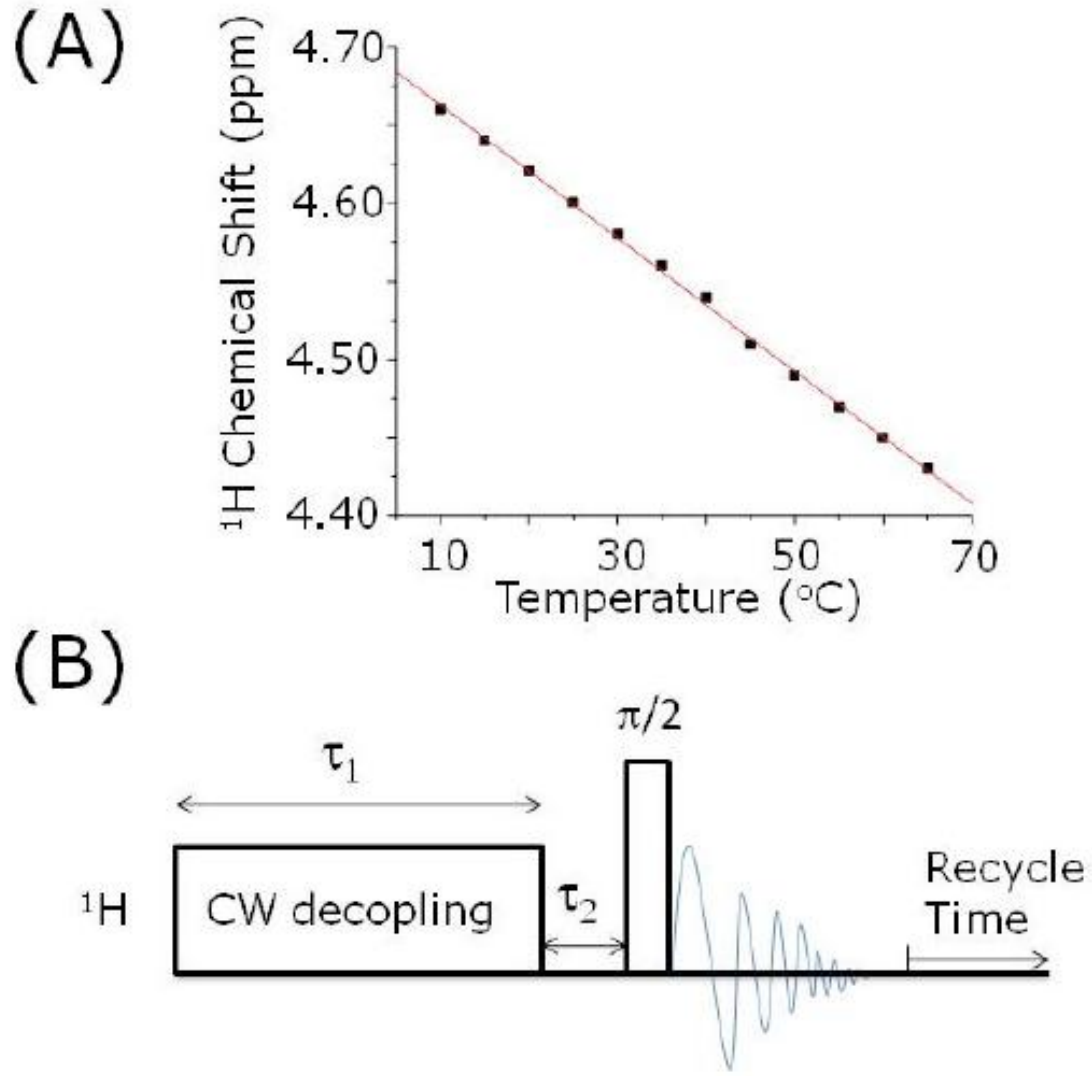

Figure II-33. (A) **Variation of the proton chemical shift of water as a function of sample temperature** measured using the pulse sequence given in (B). The proton chemical shift of water was set at 4.6 ppm at 25 ^{o}C. (B) A ^{1}H pulse sequence for evaluating RF-induced sample heating in well hydrated samples. τ_1 = 20 ms, τ_2 = 200 ms, recycle time = 4 s, 20 dummy scans, and 20 scans were used to generate each data point in (A).

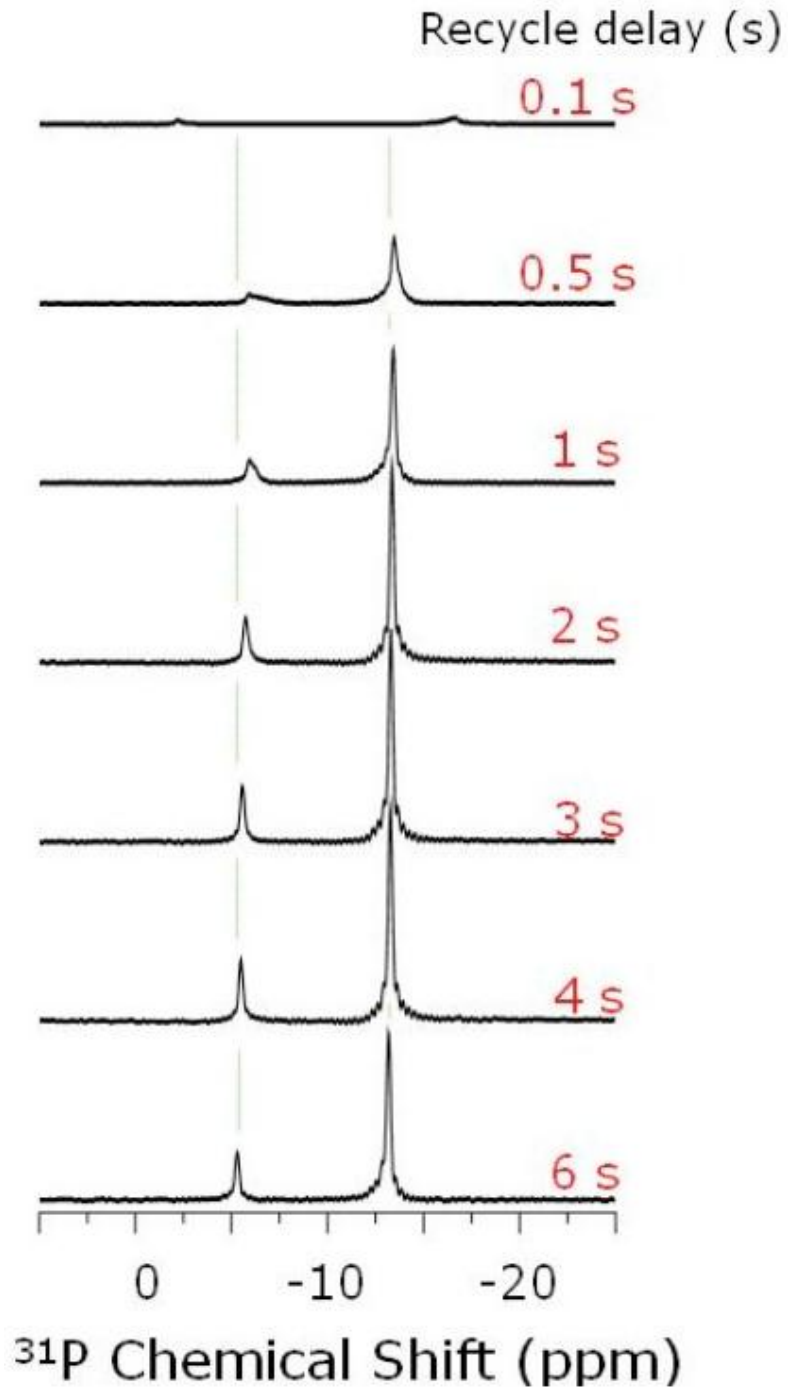

Figure II-34. **The recycle delay dependence of ^{31}P NMR spectra of q = 3.5 DMPC/DHPC bicelles at 37 ^{o}C.** The recycle delay times in the experiments are indicated in the figure. The total experimental time for each spectrum was 24 s.

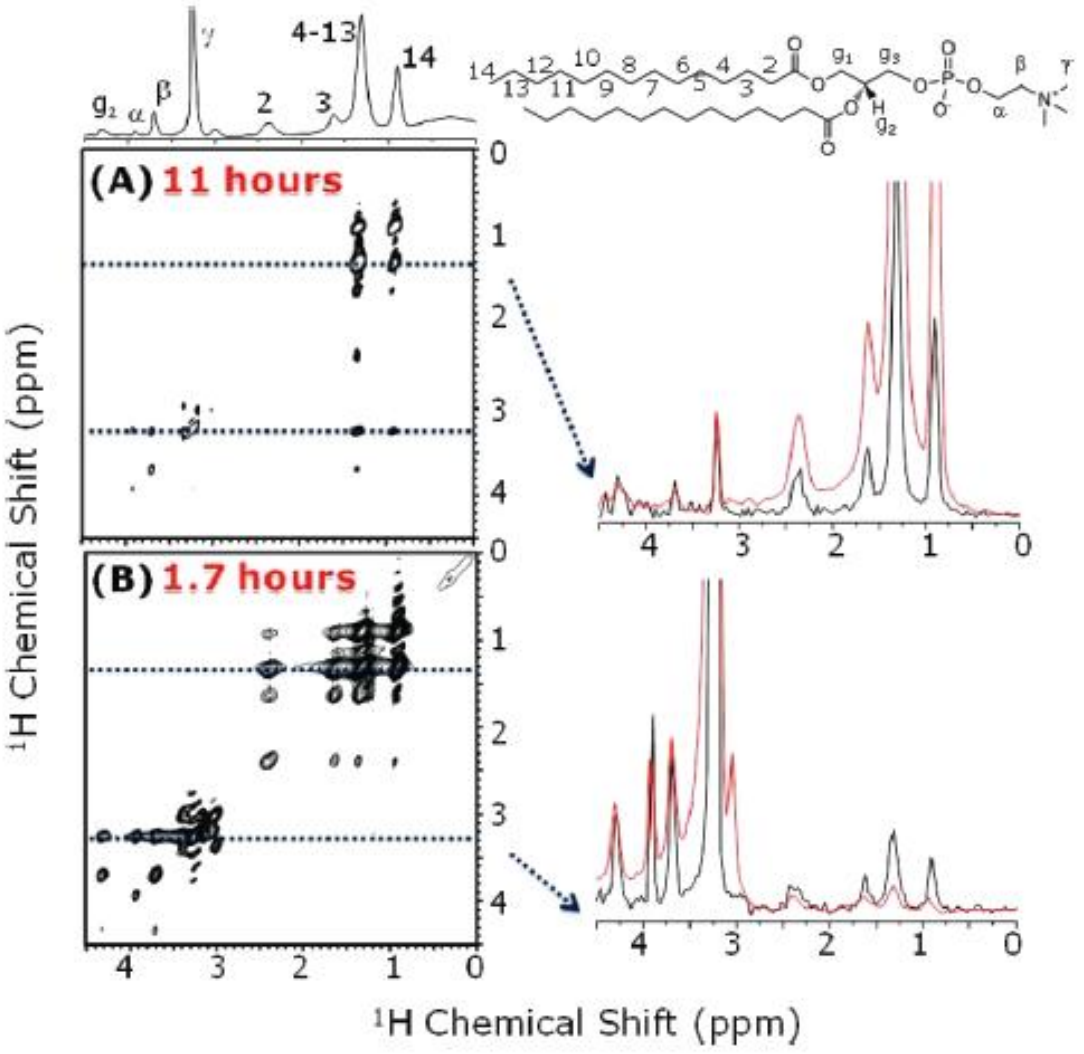

Figure II-35. **^{1}H/^{1}H 2D chemical shift correlation spectra of bicelles** without (A) and with (B) 2.56 mM copper-chelated lipid obtained under 5 kHz MAS with total data collection times of 11 and 1.77 h, respectively. A 6.2-fold reduction in data collection time with a similar S/N ratio was made possible by the use of the copper-chelated lipid, as can be seen from the 1D spectral slices taken at (top) 1.34 and (bottom) 3.25 ppm with (red) and without (black) the copper-chelating lipid. An RFDR[7] sequence with a 100 ms mixing time and a 100 ms low-power pulse for water saturation at 35 °C was used; 512 t_1 experiments with 32 scans were used, with recycle delays of 0.2 s (with copper-chelating lipid) and 2 s (without).

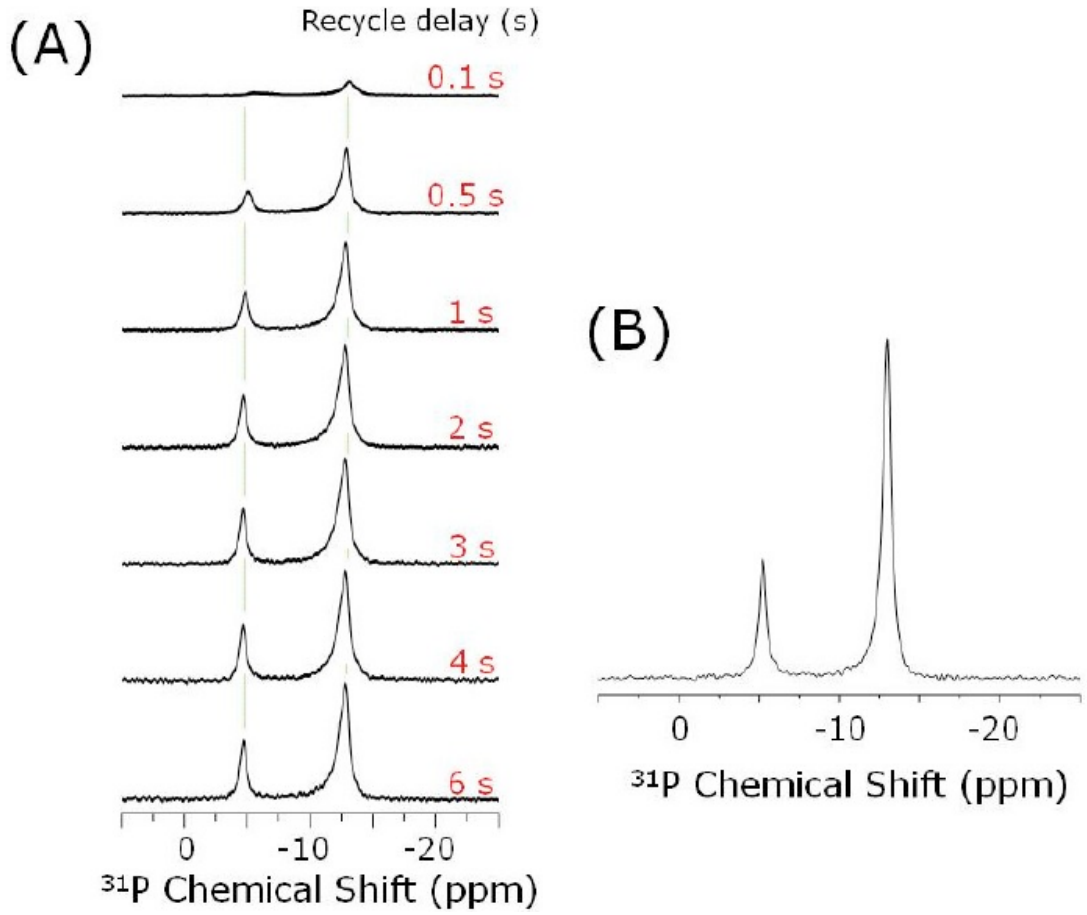

Figure II-36. (A) **The recycle delay dependence of ^{31}P NMR spectra of magnetically aligned DMPC/POPC/DHPC bicelles at 20 ^{o}C.** The recycle delay times are indicated. (B) ^{31}P NMR spectrum of DMPC/POPC/DMPE-DTPA/DHPC bicelles at 20 ^{o}C. The total experimental time for each spectrum was 24 s for spectra in Figure II-34 (A). On the other hand, 10 transients were accumulated with a 6 s recycling delay for spectra in Figure II-34 (B).

II-4-4. Use of Copper-Chelated Lipids on Solution-state NMR Spectroscopy

High-resolution structural and dynamical studies of membrane proteins and peptides are becoming increasingly important as the ability to visualize atomic-level details provides powerful insights into their functional properties. Despite the challenges posed by membrane proteins, NMR spectroscopy has been successfully utilized recently to provide a wealth of atomic-level resolution structural and dynamical information from a variety of model membranes.[9] However, in spite of the recent technical advances, relatively poor sensitivity of NMR spectroscopy continues to be a major bottleneck for high-throughput applications.[10] Specifically, stringent requirements on the quantity and stability of a sample and the long data acquisition process are not suitable for most membrane proteins that are scarcely available and/or their production could be very expensive. It is also not desirable to enhance the S/N by increasing the concentration of membrane active molecules such as antimicrobial peptides, amyloid peptides, toxins, and fusogenic peptides as they may oligomerize to disrupt the membrane.[11] The mandatory requirement for isotopic labeling of membrane proteins further limits NMR applications, as there are numerous molecules that cannot easily be biologically obtained. Therefore, there is considerable interest in the development of novel approaches to study unlabeled proteins and also to speed up the NMR data acquisition process. To overcome these difficulties, here we demonstrate an approach for NMR structural studies of a membrane protein embedded in bicelles without the need for isotopic enrichment by speeding up the spin-lattice relaxation process for protons. Our experimental results show that it is possible to obtain high-resolution multidimensional spectra from a membrane-associated peptide (MSI-78[12], Figure II-37) at natural-abundance of ^{15}N and the data can be collected four times faster, even when the SOFAST-HMQC[13] experiment is employed, using isotropic bicelles containing a copper-chelated lipid.

Since the curvature of micelles has been thought to play a role on the structural folding of certain membrane proteins, and the presence of lipids in bicelles[14] makes them better model membranes, we chose to use bicelles to investigate the paramagnetic effect of Cu^{2+} for fast NMR data acquisition. Isotropic bicelles composed of DMPC, DHPC, and MSI-78 were used in NMR experiments. Since free Cu^{2+} could interact with the protein and also could result in RF-induced heating, a Cu^{2+}-chelated DMPE lipid was used in this

Figure II-37. **Amino acid sequence of MSI-78** (also known as pexiganan).

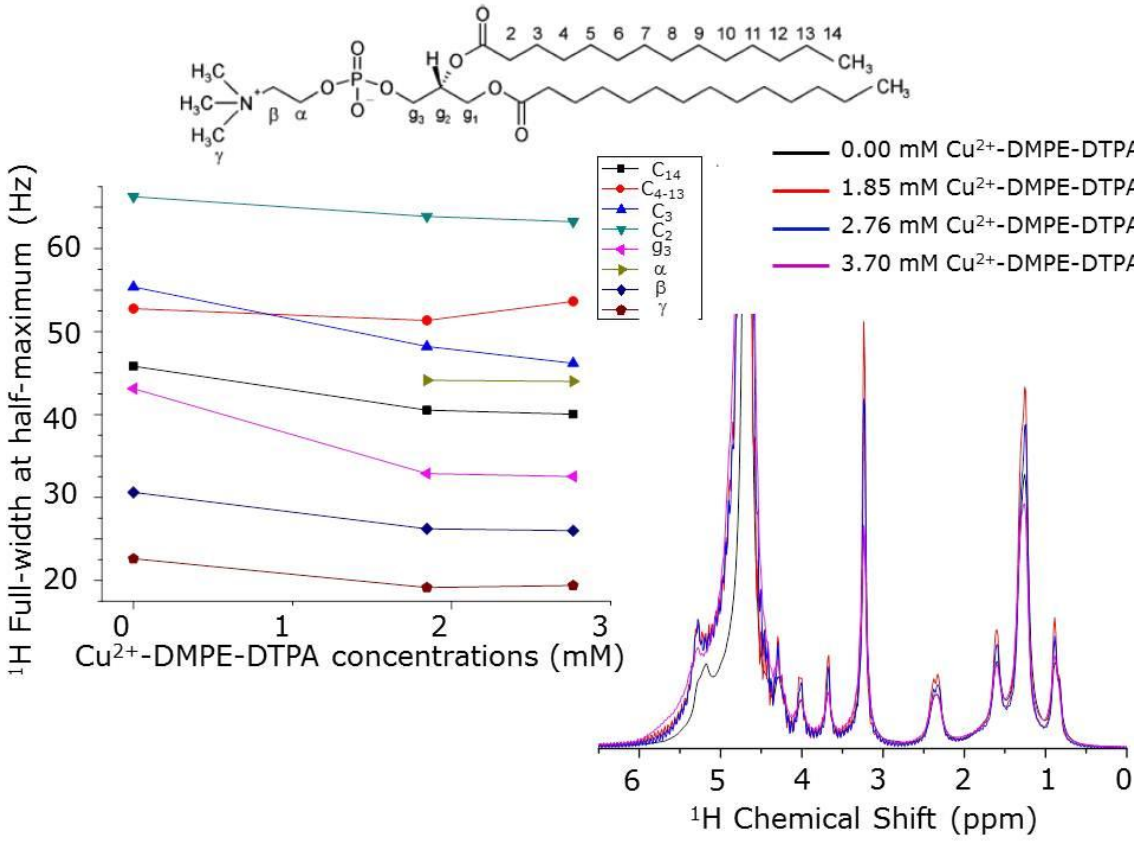

Figure II-38. **Full-width at half-maximum (FWHM) and ^{1}H NMR spectra of DMPC/DHPC isotropic bicelles (q = 0.5) for different concentrations of a copper-chelated lipid, Cu^{2+}-DMPE-DTPA, at 35 ^{o}C.** The close resemblance of spectra for different Cu^{2+}-DMPE-DTPA concentrations suggests that there is no change in the bicellar properties of the samples due to the presence of Cu^{2+} ions. The chemical structure of DMPC is shown at the top. All measurements were carried out on a 400 MHz Varian solid-state NMR spectrometer.

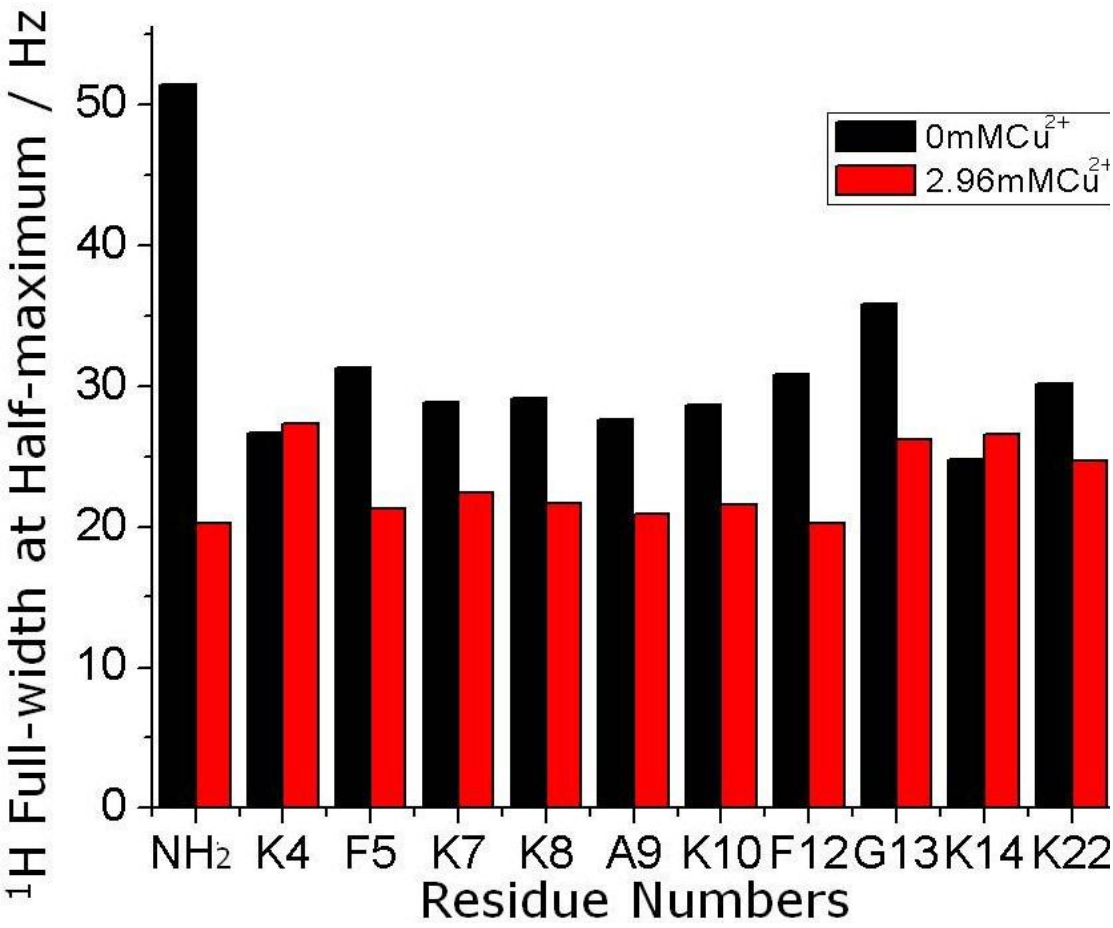

Figure II-39. **Full-width at half-maximum (FWHM) of amide-NH resonances observed from 2D SOFAST-HMQC experiments of a 9.3 mM unlabeled-MSI-78 embedded in DMPC/DHPC isotropic bicelles (q = 0.5) without Cu^{2+}-DMPE-DTPA (black) and with 2.96 mM Cu^{2+}-DMPE-DTPA (red) at 35 ^{o}C.** Spectra were obtained from a 900 MHz Bruker NMR spectrometer using a cryoprobe. Each 2D SOFAST-HMQC spectrum was obtained from 64 t_1 experiments, 256 scans, and a 100 ms recycle delay. The final 2D data matrix size after zero-filling was 2048 × 2048. 2D data were processed using TOPSPIN 2.1 (from Bruker). Squared sine-bell function was employed in both dimensions with a $\pi/4$ shift. Resonance assignment and volume fit calculations were performed using SPARKY 3.113.

~0.1 s and its presence did not alter the DMPC:DHPC bicellar properties and had no significant effect on the line width of observed peaks from both lipids and peptide present in bicelles (Figures II-38 and II-39).

II-4-5. Experimental Procedure

A Membrane-associated Antimicrobial Peptide MSI-78 (also known as pexiganan).

In this study, an antimicrobial peptide MSI-78 reconstituted in DMPC:DHPC isotropic bicelles (DMPC: 1,2-dimyristoyl-sn-glycero-3-phosphocholine, DHPC: 1,2-dihexanoyl-sn-glycero-3-phosphocholine) was used as a model system to demonstrate fast multidimensional heteronuclear NMR measurements at natural-abundance of membrane proteins. A copper-chelated lipid was used to speed up the spin-lattice relaxation time (T_1). MSI-78 is a 22-residues (a molecular weight of 2477.20 Da), linear, cationic antimicrobial peptide (Figure II-37). This peptide was designed, synthesized and donated by Genaera Corporation. Details on the synthesis and purification of MSI-78 is reported elsewhere (W. L. Maloy, U. P. Kari, *Biopolymers. 37*, **1995**, 105-122.). 3D structure of dimeric form of MSI-78 embedded in DPC micelles (Figure II-40B) determined from solution NMR experiments has been reported.[15] As shown in Figure II-37, MSI-78 was designed to exhibit an amphipathic α-helical structure between residues 4 and 19 (highlighted in red) in a membrane environment whereas it is unstructured in solution.[15] Solid-state NMR studies reported the lipid-peptide interactions, membrane-associated structure, and its mechanism of membrane disruption of MSI-78.[12,16]

Preparation of Isotropic Bicelles with a Chelated Lipid for Solution NMR Experiments.

Since isotropic bicelles tumble fast enough to result in narrow spectral lines and used in structural studies of peptides and proteins, DMPC:DHPC bicelles with *q* ratios 0.5 and 0.25 (*q* ratio = [DMPC]/[DHPC]) were used in this study for solution NMR measurements. A copper-chelated lipid was inserted in these bicelles to accelerate the spin-lattice relaxation rate ($R_1 = 1/T_1$) of protons so that the recycle delay after signal acquisition can be shortened for fast data collection. As mentioned in the main text of the manuscript, the use of copper-EDTA requires a significant amount (> 30 mM) of

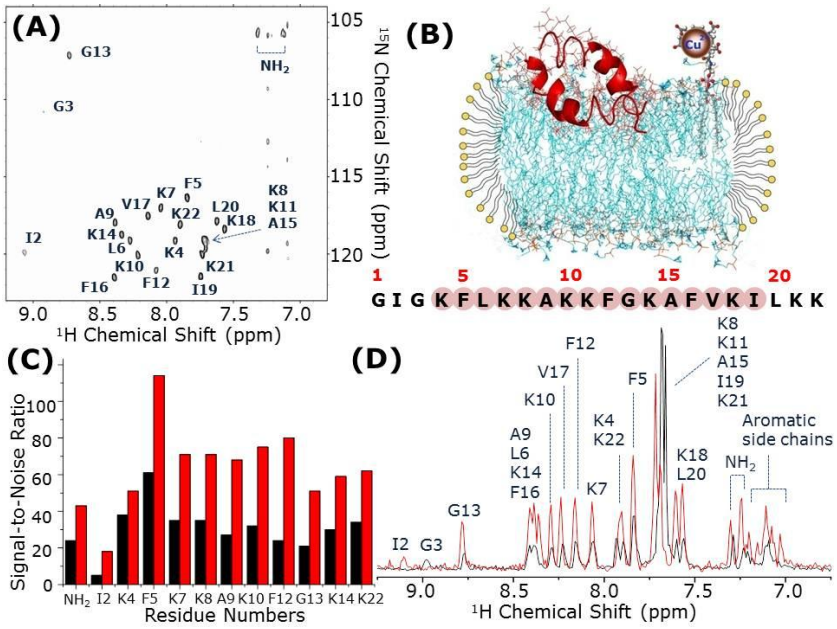

Figure II-40. **A four-fold increase in the sensitivity of 2D SOFAST-HMQC experiments**. (A) 2D SOFAST-^{1}H/^{15}N-HMQC[13] spectrum of a 9.3 mM (unlabeled) MSI-78 (also known as pexiganan) incorporated in DMPC/DHPC isotropic bicelles (q=[DMPC]/[DHPC]=0.25, DMPC: 1,2-dimyristoyl-*sn*-glycero-3-phosphocholine, DHPC: 1,2-dihexanoyl-*sn*-glycero-3-phosphocholine) containing a 2.96 mM copper-chelated DMPE lipid. (B) 3D structure of MSI-78 embedded in bicelles along with its amino acid sequence. Previous studies have shown that the potent antimicrobial peptide, MSI-78, is unstructured in solution and forms a helical dimmer in a membrane environment.[15] Solid-state NMR studies have shown the membrane-surface association of this peptide and its ability to function by forming toroidal pores.[16] The effect of a Cu^{2+}-chelated DMPE on the bicellar properties of DMPC:DHPC system and the paramagnetic ion induced shortening of spin-lattice relaxation time (T_1) were examined using a series of ^{1}H NMR experiments (Figures II-41 and II-42). (C) Signal-to-noise ratio obtained from 2D SOFAST-HMQC spectra of a 9.3 mM unlabeled MSI-78 in q=0.5 isotropic bicelles without copper-chelated lipid (black) and with a 2.96 mM copper-chelated lipid (red). S/N ratio and line widths were also measured for amide-NH resonances observed in 2D ^{1}H/^{15}N SOFAST-HMQC spectra and are compared in Figures S6 and S7. Further increase in the concentration of Cu^{2+} either did not increase the S/N or resulted in undesirable effects like line broadening (Figure II-43). (D) 1D ^{1}H chemical shift projection spectrum obtained from 2D SOFAST-^{1}H/^{15}N-HMQC spectra that were obtained with no copper (black) and a 2.96 mM Cu^{2+}-DMPE-DTPA (red). All spectra presented in this study were obtained from a 900 MHz Bruker NMR spectrometer at 35 ^{o}C using a cryoprobe. Each 2D SOFAST-HMQC spectrum was obtained from 64 t_1 experiments, 256 scans, and a 100 ms recycle delay; the total data collection time (including the acquisition time and delays in INEPT) was ~54 min. The final 2D data matrix size was 2048 X 2048 after zero-filling in both dimensions. 2D data were processed using TOPSPIN 2.1 (from Bruker). Squared sine-bell function was employed in both dimensions with a shift of $\pi/4$. Resonance assignment and volume fit calculations were performed using SPARKY 3.113.

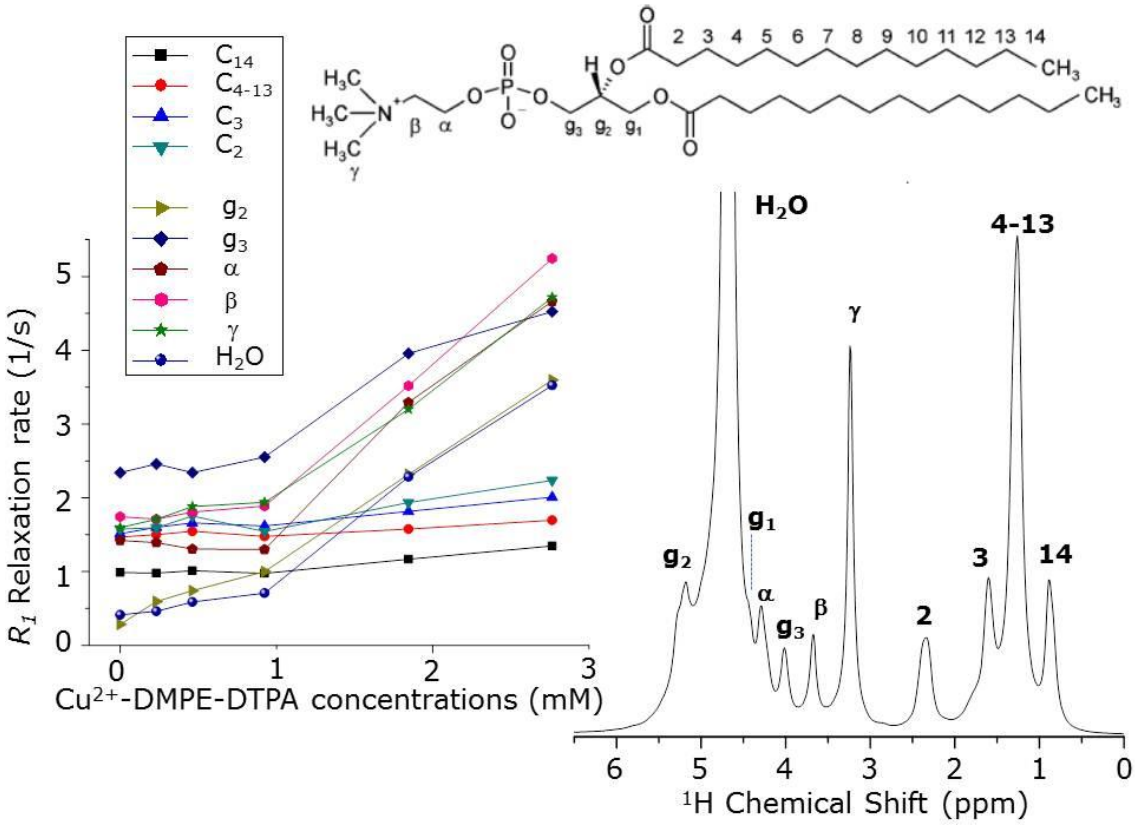

Figure II-41. **Spin-lattice relaxation rate (R_1) of protons from DMPC/DHPC isotropic bicelles (q=0.5) for different concentrations of a copper-chelated lipid, Cu^{2+}-DMPE-DTPA at 35 °C.** The R_1 values were determined from ^{1}H-spin-inversion recovery experiments and the estimated error from the best-fitting of experimental data is about ±0.05. One-dimensional ^{1}H chemical shift spectrum of DMPC/DHPC isotropic bicelles with 0 mM Cu^{2+}-DMPE-DTPA at 35 °C (bottom right). The chemical structure of DMPC is shown at the top. These measurements were performed on a 400 MHz Varian solid-state NMR spectrometer.

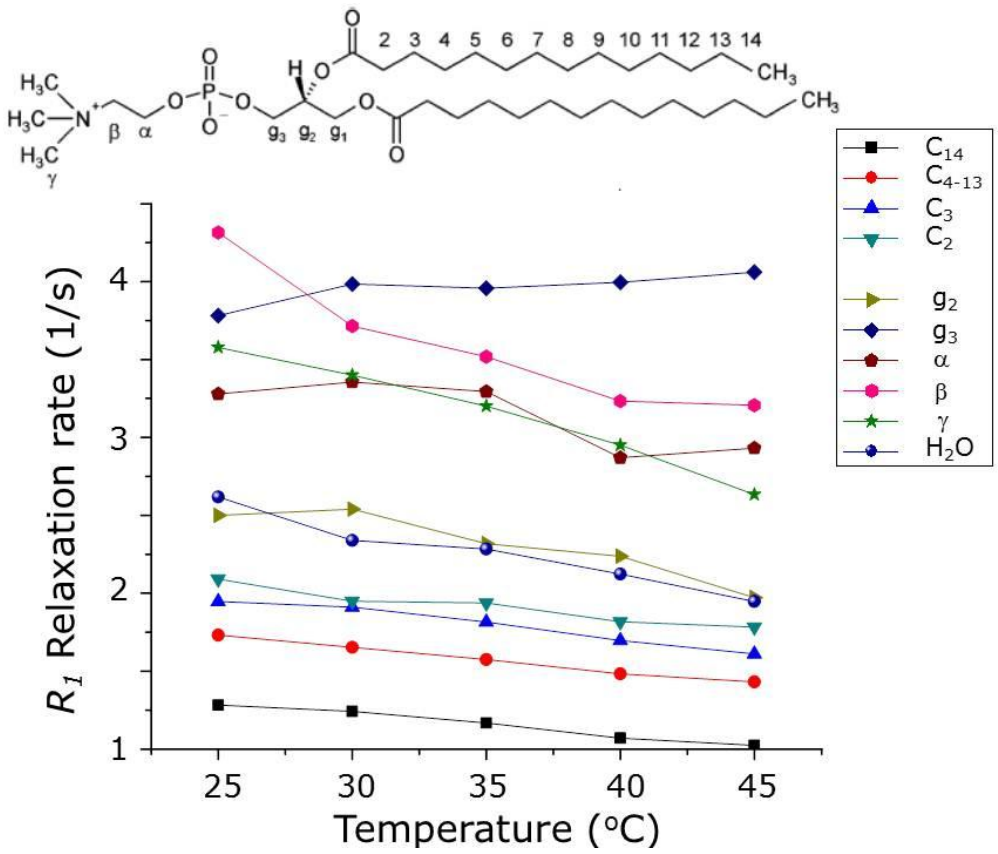

Figure II-42. **Experimentally measured spin-lattice relaxation rate (R_1) values of protons from DMPC/DHPC isotropic bicelles (q = 0.5) containing a 2.57 mM Cu^{2+}-DMPE-DTPA at different temperatures.** The R_1 values were determined from ^{1}H-spin-inversion recovery experiments and the estimated error from the best-fitting of experimental data is about ±0.05. The chemical structure of DMPC is shown at the top. All spectra were obtained from a 400 MHz Varian solid-state NMR spectrometer.

paramagnetic ions to speed up the spin-lattice relaxation rate, because the freely diffusing copper-EDTA molecules in the solution are inefficient in augmenting the T_1 process.[19] Therefore, in this study, we demonstrate an approach to enhance the paramagnetic effect on T_1 reduction for solution NMR measurements by homogeneously mixing a significantly smaller amount of paramagnetic ion-chelated phospholipid (DMPE-DTPA : 1,2-ditetradecanoyl-*sn*-glycero-3-phosphoethanolamine-N-diethylenetriaminepentaacetic acid (Figure II-25)) in the lipid bilayer. Solid-state NMR studies evaluating the paramagnetic relaxation enhancement effects on rigid solids have been reported elsewhere.[18]

Three main advantages of using a copper-chelated lipid are: (i) approximately a 10-times lower paramagnetic ion concentration was sufficient to accelerate the spin-lattice relaxation rate (R_1) than previous reports[18]; (ii) a paramagnetic ion chelated lipid (Figure II-25) can be mixed homogeneously without altering the properties of other components of bicelles used in NMR experiments in this study; (iii) the significant reduction in the amount of the copper-chelated lipid considerably reduces the sample heating effect due to radio-frequency field and enable us to collect NMR data faster.

Isotropic bicelles containing a longer acyl chain phospholipid (DMPC : 1,2-dimyristoyl-*sn*-glycero-3-phosphocholine used in the present study) and a detergent (DHPC : 1,2-diheptanoyl-*sn*-glycero-3-phosphocholine used in the present study) with and without DMPE-DTPA chelator lipid were used in this study. DMPC, DHPC and DMPE-DTPA were purchased from Avanti Polar Lipids, Inc. (Alabaster, AL). All other chemicals were purchased from Sigma-Aldrich (St. Louis, MO) and used without further purification.

DMPC/DHPC isotropic bicelles were prepared using the following procedure. In the case of q=0.5, 55.0 mg of DMPC and 73.6 mg of DHPC lipid mixture and in the case of q= 0.25, 33.5 mg of DMPC and 89.5 mg of DHPC lipid mixture were cosolubilized in 1 ml of chloroform. Subsequently, chloroform was removed under a stream of N_2 gas to form a lipid film on the walls of a glass tube and the lipid film was kept under vacuum overnight to remove all residual solvents. The q=0.5 lipid films were solubilized into 366 µl of a 10 mM phosphate buffer at pH 7.4 (the q = 0.25 lipid films were solubilized into 350 µl of a 10 mM phosphate buffer). These transparent hydrated lipid mixtures were

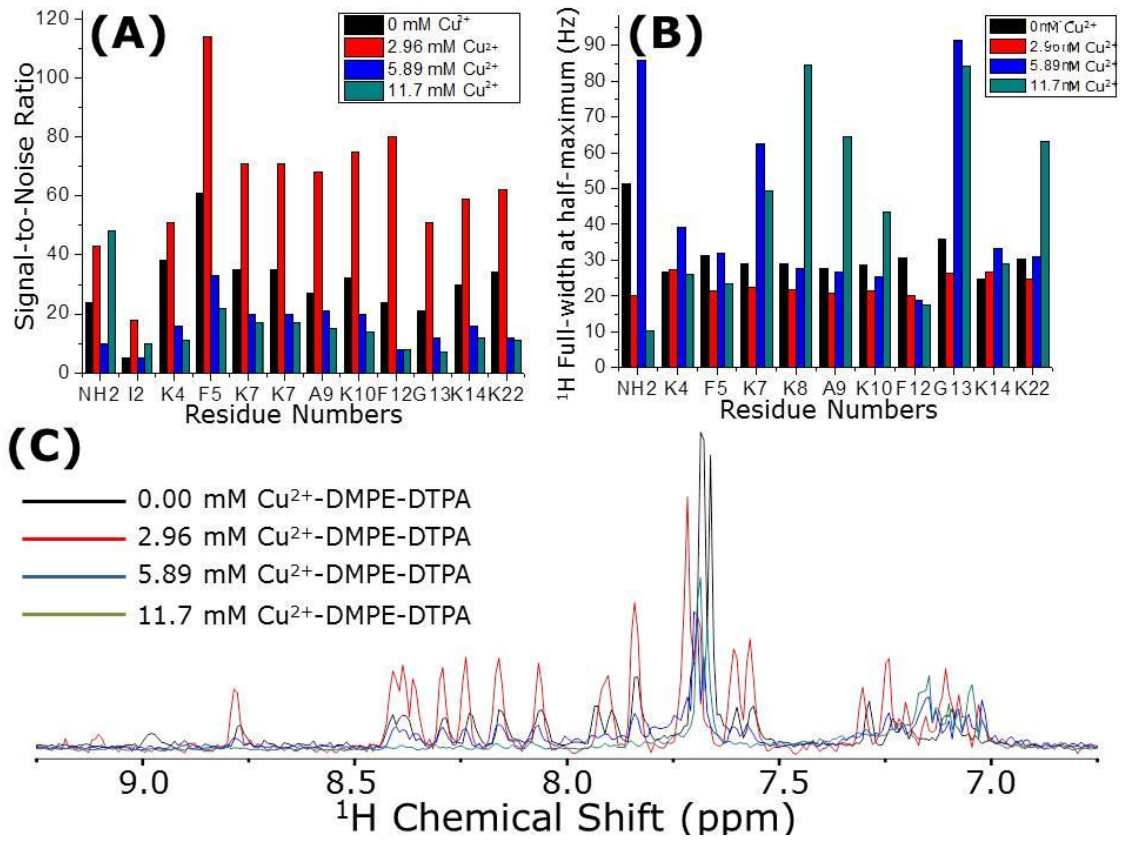

Figure II-43. **Signal-to-noise ratio (A) and Full-width at half-maximum (FWHM) values (B) obtained from 2D SOFAST-HMQC experiments** on q=0.5 isotropic bicelles containing a 6 mM unlabeled MSI-78 without Cu^{2+}-DMPE-DTPA (black), and with a 2.96 mM Cu^{2+}-DMPE-DTPA (red), 5.89 mM Cu^{2+}-DMPE-DTPA (blue) and 11.7 mM Cu^{2+}-DMPE-DTPA (green) at 35 ^{o}C. (C) One-dimensional ^{1}H chemical shift projections from 2D SOFAST-HMQC spectra. Spectra were obtained from a 900 MHz Bruker NMR spectrometer using a cryoprobe. Each 2D SOFAST-HMQC spectrum was obtained from 64 t_1 experiments, 256 scans, and a 100 ms recycle delay; the total data collection time (including the ~71 ms acquisition time and RF-free delays in the INEPT sequence) was ~54 min. The final 2D data matrix size was 2048 X 2048 after zero-filling in both dimensions. 2D data were processed using TOPSPIN 2.1 (from Bruker). Squared sine-bell function was employed in both dimensions with a π/4 shift. Resonance assignment and volume fit calculations were performed using SPARKY 3.113.

then vortexed and homogenized by gentle sonication in an ice bath for 30 minutes, and >4 freeze/heat cycles between liquid nitrogen and 40 °C of water. Once a satisfactory mixing of the components was completed, the sample (~330 µl) was transferred to a 5 mm Shigemi NMR glass tube. The isotropic bicelle formation was examined using ^{31}P-NMR experiments after 30 minutes of incubation at 35 ^{o}C in the NMR magnet.

Isotropic bicelles containing MSI-78 were prepared by mixing 130.2 mg of lipids (in the case of *q* ratio = 0.5, 1.65 mg of DMPE-DTPA, 55.0 mg of DMPC and 73.6 mg of DHPC) with 11.60 mg of (unlabeled) MSI-78. To prepare bicelles containing the copper-chelated lipid, 0.349 mg of $Cu(NO_5)_2 \cdot 2.5H_2O$ was added (for *q* ratio = 0.5 case) to a mixture of isotropic bicelles, peptide, and the chelator lipid after adding a 10 mM phosphate buffer at pH 7.4.

II-4-6. Solution-state NMR Results

Sensitivity of 2D ^{1}H/^{15}N SOFAST-HMQC experiments on bicelles containing MSI-78 was compared for various concentrations of Cu^{2+}-chelated DMPE in Figure II-40 (and also in Figure II-43). Our results suggest that, in addition to the T_1-shortening due to SOFAST effects, the presence of Cu^{2+} ions further decreased the T_1 values of amide-protons from MSI-78. As a result, the presence of a 2.96 mM Cu^{2+} was sufficient to increase the S/N by factor of 2 for all residues or to reduce the experimental time by a factor of ~4. Experiments were also performed on bicelles prepared with different concentrations of Cu^{2+}-chelated DMPE. Interestingly, 2.96 mM Cu^{2+}-chelated DMPE provided the highest sensitivity (Figure II-43). This is in agreement with an optimum T_1 reduction observed for bicelles containing 2.96 mM Cu^{2+}-chelated DMPE.

Since SOFAST-based experiments have limited applications due to the use of selective excitation RF pulses, regular 2D ^{1}H/^{15}N HSQC experiments were performed on bicelles containing MSI-78 with no ^{15}N labeling to measure the paramagnetic ion induced sensitivity gain for various concentrations of Cu^{2+}-chelated DMPE. Remarkably, bicelles containing the Cu^{2+}-chelated DMPE provided HSQC spectra with a reasonable S/N within 2 hours of experimental time, whereas there was no peak observed from a sample containing no paramagnetic ions (Figure II-44). To determine the optimized

experimental conditions, a series of 2D HSQC experiments was performed by keeping the total experimental time constant and varying the recycle delay. Results compared in Figure II-44 (and in Figure II-45) indicate that a 100 ms recycle delay is sufficient to obtain the best S/N. We also found that the 2D $^{1}H/^{15}N$ HSQC-TROSY experiment to work well on the same sample that was used to obtain results given in Figure II-44. As expected spectral lines observed in the 2D TROSY-HSQC spectrum (data not shown) were narrower than that observed in the regular HSQC spectra (Figure II-44). It is also worth mentioning that we were able to obtain a 2D $^{1}H/^{13}C$ HSQC spectrum (data not shown) from the bicelles sample containing a copper-chelated-DMPE; this was expected as a natural-abundance ^{13}C-detection based experiment is more sensitive than a natural-abundance ^{15}N-detection based experiment.

Since it is common to use isotropic bicelles with a *q* ratio <2, the effects of copper-chelated-DMPE on bicelles with *q*=0.25 and 0.5 were determined (Figure II-47). While experiments on both these samples provided excellent S/N, as seen in Figure II-47, *q*=0.25 bicelles provided better spectral resolution than that of *q*=0.5 bicelles. This could be attributed to the faster tumbling rate of *q*=0.25 bicelles than that of *q*=0.5 bicelles. These results suggest that the use of isotropic bicelles containing copper-chelated-DMPE would enable the fast acquisition of multidimensional spectra of membrane-associated proteins or peptides.

It should be noted that the measurement of functionally important data from model membranes containing membrane active peptides demands the use of a very low peptide concentration that makes NMR measurements to be difficult.[11] This becomes even more challenging when isotopically-labeled peptides are unavailable; this is unfortunately the case for a significant number of interesting systems such as mammalian membrane proteins and small peptides that lyse bacteria. It has been proven to be expensive to biologically obtain most membrane-associated peptides and proteins. Therefore, structural studies on such systems are often restricted to unlabeled peptides or site-specifically-labeled peptides. On the other hand, results presented in this study demonstrate the feasibility of NMR structural studies at natural-abundance of membrane-associated peptides and therefore could be useful to overcome the above-mentioned challenges. We note that previous studies have reported NMR spectra of short peptides

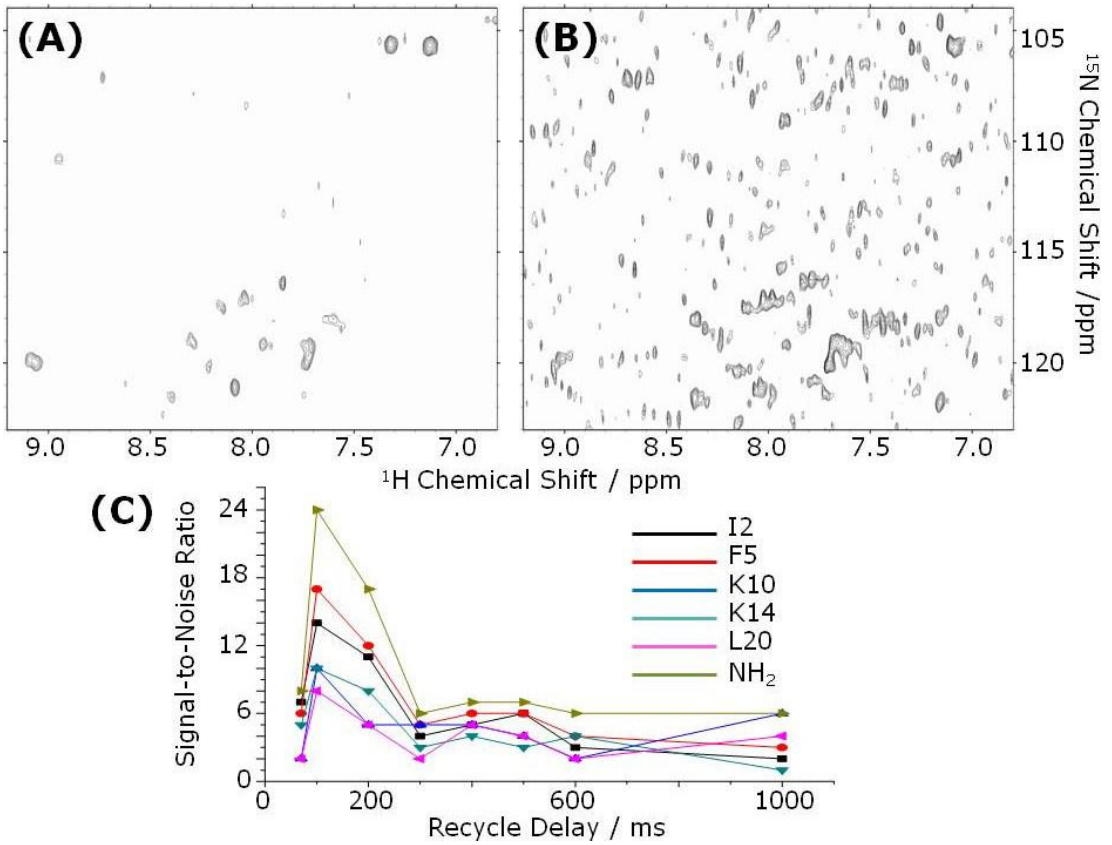

Figure II-44. **2D ^{1}H/^{15}N HSQC experiments with a 100 ms recycle delay provided the optimum S/N**. 2D HSQC spectra of *q*=0.5 isotropic bicelles containing a 9.3 mM unlabeled MSI-78 and a 2.96 mM copper-chelated lipid obtained by setting the total data collection time to 53 min with (A) 100 ms and (B) 600 ms recycle delays. (C) A comparison of the signal-to-noise ratio against recycle delay for selected peaks from 2D HSQC spectra; since the S/N observed for longer recycle delays was poor as seen in (B), only those peaks that had reasonable S/N are included in this plot. Our results indicated that there was no significant line broadening due to the paramagnetic effect was observed in any of the above-mentioned spectra (Figures II-38, II-39, II-46). Other experimental and data processing details are as mentioned in the Figure II-40 caption.

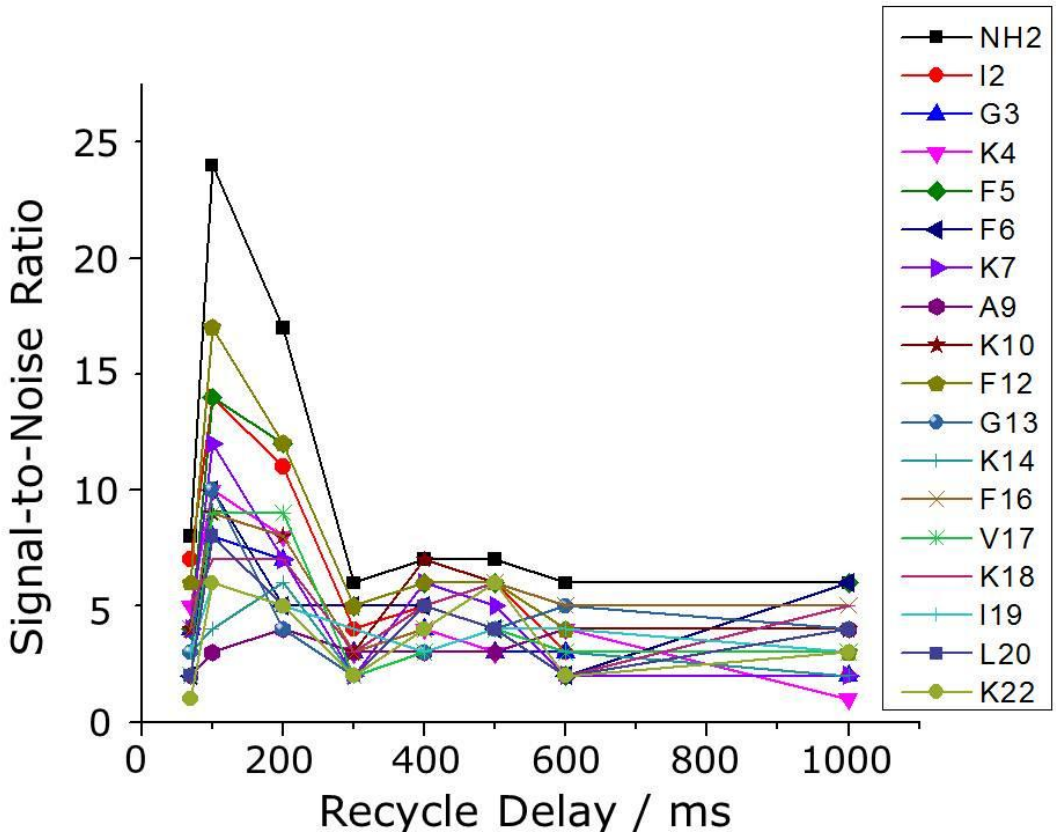

Figure II-45. **A comparison of the signal-to-noise ratios against recycle delay from 2D HSQC spectra** of 9.23 mM MSI-78 embedded in q = 0.5 DMPC/DHPC bicelles containing 2.96 mM Cu^{2+}-DMPE-DTPA cheated lipid. Each 2D ^{1}H-^{15}N HSQC spectrum was obtained from 64 t_1 experiments and the number of scans were adjusted to keep the total experimental time at 53 min. Other experimental and data processing details are as mentioned in Figure II-40 of the main text.

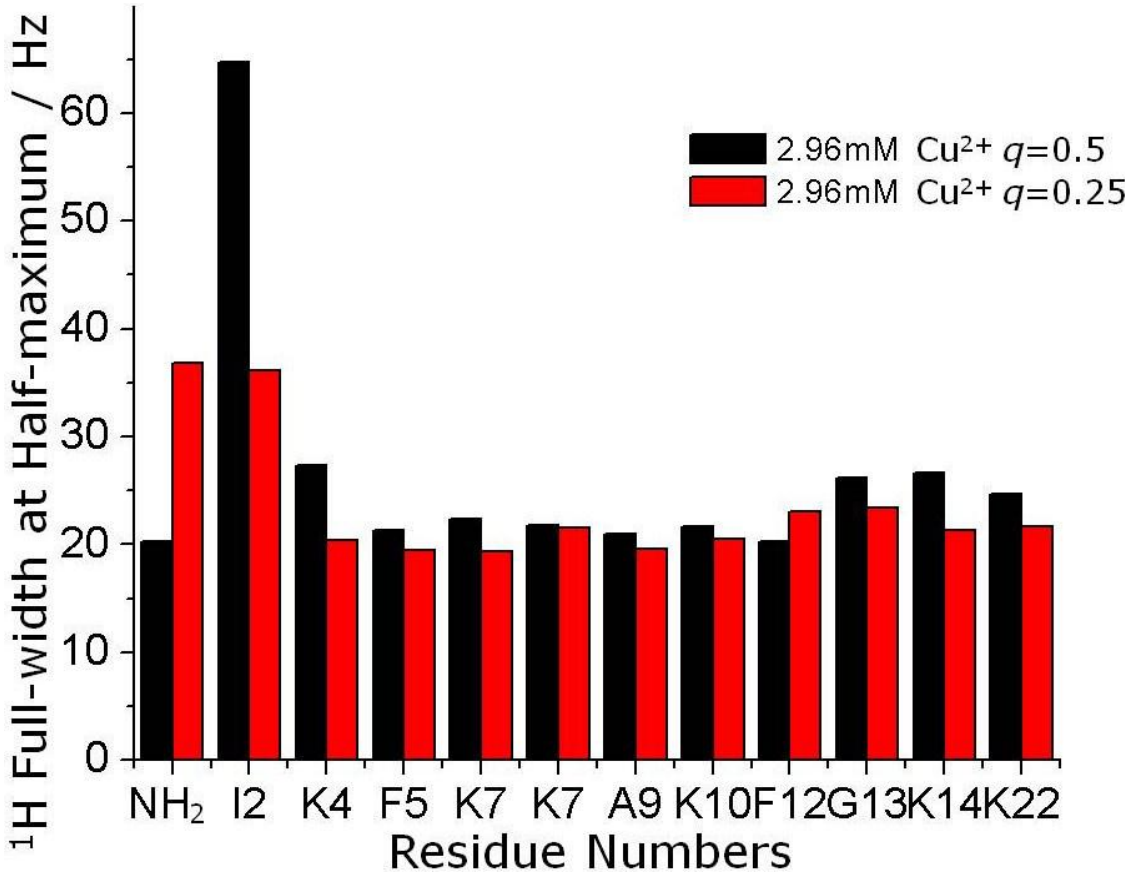

Figure II-46. **Full-width at half-maximum (FWHM) values obtained from 2D SOFAST-HMQC spectra** of a 9.23 mM unlabeled-MSI-78 embedded in DMPC/DHPC isotropic bicelles containing a 2.96 mM Cu^{2+}-DMPE-DTPA at 35 ^{o}C: q=0.5 (black) and q=0.25 (red). All spectra were obtained from a 900 MHz Bruker NMR spectrometer using a cryoprobe. Each 2D SOFAST_HMQC spectrum was obtained from 64 t_1 experiments, 256 scans, and a 100 ms recycle delay. The final 2D data matrix size was 2048 × 2048 after zero-filling in both dimensions. 2D data were processed using TOPSPIN 2.1 (from Bruker). Squared sine-bell function was employed in both dimensions with a $\pi/4$ shift. Resonance assignment and volume fit calculations were performed using SPARKY 3.113.

at natural-abundance but these studies used either high concentration of a water-soluble protein or long data acquisition and therefore such studies have not been common.[17]

Several solution and solid-state NMR studies on the successful use of paramagnetic salts to shorten the proton T_1 value of water-soluble systems have been previously reported.[18] The high concentration of paramagnetic salts (for example ~30 to 50 mM concentration) used in these studies are not suitable for membrane systems as the mobile paramagnetic ions are ineffective in shortening T_1 value of membrane embedded molecules and they could also result in RF heating and power lossy effects.[19] On the other hand, our approach effectively reduces the required concentration of the ion required to speed-up the T_1 process, and also renders the preparation of bicelles without altering their properties. The 4 times faster data acquisition than the SOFAST-based NMR experiments could be valuable to study various biochemical processes. Though line-narrowing instead of line-broadening due to the presence of Cu^{2+} was observed in our study (Figure II-39), a systematic analysis of the changes in T_2 values could be useful to determine the topology of a membrane protein as demonstrated in a previous study using Gd(DOTA).[20]

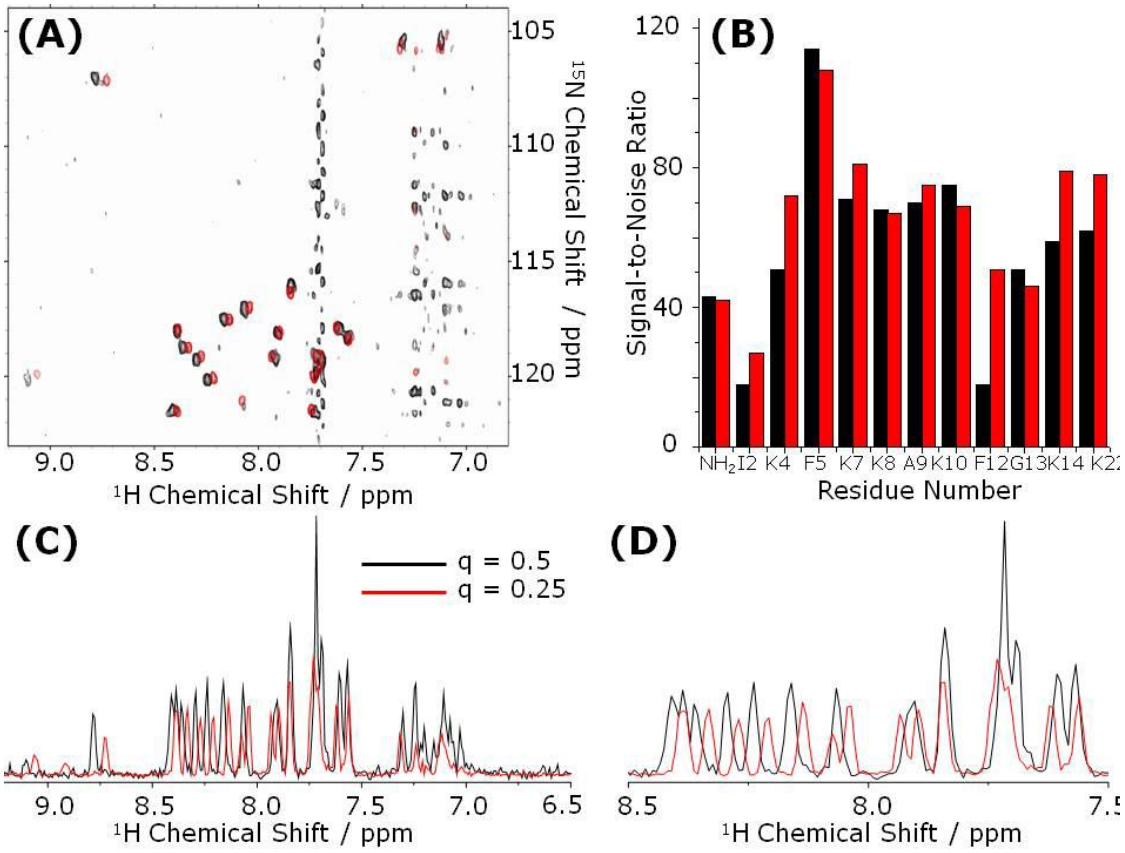

Figure II-47. **Isotropic bicelles with *q*=0.25 provided higher resolution and sensitivity than that of *q*=0.5.** (A) A comparison of 2D SOFAST-^{1}H/^{15}N-HMQC experiments of 9.3 mM unlabeled MSI-78 reconstituted in *q*=0.5 (dark) and *q*=0.25 (red) isotropic bicelles with a 2.96 mM Cu-DMPE-DTPA. Each 2D HSQC spectrum was obtained from 64 t_1 experiments and 256 scans. Other experimental and data processing details are as mentioned in Figure II-40 caption. Signal-to-noise ratio (B), 1D ^{1}H chemical shift projections (C), and expanded amide-proton chemical shift (7.5 to 8.5 ppm) regions (D) obtained from 2D SOFAST-HMQC spectra are compared.

II-5. References

II-2.

1 Ramamoorthy, A.; Wei, Y.; Lee, DK. *Annu. Rep. NMR Spectrosc.* **2004**, 52, 2.
2 Wu, CH.; Ramamoorthy, A.; Opella, SJ. *J. Magn. Reson. A.* **1994**, 109, 270.
3 Ramamamoorthy, A.; Wu, CH.; Opella SJ. *J. Magn. Reson.* **1999**, 140, 131.
4 Ramamamoorthy, A.; Opella, SJ. *Solid State Nucl. Magn. Reson.* **1995**, 4, 387.
5 Lee, M.; Goldberg, WI. *Phys. Rev. A.* **1965**, 140, 1261.
6 Mehring, M.; Waugh, JS. *Phys. Rev. B.* **1972**, 5, 3459.
7 Bielecki, A.; Kolbert AC.; de Groot HJM.; Griffin, RG.; Levitt, MH. *Adv. Magn. Reson.* **1990**, 14, 111.
8 Ravikumar, M.; Ramamoorthy, A. *Chem. Phys. Lett.* **1998**, 286, 199.
9 Vinogradov, E.; Madhu, PK.; Vega, S. *J. Chem. Phys.* **2001**, 115, 8983. Vinogradov, E.; Madhu, PK.; Vega, S. *Chem. Phys. Lett.* **1999**, 314, 443. *ibid* **2000**, 329, 207. *ibid* **2002**, 354, 193.
10 Jelinek, R.; Ramamoorthy, A.; Opella, SJ. *J. Am. Chem. Soc.* **1995**, 117, 12348.
11 Marassi, FM.; Ramamoorthy, A.; Opella, SJ. *Proc. Natl. Acad. Sci. U.S.A.* **1997**, 94, 8551.
12 Wu, CH.; Ramamoorthy, A.; Gierasch, LM.; Opella, SJ. *J. Am. Chem. Soc.* **1995**, 117, 6148.
13 Ramamoorthy, A.; Wu, CH.; Opella, SJ. *J. Am. Chem. Soc.* **1977**, 119, 10479.
14 Marassi, FM.; Opella, SJ. *J. Magn. Reson.* **2000**, 144, 150.
15 Wang, J.; Denny, J.; Tian, C.; Kim, S.; Mo, Y.; Kovacs, F.; Song, Z.; Nishimura, K.; Gan, Z.; Fu, R.; Quine, JR.; Cross, TA. *J. Magn. Reson.* **2000**, 144, 162.
16 Dvinskikh SV, Zimmermann H, Maliniak A, Sandström D. *J. Magn. Reson.* **2003**, 164, 165.
17 Ramamamoorthy, A.; Wu, CH.; Opella, SJ. *J. Magn. Reson. B.* **1995**, 107, 88.
18 Ramamamoorthy, A.; Gierasch, LM.; Opella, SJ. *J. Magn. Reson. B.* **1995**, 109, 112.
19 Ramamamoorthy, A.; Gierasch, LM.; Opella, SJ. *J. Magn. Reson. B.* **1996**, 111, 81.
20 Gu, ZT.; Opella, SJ. *J. Magn. Reson.* **1999**, 138, 193.
21 Gu, ZT.; Opella, SJ. *J. Magn. Reson.* **1999**, 140, 340.
22 Wei, Y.; Lee, D-K.; Hallock, KJ.; Ramamoorthy, A. *Chem. Phys. Lett.* **2002**, 351, 42.
23 Wei, Y.; Ramamoorthy, A. *Chem. Phys. Lett.* **2001**, 342, 312– 6.
24 Dvinskikh, SV.; Zimmermann, H.; Maliniak, A.; Sandström, D. *J. Chem. Phys.* **2005**, 122, 044512.
25 Rossum, BJV.; de Groot, CP.; Ladizhansky, V.; Vega, S.; de Groot, HJM. *J. Am. Chem. Soc.* **2000**, 122, 3465.
26 Fu RQ.; Tia, CL.; Cross, TA. *J. Magn. Reson.* **2002**, 154, 130.
27 Nevzorov, AA.; Opella, SJ. *J. Magn. Reson.* **2003**, 164, 182.

28 Yamamoto, K.; Lee, DK.; Ramamoorthy, A. *Chem. Phys. Lett.* **2005**, 407, 289–293.
29 Bak, M.; Rasmussen, JT.; Nielsen, NC. *J. Magn. Reson.* **2000**, 147, 296.
30 Lee, DK.; Wittebort, RJ.; Ramamoorthy, A. *J. Am. Chem. Soc.* **1998**, 120, 8868.
31 Lee, DK.; Ramamoorthy, A. *J. Magn. Reson.* **1998**, 113, 204.
32 Lee, DK.; Santos, JS.; Ramamoorthy, A. *Chem. Phys. Lett.* **1999**, 309, 209.
33 Lee, DK.; Wei, Y.; Ramamoorthy, A. *J. Phys. Chem. B.* **2001**, 105, 4752.
34 Wei, Y.; Lee, DK.; McDermott, AE.; Ramamoorthy, A. *J. Magn. Reson.* **2002**, 158, 23.
35 Brender, JR.; Taylor, DM.; Ramamoorthy, A. *J. Am. Chem. Soc.* **2001**, 123, 914.
36 Poon, A.; Birn, J.; Ramamoorthy, A. *J. Phys. Chem. B.* **2004**, 108, 16577.
37 Ladizhansky, V.; Vega, S. *J. Chem. Phys.* **2000**, 112, 7158.
38 Shekar, SC.; Ramamoorthy, A. *Chem. Phys. Lett.* **2001**, 342, 312.
39 Shekar, SC.; Lee, D-K.; Ramamoorthy, A. *J. Magn. Reson.* **2002**, 157, 223.
40 Shekar, SC.; Lee, D-K.; Ramamoorthy, A. *J. Am. Chem. Soc.* **1995**, 123, 7467.
41 Martin, RW.; Zilm, KW. *J. Magn. Reson.* **2004**, 168, 202.
42 Dvinskikh, SV.; Castro, D.; Sandstrom, H. *Magn. Reson. Chem.* **2004**, 42, 875.
43 Takegoshi, K.; McDowell, CA. *J. Magn. Reson.* **1986**, 67, 356.
44 Lee, DK.; Narasimhaswamy, T.; Ramamoorthy, A. *Chem. Phys. Lett.* **2004**, 399, 359.
45 Nishimura, K.; Naito, A. *Chem. Phys. Lett.* **2005**, 402, 245.
46 Gan, Z. *J. Magn. Reson.* **2000**, 143, 136.
47 Dvinskikh, SV.; Zimmermann, H.; Maliniak, A.; Sandström, D. *J. Magn. Reson.* **2003**, 163, 46.

II-3.

1 Opella, S.J.; Marassi, F.M. *Chem. Rev.* **2004**, 104, 3587–3606.
2 Prosser, R.S.; Evanics, F.; Kitevski, J.L.; Al-Abdul-Wahid, M.S. *Biochemistry* **2006**, 45, 8453–8465.
3 Sanders, C.R.; Prosser, R.S. *Structure* **1998**, 6, 1227–1234.
4 Sanders, C.R.; Prestegard, J.H. *Biophys. J.* **1990**, 58, 447–460.
5 Sanders, C.R.; Schwonek, J.P. *Biochemistry* **1992**, 31, 8898–8905.
6 Sanders, C.R.; Hare, B.J.; Howard, K.P.; Prestegard, J.H. *Prog. Nucl. Magn. Reson. Spectrosc.* **1994**, 26, 421–444.
7 Nevzorov, A.A.; DeAngelis, A.A.; Park, S.H.; Opella, S.J. in: A. Ramamoorthy (Ed.), *NMR Spectroscopy of Biological Solids*, Taylor and Francis, New York, **2005**, Chapter 7.
8 Lorigan, G.A. in: A. Ramamoorthy (Ed.), *NMR Spectroscopy of Biological Solids*, Taylor and Francis, New York, **2005**, Chapter 10.
9 Marcotte, I.; Auger, M. *Concep. Magn. Reson., Part A* **2005**, 24, 17–37.

10 Pines, A.; Gibby, M.G.; Waugh, J.S. *J. Chem. Phys.* **1973**, 59, 569–590.
11 Kim, H.; Cross, T.A.; Fu, R.Q. *J. Magn. Reson.* **2004**, 168, 147–152.
12 Lee, D.K.; Santos, J.S.; Ramamoorthy, A. *J. Phys. Chem. B*, **1999**, 103, 8383.
13 Katoh, E.; Takegoshi, K.; Terao, T. *J. Am. Chem. Soc.* **2004**, 126, 3653–3657.
14 Haeberlen, U.; Waugh, J.S. *Phys. Rev.* **1968**, 175, 453.
15 Mehring, M. *Principles of High Resolution NMR in Solids, second ed.*, Springer-Verlag, Heidelberg, **1983**.
16 Kelly, A.E.; Ou, H.D.; Withers, R.; Dotsch, V. *J. Am. Chem. Soc.* **2002**, 124, 12013–12019.
17 Li, C.G.; Mo, Y.M.; Hu, J.; Chekmenev, E.; Tian, C.L.; Gao, F.P.; Fu, R.Q.; Gor'kov, P.; Brey, W.; Cross, T.A. *J. Magn. Reson.* **2006**, 180, 51–57.
18 Lee, D.K.; Wildman, K.A.H.; Ramamoorthy, A. *J. Am. Chem. Soc.* 2004, 126, 2318–2319.
19 Martin, R.W.; Zilm, K.W. *J. Magn. Reson.* **2004**, 168, 202–209.
20 Waugh, J.S. *Proc. Natl. Acad. Sci. USA* **1976**, 73, 1394–1397.
21 Ramamoorthy, A.; Wei, Y.; Lee, D.-K. *Annu. Rep. NMR Spectrosc.* **2004**, 52, 1–52.
22 Hindman, J.C. *J. Chem. Phys.* **1966**, 44, 4582–4592.
23 Dvinskikh, S.V.; Castro, V.; Sandström, D. *Magn. Reson. Chem.* **2004**, 42, 875–881.
24 Led, J.J.; Petersen, S.B. *J. Magn. Reson.* **1978**, 32, 1–17.
25 Kugel, H. *J. Magn. Reson.* **1991**, 91, 179–185.
26 Wu, C.H.; Ramamoorthy, A.; Opella, S.J. *J. Magn. Reson. A* **1994**, 109, 270–272.
27 Ramamoorthy, A.; Opella, S.J. *Solid state NMR Spectrosc.* **1995**, 4, 387.
28 Ramamoorthy, A.; Wu, C.H.; Opella, S.J. *J. Magn. Reson.* **1999**, 140, 131–140.
29 Hester, R.K.; Ackerman, J.L.; Neff, B.L.; Waugh, J.S. *Phys. Rev. Lett.* **1976**, 36, 1081–1083.
30 Yamamoto, K.; Lee, D.K.; Ramamoorthy, A. *Chem. Phys. Lett.* **2005**, 407, 289–293.
31 Yamamoto, K.; Dvinskikh, S.V.; Ramamoorthy, A. *Chem. Phys. Lett.* **2006**, 419, 533–536.
32 Dvinskikh, S.V.; Yamamoto, K.; Ramamoorthy, A. *Chem. Phys. Lett.* **2006**, 419, 168–173.
33 Nevzorov, A.A.; Opella, S.J. *J. Magn. Reson.* **2003**, 164, 182–186.
34 Lee, D.K.; Narasimhaswamy, T.; Ramamoorthy, A. *Chem. Phys. Lett.* **2004**, 399, 359–362.
35 Dvinskikh, S.V.; Yamamoto, K.; Ramamoorthy, A. *J. Chem. Phys.* **2006**, 125, 034507.
36 Hoult, D.I.; Lauterbur, P.C. *J. Magn. Reson.* **1979**, 34, 425–433.
37 Doty, F.D. in: Grant, D.M.; Harris, R.K. (Eds.), *Encyclopedia of Nuclear Magnetic Resonance, Wiley*, Chichester, **1996**, p. 3753.
38 Marassi, F.M.; Crowell, K.J. *J. Magn. Reson.* **2003**, 161, 64–69.
39 Stringer, J.A.; Bronnimann, C.E.; Mullen, C.G.; Zhou, D.H.H.; Stellfox, S.A.; Li, Y.; Williams, E.H.; Rienstra, C.M. *J. Magn. Reson.* **2005**, 173, 40–48.

40 Gor'kov, P.L.; Chekmenev, E.Y.; Fu, R.Q.; Hu, J.; Cross, T.A. *J. Magn. Reson.* **2006**, 181, 9–20.
41 Morris, G.A. *J. Am. Chem. Soc.* **1980**, 102, 428–429.
42 Neuhaus, D. in: Grant, D.M.; Harris, R.K. (Eds.), *Encyclopedia of Nuclear Magnetic Resonance*, Wiley, Chichester, **1996**, p. 3290.
43 Hartmann, S.R.; Hahn, E.L. *Phys. Rev.* **1962**, 128, 2042.
44 Metz, G.; Wu, X.; Smith, S.O. *J. Magn. Reson. Ser. A* **1994**, 110, 219–227.
45 Warschawski, D.E.; Devaux, P.F. *J. Magn. Reson.* **2000**, 145, 367–372.
46 Khitrin, A.K.; Fung, B.M.; McGeorge, G. in Grant, D.M.; Harris, R.K. (Eds.), *Encyclopedia of Nuclear Magnetic Resonance*, Wiley, Chichester, **2002**, p. 91.
47 Bennett, A.E.; Rienstra, C.M.; Auger, M.; Lakshmi, K.V.; Griffin, R.G. *J. Chem. Phys.* **1995**, 103, 6951–6958.
48 Fung, B.M.; Khitrin, A.K.; Ermolaev, K. *J. Magn. Reson.* **2000**, 142, 97–101.
49 Shaka, A.J.; Keeler, J.; Freeman, R. *J.Magn. Reson.* **1983**, 53, 313–340.
50 Mohebbi, A.; Shaka, A.J. *Chem. Phys. Lett.* **1991**, 178, 374–378.
51 Dvinskikh, S.V.; Sitnikov, R.; Furó, I. *J. Magn. Reson.* **2000**, 142, 102–110.
52 Sinha, N.; Grant, C.V.; Wu, C.H.; De Angelis, A.A.; Howell, S.C.; Opella, S.J. *J. Magn. Reson.* **2005**, 177, 197–202.
53 Rothgeb, T.M.; Oldfield, E.J. *J. Biol. Chem.* **1981**, 256, 6004–6009.
54 Santos, J.S.; Lee, D.K.; Ramamoorthy, A. *Magn. Reson. Chem.* **2004**, 42, 105–114.
55 Smith, R.; Separovic, F.; Bennett, F.C.; Cornell, B.A. *Biophys. J.* **1992**, 63, 469–474.
56 Seelig, J.; Macdonald, P.M.; Scherer, P.G. *Biochemistry* **1987**, 26, 7535–7541.
57 Semchyschyn, D.J.; Macdonald, P.M. *Magn. Reson. Chem.* **2004**, 42, 89–104.
58 R.S. Prosser, H. Bryant, R.G. Bryant, R.R. Vold, *J. Magn. Reson.* 141 (1999) 256–260.
59 Ramamoorthy, A.; Thennarasu, S.; Lee, D.K.; Tan, A.; Maloy, L. *Biophys. J.* **2006**, 91, 206–216.
60 Lindstrom, F.; Williamson, P.T.F.; Grobner, G. *J. Am. Chem. Soc.* **2005**, 127, 6610–6616.
61 Lindstrom, F.; Bokvist, M.; Sparrman, T.; Grobner, G. *Phys. Chem. Chem. Phys.* **2002**, 4, 5524–5530.
62 Ramamoorthy, A.; Thennarasu, S.; Tan, A.; Gottipati, K.; Sreekumar, S.; Heyl, D.L.; An, F.Y.P.; Shelburne, C.E. *Biochemistry* **2006**, 45, 6529–6540.
63 Lu, J.X.; Damodaran, K.; Lorigan, G.A. *J. Magn. Reson.* **2006**, 178, 283–287.
64 Dvinskikh, S.; Dürr, U.; Yamamoto, K.; Ramamoorthy, A. *J. Am. Chem. Soc.* **2006**, 128, 6326.
65 Park, S.H.; Prytulla, S.; De Angelis, A.A.; Brown, J.M.; Kiefer, H.; Opella, S.J. *J. Am. Chem. Soc.* **2006**, 128, 7402–7403.
66 Prosser, R.S.; Hunt, S.A.; DiNatale, J.A.; Vold, R.R. *J. Am. Chem. Soc.* **1996**, 118, 269–270.
67 Prosser, R.S.; Hwang, J.S.; Vold, R.R. *Biophys. J.* **1998**, 74, 2405–2418.
68 Sternin, E.; Bloom, M.; Mackay, A.L. *J. Magn. Reson.* **1983**, 55, 274–282.

II-4.

1 (a) Lange, A.; Giller, K.; Hornig, S.; Martin-Eauclaire, M. F.; Pongs, O.; Becker, S.; Baldus, M. *Nature* **2006**, *440*, 959. (b) Dürr, U. H. N.; Waskell, L.; Ramamoorthy, A. *Biochim. Biophys. Acta* **2007**, *1768*, 3235. (c) Lorieau, J. K.; Day, L. A.; McDermott, A. E. *Proc. Natl. Acad. Sci. U.S.A.* **2008**, *105*, 10366. (d) Xu, J. D.; Dürr, U. H. N.; Im, S. C.; Gan, Z. H.; Waskell, L.; Ramamoorthy, A. *Angew. Chem., Int. Ed.* **2008**, *47*, 7864.

2 (a) Ganapathy, S.; Naito, A.; McDowell, C. A. *J. Am. Chem. Soc.* **1981**, *103*, 6011. (b) Wickramasinghe, N. P.; Kotecha, M.; Samoson, A.; Past, J.; Ishii, Y. *J. Magn. Reson.* **2007**, *184*, 350. (c) Wickramasinghe, N. P.; Parthasarathy, S.; Jones, C. R.; Bhardwaj, C.; Long, F.; Kotecha, M.; Mehboob, S.; Fung, L. W.; Past, J.; Samoson, A.; Ishii, Y. *Nat. Methods* **2009**, *6*, 215. (d) Wickramasinghe, N. P.; Shaibat, M.; Ishii, Y. *J. Am. Chem. Soc.* **2005**, *127*, 5796. (e) Weliky, D. P.; Bennett, A. E.; Zvi, A.; Anglister, J.; Steinbach, P. J.; Tycko, R. *Nat. Struct. Biol.* **1999**, *6*, 141. (f) Linser, R.; Chevelkov, V.; Diehl, A.; Reif, B. J. *J. Magn. Reson.* **2007**, *189*, 209. (g) Cai, S.; Seu, C.; Kovacs, Z.; Sherry, A. D.; Chen, Y. *J. Am. Chem. Soc.* **2006**, *128*, 13474.

3 DeMarco, M. L.; Woods, R. J.; Prestegard, J. H.; Tian, F. *J. Am. Chem. Soc.* **2010**, *132*, 1334.

4 (a) Kawulka, K.; Sprules, T.; McKay, R. T.; Mercier, P.; Diaper, C. M.; Zuber, P.; Vederas, J. C. *J. Am. Chem. Soc.* **2003**, *125*, 4726. (b) Thennarasu, S.; Lee, D. K.; Poon, A.; Kawulka, K. E.; Vederas, J. C.; Ramamoorthy, A. *Chem. Phys. Lipids* **2005**, *137*, 38.

5 Metz, G.; Wu, X.; Smith, S. O. J. Magn. Reson., Ser. A 1994, 110, 219.

6 (a) Sanders, C. R.; Hare, B. J.; Howard, K. P.; Prestegard, J. H. Prog. Nucl. Magn. Reson. Spectrosc. 1994, 26, 421. (b) Prosser, R. S.; Evanics, F.; Kitevski, J. L.; Al-Abdul-Wahid, M. S. Biochemistry 2006, 45, 8453. (c) Inbaraj, J. J.; Cardon, T. B.; Laryukhin, M.; Grosser, S. M.; Lorigan, G. A. J. Am. Chem. Soc. 2006, 128, 9549. (d) Yamamoto, K.; Soong, R.; Ramamoorthy, A. Langmuir 2009, 25, 7010. (e) Prosser, S. R.; Volkov, V. B.; Shiyanovskaya, I. V. Biophys. J. 1998, 75, 2163. (f) Dvinskikh, S. V.; Yamamoto, K.; Dürr, U. H. N.; Ramamoorthy, A. J. Magn. Reson. 2007, 184, 228.

7 Bennett, A. E.; Ok, J. H.; Griffin, R. G.; Vega, S. J. Chem. Phys. 1992, 96, 8624.

8 (a) McNeill, S. A.; Gor'kov, P. L.; Shetty, K.; Brey, W. W.; Long, J. R. J. Magn. Reson. 2009, 197, 135. (b) Gor'kov, P. L.; Chekmenev, E. Y.; Li, C.; Cotten, M.; Buffy, J. J.; Traaseth, N. J.; Veglia, G.; Brey, W. W. J. Magn. Reson. 2007, 185, 77. (c) Stringer, J. A.; Bronnimann, C. E.; Mullen, C. G.; Zhou, D. H.; Stellfox, S. A.; Li, Y.; Williams, E. H.; Rienstra, C. M. J. Magn. Reson. 2005, 173, 40.

9 (a) Lange, A.; Giller, K.; Hornig, S.; Martin-Eauclaire, M. F.; Pongs, O.; Becker, S.; Baldus, M. *Nature* **2006**, *440*, 959-962; (b) Dürr, U.H.N.; Waskell, L.; Ramamoorthy, A. *Biochim. Biophys. Acta.* **2007**, *1768*, 3235-3259. (c) Stanczak, P.; Horst, R.; Serrano, P.; Wüthrich, K. *J. Am. Chem. Soc.* **2009**,

131, 18450-18456. (d) Van Horn, W. D.; Kim, H. J.; Ellis, C. D.; Hadziselimovic, A.; Sulistijo, E. S.; Karra, M. D.; Tian, C.; Sönnichsen, F. D.; Sanders, C. R. *Science* **2009**, *324*, 1726-1729. (e) Lorieau, J. K.; Day, L. A.; McDermott, A. E. *Proc. Natl. Acad. Sci.* **2008**, *105*, 10366-10371. (f) Xu, J.D.; Dürr, U.H.N.; Im, S.C.; Gan, Z.H.; Waskell, L.; Ramamoorthy, A. *Angew. Chem. Intl. Ed*. **2008**, *47*, 7864-7867. (g) Concalves, J.A.; Ahuja, S.; Erfani, S.; Eilers, M.; Smith, S.O. *Proc. Nucl. Magn. Reson. Spectrosc.* **2010**, *57*, 159-180. (h) Akutsu, H.; Egawa, A.; Fujiwara, T. *Photosynth. Res.* **2010**, *104*, 221-231. (i) Gautier, A.; Mott, H.R.; Bostock, M.J.; Kirkpatrick, J.P.; Nietlispach, D. *Nat. Struct. Mol. Biol.* **2010**, *17*, 768-774.

10 (a) Thurber, K.R.; Yau, W.M.; Tycko, R. *J. Magn. Reson.***2010**, *204*, 303-313. (b) Fujiwara, T.; Ramamoorthy, A. *Ann.Rep.NMR Spectrosc.* **2006**, *58*, 155-175. (c) Opella, S.J.; Marassi, F.M. *Chem. Rev.***2004**, *104*, 3587-3606.

11 (a) Ieronimo, M.; Afonin, S.; Kock, K.; Berditsch, M.; Wadhwani, P.; Ulrich, A.S. *J. Am. Chem. Soc.* **2010**, *132*, 8822-8824. (b) Dürr, U.H.N.; Sudheendra, U.S.; Ramamoorthy, A. *Biochim. Biophys. Acta.***2006**, *1758*, 1408-1425. (c) Salnikov, E.; Rosay, M.; Pawsey, S.; Ouari, O.; Tordo, P.; Bechinger, B. *J. Am. Chem. Soc.* **2010**, *132*, 5940-5941.

12 Gottler, L. M.; Ramamoorthy, A. *Biochim. Biophys. Acta. 1788*, **2009**, 1680-1686.

13 Schanda, P.; Brutscher, B. *J. Am. Chem. Soc.***2005**, *127*, 8014-8015.

14 (a) Sanders, C.R.; Hare, B.J.; Howard, K.P.; Prestegard, J.H. *Prog. Nucl. Magn. Reson. Spec.* **1994**, *26*, 421-444. (b) Prosser, R.S.; Evanics, F.; Kitevski, J.L.; Al-Abdul-Wahid, M.S. *Biochemistry* **2006**, *45*, 8453-8465. (c) Inbaraj, J.J.; Cardon, T.B.; Laryukhin, M.; Grosser, S.M.; Lorigan, G.A. *J. Am. Chem. Soc.* **2006**, *128*, 9549-9554. (d) Yamamoto, K.; Soong, R.; Ramamoorthy, A. *Langmuir* **2009**, *25*, 7010-7018. (e) Dvinskikh, S.V.; Dürr, U.H.N.; Yamamoto, K.; Ramamoorthy, A. *J. Am. Chem. Soc.***2007**, *129*, 794-802.

15 Porcelli, F.; Buck-Koehntop, B.A.; Thennarasu, S.; Ramamoorthy, A.; Veglia, G. *Biochemistry*. *45*, **2006**, 5793-5799.

16 Ramamoorthy, A.; Thennarasu, S.; Lee, D.K.; Tan, A.; Maloy, L. *Biopys. J. 91*, **2006**, 206-216.

17 Ortiz-Polo, G.; Krishnamoorthi, R.; Markley, J.L. *J. Magn. Reson.* **1986**, *68*, 303-310; (b) Wang, G. *Biochim. Biophys. Acta.* **2010**, *1798*, 114-121.

18 (a) Ganapathy, S.; Naito, A.; McDowell, C.A. *J. Am. Chem. Soc.* **1981**, *103*, 6011-6015. (b) Wickramasinghe, N.P.; Kotecha, M.; Samoson, A.; Past, J.; Ishii, Y. *J. Magn. Reson.*, **2007**, *184*, 350–356. (c) Wickramasinghe, N.P.; Parthasarathy, S.; Jones, C.R.; Bhardwaj, C.; Long, F.; Kotecha, M.; Mehboob, S.; Fung, L.W.; Past, J.; Samoson, A.; Ishii, Y. *Nat. Methods* **2009**, *6*, 215-218. (d) Linser, R.; Chevelkov, V.; Diehl, A.; Reif, B. *J. Magn. Reson.* **2007**, *189*, 209-216. (e) Cai, S.; Seu, C.; Kovacs, Z.; Sherry, A.D.; Chen, Y. *J. Am. Chem. Soc.* **2006**, *128*, 13474-13478. (f) Nadaud, P.S.; Helmus, J.J.; Sengupta, I.; Jaroniec, C.P. *J. Am. Chem. Soc.* **2010**, *132*, 9561-9563. (g) DeMarco, M.L.; Woods, R.J.; Prestegard, J.H.; Tian, F. *J. Am. Chem. Soc.* **2010**, *132*, 1334-1338. (h) Otting, G. *Ann. Rev. Biophys.* **2010**, *39*, 387-405.

19 Yamamoto, K.; Xu, J.; Kawulka, K.E.; Vederas, J.C.; Ramamoorthy, A. *J. Am. Chem. Soc.***2010**, *132*, 6929-6931.
20 Hilty, C.; Wider, G.; Fernández, C.; Wüthrich, K. *ChemBioChem.* **2004**, *5*, 467-473.

Chapter III

Nuclear Magnetic Resonance Spectroscopy on Membrane Bilayers[†]

III-1. Summary

Magnetically aligned bicelles are increasingly being used as model membranes in solution- and solid-state NMR studies of the structure, dynamics, topology, and interaction of membrane-associated ligands, peptides and proteins. These studies commonly utilize the Separated-Local-Field pulse sequences such as PISEMA, HIMSELF, SAMMY and PELF to measure dipolar coupling and chemical shift, the two key parameters used in subsequent structural analysis. The results presented in this chapter demonstrate that the PISEMA-type and other rotating-frame pulse sequences are not suitable for the measurement of long-range heteronuclear dipolar couplings, and that they provide inaccurate values when multiple protons are coupled to a ^{13}C nucleus. Furthermore, we demonstrate that a laboratory-frame Separated-Local-Field experiment is capable of overcoming these difficulties in magnetically aligned bicelles. An extension of this approach to accurately measure ^{13}C-^{31}P and ^{1}H-^{31}P couplings from phospholipids, which are useful to understand the interaction of molecules with the membrane bilayers, is also described. In these two dimensional experiments, natural abundance ^{13}C was observed from bicelles containing DMPC and DHPC lipid molecules. As a first application, these solid-state NMR approaches were utilized to probe the membrane

[†] This chapter is a version of manuscripts published in *J. Am. Chem. Soc.*, 128(2006)6326-6327., *J. Am. Chem. Soc.*, 129(2007)794-802. and *Langmuir*, 25(2009)7010-7018. This study was supported by the funds from NIH and NSF.

interaction of an antimicrobial peptpide, MSI-78, and an antidepressant molecule, desipramine, and their locations in the membrane bilayers.

Bicelles of various lipid/detergent ratios are commonly used in nuclear magnetic resonance (NMR) studies of membrane-associated molecules without the need to freeze the sample. While a decrease in the size (defined at a low temperature or by the q value) of a bicelle decreases its overall order parameter, the variation of lipid dynamics with a change in the lipid/detergent ratio is unknown. In this study, we report a thorough atomistic level analysis on the variation of lipid dynamics with the size and hydration level of bicelles composed of a phospholipid, 1,2-dimyristoyl-sn-glycero-3-phosphocholine (DMPC), and a detergent, 1,2-dihexanoyl-sn-glycero-3-phosphocholine (DHPC). Two-dimensional (2D) separated-local-field NMR experiments were performed on magnetically aligned bicelles to measure ^{1}H-^{13}C dipolar couplings, which were used to determine order parameters at various (head-group, glycerol, and acyl chain) regions of lipids in the bilayer. From our analysis, we uncover the extreme sensitivity of the glycerol region to the motion of the bicelle, which can be attributed to the effect of viscosity because of an extensive network of hydrogen bonds. As such, the water-membrane interface region exhibits the highest order parameter values among all three regions of a lipid molecule. Our experimental results demonstrate that the laboratory-frame 2D proton-detected-local-field pulse sequence is well-suited for the accurate measurement of motionally averaged (or long-range) weak and multiple ^{1}H-^{13}C dipolar couplings associated with a single carbon site at the natural abundance of ^{13}C nuclei.

III-2. High Resolution Two Dimensional NMR Spectroscopy to Measure the Membrane-Ligand Interactions

While structural studies using solution NMR and crystallography have provided significant insights into the functional aspects of water-soluble molecules, extension of such studies to membrane-associated molecules has been a challenge.[1] However, a great deal of progress in obtaining high-resolution structures of membrane proteins using crystallography and solution NMR methods has recently been made.[2-9] These pioneering advances strongly rely on the preparation of samples that satisfy the requirements of the

chosen method.[3,5] For example, crystallography requires a single crystal that provides high quality diffraction data, while solution NMR experiments need well-behaved protein-containing micelles that can tumble rapidly enough to provide high-resolution spectra. These requirements are difficult to satisfy for most membrane-associated systems. In addition, such samples are not suitable to measure protein-membrane interactions at a high resolution, which determine the properties of molecules embedded in the cell membrane. This is unfortunate since the structure, dynamics, folding, and function of a significant number of proteins in the human genome are controlled by their ability to interact with the cell membrane. Therefore, it is highly valuable to measure the membrane interaction of such molecules, and it is also essential to develop biophysical techniques that can deliver such information for any membrane protein. Recent studies have shown that solid-state NMR spectroscopy of phospholipid bilayers is well-suited for such measurements.[5,10-20]

Lipid bilayers in the form of either unaligned multilamellar vesicles (MLVs) or aligned samples are typically used for solid-state NMR studies. MLVs are used under static sample conditions to measure the anisotropic interactions like chemical shift, dipolar coupling, and quadrupolar coupling which are useful to characterize the dynamics of a protein and to determine various properties of lipid bilayers including phase, domains, and curvature strain.[21,22] MLVs are also used under magic angle spinning (MAS) conditions to obtain high-resolution spectra that can be utilized to determine the high-resolution structure of embedded proteins/peptides. However, recent studies have shown that such structural studies require either low water content and/or frozen samples to suppress molecular dynamics that degrade the spectral resolution.[18,19] On the other hand, macroscopically oriented bilayer samples have been used under well-hydrated conditions to determine the backbone conformation, dynamics, and topology of transmembrane proteins.[5,10-14,23] Such samples have also been used to determine the structure and function of membrane-permeating peptides.[21,22,24-26] In these studies bilayer samples are prepared either by mechanical alignment using glass plates or by magnetic alignment. While the preparation of an aligned sample depends on the physicochemical properties of a protein present in the sample, use of well-aligned samples has the unique advantage of preserving anisotropic spin interactions, which are highly informative in the structural

studies. Recent studies demonstrated that the magnetically aligned bicelles are more suitable than mechanically aligned samples for the structural studies of membrane proteins.[5,13,27] The major advantages of using bicelles are that they occupy less volume, which reduces the radio frequency (RF) coil size and thereby the RF power requirement, are relatively easy to prepare, and are stable for a long time. Therefore, considerable efforts have been devoted to develop magnetically aligned bicelles for structural studies.[27-34]

Bicelles are aggregates composed of short- and long-chain phospholipids in an aqueous buffer that exhibit a liquid crystalline phase macroscopically orientating in the presence of an external magnetic field. The shape and size of these aggregates is controlled by the molar ratio, q, of long-chain lipids to short-chain ones. At a high $q >$ 2.5 value, the phase can be described as perforated, dynamical lamellar bilayers.[35] Decreasing the q value produces the disc-shaped bicelle morphology where a flat bilayer composed of long-chain lipids is surrounded on the perimeter by short-chain molecules.[30] Bicelles can be prepared with any desired degree of ordering: highly oriented aggregates are used in solid-state NMR studies, while weakly aligned bicelles are employed as an alignment medium for structural studies on weakly aligned biomolecules using solution NMR methods. Several studies have reported on the preparation, characterization, and applications of bicelles,[28-34] and recent publications demonstrated the usefulness of bicelles for structural studies of proteins using heteronuclear dipolar couplings.[27,36,37]

One of the most popular approaches to measure heteronuclear dipolar couplings is the 2D separation of heteronuclear dipolar interactions according to chemical shifts. Since dipolar couplings correspond to local magnetic fields in the molecule, this class of experiments is referred to as Separated-Local-Field (SLF) spectroscopy.[12,38,39] Dipolar couplings between directly bonded ^{1}H-^{13}C spin pairs as well as generally weaker dipolar interactions between remote spins can be accessed depending on the experimental design. Large ^{13}C chemical shift dispersion provides a high chemical resolution, which simplifies the assignment and allows for the separation of dipolar coupling multiplets. There are several experimental protocols for SLF spectroscopy which differ in the details of the preparation and evolution periods, while in all cases the ^{13}C signal is observed during the detection period t_2 as it evolves under the ^{13}C chemical shift interaction and in the

presence of ^{1}H decoupling. These general protocols are applicable to both the stationary and MAS sample.[12,39] In the present study, we have compared three different 2D approaches for the measurement of ^{13}C-^{1}H dipolar interactions from the lipid molecules in aligned bicelles containing DMPC and DHPC molecules under static conditions.

Our results suggest that the PISEMA (*p*olarization *i*nversion and *s*pin *ex*change at the *m*agic *a*ngle)[40-42] and other rotating-frame pulse sequences are not suitable for the measurement of long-range heteronuclear dipolar couplings, and they provide inaccurate values when multiple protons are coupled to a ^{13}C nucleus. Instead, a 2D PELF (Proton Evolved Local Field) sequence,[43] which is a laboratory-frame Separated-Local-Field experiment, is capable of overcoming these difficulties in magnetically aligned bicelles. These results are directly transferable to 2D SLF studies of ^{15}N nuclei, where they are typically applied for structural measurements on uniformly ^{15}N labeled membrane proteins. Furthermore, with a simple modification in the 2D PELF sequence, we demonstrate that, in addition to ^{1}H-^{13}C couplings, remote ^{13}C-^{31}P and ^{1}H-^{31}P couplings from phospholipids can be measured in bicelles. It should be mentioned here that the 2D PELF pulse sequence has been used in previous studies to obtain high-resolution SLF spectra of solids by overcoming the difficulties found when multiple protons are coupled with a ^{13}C nucleus.[43]

Since lipids play important roles in the folding and function of membrane-associated molecules, these experiments will be useful to measure the dynamics and conformation of lipid molecules. Such measurements also provide insights into the function of membrane-permeating peptides such as antimicrobial, toxin, fusion, and channel-forming molecules. Similar information has previously been obtained in ^{2}H NMR studies of deuterated lipids[44] and proton spin diffusion measurements.[45,46] The approach proposed in the present study, besides avoiding the isotopic labeling, benefits from the higher chemical resolution and a more straightforward signal assignment. In contrast to ^{2}H NMR, our results show that the structural information obtained in ^{13}C spectra is not limited to the orientation of a single bond C-H vector. Couplings between remote ^{13}C and ^{1}H spins and between ^{13}C and ^{31}P nuclei are also accessible. These solid-state NMR approaches are presently being utilized to understand the membrane interaction of a variety of molecules including antidepressants, dendrimers, proteins, and polypeptides.

As an application, the topology of an antidepressant molecule, desipramine, determined from these measurements is presented in this section.

III-2-1. Experimental Procedure

Sample Preparation.

1,2-Dimyristoyl-*sn*-glycero-3-phosphatidylcholine (DMPC) and 1,2-dihexanoyl-*sn*-glycero-3-phosphatidylcholine (DHPC) were purchased from Avanti Polar Lipids, Inc. (Alabaster, AL). DMPC and DHPC with a molar ratio (q = DMPC/DHPC) of 3.5:1 were dissolved in chloroform. The solvent was slowly evaporated under a stream of nitrogen gas at room temperature and completely removed by overnight lyophilization. A 100 mM HEPES buffer at pH 7.0 was added to obtain a concentration of 37.5% (w/w) phospholipids to solution. The sample was vortexed until all of the lipids were solubilized in the HEPES buffer. The solubilized sample was gently sonicated in an ice-cold water bath. The final sample was obtained by several freeze and thaw cycles until a clear transparent solution was formed. Bicelles containing desipramine were also prepared using the above-mentioned procedure.

NMR Measurements.

NMR experiments were carried out on a Chemagnetics/Varian Infinity-400 MHz solid-state NMR spectrometer using a 5 mmdouble-resonance magic-angle spinning probe under static sample conditions. About 100 mg of sample were loaded in a 5 mm NMR glass tube of 4 cm length, and the tube was closed tightly with Teflon tape and a cap. The sample was equilibrated for about 1 h in the magnet at 37 °C prior to the measurement. ^{31}P NMR spectra were recorded using Hahn-echo experiments with a 90° pulse length of 5 μs and under a 30 kHz continuous wave proton decoupling. A ramped cross-polarization (ramp-CP)[47] sequence with a contact time of 5 ms was used to record the 1D ^{13}C spectra under proton decoupling using various decoupling sequences for a comparative study, while the FLOPSY (flip-flop spectroscopy)-8[48] multiple pulse sequence was used in other experiments as it provided the best resolution. 2D ^{13}C spectra were obtained using 128 t_1 experiments, 64 scans, a 5 s recycling delay, and a 20 kHz ^{1}H decoupling. All measurements were performed at 37 °C.

III-2-2. Orientation of Bicelles in the Magnetic Field.

To obtain a highly resolved ^{13}C NMR spectrum of stationary bicelles, it is essential to align the sample in the magnetic field of the spectrometer. The degree of alignment of bicelles was examined by recording the proton decoupled ^{31}P chemical shift spectra. Figure III-1 shows the ^{31}P chemical shift spectrum of a 3.5:1 DMPC/DHPC bicelle sample at 37 °C, referenced by setting the isotropic chemical shift peak observed at 10 °C to 0 ppm. Two peaks in the spectrum are assigned to DMPC (-11.4 ppm) and DHPC (-4.4. ppm) molecules in the sample as indicated based on previous studies on bicelles;[30] the ratio of signal intensities equals the DMPC/DHPC molar ratio. The frequency position (-11.4 ppm) and a narrow line width (100 Hz) of the DMPC resonance in the spectrum suggest that the bicelle sample is well aligned with the bilayer normal (or the bicelle axis) perpendicular to the external magnetic field of the spectrometer.

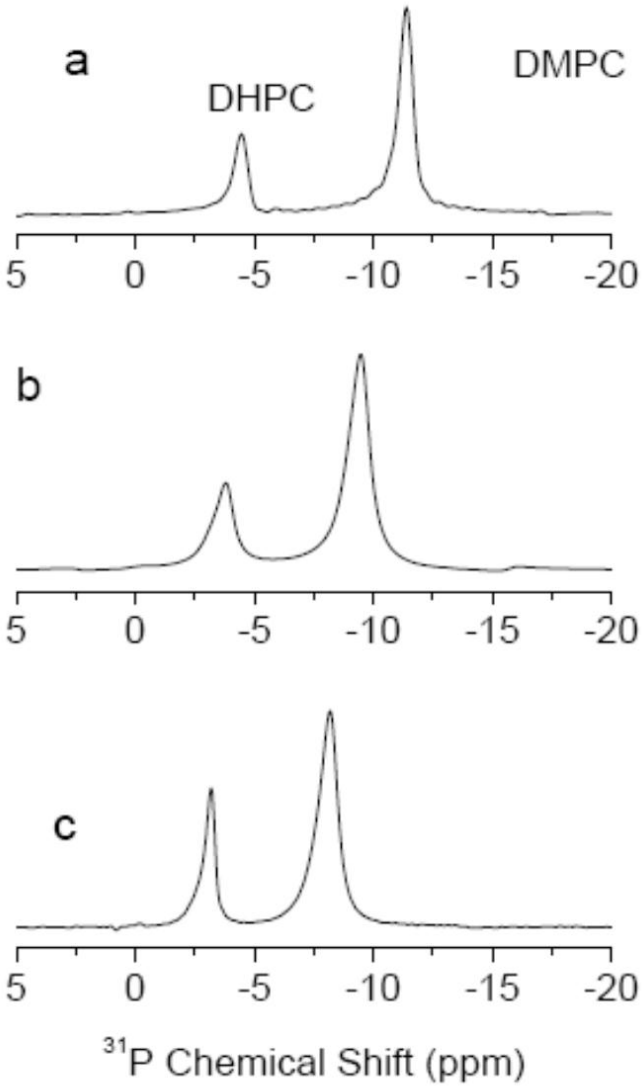

Figure III-1. **^{31}P Chemical Shift NMR spectra of bicelle samples with different concentrations of MSI-78 peptide**: (a) 0 mole %, (b) 0.5 mole % and (c) 2.0 mole % MSI-78. Spectra were obtained by acquiring the FID after a $\pi/2$ (90^{o}) R.F. pulse in the presence of 10 kHz proton decoupling. 64 transients were accumulated with a recycle delay of 3 s. The chemical shift scale was referenced by setting the isotropic peak observed at 10^{o}C to 0 ppm.

III-2-3. Two Dimensional Separated-Local-Field Experiments.

In the conventional SLF sequence,[39] the ^{13}C transverse magnetization evolves under multiple 1H-^{13}C heteronuclear dipolar couplings during the evolution period t_1 (Figure III-2a). In the proton-evolved local-field (PELF) experiment,[43] on the other hand, the ^{1}H transverse magnetization evolves under the local field of ^{13}C spins during t_1 and is subsequently transferred to carbons for detection (Figure III-2b). In the case of rare carbon-13 spins (spin *S*) coupled with abundant protons (spins *I*), the heteronuclear dipolar interaction term of the spin Hamiltonian can be written as

$$H_{IS} = \sum_i \omega_{IS}^{(i)} 2I_z^{(i)} S_z \quad (1)$$

where $\omega_{IS}^{(i)} = 2\pi d_{IS}^{(i)} = -(\mu_0/4\pi)(\gamma_I\gamma_S\hbar/r_i^3)$ is the dipolar coupling constant. Since the Hamiltonians for individual *IS* couplings commute, the time evolution of the transverse magnetization is calculated by successive action of individual dipolar coupling terms on the density operator.[39] The structure of the modulation experienced by evolved spins is, however, different in conventional SLF and PELF experiments. In the conventional SLF sequence, where an *S* spin evolves in the presence of local fields, the relevant term of the density operator contributing to the detected signal is given by

$$S_{x/y} \prod_i \cos \omega_{IS}^{(i)} \quad (2)$$

On the other hand, in the case of a PELF experiment, where each evolving spin $I^{(i)}$ is subject to the evolution under the heteronuclear coupling to a single *S* spin, the relevant density operator has the form

$$\sum_i I_{x/y}^{(i)} \cos \omega_{IS}^{(i)} \quad (3)$$

Therefore, the dipolar coupling dimension of the conventional 2D SLF spectrum, where each additional proton contributes with a successive first-order splitting, has a more complicated multiplet-type structure. In contrast, the dipolar coupling dimension of the 2D PELF spectrum is

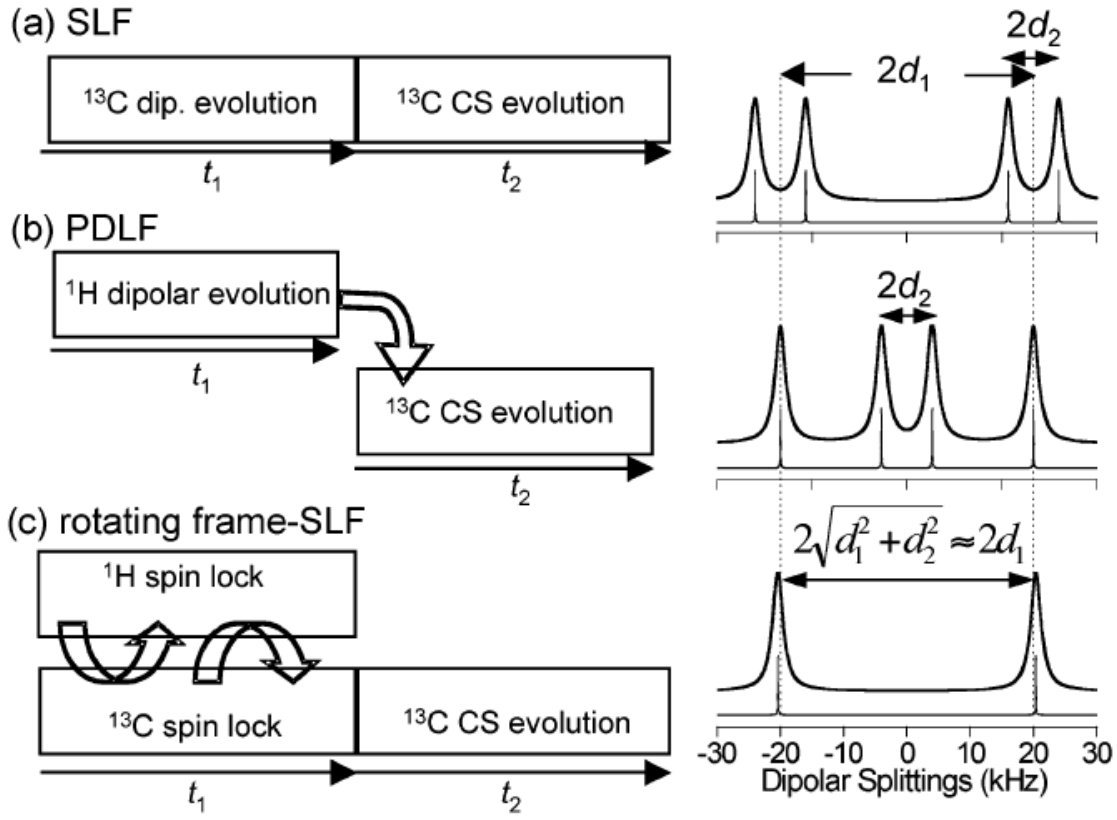

Figure III-2. **Experimental protocols of 2D experiments used for the measurements of heteronuclear dipolar couplings and the corresponding simulated dipolar coupling spectra for a three-spin system CH_2** with $d_{CH(1)}$ = 20 kHz and $d_{CH(2)}$ = 4 kHz. (a) SLF; (b) PDLF; (c) Rotating-frame SLF.

governed by a simple two spin interaction and presents a superposition of dipolar coupling doublets.

In rotating-frame local field experiments (Figure III-2c),[12] the dipolar couplings are monitored through oscillations resulting from the coherent spin exchange in the rotating frame. In the presence of the spin-lock RF fields matched at the Hartmann-Hahn condition[12,39] the heteronuclear dipolar coupling Hamiltonian is given by the flip-flop terms

$$H_{IS} = \frac{1}{2}\sum_i \omega_{IS}^{(i)}(I_+^{(i)}S_- + I_-^{(i)}S_+) \quad (4)$$

The noncommuting nature of the individual terms in this Hamiltonian results in the truncation of small heteronuclear couplings, and therefore the resolution of large dipolar coupling is enhanced.[12] This effect is well demonstrated in experiments that employed rotating-frame local field pulse sequences like PISEMA,[40] SAMMY,[49] BB-PISEMA (i.e., broadband-PISEMA), [50,51] PITANSEMA (Polarization Inversion Time Averaged Nutation Spin Exchange at the Magic Angle),[52,53] and HIMSELF (heteronuclear isotropic mixing leading to spin exchange via the local field).[54-56] Experimental and simulated results suggest that the dipolar coupling resolutions in all these methods are comparable when there are only a few protons in a spin cluster.

Efficient homonuclear ^{1}H decoupling during the evolution (or t_1) period of an SLF sequence is important for an accurate measurement of heteronuclear dipolar couplings. The windowless sequences BLEW-n[57], WIM (windowless isotropic mixing)-24,[58] LG (Lee-Goldburg),[59] FFLG (Flip-Flop Lee-Goldburg[60] or Frequency Switched Lee-Goldburg[61]), and magic echo sandwiches[62] have been employed to achieve adequate resolution in the rotating-frame SLF experiments. The uses of FFLG decoupling and magic echo sandwiches were named as PISEMA[40] and SAMMY,[49] respectively. Recently, WIM-24[54] and BLEW-type[55] sequences have also been introduced in such experiments. The unique feature of WIM and BLEW spin-locking is that they create an isotropic mixing dipolar coupling Hamiltonian, and therefore the corresponding 2D sequences are called HIMSELF.[54-56]

In a PELF experiment, where each pairwise ^{13}C-^{1}H spin interaction in a $^{13}CH_n$ spin system results in a separate doublet, the observed dipolar splitting $\Delta\nu$ is related to the coupling constant d simply by $\Delta\nu = 2kd$; $k = 0.42$ is the scaling factor of the homonuclear decoupling sequence BLEW-48. This value was calibrated using a 2D $^{1}H/^{13}C$ HETCOR experiment and closely matched the theoretically predicted value of 0.424.[57] Therefore, the measurement of heteronuclear dipolar couplings is straightforward using this 2D experiment. In contrast, in a 2D PISEMA spectrum, such a simple relationship holds only for the case of an isolated ^{13}C-^{1}H spin pair or for a CH_2 group with two equivalent C-H dipolar couplings (scaling factors are, respectively, $k = 0.79$ and $\sqrt{2} \times 0.79$, in the case of BB-PISEMA). Generally, for a CH_2 spin system the two dipolar couplings are entangled in the spectral splitting, $\Delta\nu = 2k(d_1^2 + d_2^2)^{1/2}$, and cannot easily be extracted from PISEMA and other rotating-frame experiments. For a rapidly rotating CH_3 methyl group, the theory predicts that the dipolar coupling PISEMA spectrum exhibits three different dipolar splittings: $2kd_{CH3}$, $2\sqrt{3}kd_{CH3}$, and $4kd_{CH3}$. Numerical simulations performed using the SIMPSON program[63] for a three-spin H-C-H system are given in Figure III-2. The dipolar coupling constants $d_1 = 20$ and $d_2 = 4$ kHz were used in the simulations. Increasing the number of remote protons deteriorates the resolution of large dipolar coupling spectral lines in the conventional SLF and to a lesser extent in rotating-frame SLF while it is essentially unaffected in PELF.[43,56,64] In the PELF experiment, a short contact time of the CP step suppresses signal from weak dipolar couplings, while a very long contact time could allow contributions from very remote spins which could result in doublets with very small splittings or an unresolved zero-frequency peak in the dipolar coupling spectrum. Therefore, a careful choice of contact time allows us to maximize the resolution in the 2D PELF spectrum.

III-2-4. Two Dimensional ^{13}C Separated-Local-Field Experiments on Oriented Bicelles.

In this section, we demonstrate and compare the 2D dipolar coupling spectra obtained using SLF, PELF, and PISEMA techniques. The details of the pulse sequences can be found elsewhere.[12,39,40,43] For the PISEMA experiment the frequency offset-compensated

modification of the basic sequence (called the broadband-PISEMA)[50,51] was used to suppress the effects of the chemical shifts and the proton resonance frequency offsets.

A 2D PELF spectrum that correlates the ^{13}C chemical shift and ^{1}H-^{13}C dipolar couplings is shown in Figure III-3a. Also shown is the 1D ^{13}C chemical shift spectrum of DMPC/DHPC bicelles along with the assignment of peaks to DMPC carbons. The 2D spectrum exhibits highly resolved doublets in the indirect frequency dimension corresponding to the combined dipolar and scalar interactions between directly bonded ^{13}C-^{1}H spin pairs. A number of doublets with small splittings arising from dipolar couplings between remote spins are also seen in Figure III-3a. Some of the heavily overlapped signals in the chemical shift dimension, from C_4 to C_{11} sites of acyl chains of DMPC, are resolved in the 2D spectrum. The resolution of this group is increased at a higher temperature as shown in Figure III-3b. Representative slices along the dipolar coupling dimension of the PELF spectrum are displayed in Figure III-4 (middle column). These spectral slices are compared with the corresponding slices obtained from conventional 2D SLF and PISEMA spectra. As expected, peaks in the conventional SLF spectrum are very broad. PELF provides a resolution which is better than or comparable to PISEMA. The inner doublets with smaller splittings in the PELF spectrum are due to couplings between remote spins. If assigned, these splittings could provide additional valuable structural constraints. The dipolar splitting values obtained from three different 2D experiments are, in general, in good agreement.

Experimental dipolar coupling spectra were simulated using the SIMPSON program. Simulated and experimental dipolar coupling spectra for C_2 and β carbons of the DMPC molecule are given in Figure III-5. Coupling constants used in the simulations are $d_1 = d_2 = 1.7$ kHz for C_2 and $d_1 = 1.15$ and $d_2 = 0.26$ kHz for β (as given in Table 1). For an easier comparison the frequency axes in the figure were corrected with the scaling factor of the corresponding pulse sequence, 0.42 (for SLF and PELF) and $0.79\cdot\sqrt{2}$ (for BB-PISEMA). Only couplings to directly bonded protons are accounted for in the simulations. All coupling constant d ($d = [D_{CH} + J_{CH}/2]$) values are given in Table III-1, where J_{CH} and D_{CH} are the scalar coupling constant and motionally averaged dipolar coupling constant, respectively.

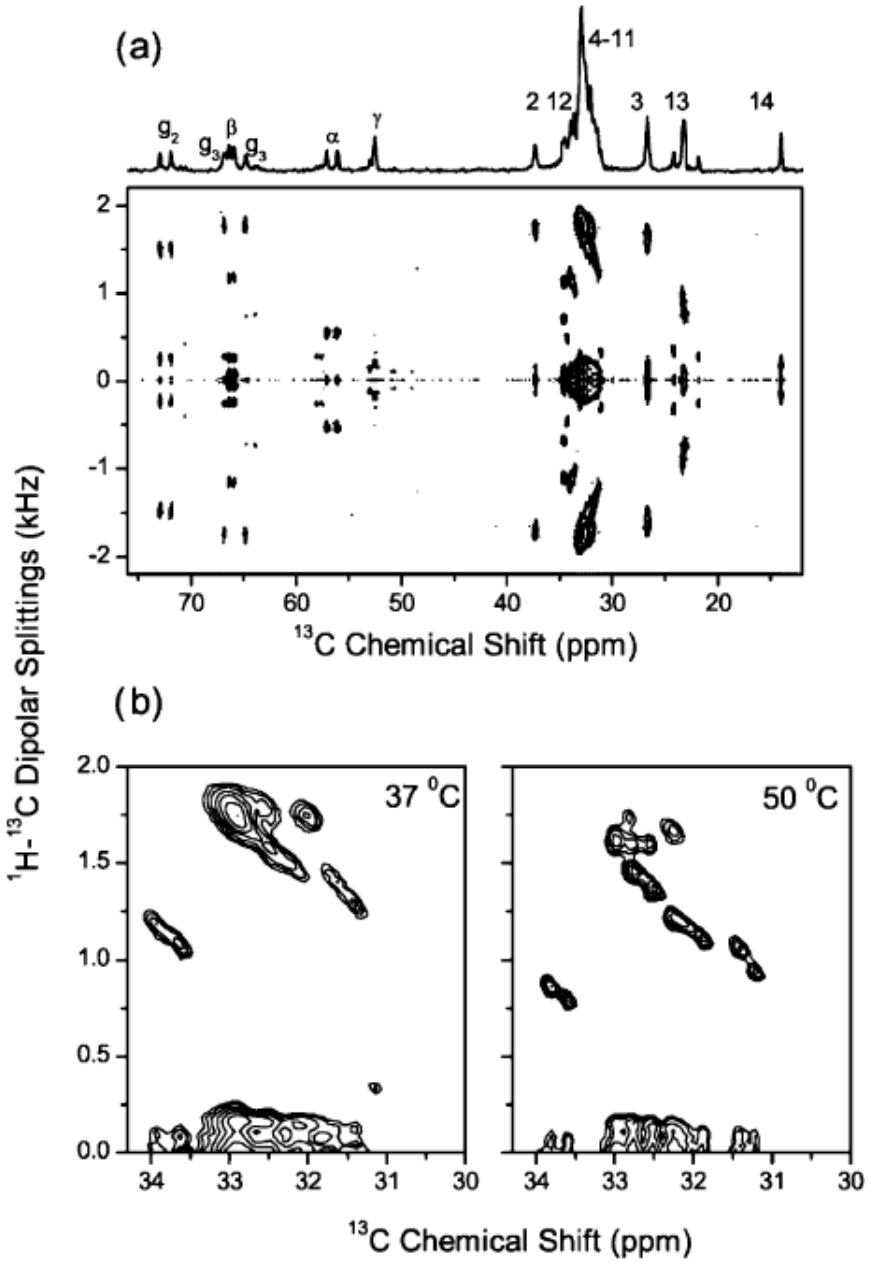

Figure III-3. (a) **A 2D PDLF spectrum of DMPC/DHPC bicelles at 37 °C.** 64 scans were accumulated for each of 200 points in the t_1 dimension with an increment time of 384 μs. The contact time for the CP transfer was set to 3.0 ms. Proton RF field during the t_1 evolution corresponded to 31 kHz. A 1D ^{13}C chemical shift spectrum is shown at the top with assignments of peaks to individual carbons of the DMPC molecule. (b) Part of the PDLF spectrum in DMPC/DHPC bicelles at 50 °C demonstrating the increased dipolar resolution in the crowded spectra range between 31 and 34 ppm. Corresponding part of the PDLF spectrum obtained at 37 °C is also shown for comparison.

Generally, C-H dipolar and scalar (or *J*) couplings are entangled in the observed splittings. The contribution from the *J*-coupling is significant for a directly bonded C-H spin pair, particularly in the highly mobile terminal groups of the lipid molecule. While the value and sign of *J*-coupling is known from other NMR studies, the ambiguity of extracting the dipolar coupling remains since the sign of the dipolar coupling term is generally not obvious. Geometry arguments can be invoked to solve this issue.[65] In addition to ^{13}C-^{1}H couplings, ^{13}C-^{31}P dipolar couplings of phospholipids can be accurately measured from the 2D PELF spectrum. Since different ^{13}C-^{31}P multiplets, overlapped in a 1D ^{13}C spectrum, are well separated in the 2D spectrum due to the difference in the ^{13}C-^{1}H coupling values for different carbon sites, the resolution is increased and the peak assignment is straightforward. (Another way to separate the ^{13}C-^{31}P multiplets is to perform the conventional ^{13}C-^{31}P 2D Separated-Local-Field experiment in the presence of proton heteronuclear decoupling.[66] This, however, requires a $^{13}C/^{31}P/\ ^{1}H$ triple channel probe.)

For most of the CH_2 sites, the spin couplings estimated from the splittings in PISEMA spectra under the assumption of equivalent dipolar couplings, $d_1 = d_2$, are in agreement with those measured directly from PELF spectra. An exception is, however, found in the case of the $\hat{a}$-carbon coupling. This is because the specific average orientation of the β-CH_2 segment with respect to the main molecular rotational axis results in inequivalent ^{13}C-^{1}H dipolar couplings. From the two distinct doublets observed for this site in the PELF spectrum, the spin couplings are estimated to be $d_1^{(PDLF)} = 1.15$ and $d_2^{(PDLF)} = 0.26$ kHz. Hence, the apparent coupling constant in the PISEMA experiment is calculated to be $(d_1^2 + d_2^2)^{1/2} = 1.18$ kHz, which is consistent with that estimated from the experimental PISEMA splitting (see Table III-1).

These experiments were also performed on 3.5:1 DMPC:DHPC bicelles containing a designed antimicrobial peptide, MSI-78 (or commercially known as plexiganan) (two dimensional spectra data is not shown). Previous studies have shown that this peptide has a broad spectrum of antimicrobial activity and is more potent than the naturally occurring magainins (magain2 and PGLa), forms an amphipathic α-helical structure in lipid bilayers, and alters the conformation of the lipid headgroup upon binding. Representative dipolar coupling slices are given in Figure 3-4(A) to show the peptide-

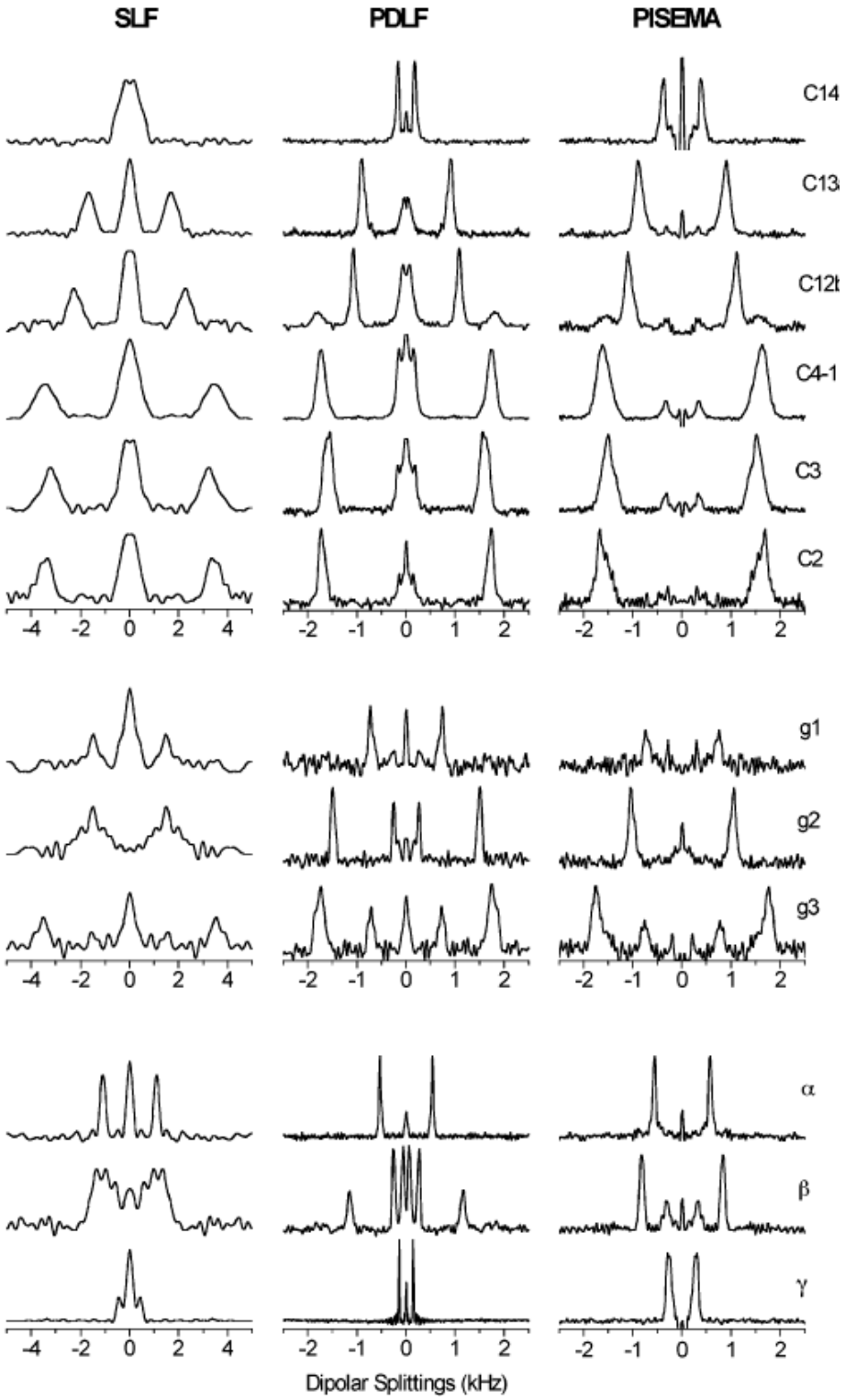

Figure III-4. **Representative slices along the dipolar coupling dimensions from SLF, PDLF, and PISEMA spectra.** Frequency axes were corrected for the respective dipolar scaling factors $k = 0.42$ (SLF and PDLF) and $0.79 \times \sqrt{2}$ (PISEMA).

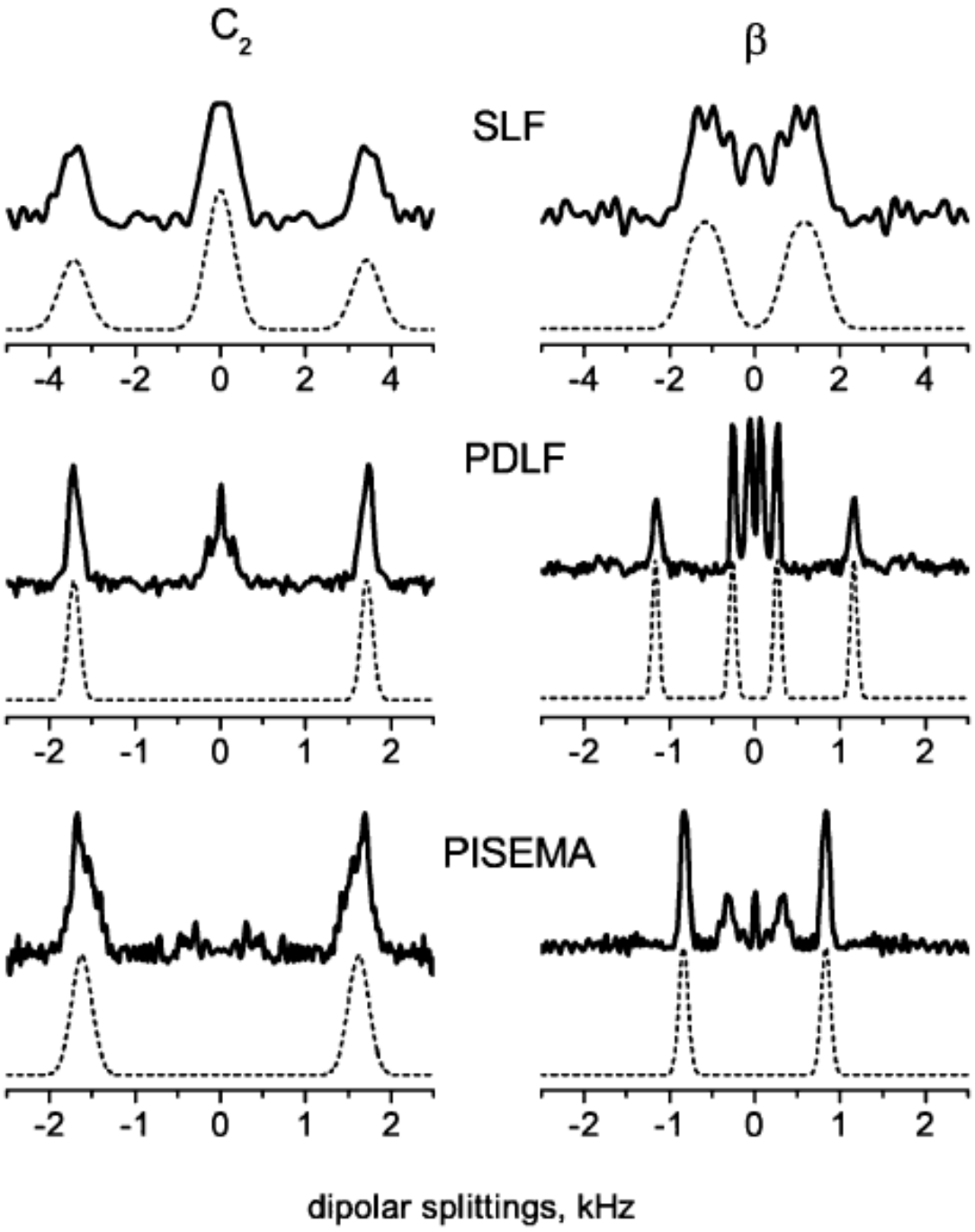

Figure III-5. **Simulated (dashed lines) and experimental (solid lines) ^{1}H-^{13}C dipolar coupling spectra corresponding to C_2 and β carbons of the DMPC molecule obtained using SLF, PDLF, and PISEMA pulse sequences.** Only couplings to directly bonded protons are accounted for in the simulations. Frequency axes were corrected for the respective dipolar coupling scaling factors k = 0.42 (SLF and PDLF) and 0.79 (PISEMA).

site	SLF[c]	PDLF[c]	PISEMA[d]	desipramine 2 mol %	desipramine 10 mol %
C_{14}		0.17(0.03)		0.13	0.13
C_{13}	0.85(0.20)	0.91(0.06)	0.90(0.10)	0.66	0.68
C_{12}	1.14(0.30)	1.08(0.05)	1.11(0.10)	1.00	0.93
C_{4-11}	1.73(0.40)	1.73(0.10)	1.63(0.16)	1.52	1.63
C_3	1.61(0.40)	1.59(0.10)	1.53(0.15)	1.51	1.61
C_2	1.72(0.30)	1.73(0.07)	1.67(0.15)	1.67	1.81
g_1	0.74(0.20)	0.72(0.05)	0.76(0.08)	0.69	0.79
g_2	1.50(0.25)	1.50(0.05)	1.48(0.08)	1.49	1.62
g_3	1.77(0.30)	1.75(0.10)	1.77(0.10)	1.68	1.77
α	0.55(0.10)	0.54(0.02)	0.56(0.03)	0.43	0.35
β		1.15/0.26 (0.05/0.03)	1.19(0.06)	1.19	1.28
γ	0.11(0.10)	0.14(0.01)		0.15	0.17

[a] Absolute values of coupling constant $|d| = [D_{CH} + J_{CH}/2]$, where J_{CH} and D_{CH} are the scalar coupling constant and motionally averaged dipolar coupling constant, respectively. [b] Full line width at half-maximum is given in parentheses. [c] $d = \Delta\nu/(2k)$, where $\Delta\nu$ is the spectral splitting and $k = 0.42$ is the scaling factor of the BLEW48 sequence. $d = \Delta\nu/(2\sqrt{2}k)$ for CH_2 methylenes (except β) and $d = \Delta\nu/(2k)$ for the CH pair (g_2 site) and for the β site, where $\Delta\nu$ is the spectral splitting and $k = 0.79$ is the scaling factor for the BB-PISEMA pulse sequence.

Table III-1. **^{1}H-^{13}C Coupling Constants[a] (Given in kHz) Measured from Magnetically Aligned DMPC/DHPC Bicelles (q = 3.5) at 37 °C** Using Different 2D Solid-State NMR Techniques[b] and Dipolar Couplings Measured Using the PDLF Technique from Bicelles (q) 3.5) Containing 2 mol % and 10 mol % of Desipramine

induced changes in the structural order of the lipid. The order parameters determined from the dipolar coupling values are given in Figure III-6(B). All ^{1}H-^{13}C dipolar couplings are reduced, and therefore, the peptide binding increases the disorder in lipid bilayers even at 0.5 mole % peptide concentration. On the other hand, this disorder is measurable using ^{2}H experiments only for a concentration $\geq$ 1% of the peptide, as shown in a recent study.[71]

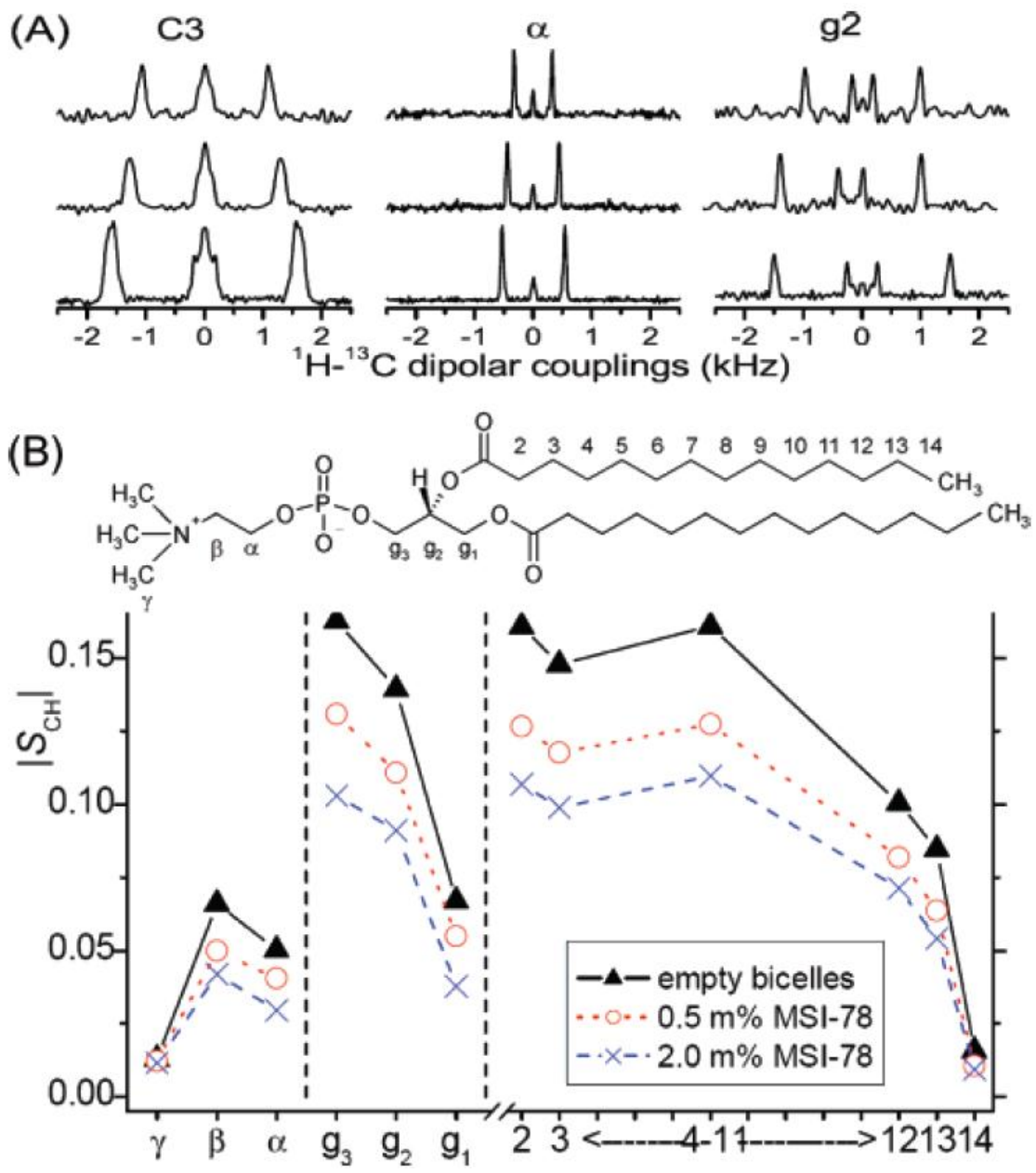

Figure III-6. (A) **^{1}H-^{13}C dipolar coupling extracted from two dimensional PELF spectra from 3.5:1 DMPC:DHPC bicelles** with 0 (bottom), 0.5 (middle), and 2 (top) mole % MSI-78. (B) The order parameter profile for DMPC determined from the dipolar coupling values.

III-2-5. Two Dimensional ^{13}C-^{31}P and ^{1}H-^{31}P Separated-Local-Field Experiments on Oriented Bicelles.

Other types of heteronuclear dipolar interactions, useful to quantify the order and conformation of the lipid headgroup and the glycerol moiety, are ^{13}C-^{31}P and ^{1}H-^{31}P dipolar couplings. Some of the ^{13}C-^{31}P dipolar splittings can be identified in the 1D ^{13}C spectrum (see Figure III-3, 1D spectrum on the top). The splitting due to the ^{1}H-^{31}P dipolar interaction can be observed in a 2D experiment which correlates the ^{1}H chemical shift and ^{1}H-^{31}P dipolar coupling evolution in the indirect dimension with the ^{13}C chemical shift and ^{13}C-^{31}P dipolar coupling evolution in the direct dimension. The RF pulse sequence is obtained from the 2D PELF sequence by removing the ^{1}H refocusing pulse in the middle of the evolution period. Note that no irradiation at the ^{31}P frequency is required in this experiment. Hence, a double resonance ^{1}H-^{13}C NMR probehead can be used. (The decoupling of ^{31}P spins to remove the coupling to ^{31}P nuclei during the evolution and/or detection period may be useful to assist the spectral assignment.)

For a dipolar coupled heteronuclear three-spin system *I*-*S*-*K* (proton, carbon-13, and phosphorus-31 spin, respectively), the spin interaction Hamiltonians effective during the evolution (t_1) and detection periods (t_2) of this pulse sequence are

$$H^{(t1)} = \omega_I I_z + \omega_{IK} 2 I_z K_z \quad (5)$$

and

$$H^{(t2)} = \omega_S S_z + \omega_{SK} 2 S_z K_z \quad (6)$$

respectively. Here, ω_I and ω_S denote the *I* and *S* spin chemical shift, and ω_{IK} and ω_{SK} are *I*-*K* and *S*-*K* dipolar coupling constants, respectively. (*J*-couplings can be accounted for as additive constants to ω_{IK} and ω_{SK}). During the *I*-*S* polarization transfer step, the spin-locked component I_x or I_y is transferred to S_x for subsequent detection. By performing the product operator calculation,[39] the following observable time domain NMR signal is obtained

$$s(t_1,t_2) \propto e^{i(\omega_I+\omega_{IK})t_1}\, e^{i(\omega_S+\omega_{SK})t_2} + e^{i(\omega_I-\omega_{IK})t_1}\, e^{i(\omega_S-\omega_{SK})t_2} \quad (7)$$

After a double Fourier transformation, a 2D spectrum results with two peaks at frequency coordinates (ω_I + ω_{IK}, ω_S + ω_{SK}) and (ω_I - ω_{IK}, ω_S - ω_{SK}). The projections on the ω_1 and ω_2 frequency axes correspond to *I-K* and *S-K* dipolar coupling spectra, respectively.

In addition to providing the information on the ^{1}H-^{31}P dipolar couplings, this experiment increases the resolution of ^{13}C-^{31}P dipolar splittings as compared to the 1D ^{13}C experiment. This is because the different ^{13}C-^{31}P dipolar doublets overlapped in the 1D ^{13}C spectrum are well separated in a 2D plane due to the difference in the chemical shifts of protons to which a particular carbon is correlated.

Part of the 2D ^{13}C-^{1}H-^{31}P correlation spectrum shown in Figure III-7 contains the resonances from the atoms in the head group and glycerol region. The ^{1}H-^{31}P couplings are easily recognized in the g_2 and α signals, which appear as tilted doublets. This tilt arises from simultaneous splittings by ^{13}C-^{31}P and ^{1}H-^{31}P interactions along the horizontal (direct dimension) and vertical (indirect dimension) axes, respectively. Similar splittings for the g_3 and β sites were assigned by comparison to the peaks in the PELF spectrum. Since in the PDLF spectrum the ^{1}H-^{31}P couplings are refocused at the end of the evolution period by the ^{1}H 180° pulse, both doublet peaks are located on the same horizontal line in the bottom spectrum of Figure III-7. Experimentally measured dipolar couplings are given in Table III-2. Since ^{13}C-^{31}P and ^{1}H-^{31}P dipolar couplings are not between directly bonded nuclei, they could be very sensitive to the conformational changes in the headgroup region around the phosphorus site. Therefore, the changes in the lipid headgroup conformation can be measured using this experimental approach. Spin pairs in the headgroup for which dipolar couplings were measured are indicated in Figure III-8(B).

Another significant advantage of this two dimensional NMR approach is in assigning and separating peaks in the ^{13}C spectrum that otherwise overlap due to ^{13}C-^{31}P dipolar coupling. This difficulty can be seen for g_3 and β carbon sites, while the peaks from g_2 and α are assignable in pure bicelles but may not be possible in bicelles containing additives. We expect this approach to be useful in the structural studies of membrane-associated molecules and also in studies that utilize bicelles as an alignment medium.

The ^{1}H-^{31}P dipolar couplings can also be measured in a more direct way by recording a 2D ^{31}P-^{1}H PELF spectrum. We performed such an experiment, and the dipolar coupling slices taken at the ^{31}P resonances are shown in Figure III-9. While the observed splitting for DMPC signal is generally consistent with the values given in Table III-2, the lines in Figure III-9 are broad and the individual dipolar coupling doublets are not resolved in contrast to the data from the 2D ^{13}C-^{31}P-^{1}H experiment (Figure III-7).

III-2-6. Topology of Desipramine.

An antidepressant, desipramine, was introduced into bicelles in order to study its effect on the heteronuclear dipolar couplings investigated above. DMPC/DHPC (q = 3.5) bicelles containing 2 and 10 mol % of desipramine were prepared. ^{31}P chemical shift spectra (data not shown) were used to judge the alignment of samples as mentioned earlier, which were found to be of comparably high quality. 2D PELF experiments were performed on the desipramine/bicelle samples. The 2D data (spectra not shown) consisted of well-resolved peaks, which enabled the measurement of ^{1}H-^{13}C dipolar coupling values for each carbon site; the values are given in Table III-1. We have also performed similar experiments to understand the membrane interaction of polypeptides and proteins with bicelles (data not shown). The presence of desipramine or other molecules did not alter the line width of dipolar spectral lines suggesting that the pulse sequence performs well when bicelles contain ligands such as drugs, peptides, and proteins. Therefore, this method provides a straightforward and highly informative way to investigate the effect that such ligands have on lipid bilayer properties. The experimental data obtained from desipramine-doped bicelles (Table III-1) consist of several interesting features that are worth noting. In the terminal carbons (C_{12}, C_{13}, and C_{14}) of DMPC, the measured C-H dipolar coupling values decrease with the increasing desipramine concentration. The response from carbons 2 to 11 of DMPC, as well as from the glycerol backbone carbons (g_1 and g_3), is more complex. As a general trend, a slight decrease of dipolar couplings was observed in the sample with 2 mol % desipramine incorporated. In contrast, when the desipramine concentration was increased to 10 mol %, the ^{1}H-^{13}C dipolar couplings in this region generally are increased above the values observed in pure bicelles. In the choline headgroup region, the α carbon site

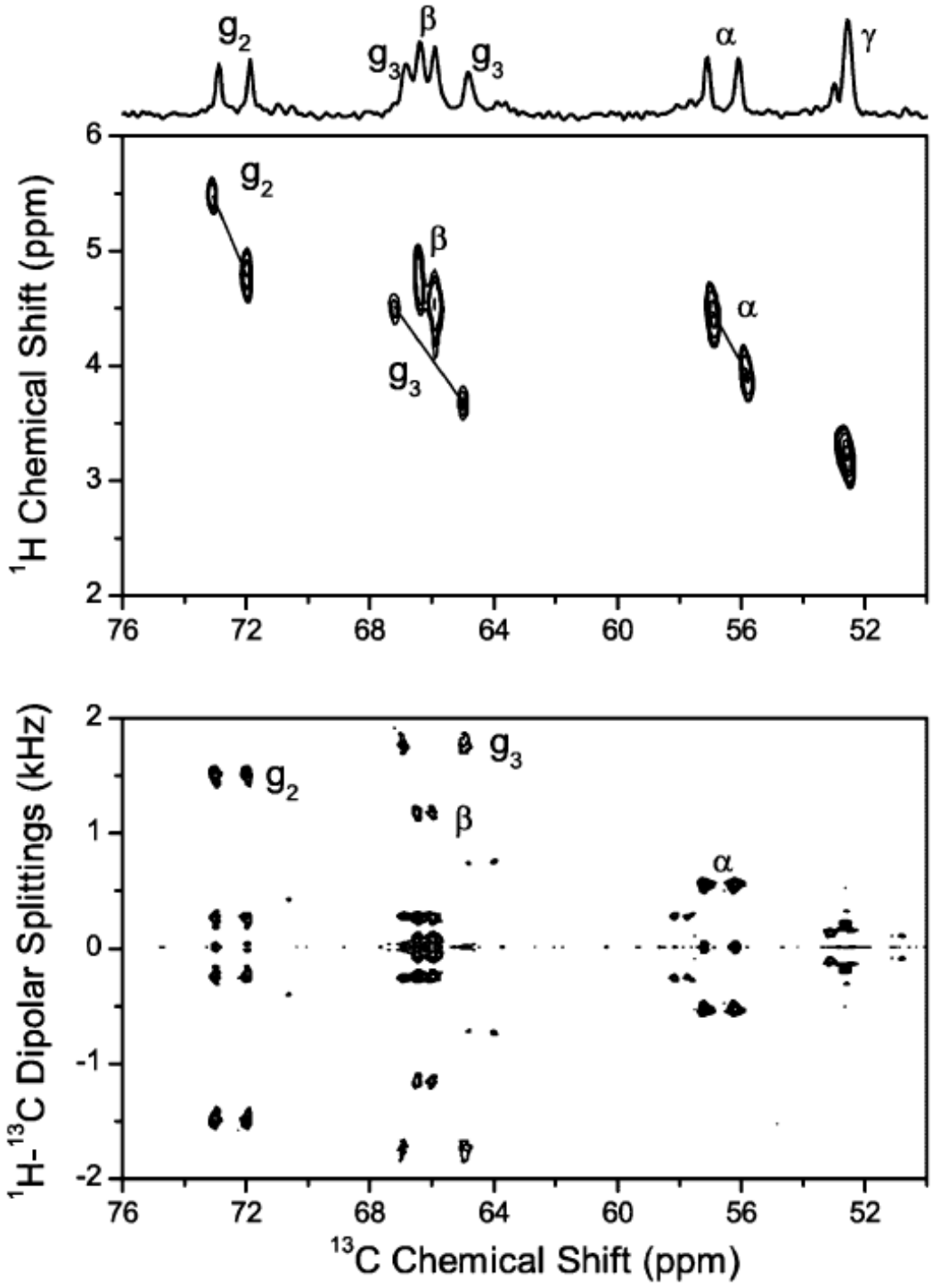

Figure III-7. **Contour plot of the headgroup and glycerol region of the 2D ^{13}C-^{1}H correlation spectrum** (top). The tilted dipolar doublets are indicated by solid lines. The doublets are due to ^{13}C-^{31}P and ^{1}H-^{31}P dipolar interactions resulting in splittings of the ^{13}C-^{1}H cross-peaks along the horizontal axis and vertical axis, respectively. The experimental conditions are as mentioned for the PDLF spectrum in Figure III-3. Comparison to the ^{13}C-^{1}H PDLF spectrum (bottom) was used to assign the peaks.

carbon site	pure bicelles		2 mol % desipramine		10 mol % desipramine	
	$^{13}C–^{31}P$	$^{1}H–^{31}P$	$^{13}C–^{31}P$	$^{1}H–^{31}P$	$^{13}C–^{31}P$	$^{1}H–^{31}P$
g_2	52	138	48	112	55	130
g_3	102	163	118	100	135	147
α	51	107	42	71	40	71
β	25	48	18	18	25	88

Table III-2. **^{13}C-^{31}P and ^{1}H-^{31}P Dipolar Couplings (Given in Hz (10 Hz) Measured from Magnetically Aligned DMPC/DHPC Bicelles (q = 3.5) at 37 °C**

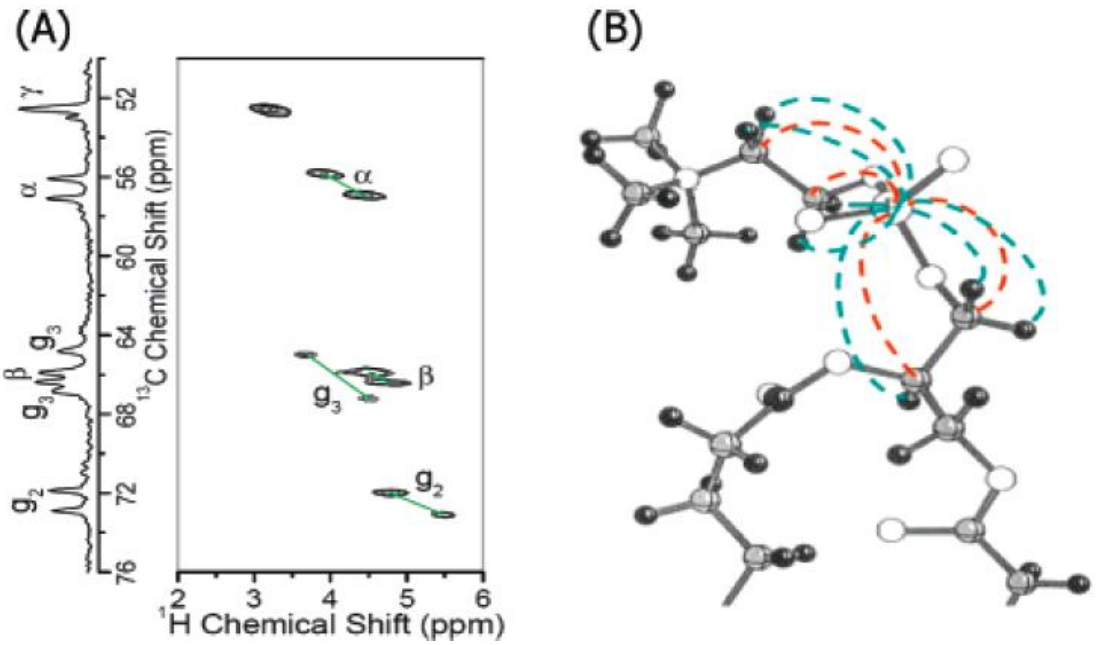

Figure III-8. (A) **A two dimensional correlation (Hetero Nuclear Correlation, HETCOR) spectrum of ^{13}C chemical shift and ^{13}C-^{31}P dipolar coupling (*y*-axis) with the ^{1}H chemical shift and ^{1}H-^{31}P dipolar coupling (*x*-axis) of 3.5:1 DMPC:DHPC bicelles (left).** The ^{1}H-^{31}P dipolar split peaks of α, β, g_2, and g_3 are connected by a green line. (B) The measured ^{1}H-^{31}P (blue) and ^{13}C-^{31}P (red) dipolar couplings in DMPC lipid molecule are highlighted.

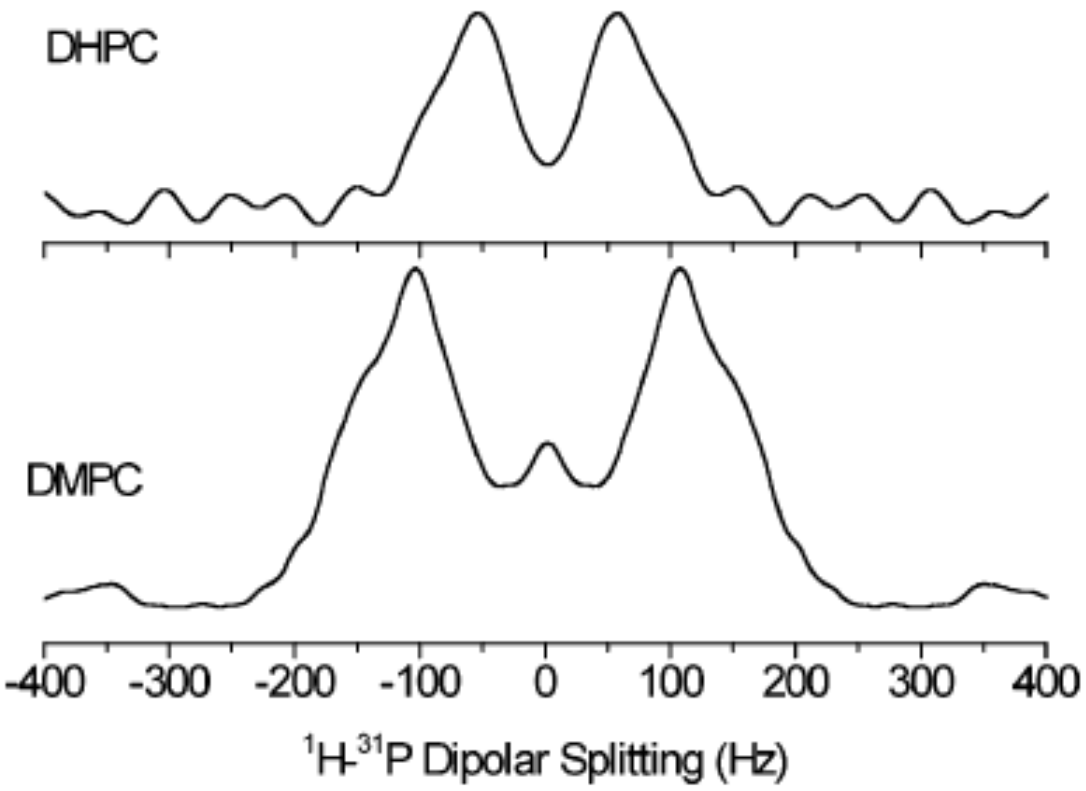

***Figure III-9*. Cross sections from the 2D ^{31}P-^{1}H PDLF spectrum at the chemical shift of the ^{31}P resonance in DMPC and DHPC molecules.** 64 transients were accumulated for each of 32 points in the t_1 dimension with an increment time of 2300 s.

shows a linear decrease of ^{1}H-^{13}C dipolar coupling, while the ^{13}C-^{1}H dipolar coupling increases with the desipramine concentration. The γ position shows a very slight increase in dipolar coupling, analogous to the β position. The complex response of the upper acyl chain and the glycerol backbone regions of the DMPC bilayer to the incorporation of desipramine could be further confirmed by ^{13}C-^{31}P and ^{1}H-^{31}P SLF experimental results. The ^{13}C-^{31}P and ^{1}H-^{31}P dipolar coupling values measured from the desipramine/bicelle samples are given in Table 2. For none of the observable carbon sites (α, β, g_2, g_3) was a linear change of the dipolar splitting with the desipramine content observed.

The above-mentioned experimental findings can be rationalized as follows. The desipramine molecule consists of a hydrophobic tricyclic "core" segment and an aliphatic "side chain" that carries a positive charge on a secondary amine (Figure III-10). An incorporation of this molecule into lipid bilayers has to accommodate the amphiphilic properties of the molecule. Most likely, the bulky hydrophobic tricycle will partition into the hydrophobic portion of the lipid bilayer, while the hydrophobic polar side chain will reach (or "snorkel") into the hydrophilic headgroup region of lipids. An earlier ^{14}N NMR study indeed found the desipramine molecule to be located near the headgroup region in lipid bilayers.[67] Since the hydrophobic region of desipramine is bulky and rather short when compared to the DMPC molecule, such an arrangement in the interface between hydrophobic and hydrophilic bilayer regions will affect DMPC molecules in bilayers. Figure III-10 shows both molecules in comparison; striking differences in their size and shape are evident. The presence of desipramine would most likely restrict DMPC molecules in their upper acyl chain and glycerol backbone regions, while the terminal segments of a DMPC molecule would experience a reduced steric hindrance resulting in an increased segmental mobility. These considerations are in full agreement with the experimental data reported in this study. An increase in the mobility in the terminal acyl chain carbons would result in decreased ^{1}H-^{13}C dipolar coupling values, as observed. A strong interaction of desipramine with the upper acyl chain and glycerol backbone carbons of DMPC is reflected in the nonmonotonous response of the observed ^{1}H-^{13}C dipolar couplings (Table III-1), as well as ^{13}C-^{31}P and ^{1}H-^{31}P dipolar couplings (Table III-2), to desipramine content.

In the headgroup region of DMPC, the observed ^{1}H-^{13}C dipolar couplings can be interpreted in terms of desipramineinduced changes in the headgroup dynamics and/or conformation. Any changes in the dynamics of the lipid headgroup would have the same effect on both α and β carbon sites, and the ^{1}H-^{13}C dipolar couplings at both sites would be expected to change in the same direction. Therefore, the measured counterdirectional changes in the ^{1}H-^{13}C dipolar couplings at α and β carbon sites cannot be explained solely by the changes in the dynamics of the headgroup. On the other hand, these results can be explained in terms of a conformational change in the phosphocholine headgroup of DMPC. Previous NMR studies have shown that the addition of a cationic amphiphile to lipid bilayers can move the N^{+} end of the lipid's P^{-}-N^{+} dipole toward the water phase of the bilayer, whereas an anionic amphiphile has the opposite effect.[9,68-70] Since the desipramine side chain is positively charged, it could repel the N^{+} end of the P^{-}-N^{+} dipole vector that would move the dipole toward the water phase of the bilayer. This would alter the conformation of the phosphocholine headgroup of the DMPC molecule. This interpretation is in excellent agreement with a previous ^{14}N NMR study that reported a significant reduction in the ^{14}N quadrupole coupling due to the electrostatic interaction between the positively charged N-H group of the drug and the C=O and P-O^{-} groups of the DMPC molecule.[67] This interaction causes the lipid head group to move toward the water phase of bilayers, thereby increasing the symmetry at the ^{14}N nucleus of the choline group and decreasing the quadrupolar interaction.[67] In addition, our interpretation is in good agreement with previous ^{2}H NMR studies that reported the effects of cations[68] and cationic peptides[9,70] on the conformation of the lipid headgroup.

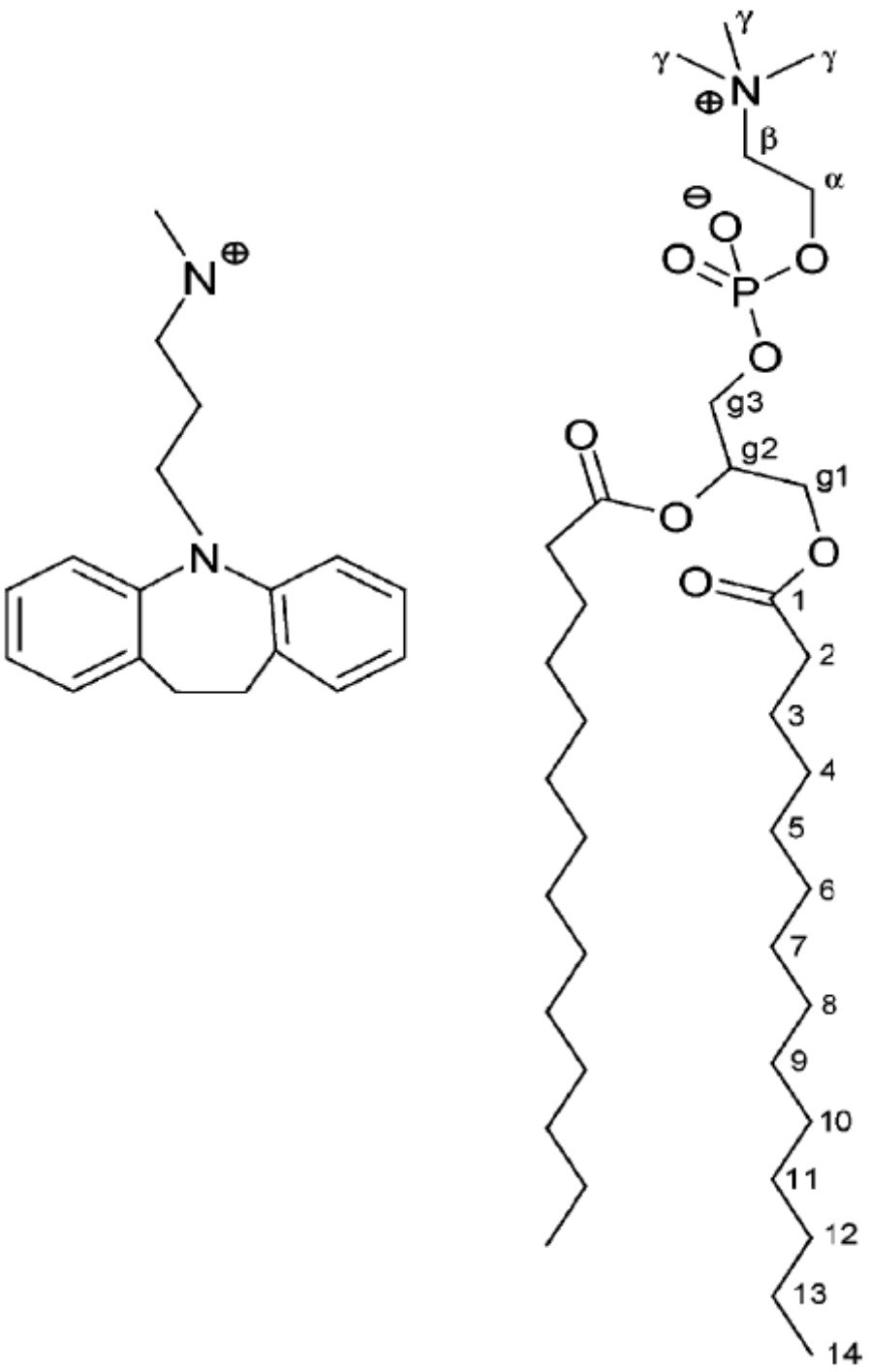

Figure III-10. **Molecular structures of desipramine (left) and DMPC (right).**

III-3. Comprehensive Analysis of Lipid Dynamics Variation with Lipid Composition and Hydration of Bicelles Using NMR Spectroscopy

As we discussed in previous sections, bicelles are rapidly becoming an important class of biomembrane mimics used in the high-resolution structural studies of membrane proteins.[1-4] Bicelles are a fascinating category of versatile and robust lipid assemblies that bridge the gap between micelles and lipid vesicles. One of the often-exploited features of bicelles is their propensity to spontaneously align in the presence of an external magnetic field.[5-7] This macroscopic alignment enables one to acquire high-resolution solid-state nuclear magnetic resonance (NMR) spectra while retaining various essential anisotropic interactions, such as dipolar coupling, chemical-shift anisotropy (CSA), and quadrupole coupling, which are rich in dynamic and structural information.[8-10] The easy and quick preparation of bicelles, in conjunction with their excellent filling factor in a NMR RF coil for better sensitivity, enable one to address some of the complex problems related to biological membranes at atomic-level resolution. The magnetic alignment of bicelles can be maintained over a reasonable range of physiological conditions, making bicelles an attractive class of model membranes for studies of structure, dynamics, molecular imaging, and functional properties of a variety of exciting biological systems, such as antimicrobial peptides, amyloid peptides, toxins, fusion peptides, membrane proteins, and membrane-binding pharmaceutical compounds.[10-13]

While bicelles display many features comparable to a lipid bilayer, they differ in several aspects, such as compositions and morphology. Bicelles are primarily composed of a mixture of long- and short-chain lipids, such as 1,2-dimyristoyl-*sn*-glycero-3-phosphocholine (DMPC) and 1,2-dihexanoyl-*sn*-glycero-3-phosphocholine (DHPC) (Figure III-11). They exhibit a wide spectrum of fascinating yet controversial morphologies, ranging from perforated lamellae to giant worm-like micelles, as dictated by sample conditions, such as the q ratio (q=[DMPC]/[DHPC]), temperature, and lipid composition.[14-18] Over the years, the morphology of bicelles has been exhaustively investigated using ^{2}H and ^{31}P NMR spectroscopy.[6,19-21] Despite the fact that bicelles have become an excellent platform for functional reconstitution of membrane proteins, a complete mapping of lipid dynamics that correlates all three regions (head-group, glycerol, and acyl chains) of bicelles as a function of the *q* ratio, temperature, and

hydration remains to be elucidated. These parameters are essential for formulating a proper bilayer environment for relevant biological studies of membrane proteins. In previous studies, the effect of hydration has shown to be highly critical in maintaining bilayer fluidity, which facilitates proper functioning of membrane proteins.[22,23] For example, many signaling proteins rely on the membrane fluidity for signal transduction and domain formation in the plasmamembrane.[22] In addition, *q* ratios and temperatures can strongly influence the dynamics of lipids in bicelles and may alter their interactions with other membrane constituents. Therefore, to effectively use bicelles for NMR structural studies, an optimization of these parameters is essential and an understanding of how the three lipid regions are correlated with each other as a function of these parameters is an important first step in formulating a suitable bilayer environment for biophysical applications.[17,24-27]

Separate-Local-Field (SLF) experiments, such as polarization inversion spin exchange at the magic angle (PISEMA), broadband PISEMA, heteronuclear isotropic mixing leading to spin exchange via the local field (HIMSELF), or heteronuclear rotating-frame leading to spin exchange via the local field (HERSELF), and SAMMY, which correlate heteronuclear dipolar couplings with chemical shifts while suppressing the dominant dipolar couplings among protons, are employed in solid-state NMR studies of membrane proteins embedded in aligned lipid bilayers.[9,10,28,29] Experimentally measured heteronuclear dipolar couplings can provide atomic-level detailed information regarding segmental mobility and orientation of molecules.[9,10,30-32] The order parameter gives a measure of the mobility of a chemical bond in a molecule with respect to a molecular frame and can be determined from the observed dipolar coupling $\langle D_{ij} \rangle$ values using the following equation:

$$\langle D_{ij} \rangle = D_{ij} S_{ij} \langle 3\cos^2\theta - 1 \rangle \quad (1)$$

where $$D_{ij} = \frac{(\mu_0/4\pi)\gamma_i\gamma_j}{r^3} \quad (2)$$

D_{ij} is the static dipolar coupling between nuclei *i* and *j*, S_{ij} is an order parameter ($0 \leq S_{ij} \leq 1$), and θ is the angle between the *i*-*j* internuclear vector and the external magnetic field

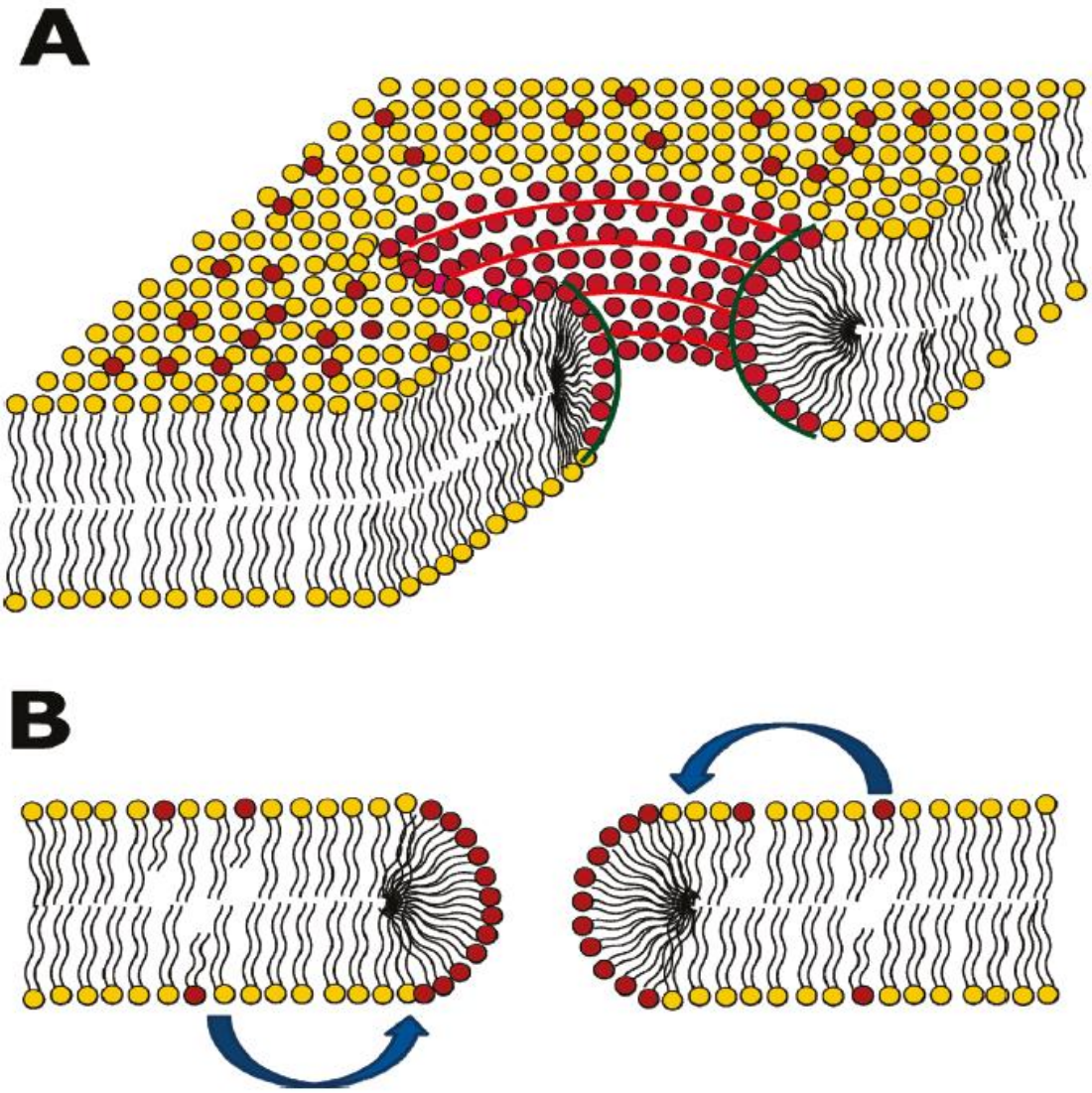

Figure III-11. **Schematic representations of lamellar phase bicelles.** (A) Schematic representation of the perforated lamellae morphology of magnetically aligned DMPC/DHPC bicelles consisting of both planar and high-curvature regions. DMPC and DHPC molecules are represented by the yellow and red colors, respectively. (B) Schematic representation of DHPC undergoing fast exchange between the planar and highly curved toroidal pore regions, as indicated by the arrows.

axis. While most SLF pulse sequences can be used to measure dipolar couplings on aligned samples, rotating-frame pulse sequences, such as HIMSELF, have been shown to provide superior resolution in the heteronuclear dipolar coupling dimension of a 2D SLF spectrum and, hence, commonly used in the structural studies of membrane proteins.[11,12] On the other hand, these rotating-frame SLF sequences provide higher resolution by suppressing weak heteronuclear dipolar couplings, which are essential for the present study on bicelles. To overcome this problem, a variation of a SLF pulse sequence called proton-evolved-local-field [PELF, also called as proton-detected local field (PDLF), but protons are not detected in the present study][31] experiment was successfully applied in a high-resolution NMR study of magnetically aligned bicelles and provided a comprehensive mapping of lipid dynamics at each carbon position, from the head-group to the acyl chains, in response to various ligands.[9,10] It has been shown that this 2D PELF technique is capable of providing high-resolution ^{13}C-^{1}H dipolar coupling spectral lines at the natural abundance of ^{13}C nuclei and also enables the measurement of multiple couplings associated with a single carbon site.[10] Therefore, we chose to use this PELF technique for the present study to accomplish a complete mapping of lipid dynamics as a function of the q ratio, hydration, and temperature of bicelles. Unlike the requirement of deuterated lipids for deuterium NMR studies, PELF measurement can be carried out on normal lipids with the natural abundance of ^{13}C and can also be used to measure long-range C-H dipolar couplings.[10,28]

III-3-1. Experimental Procedure

Materials.

DMPC and DHPC were purchased from Avanti Polar Lipids, Alabaster, AL, and used without further purification. All other biochemicals and reagents used in this study were purchased from Sigma-Aldrich, St. Louis, MO.

Preparation of Bicelles.

Bicelles were prepared with a desired amount of lipid in buffered D_2O. The ratio q was calculated as moles of DMPC per mole of DHPC. A typical preparation involved dissolving the desired quantities of DMPC and DHPC in buffered D_2O solution (10 mM Tris at pH 7.4 and 150 mM NaCl), followed by a series of cycles of freezing, thawing,

and gentle vortexing until a clear solution, was obtained. The solution was then stored at 4 ^{o}C for up to 24 h before use.

NMR Spectroscopy.

NMR experiments were carried out on a Chemagnetics/Varian Infinity 400MHz solid-state NMR spectrometer using a 5 mm double-resonance magic-angle spinning probe under static sample conditions. About 150-200 mg of bicelles was loaded in a 5mmNMRglass tube of 4 cm length, and the tube was closed tightly with a Teflon tape and a cap. The sample was then equilibrated for about 30 min in the magnet at the desired temperature prior to signal acquisitions. ^{31}P chemical shift spectra were recorded using the Hahn echo (90^{o}-τ-180^{o}-τ acquire) experiment with a 90^{o} pulse length of 5 μs, an echo delay of 100 μs, and under a 15-25 kHz continuous-wave proton decoupling. A total of 32 transients were sufficient to acquire reasonable signal-to-noise ratio ^{31}P chemical-shift spectra of well aligned samples, while about 64 scans were acquired for relatively poorly aligned samples. The chemical-shift scale was referenced by setting the ^{31}P chemical-shift peak from phosphoric acid (H_3PO_4) to 0 ppm at 37 ^{o}C. A ramped-cross-polarization (ramp-CP) sequence with a contact time of 5 ms was used to record the 1D ^{13}C chemical-shift spectra under proton decoupling using various decoupling sequences for a comparative study, while the flip-flop spectroscopy (FLOPSY)-8[48] multiple pulse sequence was used in our experiments because it provided the best resolution. The 2D PELF spectra were obtained using 64 t_1 experiments, 64 scans, a 5 s recycling delay, and a 20 kHz ^{1}H decoupling.

III-3-2. ^{31}P Chemical-Shift Spectra of Magnetically Aligned Bicelles as a Function of the *q* Ratio.

^{31}P NMR spectroscopy is a convenient and reliable tool commonly used to assess the quality of bicelles alignment and the angle between the bilayer normal and the applied magnetic field.[20] Parts A and C of Figure III-12 show a series of ^{31}P chemical-shift spectra as a function of the hydration and q ratio obtained at 35 ^{o}C, and Figure III-12B shows a series of ^{31}P spectra obtained as a function of the temperature of the sample. In these spectra, two well-resolved resonances corresponding to DMPC and DHPC were observed. These spectra are typical of magnetically aligned bicelles, as shown in

previous studies.[6,20] The low- and high-field peaks are assigned to DMPC and DHPC, respectively. The chemical-shift frequency of the DMPC peak corresponds to the perpendicular shoulder of the ^{31}P CSA powder pattern of DMPC in the liquid-crystalline phase, indicating that magnetic alignment of bicelles was indeed achieved. The difference between the chemical-shift values of DHPC and DMPC is the direct consequence of the difference in their residual CSA spans. DHPC molecules in bicelles are highly mobile compared to DMPC; DHPC molecules undergo a fast exchange between the planar regions and the toroidal-pore regions of bicelles, whereas the DMPC molecules are confined to the planar region of the bilayer as shown in Figure III-11. This mobility scales down the CSA of DHPC, leading to a smaller absolute chemical-shift value, as seen in Figure III-12.

^{31}P chemical shifts of both DMPC and DHPC measured as a function of the *q* ratio, hydration, and temperature are consistent with the results reported in previous studies. With the increasing *q* ratio, the observed chemical-shift frequency of DMPC progressively increased from -11.25 to -13.46 ppm, while that of DHPC increased from -5.31 to -6.79 ppm. A similar but gradual trend was observed in the chemical-shift values of DMPC and DHPC as a function of the hydration level and temperature of bicelles. The chemical-shift values of both DMPC and DHPC decrease as hydration increases and plateau for hydration levels greater than 60%. On the other hand, the ^{31}P chemical shifts of both DMPC and DHPC increase as a function of the temperature and are consistent with previous studies. The changes in the observed ^{31}P chemical-shift value as a function of the *q* ratio, temperature, and hydration are a manifestation of the scaling of the bicelles order parameter $S_{bicelles}$.[6] Sanders *et al.* first introduced the $S_{bicelles}$ order parameter as a measure of the additional local "wobbling" effect experienced by a phospholipid within the bicelle relative to a unoriented bilayer.[6] The Sbicelles parameter is calculated from the ^{31}P residual CSA using the following equation:

$$S_{\text{bicelles}} = \frac{\delta_{\text{obs}} - \delta_{\text{iso}}}{\delta_{90} - \delta_{\text{iso}}} \quad (3)$$

where δ_{obs} is the observed ^{31}P chemical-shift frequency, δ_{iso} is the isotropic chemical shift, and δ_{90} is the perpendicular edge frequency of the ^{31}P CSA powder pattern spectrum of

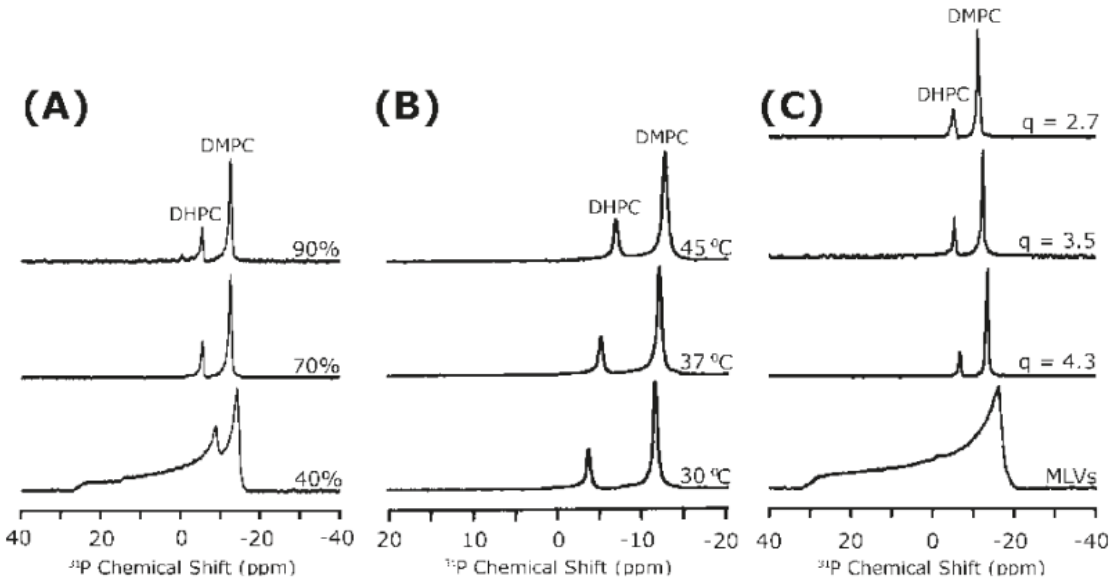

Figure III-12. **^{31}P chemical-shift spectra of magnetically aligned bicelles for various (A) hydration levels with q = 3.5 at 37°C, (B) temperatures with *q* = 3.5 and 77% hydration, and (C) q ratios at 37°C with 77% hydration.** ^{31}P pectrumof partially aligned bicelles is given at the bottom of A for 0%hydration (spectra of bicelles with 50 and 40% hydration levels are similar), and that of unalignedmultilamellar vesicles (MLVs) is given at the bottom of C for 63%hydration at 37 °C. The hydration level is given in (w/v)% of water.

unaligned DMPC in the liquid-crystalline phase. $S_{bicelles}$ values of bicelles are summarized in Tables III-3.

^{31}P spectra at relatively low hydration levels show significant deviation from the typical ^{31}P NMR spectrum of magnetically aligned bicelles. Poor alignment of bicelles was observed at 50 and 40% hydration levels. In these samples, a broad powder pattern, such as ^{31}P line shape, was observed, indicating the presence of unaligned lipids. Under these conditions, bicelles most likely exhibit an ellipsoidal morphology with a dispersion of ^{31}P chemical shifts, which is commonly observed for bicelles at high q ratios.[21,33] The lack of alignment at these hydration levels can be attributed to numerous factors; however, the most likely factor under these circumstances is the sample viscosity. The kinetic of bicelles alignment is a function of two intrinsic parameters: the size of aggregates and the sample viscosity. Because of low hydration levels for these samples, they exhibit the highest viscosity, preventing them from proper magnetic alignment and leading to a mosaic spread of bicelle orientations. Therefore, a broad ^{31}P chemical-shift spectrum was observed for these samples.

temperatures (°C)	δ_{DMPC}	δ_{DHPC}	$S^{DMPC}_{bicelles}$	$S^{DHPC}_{bicelles}$
30	−12.5	−4.8	0.83	0.32
37	−12.7	−5.5	0.85	0.36
45	−13.2	−7.5	0.88	0.5

Table III-3. $S_{bicelle}$ **Order Parameter of DMPC and DHPC Molecules Determined from NMR Experiments on Magnetically Aligned Bicelles at Different Temperatures**

hydration levels (%)	δ_{DMPC}	δ_{DHPC}	$S^{DMPC}_{bicelles}$	$S^{DHPC}_{bicelles}$
40	−14.2	−8.7	0.94	0.58
50	−13.0	−6.8	0.86	0.45
60	−12.5	−5.5	0.83	0.36
70	−12.4	−5.4	0.82	0.36
80	−12.5	−5.5	0.83	0.36
90	−12.4	5.3	0.83	0.35

Table III-4. $S_{bicelle}$ **Order Parameter of DMPC and DHPC Molecules Determined from NMR Experiments on Magnetically Aligned Bicelles at Different Hydration Levels**

q ratio	δ_{DMPC}	δ_{DHPC}	$S^{DMPC}_{bicelles}$	S^{DHP}_{bicel}
2.7	−11.2	−5.3	0.75	0.3
3.5	−12.2	−5.3	0.82	0.3
4.3	−13.4	−6.7	0.89	0.4

Table III-5. $S_{bicelle}$ **Order Parameter of DMPC and DHPC Molecules Determined from NMR Experiments on Magnetically Aligned Bicelles at Different** q **Ratios**

III-3-3. Two Dimensional PELF Spectra of Magnetically Aligned Bicelles.

A 2D PELF experiment was used to measure ^{13}C-^{1}H dipolar couplings from magnetically aligned bicelles. A typical 2D PELF spectrum that correlates ^{13}C-^{1}H dipolar couplings with ^{13}C chemical shifts is shown in Figure III-13A for bicelles with q = 3.5 at 35 ^{o}C. Each representative ^{13}C-^{1}H dipolar-coupling slice corresponds to a specific carbon site of a phospholipid in bicelles. The 2D spectrum exhibits well-resolved doublets in the indirect frequency dimension, corresponding to the combined dipolar and scalar couplings between ^{13}C and ^{1}H spins. A 1D ^{13}C chemical-shift spectrum of bicelles is also shown; a significant overlap of resonances, especially for the C_4-C_{11} region of acyl chains, was observed. Interestingly, these resonances are resolved in the 2D spectrum. Because experimental conditions were optimized for the observation of resonances from DMPC, ^{13}C NMR resonances from DHPC were not readily observed. In the PELF spectrum, multiplets with small splittings were observed because of interactions between ^{13}C and remote protons.[9,10]

Interestingly, additional dipolar couplings were observed for carbons in the head-group and the glycerol moiety of lipids. A 2D $^{13}C/^{1}H$ heteronuclear chemical-shift correlation spectrum of bicelles is shown in Figure III-13B, with resonances only from the glycerol and head-group regions displayed. The doublets observed in the spectrum are the direct consequences of the dipolar interactions between ^{13}C-^{31}P nuclei.[6,34,35] The ^{13}C-^{13}P dipolar couplings were observed for carbons in these regions (that is for g_1, g_2, g_3, C_α, and C_β carbon sites) because they are geometrically in close proximity with the ^{31}P nucleus of the phosphate headgroup. However, for the C_γ of the choline head-group, no ^{13}C-^{13}P dipolar coupling was observed. This is mainly due to the large distance separation between C_γ and ^{31}P nucleus. In general, dipolar couplings associated with the $C\alpha$ and g_3 carbons are the largest among all measured.

III-3-4. Lipid Order Parameters as a Function of the *q* Ratio.

Dipolar couplings are sensitive to the motional properties of lipids in a bilayer membrane and can provide valuable dynamic information. The order parameter of C-H bonds (S_{CH}) in the acyl

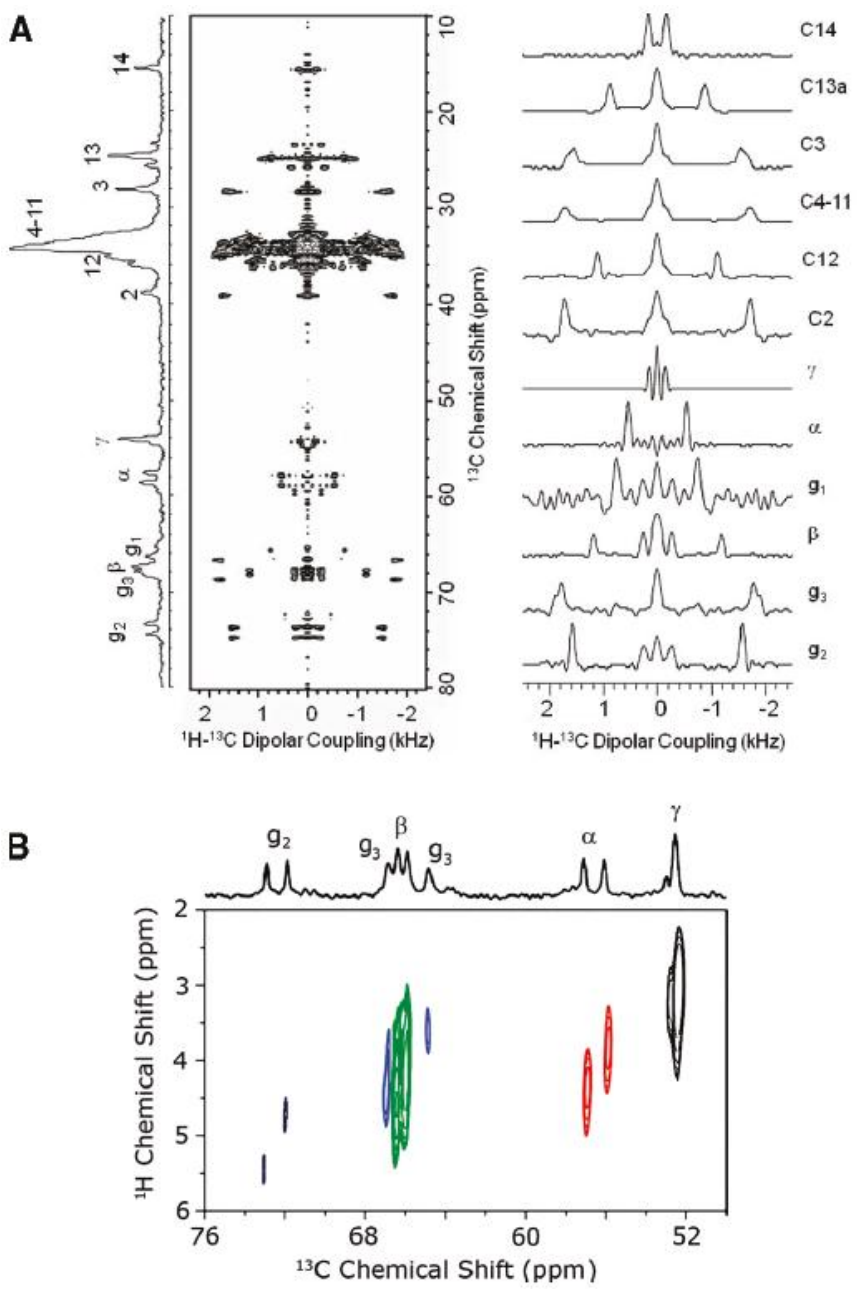

Figure III-13. (A) **^{13}C chemical-shift spectrum (left), a 2D PELF spectrum (middle) that correlates the ^{13}C chemical shifts (vertical dimension) and ^{1}H-^{13}C dipolar coupling (horizontal dimension), and individual ^{1}H-^{13}C dipolar coupling slices (right) of q = 3.5 magnetically aligned bicelles with 77% hydration level [given in (w/v)% of water] at 37°C.** The details on the pulse sequence used in these experiments can be found elsewhere.[8] The acquisition parameters used to obtain these spectra are 64 scans, 200 t_1 points with an increment time of 384 μs, a recycle delay of 5 s, a 31 kHz ^{1}H RF field strength during t_1, and a 3.0 ms CP contact time. (B) 2DPELF spectrum showing distinct doublets for g_2, $C\alpha$, and C_β carbons because of residual ^{13}C-^{31}P dipolar couplings.

chains of DMPC can be determined from the residual ^{13}C-^{1}H dipolar couplings measured from 2D PELF spectra of bicelles. PELF experiments were performed on bicelles under various conditions to understand the effects of the q ratio, hydration level, and temperature. The data were processed and interpreted as discussed above. The S_{CH} values are given in Figure III-14 for all carbon sites of DMPC in bicelles for different q ratios, hydration levels, and temperatures. Because the C-H order parameters are determined from the experimentally measured C-H dipolar coupling values, the accuracy of S_{CH} values strongly depends upon the resolution of 2D PELF spectral lines in the C-H dipolar coupling dimension. As can be seen from the spectral slices provided in Figure III-14, the lines are narrow, with the full width at half-maximum varying from ~50 Hz (119 Hz after taking the scaling factor of the BLEW-48 multiple pulse sequence in the t1 period into account) to 111Hz (264Hz after the inclusion of the scaling factor). Therefore, the reported S_{CH} values are of high accuracy.

Here are some common features among the plots of S_{CH} values. The magnitude of S_{CH} homogenously decreases along the acyl chains of lipids, reflecting an increase in the overall motions down the acyl chains, which is consistent with previous ^{2}H NMR studies. Similarly, the head-group moiety of lipids also displayed a similar trend.[19,36] Because of the rapid rotation of the methyl group, the residual dipolar coupling associated with C_γ is projected along an additional director axis of motion defined by the methyl rotor, leading to a lower S_{CH} value for C_γ relative to that of C_α and C_β. Interestingly, the order parameter associated with C_β is significantly higher than that of C_α of the choline headgroup. This can be attributed to a higher range of motions experienced by C_α, while themotions around the C_β are restricted by the electrostatic interaction between the positively charged nitrogen and the negatively charged phosphate group. As such, this interaction will significantly hinder motions around the C_β-N bond, leading to a higher order parameter, as observed for C_β. Furthermore, the order parameters associated with glycerol carbons display a gradual decrease from positions g_3 to g_1. The glycerol section of a lipid bilayer is highly viscous because of an extensive network of hydrogen bonds near the water-membrane interface; this will considerably hinder the overall motions of the C-H bond at the g_3 position, leading to a higher S_{CH} value relative to that of g_1, which is buried closer to the hydrophobic core of the membrane.

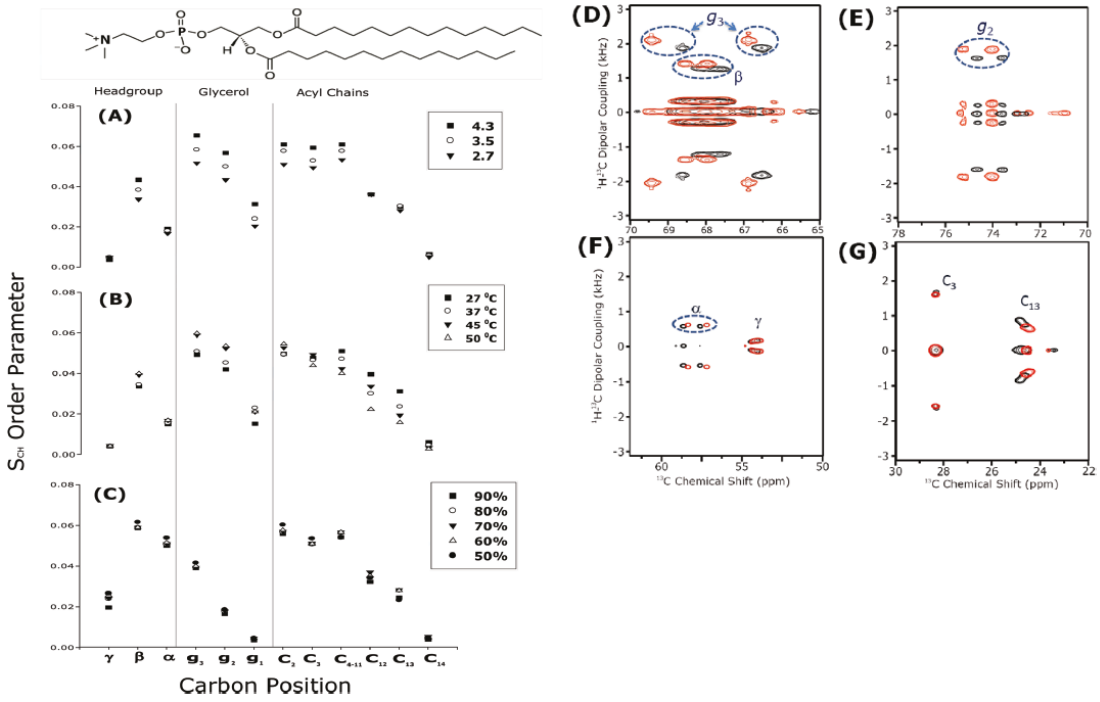

Figure III-14. **Order parameter of bicelles.** The order parameter profile determined from experimentally measured ^{1}H-^{13}C dipolar coupling values at different (A) q ratios at 37 ^{o}C with 77% hydration level [given in (w/v) % of water], (B) temperatures with q = 3.5 and 77% hydration, and (C) hydration levels with q=3.5 at 37^{o}C. Selective regions of 2D PELF spectra for g_3, g_2, C_α, C_β, C_γ, C_3, and C_{13} carbons at two different temperatures of 37^{o}C (black) and 45^{o}C (red) are given in parts D-G.

The dependence of S_{CH} upon the q ratio and hydration level is gradual, but interestingly, only specific regions, in particular, near the water-membrane interface, are significantly affected. In general, the S_{CH} values vary proportionally to both the q value and the extent of hydration, indicating an overall increase in the $S_{bicelles}$ value. However, one should be cautious when examining the order parameter at a very low hydration level, for example, 40%, because of the poor alignment of the bicelles (data not included). Because of the rapid motion exhibited by the terminal methyl groups of the acyl chains and the head-group, these regions are reasonably insensitive to the additional local "wobbling" effect in bicelles, as defined by the $S_{bicelle}$ value. Therefore, their S_{CH} order parameters remain relatively constant as a function of both the q ratio and hydration level. In contrast, the region near the water-membrane interface, where an extensive network of hydrogen bonds considerably hinders motions, will be particularly sensitive to the local wobbling effect of bicelles, leading to a gradual dependence of S_{CH} upon the q ratio. On the other hand, the dependence of S_{CH} values upon the hydration level of bicelles is only moderate at best because all of the plots in Figure III-14C virtually overlap with each other.

Interestingly, the S_{CH} values vary differently at different regions of the bilayer as a function of the temperature of bicelles: the S_{CH} values of carbon sites in the acyl chains uniformly decrease as the temperature increases, while S_{CH} values in the head-group and glycerol moieties increase as the temperature increases. This could be a consequence of the dynamical difference exhibited at different regions of the lipid bilayer. The S_{CH} values homogeneously decrease in the acyl chain region as a function of the temperature, indicating an increase in the motion of acyl chains of lipids from the additional thermal energy. In contrast, the S_{CH} values of the head group moiety are inversely proportional to the temperature, which can be attributed to the combined effects of water dynamics and an increase in the $S_{bicelles}$ order parameter value. Representative PELF spectra for carbon positions g_3, g_2, C_α, C_β, C_γ, C_3, and C_{13} at 37 and 45 ^{o}C are shown in parts D-G of Figure III-14. These spectra showa clear difference in the ^{13}C-^{1}H dipolar couplings at two different temperatures. In addition, the increase in the ^{13}C chemical shift of these resonances is indicative of an increase in their overall $S_{bicelles}$ order parameter as the temperature of the sample increases. The hydration shell close to the surface of the lipid bilayer is highly dynamic in nature: water molecules exchange rapidly between the bound

and free states. The increase in temperature depletes this hydration shell around the bilayer because of an increase in kinetic energy, which prompts water molecules to be in the free state, leading to dehydration of the membrane surface. Therefore, this effect can increase the ordering of the head-groupmoiety (particularly in the glycerol region) as evident in the raise of the S_{CH} order parameter.[37-40] In addition, an increase in temperatures also increases the value of $S_{bicelles}$, as evident in numerous studies in the past. At high temperatures, the DHPC becomes miscible with DMPC, which reduces the surface area of perforations and local "wobbling" motions of the bicelle. Therefore, a higher $S_{bicelles}$ value or ^{1}H-^{13}C dipolar coupling is observed.

Interestingly, additional heteronuclear dipolar couplings, particularly ^{13}C-^{31}P couplings (D_{CP}), are observed in the glycerol and head-group regions of the bicelle. These couplings provide specific details regarding the motions and dynamics at the water membrane interface. In general, the magnitude of D_{CP} varies proportionally with the q ratio, as shown in Figure III-15, similar to that of ^{13}C-^{1}H dipolar couplings observed in this study, which is a manifestation of the global $S_{bicelles}$ order parameter. Furthermore, the effect of hydration has a rather complicated effect on the observed values of D_{CP}, particularly at C_{β} and g_3 carbons, as shown in Figure III-16.

In general, an increase in the hydration level reduces the ordering of bicelles, particularly in the head-group region, and is consistent with previous ^{2}H NMR studies.[40] The profound sensitivity of D_{CP} at the C_{β} and g_3 carbon positions can be attributed to their local motions and dynamics. Motions at the site of C_{β} are highly restricted because of the electrostatic interactions associated with the P^{-}-N^{+} dipole. Therefore, any change in the ordering of this dipole will have a dramatic impact on the local dynamics around C_{β}, which results in a notable change in its D_{CP} value. Furthermore, the sensitivity of D_{CP} at the g_3 position is attributed to the ordering of water at the membrane surface. An increase in hydration reduces ordering of water at the bilayer surface and ultimately influences the local dynamics at the glycerol region, particularly near g_3 because of its close proximity to the network of hydrogen bonding at the surface-membrane surface. Therefore, a change in the hydration of bicelles leads to a profound change in the value of D_{CP} at the g_3 position.

III-3-5. Discussion.

Dynamics of lipids in bicelles are crucial in producing a native bilayer environment for in-depth biophysical studies of membrane-associated amphiphiles, in particular, membrane proteins. In previous studies, the basic dynamics of both head-group and acyl chains were extensively investigated using ^{2}H NMR experiments. However, the intricate relationship between the dynamics at different regions of the bilayer under various sample conditions remains an issue that requires attention. In this study, we have revealed the complex influence of the *q* ratio, hydration level, and temperature on the motion of lipids in bicelles using both ^{13}C-^{1}H and ^{13}C-^{31}P dipolar couplings. The order parameter, which is a measure of motions, was carefully extracted from the dipolar coupling for different regions of the lipid. In general, the basic behavior of order parameters in the acyl chains as a function of the *q* ratio, temperature, and hydration is consistent with previous ^{2}H NMR studies. Surprisingly, the glycerol region of the bilayer is extremely sensitive to the conditions of bicelles compared to other regions of the bilayer. Because of an extensive hydrogen-bonding network in the water-membrane interface, the motional freedom at the glycerol region is profoundly restricted, such that larger order parameters are observed in this region.

The phosphocholine head-group is highly flexible and exhibits a wide range of orientations that can be determined using ^{13}C-^{1}H dipolar couplings from different carbon positions, C_{α}, C_{β}, and C_{γ}, along the phosphocholine moiety. For a lipid molecule in the liquid-crystalline phase undergoing a rapid anisotropic rotation about its long axis, many anisotropic interactions, such as dipolar coupling and chemical-shift anisotropy, are projected along this director axis of motion and only the motionally averaged values of these nuclear spin interactions influence the observed NMR spectrum. Interestingly, the motions of the phosphocholine moiety will have an additional averaging effect on the magnitude of nuclear spin interactions exhibited in the choline head-group. Therefore, the ^{13}C-^{1}H dipolar couplings associated with C_{α} and C_{β} are motionally averaged along two different director axes: the long axis of the lipid and an axis defined by the phosphocholine moiety. For C_{γ}, its ^{13}C-^{1}H dipolar coupling is motionally averaged along an additional director axis defined by the methyl rotor. The orientation of the different director axiswith respect to the external magnetic field is shown in Figure III-17.

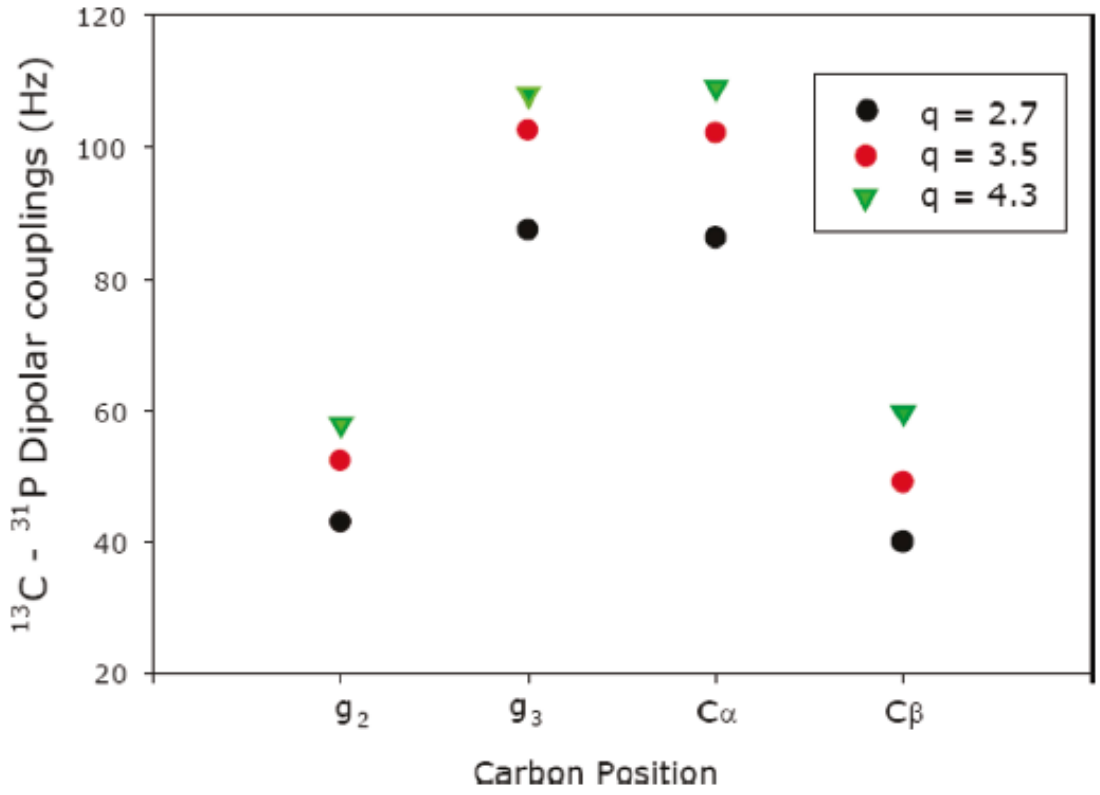

Figure III-15. **Plot of experimentally measured ^{13}C-^{31}P dipolar couplings from magnetically aligned bicelles at 37°C** with 77% hydration level [given in (w/v) % of water] and q ratios (black circle) 2.7, (red circle) 3.5, and (green inverted triangle) 4.3 at g_2, g_3, C_α, and C_β carbons.

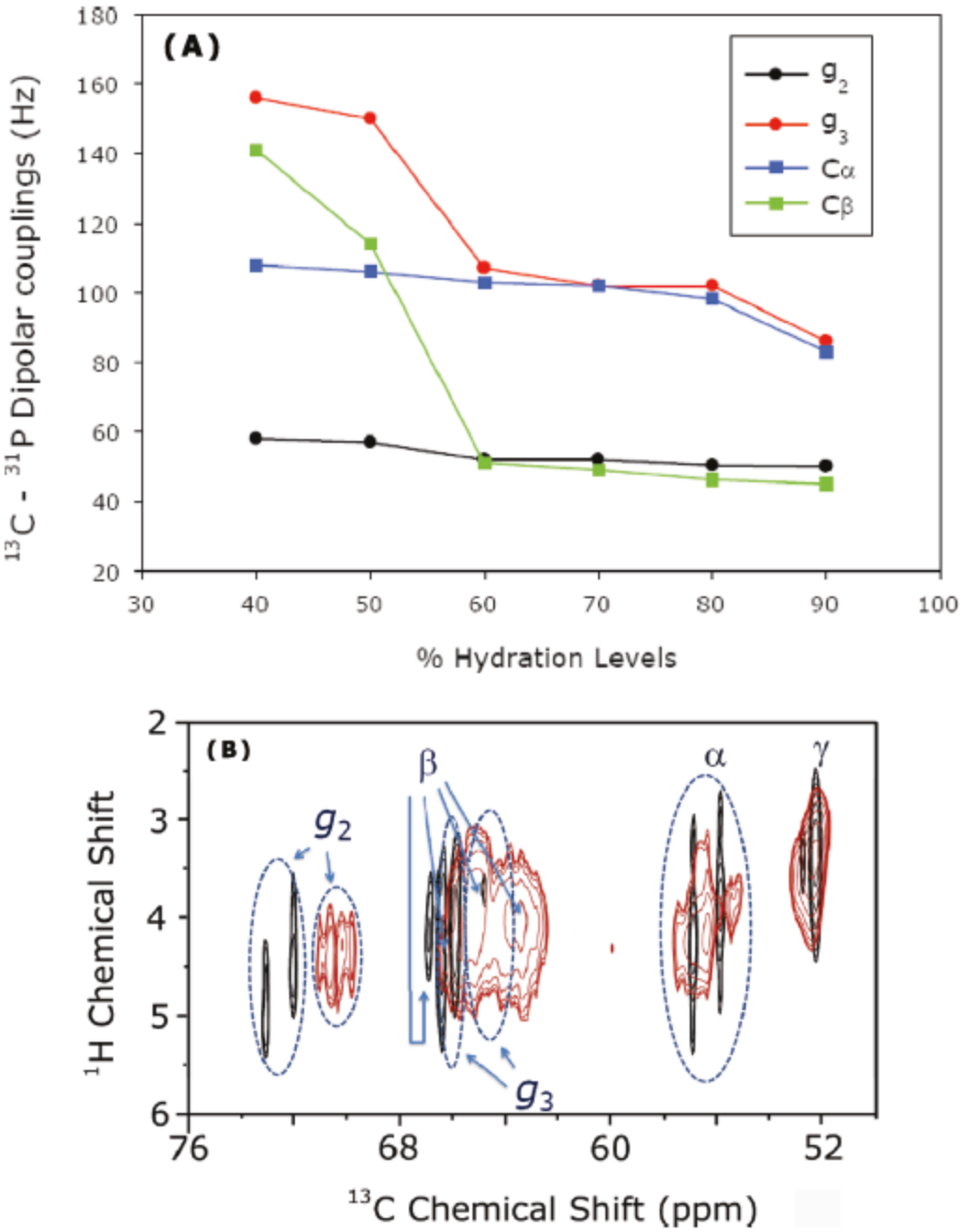

Figure III-16. (A) **Plot of experimentally measured ^{13}C-^{31}P dipolar couplings as a function of the hydration level** [given in (w/v)%of water] for (black circle) g_2, (red circle) g_3, (blue square) Cα, and (green square) C$_\beta$ carbons from bicelles with a q ratio of 3.5 at 37 ^{o}C. (B) 2D ^{1}H/^{13}C chemical-shift correlation spectrum that shows the dipolar couplings among ^{13}C and ^{31}P nuclei at 40% (red) and 70% (black) hydration level [given in (w/v)% of water]. Line broadening because of poor alignment of bicelles at 40% hydration and a significant increase in ^{13}C-^{31}P dipolar couplings at a higher hydration level are evident from the 2D spectrum.

The angle of the phosphocholine head-group with respect to the surface of the bilayer is summarized in Tables III-4 for different q ratios, temperatures, and hydration levels.

The average angle $<\varphi>$ between the phosphocholine moiety with respect to the bilayer surface is $\sim 30^{o}$ and is consistent among the series of q ratios, indicating that changes in the observed dipolar couplings in the head-group moiety are indeed due to the $S_{bicelles}$ order parameter and not because of the reorientation of the headgroup. Furthermore, the values of $<\varphi>$ that we obtained from measured dipolar couplings are consistent with observations reported in the literature.[35,37,39,41] Because of the dynamic nature of the phosphocholine head-group, the value of $<\varphi>$ is not unique, rather a collection of values is observed; however, the head-group prefers to be in close proximity to the bilayer surface because of an electrostatic interaction associated with the P^{-}-N^{+} dipole. This result is consistent with the crystal structure of POPE and small angle neutron scattering studies, where the P^{-}-N^{+} dipole is seen to be approximately perpendicular to the bilayer normal.[39,42] Interestingly, the effect of temperature has a minimal impact on lipid head-group orientations. The value of $<\varphi>$, defined as the angle between the choline lipid head-group and the bilayer surface (Figure III-17), does not significantly vary with temperature. Therefore, the increase in the observed dipolar couplings in C_{α} and C_{β} positions is a consequence of an increase in the $S_{bicelles}$ order parameter. Similar trends are observed for the effect of hydration on the head-group moiety. The values obtained for $<\varphi>$ are constant among various hydration levels, indicating the changes in the dipolar couplings are due to an increase in the ordering of the head-group region. At the lowest hydration level of 50%, which corresponds to 37 water molecules per lipid, the surface of the bilayer still remains properly hydrated and well above the critical number of 25 water molecules per lipid; in fact, only when the number of water molecules per lipid is < 18 should one expects a reorientation of the head-group moiety.[40] Therefore, at these hydration levels, it is not surprising that the orientation of the lipid head-group remains relatively constant.

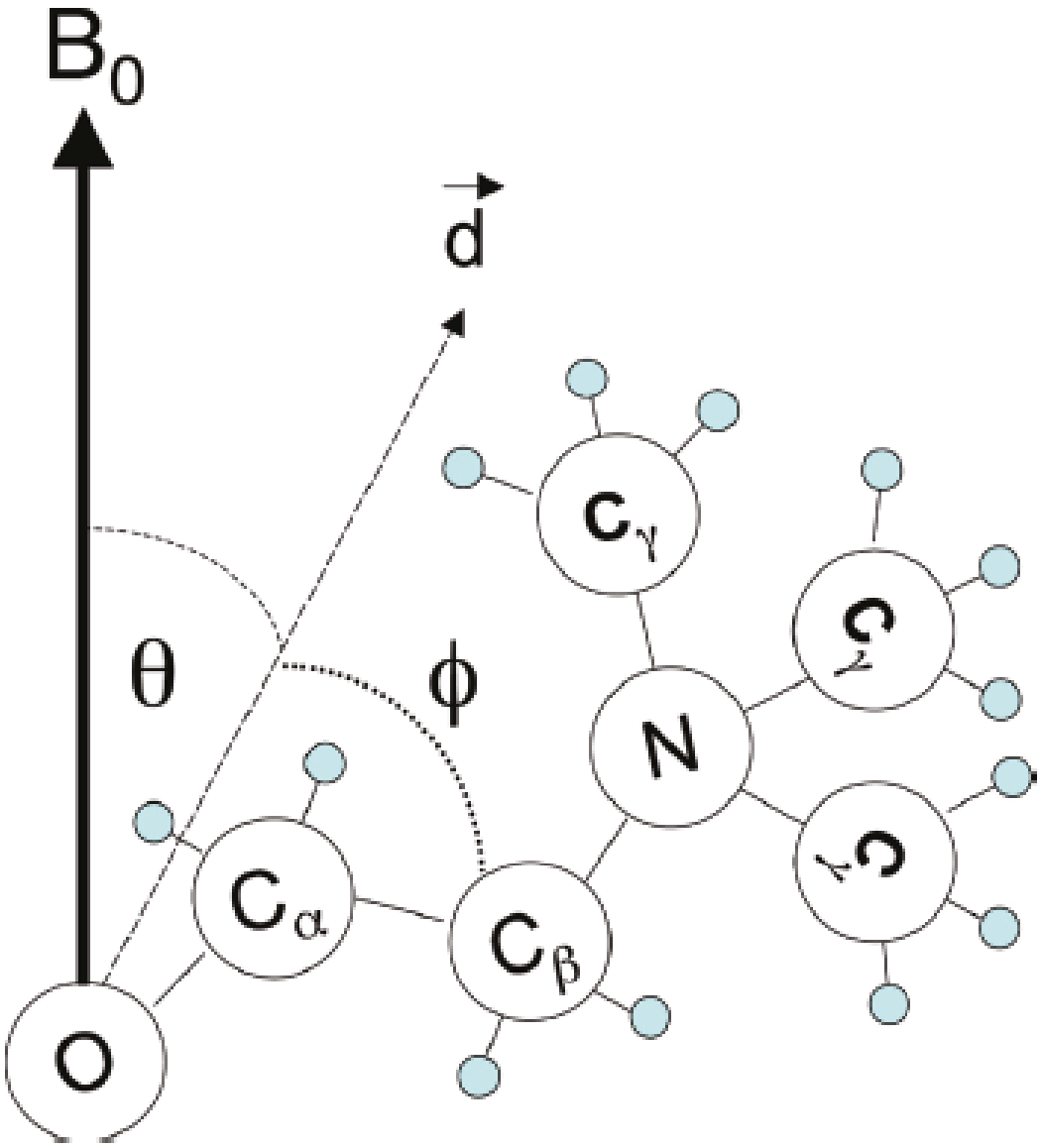

Figure III-17. **Orientation of the choline head-group of DMPC is represented**, by two angles φ and $\varphi + \theta$, with respect to the director of the lipid (d) and the external magnetic field axis (B_0). The relationship between φ and ϕ is j = 90^o - ϕ; φ is the angle between the bilayer surface and the choline lipid head-group.

q ratio	C_α (Hz)	C_β (Hz)	C_γ (Hz)	average angle $\langle\varphi\rangle$
2.7	32.1	28.4	24.8	28.4
3.5	32.7	29.6	25.8	29.3
4.3	32.1	28.8	26.1	29.0

Table III-6. **Angle φ (in Degrees) Calculated from Experimentally Measured ^{13}C-^{1}H Dipolar Couplings at Different Carbon sites of DMPC Head-Group in Bicelles of Different *q* Ratio**

temperatures (°C)	C_α (Hz)	C_β (Hz)	C_γ (Hz)	average angle $\langle\varphi\rangle$
30	33.1	30.3	28.2	30.5
37	33.0	30.2	27.9	30.4
45	32.8	29.4	27.2	29.8
50	32.8	29.3	27.1	29.7

Table III-7. **Angle φ (in Degrees) Calculated from Experimentally Measured ^{13}C-^{1}H Dipolar Couplings at Different Carbon sites of DMPC Head-Group in Bicelles of Different Temperatures**

water molecules per lipid	C_α (Hz)	C_β (Hz)	C_γ (Hz)	average angle $\langle\varphi\rangle$
338	27.4	25.9	25.4	26.3
151	27.0	25.4	22.1	25
87	26.9	25.5	22.1	24.8
56	26.8	25.5	21.4	24.6
37	26.7	25.4	21.26	24.5

Table III-8. **Angle φ (in Degrees) Calculated from Experimentally Measured ^{13}C-^{1}H Dipolar Couplings at Different Carbon sites of DMPC Head-Group in Bicelles of Different Hydration Levels**

Both the q ratio and the hydration level exert similar effects on the dynamics of bicelles: they mainly influence the global $S_{bicelles}$ order parameter. This order parameter influences each region of the bilayer equally; most changes observed in the dipolar coupling as a function of either the q ratio or hydration level can be attributed to a change in this parameter. In contrast, the influence of the temperature has a differential effect on the dynamics of lipids at different regions of the bilayer. The S_{CH} order parameter scales inversely with the temperature as motions in the acyl chains increase. The increase in the thermal kinetic energy translates to a higher degree of overall motion in the acyl chains, leading to a significant decrease in the order parameter. Interestingly, the head-group and glycerol regions respond slightly different from that of acyl chains for a change in the temperature. The increase in temperature causes an increase in ordering of these regions and can be attributed to the dehydration effects with increasing temperature. It would be interesting to use the measured C-H dipolar couplings and the C-H order parameters to probe the dehydration induced by ligand binding to membrane bilayers. For example, such measurements will be useful in understanding the membrane fusogenic activities by viral peptides[43] and also the membrane-disrupting mechanisms by antimicrobial peptides[44] or amyloid peptides.[45]

III-4. References

III-2.

1 Gao, F.P.; Cross, T.A. *Genome Biol.* **2005**, *6*, Art. No. 244.

2 Hwang, P.M.; Kay, L.E. *Methods Enzymol.* **2005**, *394*, 335-50.

3 (a) Tian, C.L.; Karra, M.D.; Ellis, C.D.; Jacob, J.; Oxenoid, K.; Sonnichsen, F.; Sanders, C.R. *Methods Enzymol.* **2005**, *394*, 321-334. (b) Sanders, C.R.; Sonnichsen, F. *Magn. Reson. Chem.* **2006**, *44*, 24-40.

4 (a) Tian, C.L.; Breyer, R.M.; Kim, H.J.; Karra, M.D.; Friedman, D.B.; Karpay, A.; Sanders, C.R. *J. Am. Chem. Soc.* **2006**, *128*, 5300-5300. (b) Evanics, F.; Hwang, P. M.; Cheng, Y.; Kay, L.E.; Prosser, R.S. *J. Am. Chem. Soc.* **2006**, *128*, 8256-64.

5 Opella, S.J.; Marassi, F.M. *Chem. Rev.* **2004**, *104*, 3587-3606.

6 (a) Arora, A.; Tamm, L.K. *Curr. Opin. Struct. Biol.* **2001**, *11*, 540-7. (b) Cierpicki, T.; Liang, B.; Tamm, L.K.; Bushweller, J.H. *J. Am. Chem. Soc.* **2006**, *128*, 6947-51.

7 Fernandez, C.; Hilty, C.; Wider, G; Guntert, P.; Wüthrich, K. *J. Mol. Biol.* **2004**, *336*, 1211-21.

8 Porcelli, F.; Buck-Koehntop, B.A.; Thennarasu, S.; Ramamoorthy, A.; Veglia, G. *Biochemistry* **2006**, *45*, 5793-5799.

9 Porcelli, F.; Buck, B.; Lee, D.K.; Hallock, K. J.; Ramamoorthy, A.; Veglia, G. *J. Biol. Chem.* **2004**, *279*, 45815-45823.

10 Marassi, F.M.; Opella, S.J. *J. Magn. Reson.* **2000**, *144*, 150-155.

11 Wang, J.; Denny, J.; Tian, C.; Kim, S.; Mo, Y.; Kovacs, F.; Song, Z.; Nishimura, K.; Gan, Z.; Fu, R.; Quine, J.R.; Cross, T.A. *J. Magn. Reson.* **2000**, *144*, 162-167.

12 Ramamoorthy, A.; Wei, Y.; Lee, D.K. *Annu. Rep. NMR Spectrosc.* **2004**, *52*, 1-52.

13 De Angelis, A.A.; Nevzorov, A.A.; Park, S.H.; Howell, S.C.; Mrse, A.A.; Opella, S.J. *J. Am. Chem. Soc.* **2004**, *126*, 15340-15341.

14 Kamihira, M.; Vosegaard, T.; Mason, A.J.; Straus, S.K.; Nielsen, N.C.; Watts, A. *J. Struct. Biol.* **2005**, *149*, 7-16.

15 Crocker, E.; Eilers, M.; Ahuja, S.; Hornak, V.; Hirshfeld, A.; Sheves, M.; Smith, S. O. *J. Mol. Biol.* **2006**, *357*, 163-172.

16 Yamamoto, K.; Tuzi, S.; Saito, H.; Kawamura, I.; Naito, A. *Biochim. Biophys. Acta* **2006**, *1758*, 181-189.

17 Yao, X.L.; Hong, M. *Biochemistry* **2006**, *45*, 289-295.

18 (a) Lange, A.; Giller, K.; Hornig, S.; Martin-Eauclaire, M.F.; Pongs, O.; Becker, S.; Baldus, M. *Nature* **2006**, *440*, 959-962. (b) Andronesi, O.C.; Becker, S.; Seidel, K.; Heise, H.; Young, H.S.; Baldus, M. *J. Am. Chem. Soc.* **2005**, *127*, 12965-12974. (c) Baldus, M. In *NMR spectroscopy of biological solids*; Ramamoorthy, A., Ed.; Taylor & Francis: New York, 2006; pp 39-56.

19 Todokoro, Y.; Yumen, I.; Fukushima, K.; Kang, S.W.; Park, J.S.; Kohno, T.; Wakamatsu, K.; Akutsu, H.; Fujiwara, T. *Biophys. J.* **2006**, *91*, 1368- 1379.

20 Luca, S.; Heise, H.; Baldus, M. *Acc. Chem. Res.* **2003**, *36*, 858-865.

21 Hallock, K.J.; Lee, D.K.; Ramamoorthy, A. *Biophys. J.* **2003**, *84*, 3052-3060.
22 Henzler-Wildman, K.A.; Martinez, G.V.; Brown, M.F.; Ramamoorthy, A. *Biochemistry* **2004**, *43*, 8459-8469.
23 Hallock, K.J.; Henzler-Wildman, K.A.; Lee, D.K.; Ramamoorthy, A. *Biophys. J.* **2002**, *82*, 2499-2503.
24 Strandberg, E.; Ulrich, A.S. *Concepts Magn. Reson.* **2004**, *23*, 89-120.
25 Hallock, K.J.; Lee, D.K.; Omnaas, J.; Mosberg, H.I.; Ramamoorthy, A. *Biophys. J.* **2002**, *83*, 1004-1013.
26 Henzler-Wildman, K.A.; Lee, D.K.; Ramamoorthy, A. *Biochemistry* **2003**, *42*, 6545-6558.
27 Park, S.H.; Prytulla, S.; De Angelis, A.A.; Brown, J.M.; Kiefer, H.; Opella, S.J. *J. Am. Chem. Soc.* **2006**, *128*,7402-7403.
28 Sanders, C.R.; Prestegard, J.H. *Biophys. J.* **1990**, *58*, 447.
29 Sanders, C.R.; Schwonek, J.P. *Biochemistry* **1992**, *31*, 8898.
30 Sanders, C.R.; Hare, B..; Howard, K.P.; Prestegard, J.H. *Prog. Nucl. Magn. Reson. Spectrosc.* **1994**, *26*, 421.
31 Howard, K.P.; Opella, S.J. *J. Magn. Reson. B* **1996**, *112*, 91-4.
32 Sanders, C.R.; Prosser, R.S. *Structure* **1998**, *6*, 1227-1234.
33 Cardon, T.B.; Dave, P.C.; Lorigan, G.A. *Langmuir* **2005**, *21*, 4291-4298.
34 Minto, R.E.; Adhikari, P.R.; Lorigan, G.A. *Chem. Phys. Lipids* **2004**, *132*, 55-64.
35 Gaemers, S.; Bax, A. *J. Am. Chem. Soc.* **2001**, *123*, 12343.
36 Lu, J.X.; Damodaran, K.; Lorigan, G.A. *J. Magn. Reson.* **2006**, *178*, 283-287.
37 Dvinskikh, S.V.; Dürr, N.H.U.; Yamamoto, K.; Ramamoorthy, A. *J. Am. Chem. Soc.* **2006**, *128*, 6326-6327.
38 Hester, R.K.; Ackerman, J.L.; Neff, B.L.; Waugh, J.S. *Phys. Rev. Lett.* **1976**, *36*, 1081.
39 Schmidt-Rohr, K.; Spiess, H.W. *Multidimensional Solid-state NMR and Polymers*; Academic Press: San Diego, CA, 1994.
40 Wu, C.H.; Ramamoorthy, A.; Opella, S.J. *J. Magn. Reson., Ser. A* **1994**, *109*, 270.
41 Ramamoorthy, A.; Opella, S.J. *Solid State NMR Spectrosc.* **1995**, *4*, 387.
42 Ramamoorthy, A.; Wu, C.H.; Opella, S.J. *J. Magn. Reson.* **1999**, *140*, 131.
43 (a) Schmidt-Rohr, K.; Nanz, D.; Emsley, L.; Pines, A. *J. Phys. Chem.* **1994**, *98*, 6668-6670. (b) Hong, M.; Pines, A.; Caldarelli, S. *J. Phys. Chem.* **1996**,*100*, 14815.
44 Seelig, J. *Q. Rev. Biophys.* **1977**, *10*, 353.
45 Kumashiro, K.K.; Schmidt-Rohr, K.; Murphy, O.J.; Ouellette, K.L.; Cramer, W.A.; Thompson, L.K. *J. Am. Chem. Soc.* **1998**, *120*, 5043-5051.
46 Gallagher, G.J.; Hong, M.; Thompson, L.K. *Biochemistry* **2004**, *43*, 7899-7906.
47 Metz, G.; Wu, X.L.; Smith, S.O. *J. Magn. Reson., Ser. A* **1994**, *110*, 219-227.
48 Kadkhodaie, M.; Rivas, O.; Tan, M.; Mohebbi, A.; Shaka, A.J. *J. Magn. Reson.* **1991**, *91*, 437-4349.
49 Nevzorov, A.A.; Opella, S.J. *J. Magn. Reson.* **2003**, *164*, 182.

50 Yamamoto, K.; Lee, D.K.; Ramamoorthy, A. *Chem. Phys. Lett.* **2005**, *407*, 289-293.
51 Dvinskikh, S.V.; Sandström, D. *J. Magn. Reson.* **2005**, *175*, 163.
52 Lee, D.K.; Narasimhaswamy, T.; Ramamoorthy, A. *Chem. Phys. Lett.* **2004**, *399*, 359-362.
53 Yamamoto, K.; Ermakov, V.L.; Lee, D.K.; Ramamoorthy, A. *Chem. Phys. Lett.* **2005**, *408*, 118-122.
54 Dvinskikh, S.V.; Yamamoto, K.; Ramamoorthy, A. *Chem. Phys. Lett.* **2006**, *419*, 168.
55 Yamamoto, K.; Dvinskikh, S.V.; Ramamoorthy, A. *Chem. Phys. Lett.* **2006**, *419*, 533.
56 Dvinskikh, S.V.; Yamamoto, K.; Ramamoorthy, A. *J. Chem. Phys.* **2006**, *125*, 034507.
57 Burum, D.P.; Linder, M.; Ernst, R.R. *J. Magn. Reson.* **1981**, *44*, 173.
58 Caravatti, P.; Braunschweiler, L.; Ernst, R.R. *Chem. Phys. Lett.* **1983**, *100*, 305.
59 Lee, M.; Goldburg, W.I. *Phys. Rev. A* **1965**,*140*, 1261.
60 Mehring, M.; Waugh, J.S. *Phys. Rev. B* **1972**, *5*, 3459.
61 Bielecki, A.; Kolbert, A.C.; de Groot, H.J.M.; Griffin, R.G.; Levitt, M.H. *Adv. Magn. Reson.* **1990**, *14*, 111.
62 Takegoshi, K.; Mcdowell, C.A. *Chem. Phys. Lett.* **1985**, *116*, 100.
63 Bak, M.; Rasmussen, J.T.; Nielsen, N.C. *J. Magn. Reson.* **2000**, *147*, 296.
64 Dvinskikh, S.V.; Sandström, D.; Zimmermann, H.; Maliniak, A. *Chem. Phys. Lett.* **2003**, *382*, 410-417.
65 Hong, M.; Schmidt-Rohr, K.; Pines, A. *J. Am. Chem. Soc.* **1995**, *117*, 3310.
66 Hong, M.; Schmidt-Rohr, K.; Nanz, D. *Biophys. J.* **1995**, *69*, 1939.
67 Santos, J.S.; Lee, D.K.; Ramamoorthy, A. *Magn. Reson. Chem.* **2004**, *42*, 105-114.
68 Scherer, P.G.; Seelig, J. *Biochemistry* **1989**, *28*, 7720-7728.
69 Semchyschyn, D.J.; MacDonald, P.M. *Magn. Reson. Chem.* **2004**, *42*, 89-104.
70 Ramamoorthy, A.; Thennarasu, S.; Tan, A.; Lee, D.K.; Clayberger, C.; Krensky, A.M. *Biochim. Biophys. Acta, Biomembranes* **2006**, *1758*, 154-163.
71 Mecke, A.; Lee, D.K.; Ramamoorthy, A.; Orr, B.G.; Holl, M.M.B. *Biophys. J.* **2005**, *99*, 4043-4050.

III-3.

1 (a) Sanders, C. R.; Hare, B. J.; Howard, K. P.; Prestegard, J. H. *Prog. NMR Spectrosc.* **1994**, 26, 421–444. (b) Mecke, A.; Lee, D.K.; Ramamoorthy, A.; Orr, B.G.; Holl, M.M.B. *Biophys. J.* **2005**, *99*, 4043-4050.
2 Prosser, R.S.; Evanics, F.; Kitevski, J.L.; Al-Abdul-Wahid, M.S. *Biochemistry* **2006**, 45, 8453–8465.
3 Marcotte, I.; Auger, M. *Concepts Magn. Reson., Part A* **2005**, 24, 17–37.
4 Sanders, C.R.; Prosser, R.S. *Structure* **1998**, 6, 1227–1234.

5 Prosser, R.S.; Hwang, J.S.; Vold, R.R. *Biophys. J.* **1998**, 74, 2405–2418.
6 Sanders, C.R.; Schwonek, J.P. *Biochemistry* **1992**, 31, 8898–8905.
7 Vold, R.R.; Prosser, R.S. *J. Magn. Reson. B* **1996**, 113, 267–271.
8 De Angelis, A.A.; Howell, S.C.; Nevzorov, A.A.; Opella, S.J. *J. Am. Chem. Soc.* **2006**, 128, 12256–12267.
9 (a) Dvinskikh, S.V.; Dürr, U.H.N.; Yamamoto, K.; Ramamoorthy, A. *J. Am. Chem. Soc.* **2006**, 128, 6326–6327. (b) Dvinskikh, S.V.; Yamamoto, K.; Scanu, D.; Deschenaux, R.; Ramamoorthy, A. *J. Phys. Chem.* **2008**, 112, 12347–12353.
10 Dvinskikh, S.V.; Dürr, U.H.N.; Yamamoto, K.; Ramamoorthy, A. *J. Am. Chem. Soc.* **2007**, 129, 794–802.
11 Dürr, U.H.N.; Waskell, L.; Ramamoorthy, A. *Biochim. Biophys. Acta, Biomembr.* **2007**, 1768, 3235–3259.
12 Dürr, U.H.N.; Yamamoto, K.; Im, S.C.; Waskell, L.; Ramamoorthy, A. *J. Am. Chem. Soc.* **2007**, 129, 6670–6671.
13 Li, C.; Yi, M.; Hu, J.; Zhou, H.X.; Cross, T.A. *Biophys. J.* **2008**, 94, 1295–1302.
14 Nieh, M.P.; Glinka, C.J.; Krueger, S.; Prosser, R.S.; Katsaras, J. *Langmuir* **2001**, 17, 2629–2638.
15 Nieh, M.P.; Glinka, C.J.; Krueger, S.; Prosser, R.S.; Katsaras, J. *Biophys. J.* **2002**, 82, 2487–2498.
16 Nieh, M.P.; Raghunathan, V.A.; Glinka, C.J.; Harroun, T.A.; Pabst, G.; Katsaras, J. *Langmuir* **2004**, 20, 7893–7897.
17 Soong, R.; Macdonald, P.M. *Biophys. J.* **2005**, 88, 255–268.
18 Soong, R.; Macdonald, P.M. *Biophys. J.* **2005**, 89, 1850–1860.
19 Aussenac, F.; Laguerre, M.; Schmitter, J.M.; Dufourc, E.J. *Langmuir* **2003**, 19, 10468–10479.
20 Triba, M.N.; Warschawski, D.E.; Devaux, P.F. *Biophys. J.* **2005**, 88, 1887–1901.
21 Raffard, G.; Steinbruckner, S.; Arnold, A.; Davis, J.H.; Dufourc, E.J. *Langmuir* **2000**, 16, 7655–7662.
22 Kusumi, A.; Nakada, C.; Ritchie, K.; Murase, K.; Suzuki, K.; Murakoshi, H.; Kasai, R.S.; Kondo, J.; Fujiwara, T. *Ann. Rev. Biophys. Biomol. Struct.* **2005**, 34, 351–354.
23 Lindblom, G. *Curr. Opin. Colloid Interface Sci.* **1996**, 1, 287–295.
24 Mangels, M.L.; Cardon, T.B.; Harper, A.C.; Howard, K.P.; Lorigan, G.A. *J. Am. Chem. Soc.* **2000**, 122, 7052–7058.
25 Tiburu, E.K.; Moton, D.M.; Lorigan, G.A. *Biochim. Biophys. Acta, Biomembr.* **2001**, 1512, 206–214.
26 Soong, R.; Macdonald, P.M. *Biochim. Biophys. Acta, Biomembr.* **2007**, 1768, 1805–1814.
27 Soong, R.; Macdonald, P. M. *Langmuir* **2008**, 24, 518–527.
28 Lu, J.X.; Damodaran, K.; Lorigan, G.A. *J. Magn. Reson.* **2006**, 178, 283–287.
29 Dvinskikh, S.V.; Yamamoto, K.; Dürr, U.H.N.; Ramamoorthy, A. *J. Magn. Reson.* **2007**, 184, 228–235.
30 Koenig, B.W.; Gawrisch, K. *J. Phys. Chem. B* **2005**, 109, 7540–7547.

31 Schmidt-Rohr, K.; Nanz, D.; Emsley, L.; Pines, A. *J. Phys. Chem.* **1994**, 98, 6668–6670.
32 Bertram, R.; Asbury, T.; Fabiola, F.; Quine, J.R.; Cross, T.A.; Chapman, M.S. *J. Magn. Reson.* **2003**, 163, 300–309.
33 Cardon, T.B.; Dave, P.C.; Lorigan, G.A. *Langmuir* **2005**, 21, 4291–4298.
34 Sanders, C.R. *Biophys. J.* **1993**, 64, 171–181.
35 Semchyschyn, D.J.; Macdonald, P.M. *Magn. Reson. Chem.* **2004**, 42, 89–104.
36 Davis, J. H. *Biochim. Biophys. Acta.* **1983**, 737, 117–171.
37 Seelig, J.; Gally, H.U.; Wohlgemuth, R. *Biochim. Biophys. Acta.* **1977**, 467, 109–119.
38 (a) Brown, M.F.; Seelig, J. *Nature* **1977**, 269, 721–723. (b) Buldt, G.; Gally, H.U.; Seelig, A.; Seelig, J. *Nature* **1978**, 271, 182–184.
39 Lee, D.L.; Kwon, B.S.; Ramamoorthy, A. *Langmuir* **2008**, 24, 13598–13604.
40 Bechinger, B.; Seelig, J. *Chem. Phys. Lipids* **1991**, 58, 1–5.
41 Scherer, P.G.; Seelig, J. *Biochemistry* **1989**, 28, 7720–7728.
42 Akutsu, H.; Seelig, J. *Biochemistry* **1981**, 20, 7366–7373.
43 Wasniewski, C.M.; Parkanzky, P.D.; Bodner, M.L.; Weliky, D.P. *Chem. Phys. Lipids* **2004**, 132, 89–100.
44 Hallock, K.J.; Lee, D.K.; Ramamoorthy, A. *Biophys. J.* **2002**, 83, 1004–1013.
45 Brender, J.R.; Durr, U.H.N.; Heyl, D.; Budarapu, M.B.; Ramamoorthy, A. *Biochim. Biophys. Acta, Biomembr.* **2007**, 1768, 2026–2029.
46 (a) Ramamoorthy, A.; Lee, D.K.; Santos, J.S.; Henzler-Wildman, K.A. *J. Am. Chem. Soc.* **2008**, 130, 11023–11029. (b) Ramamoorthy, A. *Solid State Nucl. Magn. Reson.* **2009**, in press.
47 Smith, P.E.S.; Brender, J.R.; Ramamoorthy, A. *J. Am. Chem. Soc.* **2009**, 131, 4470–4478.
48 Barry, J.; Fritz, M.; Brender, J.R.; Smith, P.E.S.; Lee, D.K.; Ramamoorthy, A. *J. Am. Chem. Soc.* **2009**, 131, 4490–4498.

Chapter IV

Nuclear Magnetic Resonance Spectroscopy on Membrane Proteins‡

IV-1. Summary

Structural biology of membrane proteins has rapidly evolved into a new frontier of science. Although solving the structure of a membrane protein with atomic-level resolution is still a major challenge, Separated-Local-Field (SLF) NMR spectroscopy has become an invaluable tool in obtaining structural images of membrane proteins under physiological conditions. Recent studies have demonstrated the use of rotating-frame SLF techniques to accurately measure strong heteronuclear dipolar couplings between directly bonded nuclei for the structural determination of membrane proteins. In this chapter the structure and dynamics determinations of cytochrome b_5 and cytochrome P450 membrane protein complex, using newly developed SLF techniques, which we already discussed in previous chapters, are discussed.

IV-2. Solid-State NMR Reveals Structural and Dynamical Properties of a Membrane-Anchored Electron-Carrier Protein, Cytochrome b_5

The vast majority of pharmaceutical compounds in use today are hydrophobic compounds. The human metabolism oxidizes them to water-soluble, excretable compounds by a superfamily of enzymes known as the cytochromes P450 (Cyt P450).[1] These enzymes are sometimes referred to as “Mother Nature’s blowtorch” because they

‡ This chapter is a version of manuscripts published in *J. Am. Chem. Soc.*, 129(2007)794-802., *Mag. Lab. Reports.*, 14(2008)7-8. and *J. Am. Chem. Soc.*, 132(2010)5779-5788. This study was supported by the funds from NIH and NSF.

are such strong and versatile oxidizing agents. Cytochrome *b*5 (Cyt *b*5) is a membrane-bound protein which enhances the efficiency of the metabolism of selected drugs by Cyt P450, by donating an electron to Cyt P450.[2,3] Besides augmenting drug metabolism, Cyt b_5 is also essential for the biosynthesis of testosterone and numerous unsaturated lipids which are necessary for maintaining the integrity of cellular membranes.[3] In order to understand the molecular mechanism by which Cyt b_5 increases the efficiency of oxidation by Cyt P450 in vivo, one must understand the structural folding of Cyt b_5 that enables it to interact with Cyt P450.

Full-length rabbit Cyt b_5 is a 16.7 kDa protein consisting of three domains: a 95 amino acid amino terminal heme-containing domain, a 25 amino acid carboxyl terminal membrane anchor domain, and a 14 amino acid linker region which connects the former two.[3,4] Figure IV-1A shows a model constructed from the solution NMR structure of the soluble domain of rabbit Cyt b_5;[5] the full amino acid sequence is given as Figure IV-2. Because of the difficulties in preparing suitable samples of full-length Cyt b_5, X-ray[6] and solution NMR[5,7] studies reported the structure of the water-soluble domain of Cyt b_5 that lacks the transmembrane domain. Remarkably, the soluble domain alone is not able to fulfill its physiological functions.[3,8] Hence, it is vital to investigate the role of the membrane-bound domain and the linker region in the function of Cyt b_5 in order to fully understand the interaction with Cyt P450. A determination of the three-dimensional structure, dynamics, and the relative orientation of these domains in a membrane environment will shed light on how Cyt b_5 carries out its function. Here, we revealed the first solid-state NMR investigation of the membrane topology and related dynamic properties of full-length rabbit Cyt b_5 in a membrane environment.

Lipid bicelles[9] were prepared from dimyristoylphosphatidylcholine (DMPC) and dihexanoylphosphatidylcholine (DHPC) in a 3.5:1 molar ratio; Cyt b_5 was added in different amounts as described in the Supporting Information. The bicelle samples were magnetically aligned with the bilayer normal perpendicular to the external magnetic field for solid-state NMR experiments. The quality and extent of magnetic alignment of the bicelles containing various concentrations of Cyt b_5 were examined using ^{31}P chemical shift spectra of samples (representative spectra are given as Figure IV-3). Bicelles containing high concentrations (>0.5 mol %) of protein did not align well, while they did

align well upon lowering the protein concentration and are suitable for solid-state NMR studies. At the end of the experiments, the ^{15}N NMR spectra and the molecular weight of Cyt b_5 were checked to rule out protein degradation.

^{15}N chemical shift spectra of uniformly ^{15}N-labeled Cyt b_5 in aligned DMPC:DHPC bicelles show a strong dependence of the spectral line shape on experimental conditions (Figure IV-1). The ^{15}N cross-polarization (CP) spectrum obtained at 0.8 ms contact time (Figure IV-1D) displays the strongest overall intensity and most likely contains signal from the entire protein. It may be expected that the transmembrane (TM) domain of Cyt b_5 is relatively more rigid on the NMR time scale, while the water-soluble domain is less rigid. Therefore, it should be possible to distinguish resonances from these two regions based on the difference in ^{15}N-^{1}H dipolar coupling values. Indeed, we have obtained markedly different ^{15}N spectra when the CP contact time was varied to control the extent of magnetization transfer from ^{1}H to ^{15}N nuclei (Figure IV-1C-E). The spectra suggest that a shorter contact time of 0.1 ms is sufficient to transfer magnetization from ^{1}H to ^{15}N in the rigid residues as found in the TM domain. These experimental conditions result in resonances in the 40-90 ppm range (Figure IV-1E). Interestingly, the signal in the 100-130 ppm region is suppressed to a great extent. On the other hand, since a longer contact time transfers magnetization to all parts of the molecule due to ^{1}H spin diffusion, the spectra at 3 ms (Figure IV-1C) and 0.8 ms (Figure IV-1D) contact time contain peaks in the entire ^{15}N chemical shift frequency range. Hence, we presume that the signal appearing between 100 and 130 ppm originates from the less rigid residues in the soluble domain. This supposition is confirmed by a RINEPT (refocused insensitive nuclei enhanced by polarization transfer) experiment[10] shown in Figure IV-1B. Since no decoupling pulses were employed during the evolution and refocusing delays of the RINEPT sequence, the ^{15}N transverse magnetization evolves under the motionally averaged ^{1}H-^{15}N and ^{1}H-^{1}H dipolar and ^{1}H-^{15}N scalar couplings. The time delays in the RINEPT sequence were experimentally optimized to obtain the signal from the less rigid residues found in the soluble domain of the protein. Interestingly, the RINEPT sequence significantly suppressed the peaks from the TM domain that resonate between 40 and 90 ppm. This is mainly because the transverse magnetization from the TM region dephases

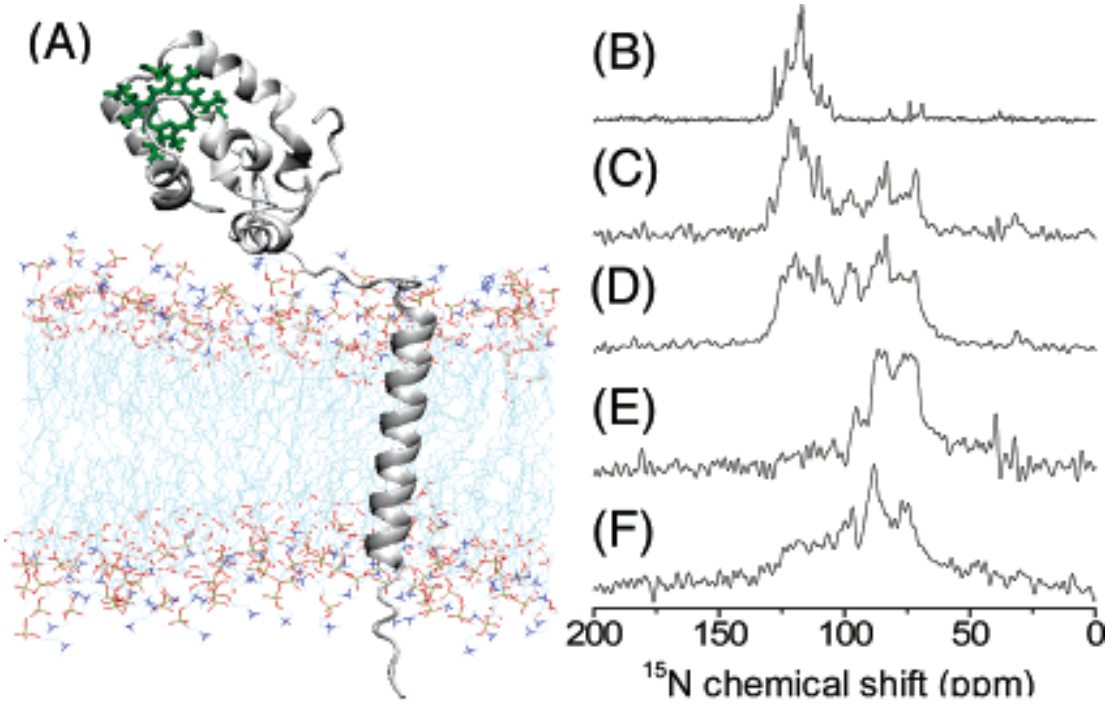

Figure IV-1. **Molecular model and ^{15}N NMR spectra of uniformly aligned DMPC:DHPC bicelles containing ^{15}N-labeled Cyt b_5.** The model (A) shows Cyt b_5 in the context of a DMPC bilayer; the transmembrane, linker, and heme-carrying soluble domains are evident. The ^{15}N RINEPT spectrum (B) shows spectral intensity only in the 100-130 ppm region, consistent with a high mobility of the soluble domain. In the RINEPT sequence, 2.6 and 1.3 ms were used in the first (before the pair of 90° pulses) and second (after the pair of 90° pulses) delays, respectively. This spectral region (100-130 ppm) also shows peaks in cross-polarization (CP) spectra at 3.0 ms (C) and 0.8 ms (D) contact times. At a short contact time of 0.1 ms (E), however, spectral intensity is mostly observed in the range from 40 to 90 ppm. This spectral component is most likely from the relatively immobile transmembrane domain. A D_2O exchange experiment (F) with a 0.8 ms contact time confirms this spectral assignment.

MAAQSDKDVK$_{10}$-YYTLEEIKKH$_{20}$-NHSKSTWLIL$_{30}$ -HHKVYDLTKF$_{40}$ -
LEEHPGGEEV$_{50}$ -LREQAGGDAT$_{60}$ -ENFEDVGHST$_{70}$-DARELSKTFI$_{80}$-
IGELHPDDRS$_{90}$-KLSKPMETLI$_{100}$-TTVDSNSSWW$_{110}$-TNWVIPAISA$_{120}$-
LIVALMYRLY$_{130}$-MADD

Figure IV-2. **Amino acid sequence of rabbit cytochrome b_5,** predicted transmembrane domain is underlined.

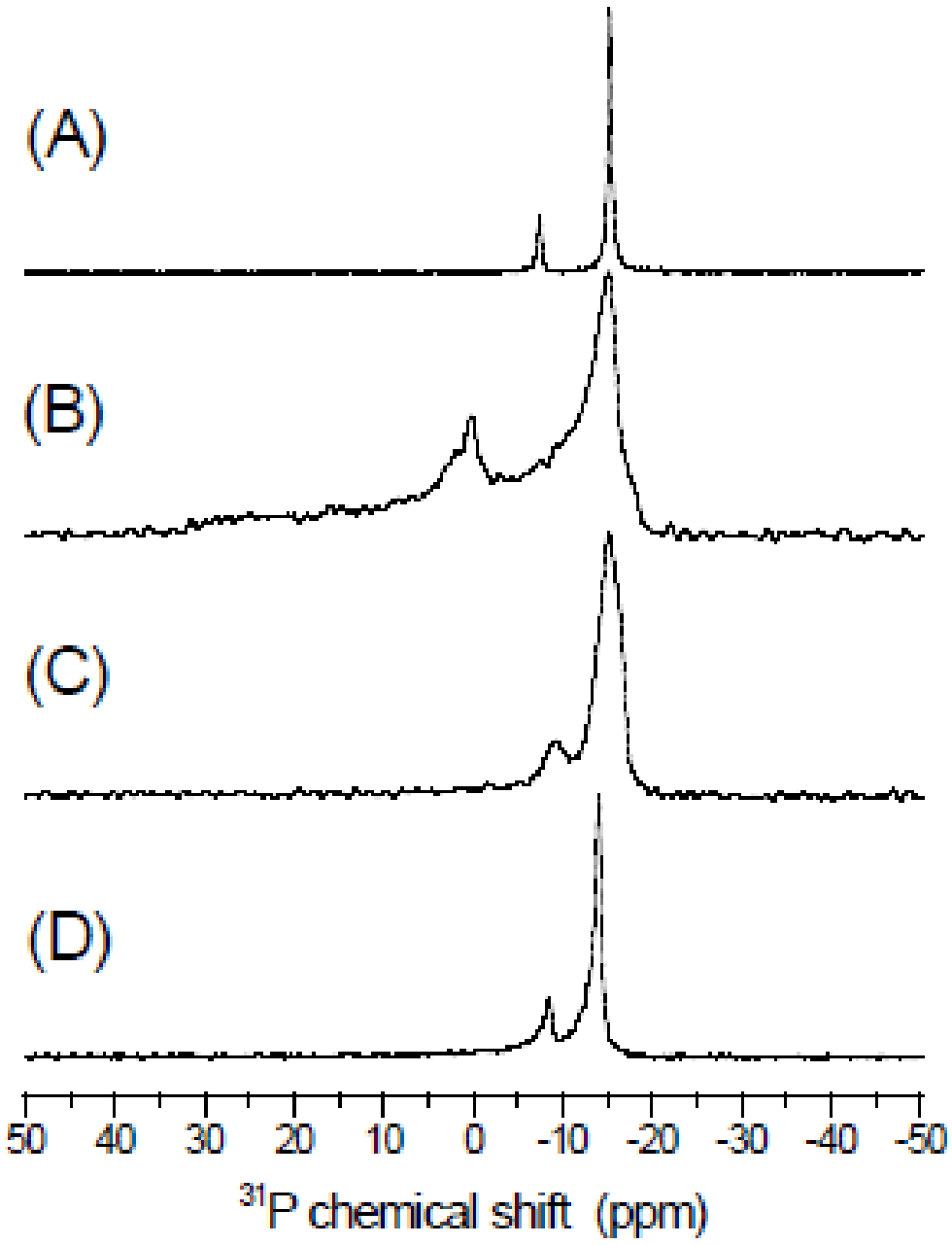

Figure IV-3. **Proton-decoupled ^{31}P-chemical shift spectra of 3.5:1 DMPC/DHPC bicelles containing different concentrations of Cyt b_5.** (A) Pure bicelles without Cyt b_5 show a high degree of alignment as suggested by the narrow lines for DMPC (a peak observed in the high field region) and DHPC (a peak observed in the low field region), while addition of 1:86 Cyt b_5:DMPC (B) completely prohibits any macroscopic orientation. At 1:170 *Cyt* b_5 content (C) macroscopic alignment is observed, albeit broadened lines indicate a low degree of alignment. Only when Cyt b_5 content is further lowered to 1:212 (D), a macroscopic alignment comparable to that observed for pure bicelles (A) can be achieved.

relatively quickly in the evolution and refocusing periods of the RINEPT sequence due to relatively strong ^{1}H-^{15}N and ^{1}H-^{1}H dipolar couplings.

Amide protons can be exchanged with deuterons when exposed to D_2O, thus suppressing the ^{15}N signal from water-exposed protein domains.[11] This approach was utilized to suppress amide ^{15}N signals from the Cyt b_5 ^{15}N spectrum. The ^{15}N CP spectrum of bicelles, where water was exchanged with D_2O, is given in Figure IV-1F. It contains peaks from the TM region (40-90 ppm) but not from the soluble domain (100-130 ppm) of the protein, again supporting our assignment. These 1D spectral editing approaches demonstrate that the dynamics of the transmembrane and soluble domains are very different and that it is possible to differentiate between the resonances from these domains, which is highly valuable to interpret data from PISEMA[12] (polarization inversion and spin exchange at the magic angle)-type experiments in terms of structure and geometry of Cyt b_5.

Two-dimensional Separated-Local-Field spectra, which correlate ^{15}N chemical shift with ^{1}H ^{15}N dipolar coupling, were recorded on well-oriented bicelles and are given in Figure IV-4. A HIMSELF[13] (heteronuclear isotropic mixing leading to spin exchange via the local field) sequence based on the PIWIMz (polarization inversion by windowless isotropic mixing) pulse scheme was used, which we recently found to give better resolution when compared to the more commonly employed PISEMA sequence.[12] Figure IV-4A shows that the 1D spectral region assigned to the TM anchor region of the protein assumes a distinct circular PISA (polarity index slant angle)-wheel pattern[14] when expanded into the second dimension of ^{1}H-^{15}N dipolar coupling, indicative of α-helical conformation. Spectrum Figure IV-4A also proves that the signal from the soluble domain, although resonating in the 100-130 ppm region characteristic for isotropic ^{15}N chemical shifts, shows clearly resolved residual ^{1}H-^{15}N dipolar couplings. This suggests that the soluble domain is weakly aligned. When performed in combination with the abovementioned spectral editing techniques, the 2D HIMSELF experiments demonstrate that it is possible to obtain the resonances from the transmembrane helical region alone by suppressing most other resonances from Cyt b_5 (Figure IV-4B,C).

Spectral simulations were carried out to infer the tilt of the TM α-helix from the observed PISA wheel. The dispersion of resonances in the PISA wheel is consistent with

a 15(±3)° tilt of the TM helix relative to the bilayer normal. However, no single PISA wheel could give a satisfactory fit to all resonances present in the circular pattern, indicating that the helical TM domain may not be a perfect α-helix. The Pro-116 residue located in the middle of the TM region could induce a kink in the helical structure, which may be responsible for this observation of an imperfect PISA wheel. Further experimental studies are in progress to completely assign the spectrum.

IV-2-1. Experimental Procedure

Protein Expression Protocol.

^{15}N labeled full length rabbit cytochrome b5 was expressed in *E.coli* C41 cells using the pLW01 plasmid (Bridges A.; Gruenke, L.; Chang, Y. T.; Vakser, I. A.; Loew, G.; Waskell, L. *J. Biol. Chem.* **1998**, *273*, 17036). The cells were grown from a single colony in LB medium to an OD of 1 at 600 nm. The culture was diluted 100-fold into 10 ml of ^{15}N-Celtone medium. This culture was grown at 35° C with shaking at 250 rpm until an OD of 1 at 600 nm was achieved. The cells were pelleted and resuspended in 10 ml of fresh ^{15}N-Celtone medium. The resuspended cell culture was added to the final 1 L of culture medium. The final culture medium contained 880 ml of ^{15}N-Celtone solution, 112 ml of M9 solution, 2 ml of glycerol, 2 g of [^{15}N] ammonium sulfate, 0.24 mM carbenicillin, 1 mM $CaCl_2$, 10 mM $MgSO_4$, 10 μM $FeCl_3$, 25 μM $ZnSO_4$, 20 μM $MnCl_2$, 250 μM δ-aminolaevulinic acid and vitamin mix (25 μg of biotin, choline chloride, folic acid, niacinamide, D-pantothenate, pyridoxal-HCl, riboflavin and 250 μg of thiamine). Optimal expression was achieved with a 100 mL culture volume in a 500 mL Erlenmeyer flask. The flask was incubated at 35 ^{o}C with shaking at 250 rpm until the OD at 600 nm was 1.2. Isopropyl β-D-thiogalactopyranoside was added to a final concentration of 10 μM, and incubation was continued for 20 h, at which time the cells were harvested. Purification of the ^{15}N cytochrome b_5 was performed as described previously (Mulrooney, S. B.; Waskell, L. *Protein Expr. Purif.* **2000**, *19*, 173).

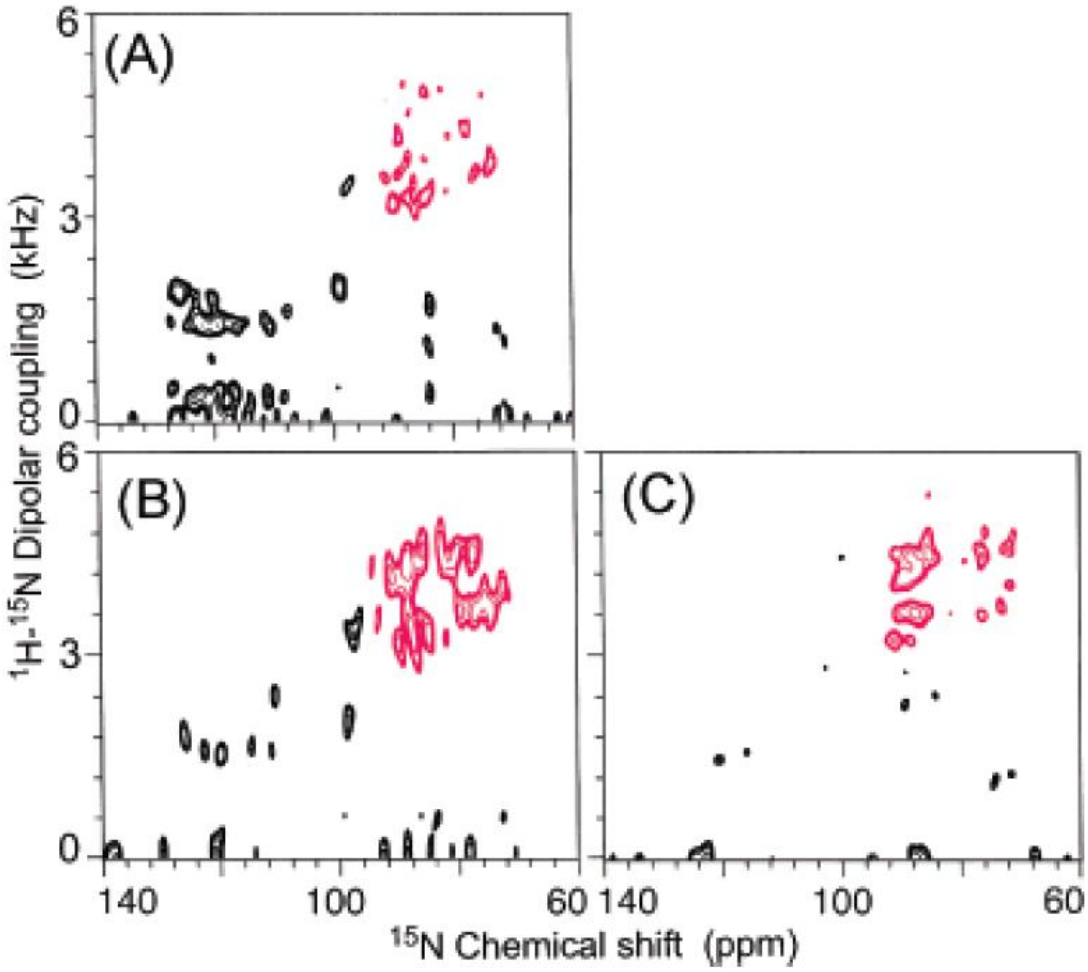

Figure IV-4. **^{15}N-HIMSELF spectra of U-^{15}N-Cyt b_5**, recorded with a CP contact time of 0.8 ms (A) and 0.1 ms (B). (C) Recorded after the water in the bicelle sample was replaced by D_2O, suppressing the spectral contributions of the soluble domain.

Bicelles Preparation Protocol.

40 mg DMPC and 7.6 mg DHPC corresponding to a molar ratio of q=[DMPC]/[DHPC]=3.5 were cosolubilized in chloroform. Solvent was removed under a stream of N_2 gas to give a lipid film on the walls of a glass vessel, which was kept under vacuum overnight to remove all residual solvent. The lipid film was then scratched off the glass and transferred to the 5 mm NMR tube that was used for the experiments. In the NMR tube, 53.5 µl of 50 mM HEPES buffer, pH 7.4, with 10% glycerol content was added to the lipids. The resulting mixture of extreme viscosity was homogenized by vortexing, 30 min sonication in an ice bath, and 4 freeze/heat cycles between liquid nitrogen and 50°C. The resulting turbid gel is still extremely viscous, but viscosity is slightly reduced at 0°C, as is common for all bicellar preparations. Protein was added in the final step of the preparation. Adding 89.3 µl of 3.0 mM cyt b5 solution corresponding to 4.3 mg or 268 nmol protein resulted in a protein:DMPC ratio of 1:220. Because of extreme viscosity, in some samples mechanical mixing with a sterile needle was necessary to mix both phases. Once a satisfactory mixing of the components was reached, the sample tube was sealed and the sample transferred to the magnet for subsequent NMR experiments. Quality of orientation was measured using ^{31}P-NMR and was found to be stable after 1 h of equilibration.

PISA wheel Best-Fit Details.

Best-fit analysis of PISA wheel patterns was done using a home-written software routine. The positions of all clearly resolved peaks were extracted as pairs of ^{15}N chemical shift and ^{1}H-^{15}N dipolar coupling values. These pairs were fit to PISA wheels predicted from geometrical calculations. The formulas used for the calculation of predicted PISA wheels are those given in A. Ramamoorthy et al., *Ann. Rep. NMR Spectrosc*. **2004**, *52*, 1-52. The best-fit helix tilt was found to be 15.3° at a molecular order parameter of Smol=0.88. The corresponding PISA wheel is included in the HIMSELF-spectrum given above. From calculating PISA wheels at slightly differing tilt angles, the error in the fit was estimated to be ±3°. A recent paper from our lab discusses the error in the measurement of the tilt angle (A. Ramamoorthy, S. K. Kandasamy, D. K. Lee, S. Kidambi, and R. G. Larson, Structure, Topology and Tilt of Cell-Signaling

Peptides Containing Nuclear Localization Sequences in Membrane Bilayers Determined by Solid-State NMR and Molecular Dynamics Simulation Studies, *Biochemistry* **2007**, *46*, 965-975).

IV-2-2. ^{31}P-NMR Spectra of Cyt b_5 bicelles samples.

Proton-decoupled ^{31}P-chemical shift spectra of 3.5:1 DMPC/DHPC bicelles containing different concentrations of Cyt b_5 (Figure IV-3). (A) Pure bicelles without Cyt b_5 show a high degree of alignment as suggested by the narrow lines for DMPC (a peak observed in the high field region) and DHPC (a peak observed in the low field region), while addition of 1:86 (Cyt b_5:DMPC) (B) completely prohibits any macroscopic orientation. At 1:170 Cyt b_5 content (C) macroscopic alignment is observed, albeit broadened lines indicate a low degree of alignment. Only when Cyt b_5 content is further lowered to 1:212 (D), a macroscopic alignment comparable to that observed for pure bicelles (A) can be achieved.

IV-2-3. Comparison of Two Dimensional HIMSELF and PISEMA Spectra.

The frequently used 2D PISEMA pulse sequence is very sensitive to the proton frequency offset in the indirect dimension (that is the heteronuclear dipolar coupling frequency dimension). At on-resonance frequency of protons, PISEMA provides the best resolution. However, the dipolar coupling spectral lines are not as narrow at off resonance as they are at on-resonance. The presence of an offset distorts the spectral lines in two ways: (1) increases the scaling factor, which makes the measured dipolar coupling values larger; (2) line narrowing by PISEMA is not efficient, which results in broad dipolar coupling lines. In addition, the PISEMA technique does not enable the measurement of small dipolar coupling values in the presence of large dipolar couplings. These disadvantages of the PISEMA sequence become obvious when experiments are performed on a uniformly labelled protein, where the proton offset problem is unavoidable. To demonstrate these points, we have carried out experiments on an *n*-acetyl-L-valyl-L-leucine single crystal (Figure IV-5) and also on aligned DMPC/DHPC bicelles containing Cyt b_5 (Figure IV-6). 2D HIMSELF and PISEMA data obtained under the same experimental conditions are also given below for comparison. As the data suggest the HIMSELF experiment, unlike the PISEMA method, overcomes the

proton off resonance problem and also performs well for small heteronuclear dipolar couplings. This enables the measurement of motionally averaged ^{1}H-^{15}N dipolar couplings from the soluble domain of Cyt b_5 using the HIMSELF sequence.

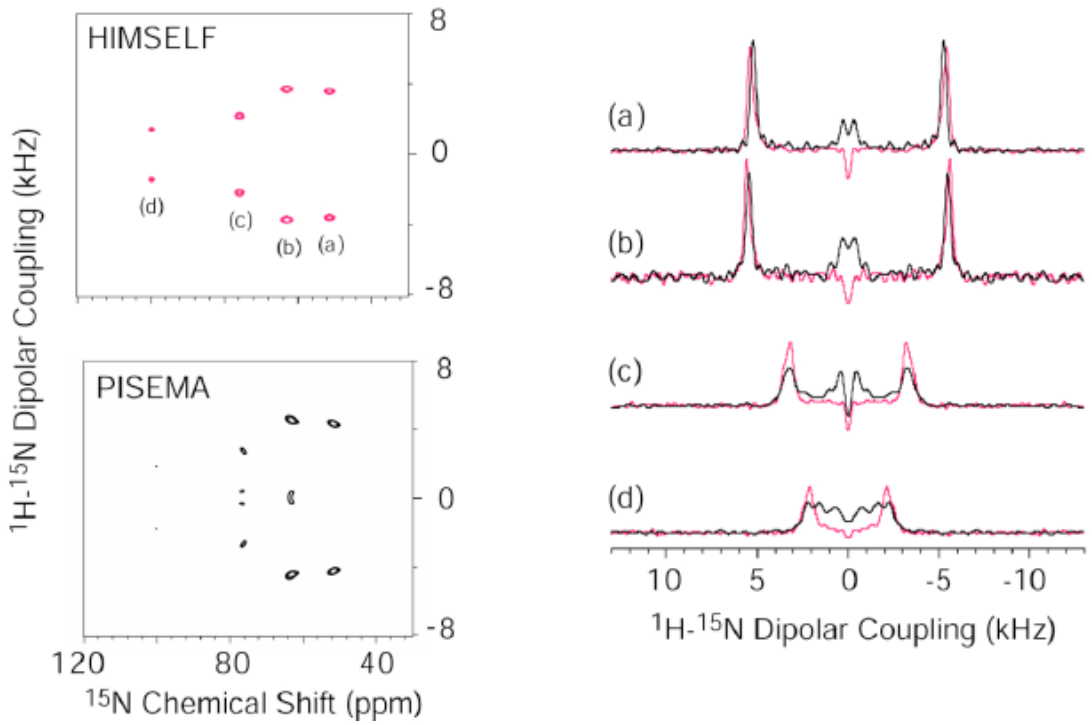

Figure IV-5. **2D HIMSELF (red color) and PISEMA (dark color) spectra of an ^{15}N-labeled *n*-acetyl-L-valyl-L-leucine single crystal.** The dipolar coupling spectral slices clearly demonstrate the better performance of HIMSELF over PISEMA.

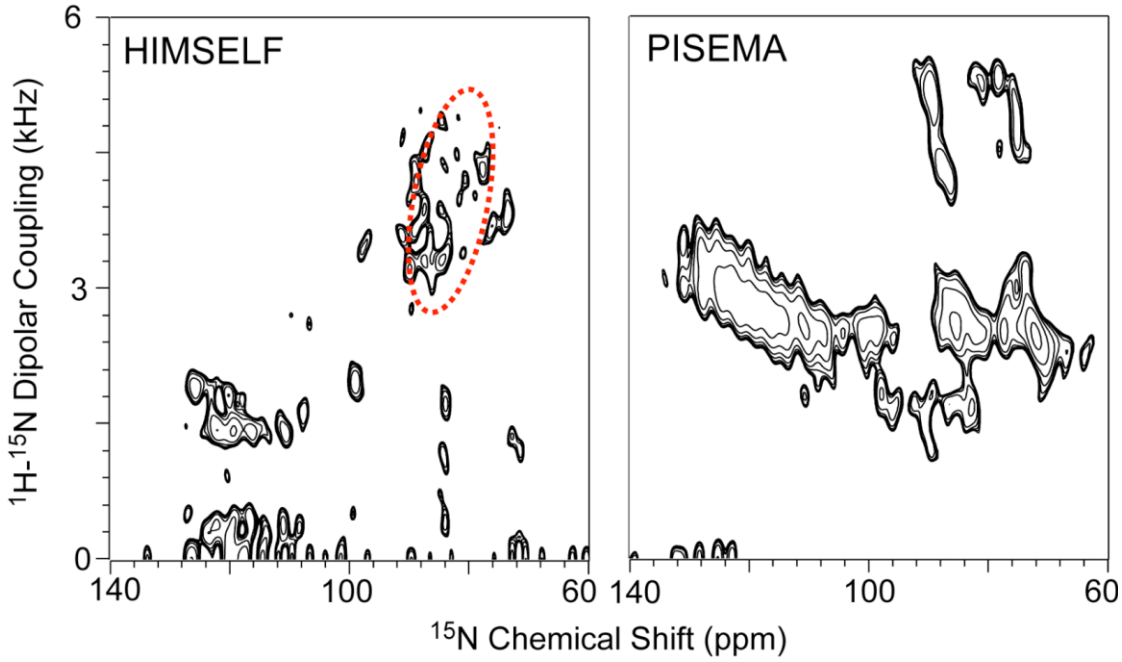

Figure IV-6. **2D HIMSELF (left; the same spectrum as given in Figure IV-4) and PISEMA (right) spectra of 3.5:1 DMPC/DHPC bicelles containing uniformly ^{15}N-labeled Cyt *b*$_5$;** other experimental details are as given in the main text of the paper. The dipolar coupling values appear different in these two spectra because the scaling factor for the PISEMA pulse sequence is larger due to proton offset effects as mentioned above. The simulated PISA wheel (red dashed lines) is shown in the HIMSELF spectrum.

IV-3. Proton-Evolved Local-Field Solid-State NMR Studies of Cytochrome b_5 Embedded in Bicelles, Revealing both Structural and Dynamical Information

Membrane proteins, which constitute a third of all proteins in nature, regulate and direct a host of important cellular processes, ranging from transport of nutrients to generation of energy. Membrane proteins exhibit molecular motions on a wide range of time-scales under physiological conditions and insight into their motions is the key to understanding their functions.

Molecular motions on the order of milliseconds are frequently observed in many essential and fascinating biological processes ranging from ligand binding to enzyme catalysis.[1-4] Fast time scale side-chain dynamics can provide clues into the mechanism by which ions migrate through membrane protein channels. Many membrane-associated enzymes, such as microsomal cytochrome P450, exhibit dynamic structural plasticity that enables the binding of substrates with various sizes and stereochemistry.[5,6] Over the years, significant efforts have been devoted to understand the intricate molecular dynamics of soluble proteins; however, complete characterization of membrane protein dynamics continues to be a challenge.[7-14]

In principle, solid-state NMR spectroscopy is a versatile tool for probing molecular dynamics occurring on time scales that vary from picoseconds (bond libration) to days (protein aggregation). These motions often influence various NMR observables such as chemical shift anisotropy, dipolar coupling and quadrupole coupling. Standard high-resolution solution NMR techniques have provided valuable insights into membrane protein structure-function relationships, but information regarding protein dynamics in lipid bilayers remains elusive.[7-11,15] The slow tumbling rate of most lipid membrane systems leads to various undesirable line broadening effects that make solution NMR techniques not applicable. Therefore, most solution NMR studies of membrane protein are restricted to proteins reconstituted in detergent micelles in cases where they may retain their functions and tumble rapidly enough to average out various undesirable line broadening effects. However, the dynamics observed in these systems can be different from those in a lipid bilayer environment. Solid-state NMR can overcome the undesirable line broadening effects associated with membrane proteins in lipid bilayers. High-resolution solid-state NMR requires the sample to be mechanically aligned or spun at the

magic angle (54.7°) relative to the external magnetic field direction to suppress the line-broadening effects associated with nuclear spin interactions and allows for the reconstitution and study of membrane proteins in their native environment.[16-19]

Separated-Local-Field (SLF) spectroscopy of aligned samples holds a great promise as a practical tool for studying membrane proteins in lipid bilayers.[20-23] Alignment media used for membrane protein structural studies can be made to closely mimic the native membrane and experiments can be carried out under physiological conditions.[13,24-26] Indeed, SLF has been successful in providing detailed structural information of α-helical membrane proteins in well-hydrated bilayer environments. A typical SLF spectrum correlates heteronuclear dipolar couplings between low-γ nuclei and their directly bonded ^{1}H nuclei (such as ^{15}N-^{1}H) with the CSAs of the low-γ nuclei (^{15}N, in this case). Importantly, these NMR observables are sensitive to the whole body motions of a protein, and are therefore capable of providing detailed dynamical and structural information.[27-29] In order to extract dynamical and structural information from an SLF spectrum, one must be able to accurately measure a broad range of dipolar couplings between directly bonded spin pairs. However, in most commonly used rotating-frame SLF protocols, such as heteronuclear isotropic mixing spin exchange via local field (HIMSELF), polarization inversion spin exchange at the magic angle (PISEMA), and SAMMY, various weak heteronuclear dipolar couplings are effectively suppressed in favor of simple spectral line-shape and improved resolution in the indirect dipolar coupling dimension.[30,31] Laboratory-frame SLF experiments such as proton-evolved local field (PELF) provide high sensitivity and resolution for loop regions, soluble domains, and mobile parts of membrane proteins such that structural and dynamical information can be extracted from these regions in a SLF spectrum.[31,32] Also, PELF is capable of resolving a broad range of dipolar couplings from directly bonded spin pair, which is absolutely necessary for determining both dynamics and structures of membrane proteins. Despite these unique advantages, applications of PELF in structural biology remain to be established.

In the present work, we demonstrate the use of the PELF method to extract dynamical and structural information from cytochrome b_5 (Cyt b_5), a membrane-anchored protein. Cytochrome b_5 consists of a transmembrane domain near the C-terminal, a water-soluble heme-containing domain, and a linker region that connects these two domains.

Functional studies have shown that the length of the linker region is crucial for cytochrome *b*5 to interact with and donate an electron to activate cytochrome P450.[33] In the present study, a mutant of cytochrome b_5 (mutant- Cyt b_5), which lacks eight residues in its linker region, is used to demonstrate the efficiency of the PELF sequence. The amino acid sequence of a wild-type rabbit cytochrome b_5 is given in Figure IV-7. A previous solid-state NMR study revealed the various domains of this protein display motions occurring on a wide range of time scales.[23] Since the mutant protein used in this study lacks eight residues in the linker region, the motion of the soluble domain should be significantly reduced such that small, yet measurable, dipolar couplings can be observed. Therefore, it is an ideal system to firmly establish and demonstrate the effectiveness of using the PELF sequence to study the structure and dynamics of membrane proteins in magnetically aligned bicelles.

IV-3-1. Experimental Procedure.

Materials.

DMPC and DHPC were purchased from Avanti Polar Lipids, Alabaster, AL, and used without further purification. All other biochemicals and reagents used in this study were purchased from Sigma-Aldrich, St. Louis, MO.

Preparation of Bicelles.

Bicelleswere prepared with a desired amount of lipid in a buffer. The ratio q was calculated as moles of DMPC per mole of DHPC. A typical preparation involved dissolving the desired quantities of DMPC and DHPC in a buffer solution (10 mM Tris at pH 7.4 and 150 mM NaCl), followed by a series of cycles of freezing, thawing, and gentle vortexing until a clear solution, was obtained. The solution was then stored at 4 ^{o}C for up to 24 h before use.

NMR Spectroscopy.

NMR experiments were carried out on a Chemagnetics/Varian Infinity 400MHz solid-state NMR spectrometer using a 5 mm double-resonance magic-angle spinning probe under static sample conditions. About 150-200 mg of bicelles was loaded in a 5mm

NMR glass tube of 4 cm length, and the tube was closed tightly with a Teflon tape and a cap. The sample was then equilibrated for about 30 min in the magnet at the desired temperature prior to signal acquisitions. ^{31}P chemical shift spectra were recorded using the Hahn echo (90^{o}-τ-180^{o}-τ acquire) experiment with a 90^{o} pulse length of 5 μs, an echo delay of 100 μs, and under a 15-25 kHz continuous-wave proton decoupling. A total of 32 transients were sufficient to acquire reasonable signal-to-noise ratio ^{31}P chemical-shift spectra of well aligned samples, while about 64 scans were acquired for relatively poorly aligned samples. The chemical-shift scale was referenced by setting the ^{31}P chemical-shift peak from phosphoric acid (H_3PO_4) to 0 ppm at 37 ^{o}C. A ramped-cross-polarization (ramp-CP) sequence with a contact time of 5 ms was used to record the 1D ^{13}Cchemical-shift spectra under proton decoupling using various decoupling sequences for a comparative study, while the flip-flop spectroscopy (FLOPSY)-8[48] multiple pulse sequence was used in our experiments because it provided the best resolution. The 2D PELF spectra were obtained using 64 t_1 experiments, 64 scans, a 5 s recycling delay, and a 20 kHz ^{1}H decoupling.

Simulations and Data Analysis.

Numerical simulations were performed using the program SPINEVOLUTION.[39] The simulated spectra and CP buildup curve were plotted using *SigmaPlot 9.0*. The details of the simulation are described in the Results section below. All numerical simulations were performed on a 2.0 GHz Intel Quad Core HP desktop running Windows Vista.

Figure IV-7. **Amino acid sequence of a full-length wild-type rabbit cytochrome b_5.** High-resolution structures of the soluble domain of the protein have been reported from solution NMR and X-ray crystallography studies, whereas the structure of the full-length protein is unknown as it has not been amenable for studies using high-resolution methods. Secondary structures such as α-helix (blue) and β-sheet (green) are indicated based on previous studies. The eight amino acids that were deleted from the linker region of the wild-type cytochrome b_5 to obtain a mutant are shown in red.

IV-3-2. Theory of Two Dimensional Proton-Evolved Local Field (PELF).

A typical PELF radio frequency (RF) pulse sequence is given in Figure IV-8. In the PELF sequence, the transverse magnetizations of protons evolve under heteronuclear dipolar coupling (with an evolution frequency Ω_{IS}) during the incrementable t_1 period, while chemical shifts of protons and ^{1}H-^{1}H homonuclear dipolar couplings are suppressed.[32,34,35] After the t_1 period, the transverse ^{1}H magnetization is transferred to the rare nucleus (referred to as X, often either ^{13}C or ^{15}N) for detection as shown in Figure IV-8.

Since there is no homonuclear dipolar coupling between rare X nuclei and each ^{1}H spin is coupled to a single X nuclear spin, for every resolvable X resonance, either a single doublet corresponding to a single ^{1}H-X dipolar coupling or a simple superposition of doublets corresponding to different sets of ^{1}H-X pairs is observed in the indirect frequency dimension of a two-dimensional (2D) PELF spectrum. The elegant PELF technique thereby avoids the complicated multiplet-type spectral pattern typically observed in the indirect dimension of other SLF sequences where X spin transverse magnetizations are allowed to evolve under the dipolar couplings to many ^{1}H nuclei.[31,32] In other words, after dipolar coupling between a rare X nucleus and the ^{1}H nuclei has evolved for a period of t_1, the relevant term of the density operator contributing to the detected signal is given as

$$\sum_j I^j_{x/y} \cos \Omega^j_{IS} \quad (1)$$

Magnetization transfer in a PELF pulse sequence can be accomplished by any of the following means, depending on sample conditions and the spin system dynamics: a standard cross-polarization (CP) scheme, a CP scheme based on the Lee-Goldburg homonuclear dipolar decoupling, windowless isotropic mixing (WIM),) composite zero cross-polarization (COMPOZER-CP, or insensitive nuclei enhanced by polarization transfer (INEPT)/refocused insensitive nuclei enhanced by polarization transfer (RINEPT). The resolution and sensitivity of a 2D PELF spectrum critically depends on the details of the pulse sequence used to transfer the ^{1}H transverse magnetization.[31,32] For example, a short transfer time is required to suppress ^{1}H spin diffusion, which manifests

as a broad zero-frequency peak in the indirect dipolar coupling frequency dimension that severely obscures the spectrum.[32] Furthermore, for most solid-state systems the rapid rotating-frame relaxation ($T_{1\rho}$) of protons could hamper the efficiency of magnetization transfer, particularly in the standard CP sequence where the transverse magnetization is transferred from protons to less-sensitive nuclei like ^{13}C or ^{15}N. Since for most systems the proton T_1 (spin-lattice relaxation time) is much longer than $T_{1\rho}$, it is advantageous to use a magnetization transfer scheme whereby the transfer of magnetization occurs along the *z*-axis. Currently, two schemes, WIM and COMPOZER-CP, can render such a magnetization transfer while providing homonuclear decoupling to dampen the ^{1}H-^{1}H spin diffusion process.[31,36] It may be noted that the homonuclear decoupling of WIM sequence is more effective than that of the COMPOZER-CP. Therefore, in this study, the performances of these two schemes (COMPOZER-CP and WIM) in PELF sequences are compared with that of the standard CP. The other two magnetization transfer sequences, namely Lee-Goldburg-CP and INEPT, are excluded from this study. Lee-Goldburg-CP is highly sensitive to the frequency offset and may not be appropriate as a general magnetization transfer protocol.[31] Furthermore, magnetization transfer by INEPT sequences only occurs in highly mobile samples and is therefore limited in their applicability to only the mobile regions of membrane proteins.[23]

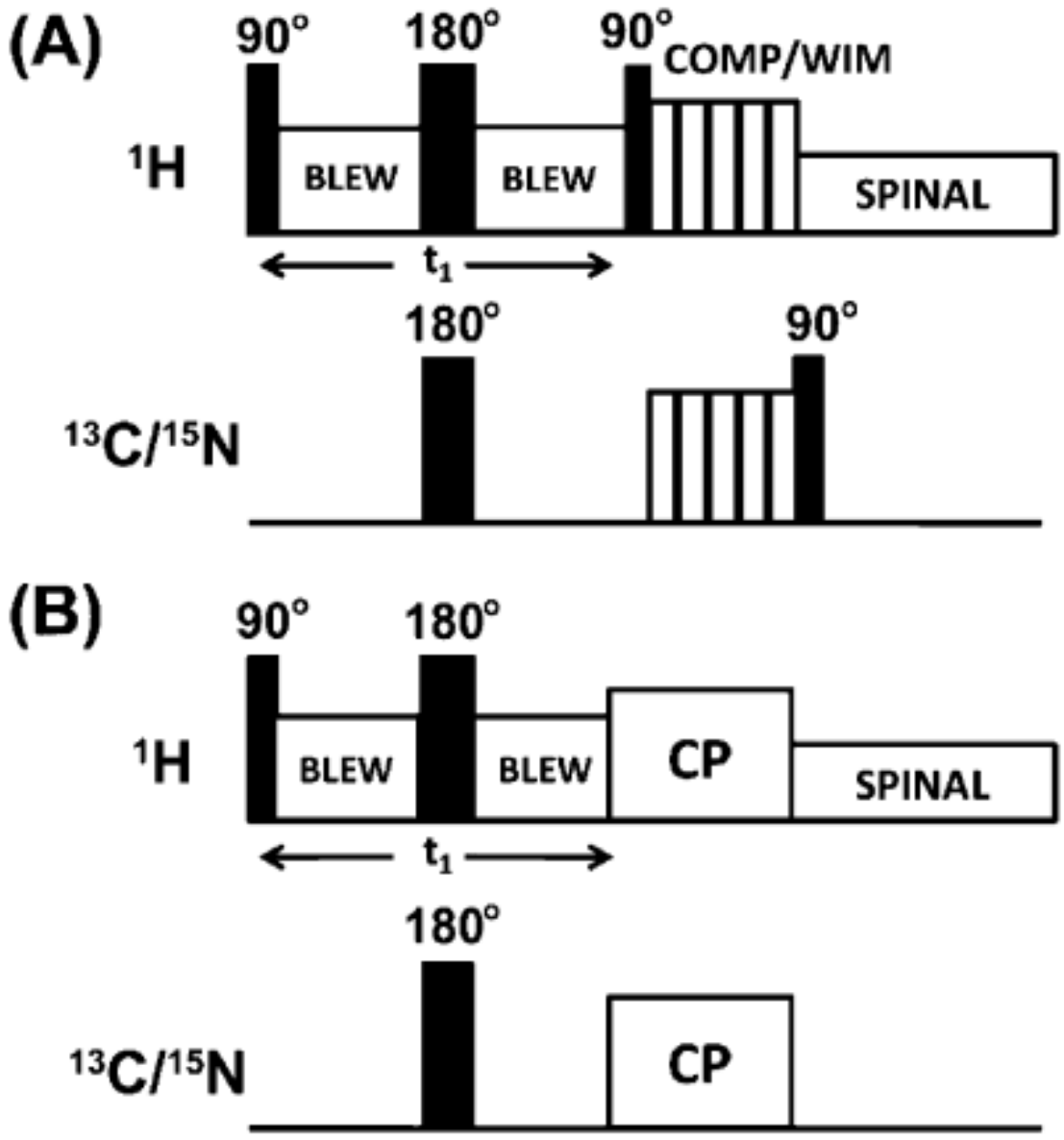

Figure IV-8. **Radio frequency PELF pulse sequences for two-dimensional (2D) SLF spectroscopy of solids.** In these pulse sequences, proton homonuclear decoupling in the *t*1 period is achieved using the BLEW-12 sequence and SPINAL-64 is used to decouple protons during acquisition. Proton transverse magnetization after the t_1 period is transferred to X nuclei using the composite zero degree cross-polarization (COMPOZER-CP) or windowless isotropic mixing (WIM) pulse sequence. (A) or by the standard cross-polarization sequence (B). A supercycled COMPOZER sequence consists of a series of 360° pulses with phases *x*, *-x*, *y*, *-y*, *-y*, *y*, *-x*, *x*. The WIM sequence consists of a series of 90° pulses of phases *-x*, *y*, *-x*, *-x*, *y*, *-x*, *x*, *y*, *x*, *x*, *y*, *x*. Since the *z*-component of proton magnetization is transferred as the *z*-component of ^{15}N or ^{13}C spin magnetization under both WIM and COMPOZER-CP sequences, a 90° read pulse on the ^{15}N or ^{13}C channel is used for detection.

IV-3-3. Simulations of PELF Spectra under Different Magnetization Transfer Schemes.

The influence of magnetization transfer schemes on the resolution and sensitivity of a 2D PELF spectrum, specifically in the heteronuclear dipolar coupling dimension, is investigated through numerical simulations on a hypothetical spin system defined in Figure IV-9 using the SPINEVOLUTION software.[39] In this spin system, an NH group is weakly coupled to an neighboring proton such that it demonstrates the case of biomolecules embedded in the membranes and/or to reflect motionally averaged N-H dipolar couplings as found in relatively mobile regions of a protein. N-H dipolar coupling slices taken from the indirect dimension of the simulated SLF spectrum are shown in Figure IV-10. As illustrated by our numerical simulations (Figures IV-10 and IV-11), not only the choice of the magnetization transfer scheme but also the duration of the magnetization transfer significantly influences the resolution of a PELF spectrum. With a transfer contact time of approximately 250 μs, all of the magnetization transfer schemes give identical dipolar doublets corresponding to the large dipolar coupling (D_1). As the transfer time is increased, significant differences between the spectra are observed, which is a direct consequence of the differences among the magnetization transfer schemes employed (see Figure IV-11). Figure IV-11 shows that the intensity of the strong dipolar coupling (the outer doublet in Figure IV-10) oscillates strongly as a function of magnetization transfer time when WIM or regular CP was used as a magnetization transfer sequence. The WIM sequence offers the highest homonuclear decoupling and therefore allows for the detection and isolation of the weak dipolar coupling D_2 in the presence of the strong coupling D_1, which could be suppressed by the choice of an appropriate magnetization transfer time. As the strength of the homonuclear decoupling decreases, the spectral resolution deteriorates because of the obscuring effect of spin diffusion. Spin diffusion manifests as a zero frequency artifact in the indirect dimension (see E and F of Figure IV-10). As a result, an intense central peak at the zero frequency is observed, obstructing the measurements of weak dipolar couplings. Also, for a long contact time, D_1 is more effectively suppressed when COMPOZER-CP or WIM magnetization transfer schemes are used, which is a consequence of the spin diffusion facilitated by the proton bath. Therefore, the use of these magnetization transfer schemes

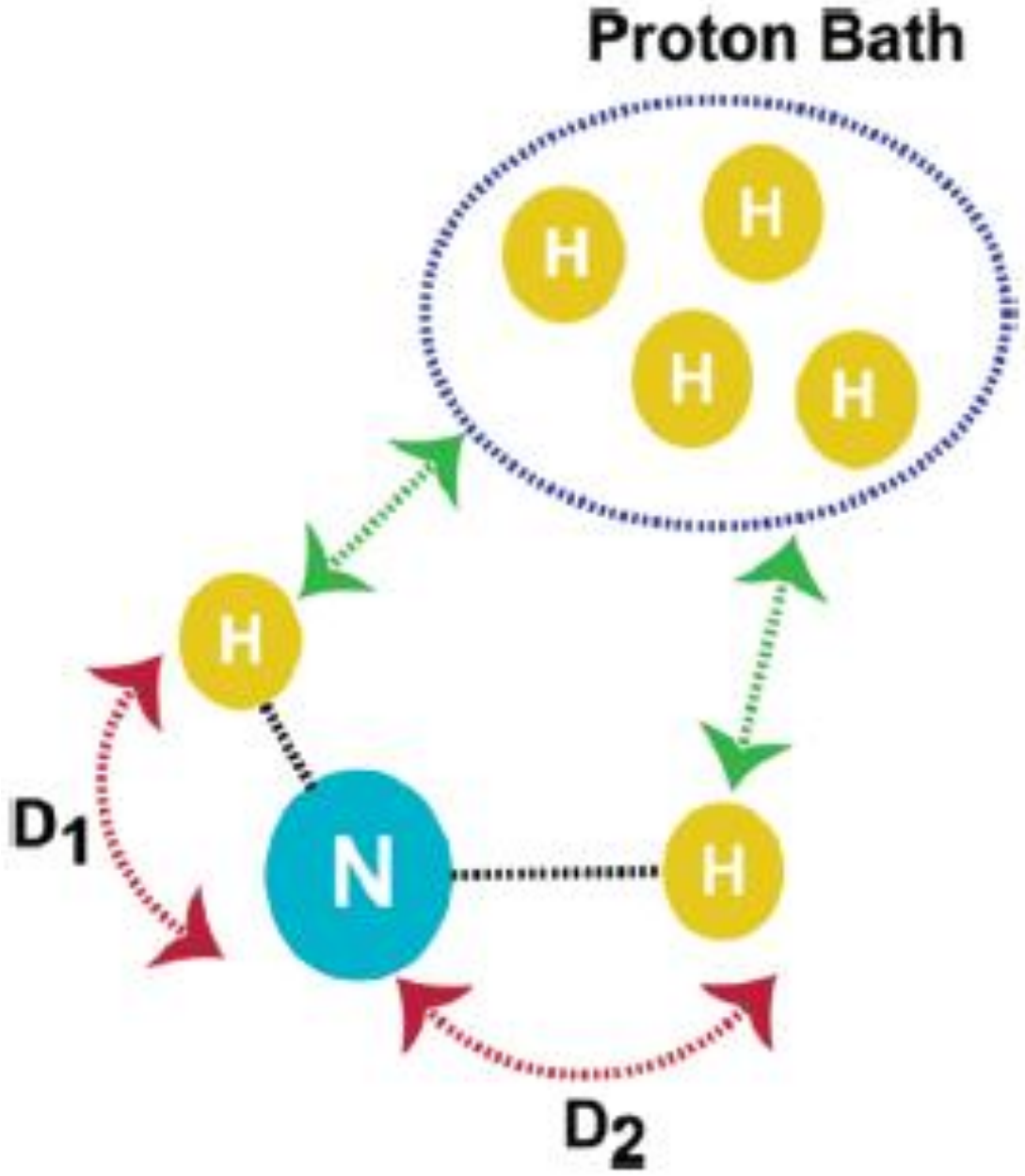

Figure IV-9. **A schematic of a hypothetical spin system to evaluate the PELF pulse sequence.** In this system, a ^{15}N nucleus is strongly dipolar coupled to two nearby protons. The dipolar coupling values used in the simulations are D_1 = 1750 Hz and D_2 = 500 Hz. The ^{15}N-^{1}H dipolar couplings are arranged such that $D_1 > D_2$, and each of these protons is weakly dipolar coupled to a proton bath as indicated by the green arrows.

allow for broader optimal contact time conditions. In summary, from these numerical simulations, we may conclude the following: (1) significant resolution is gained by using a magnetization transfer scheme that suppresses ^{1}H-^{1}H interactions, (2) the main contributors to the central peak observed in the 2D PELF spectrum using the COMPOZER-CP and the regular CP originate from the proton spin diffusion process, and (3) weak ^{1}H-^{1}H dipolar coupling ensures that the amount of ^{1}H magnetization transferred to an X nucleus builds up steadily, which enables a broad range of transfer times to be used. In contrast, when a ^{1}H-^{1}H dipolar coupling is completely eliminated, magnetization is transferred back and forth between insensitive X nuclei and sensitive ^{1}H nuclei, and therefore the transfer time has to be carefully calibrated. This makes PELF-COMPOZER the most generally suitable technique for measuring weak X-^{1}H dipolar couplings (X may be ^{13}C or ^{15}N). Thus, in order to acquire a highly resolved SLF spectrum of an aligned membrane protein using the 2D PELF pulse sequence, one must use a magnetization transfer scheme that suppresses ^{1}H-^{1}H dipolar coupling interactions while using the shortest contact time that permits the observation of the desired range of dipolar coupling frequencies.

IV-3-4. Application of PELF Techniques To Study the Structure and Dynamics of 15N-Labeled Mutant-Cyt b5 in Magnetically Aligned Bicelles.

Low resolution and low sensitivity are often the major obstacles in solid-state NMR studies of membrane proteins. The introduction of magnetically aligned bicelles as an alignment medium has dramatically improved the sample filling factor of the RF coil, reduced the sample preparation time, and improved the quality of alignment when compared to mechanically aligned glass plate samples.[24,40-42] The use of bicelles has been shown to sufficiently improve the sensitivity and resolution of NMR spectra. Studies have shown that bicelles prepared with different *q* ratios can be used for solution-like and solid-state-like NMR experiments, enabling the complete characterization of protein structure, protein dynamics, and protein-membrane interactions.[43,44] Recently, the 2D PELF sequence was demonstrated to be well suited for structural studies of membrane-associated ligands in magnetically aligned bicelles.[44,45] In the present work, we demonstrate the unique advantages of combining the PELF sequence with WIM or

COMPOZER-CP magnetization transfer scheme for structural studies of membrane proteins in aligned bicelles. To this end, we have acquired a series of 2D PELF spectra of mutant-Cyt*b*5 in magnetically aligned bicelles using WIM, COMPOZERCP, or ramp-CP as the magnetization transfer step (Figure IV-12). The contact time used in these experiments was optimized for the maximum signal intensity and spectral resolution.

In general, the 2D PELF sequence implemented with WIM or COMPOZER-CP offers a substantial improvement in resolution when compared to the one with ramp-CP. The resolution gained using a PELF-COMPOZER or PELF-WIM sequence is due to the ability of COMPOZER-CP and WIM to suppress the ^{1}H-^{1}H dipolar interactions as well as the use of a short contact time, which effectively suppresses the contribution from remote spins due to ^{1}H spin diffusion.[31] The central bands (or the zero-frequency peaks) in these experimental spectra are effectively suppressed, suggesting a significant reduction in the spin diffusion process as is also illustrated in our simulations. Therefore, clear dipolar coupling doublets are resolved in the indirect frequency dimension. On the other hand, the central bands severely obscure the spectrum when a regular CP sequence is used in the magnetization transfer step, making accurate measurements of the weak dipolar couplings difficult. These experimental results are in good agreement with the numerical simulations for PELF-COMPOZER, PELF-WIM, and regular PELF protocols presented in Figures IV-10 and IV-11.

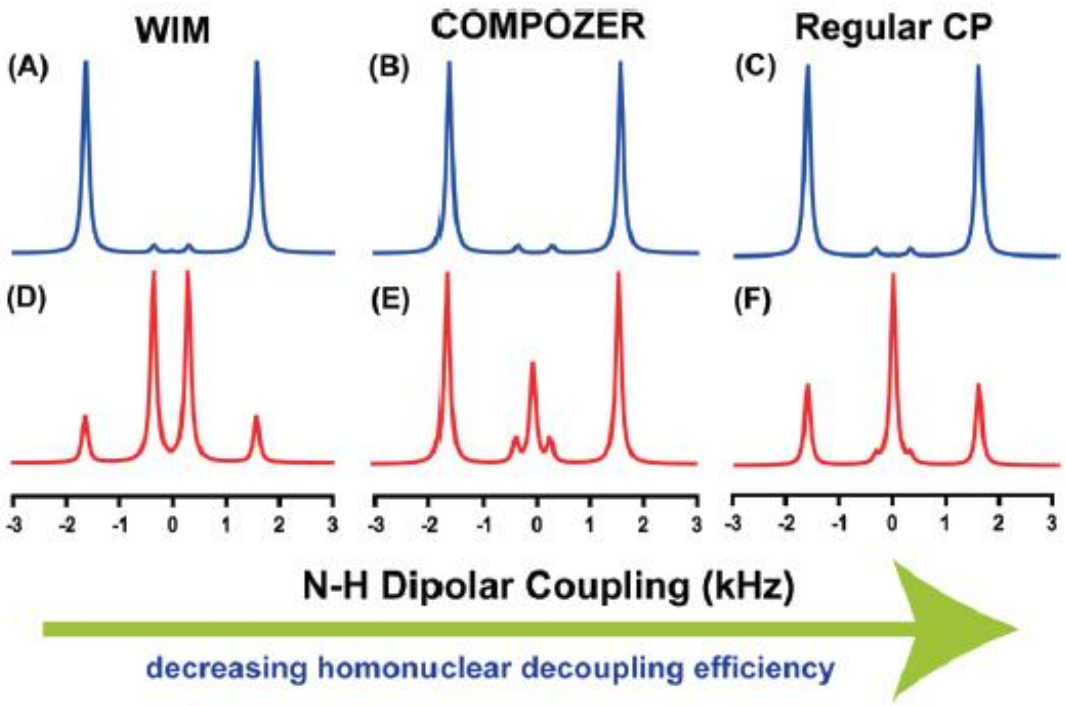

Figure IV-10. **Numerically simulated PELF spectra under different magnetization transfer schemes.** It should be noted that WIM is known for its efficient suppression of ^{1}H-^{1}H dipolar couplings and is better than the COMPOZERCP sequence. On the other hand, the regular CP sequence does not employ any special sequence to suppress ^{1}H-^{1}H dipolar couplings. Spectra A-C were simulated using a contact time of 250 μs and spectra D-F were simulated using a contact of 3 ms.

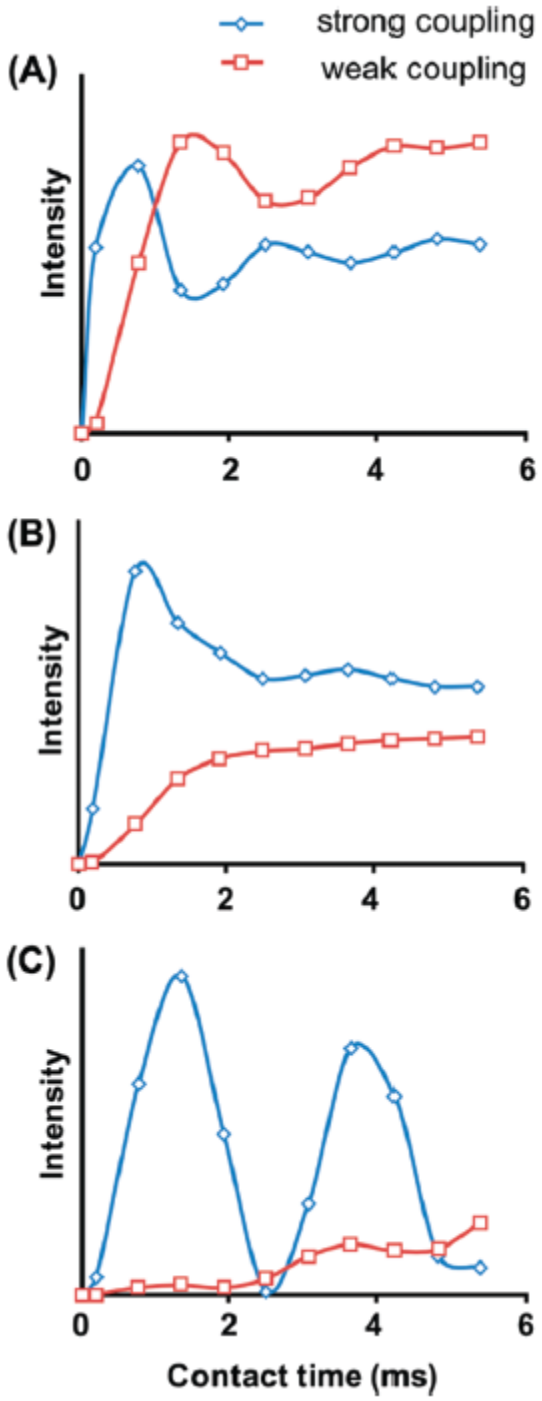

Figure IV-11. **Simulated magnetization transfer efficiency** as a function of transfer time by a regular-CP (A), COMPOZER-CP (B), and WIM (C) in a 2D PELF experiment. Details are discussed in the text.

As shown in A and B of Figure IV-12 two sets of resonances with vastly different dipolar coupling values are clearly observed. The magnitudes of their dipolar couplings indicate that they correspond to different regions of the proteins.[23] The resonances with large dipolar couplings correspond to the membrane-spanning domain, while the small dipolar couplings correspond to a more mobile region of the protein, which probably lies near the membrane surface. The spectral resolution of the transmembrane region in the PELF-COMPOZER and PELF-WIM is comparable to that obtained using the rotating frame sequences like HIMSELF and broad-band-PISEMA (BB-PISEMA).[23] For dipolar couplings originating from the mobile regions of the protein, the gain in spectral resolution when either COMPOZER-CP or WIM is used as the magnetization transfer step (as shown in Figure IV-13) represents a remarkable improvement over previous PELF studies and demonstrates the effectiveness of this new approach. Thus, these experiments demonstrate the practical application of the 2D PELF pulse sequence with the appropriate magnetization transfer scheme to accurately measure a wide range of heteronuclear dipolar couplings for membrane proteins embedded in magnetically aligned bicelles.

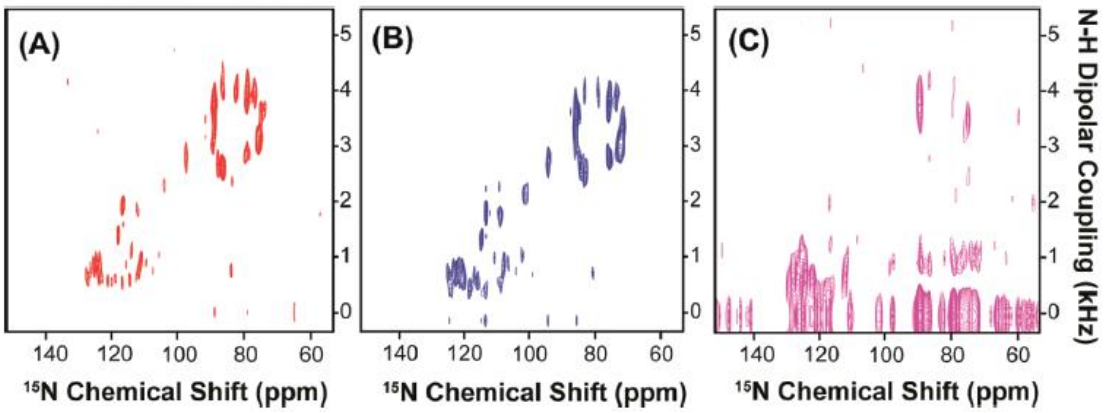

Figure IV-12. **Two-dimensional PELF spectra of magnetically aligned bicelles containing a uniformly ^{15}N-labeled cytochrome b_5.** Spectra were obtained using (A) WIM for 210 μs contact time, (b) COMPOZER-CP with an optimized contact time of 240 μs, and (c) RAMP-CP with an optimized contact time of 800 μs. All PELF spectra were acquired using a ^{1}H RF field strength of 41 kHz and SPINAL proton decoupling during acquisition. All spectra are shown at the same contour level for a direct comparison.

IV-3-5. Wobbling of the Transmembrane Helix of Cytochrome b_5 and Its Influence on the Helical Wheel Pattern of Resonances.

The proposed average 13° tilt of the mutant-Cyt b_5 transmembrane domain relative to the membrane normal determined from our PELF experimental data is illustrated in Figure IV-14A. The resonances corresponding to the transmembrane region are dispersed in a circular pattern, which is unique to proteins with α-helical secondary structure, and the best-fitting helical wheel projection circle is indicated in blue in Figure IV-14B.[46-48] This is expected for the transmembrane helix of mutant-Cyt b_5 since both mutant-Cyt b_5 and the full-length Cyt b_5 share identical amino acid sequences in their membrane-spanning domain. Importantly, the degree of dispersion in the resonances of the helical wheel directly reflects the average tilt angle (τ) of the helix with respect to the bilayer normal.[46,47] In Figure IV-14B, the PISA wheel of an ideal helix was empirically fitted with an average helical tilt angle of 13°, and the value of the overall order parameter (S) is estimated to be 0.42. However, no single helical wheel can provide an ideal fit to all the resonances presented in the circular pattern, which indicates non-ideality of the transmembrane helix. A kink due to the Pro residue in the middle of the TM region could be the main reason for the observation of an imperfect polarity index slant angle (PISA) wheel. Further experimental studies are required to completely assign the spectrum and determinate the origin of this imperfect helix.

Over the years, the structure of the membrane-spanning region of Cyt b_5 has been a source of constant debate.[49,50] It was proposed that the transmembrane domain of Cyt b_5 could adopt two conformations: a helical hairpin conformation or a membrane spanning α-helix. Fluorescence quenching and trypsin digestion assays show that the helical hairpin conformation is a "loose-binding" form of Cyt b_5, which allows it to exchange between lipid vesicles and does not span the membrane.[51] On the other hand, the "tight-binding" form of Cyt b_5 is believed to span the entire membrane and is firmly anchored to the lipid bilayer.[51] Interestingly, the hairpin helical conformation can be converted to the membrane spanning form by increasing the temperature or adding detergents.[51] In our case, mutant-Cyt b_5 most likely incorporates into the bicelle assembly and spans the bilayer due to the presence of DHPC. Also, the value of the overall order parameter is comparable to a single transmembrane helix spanning the whole bilayer as reported in the

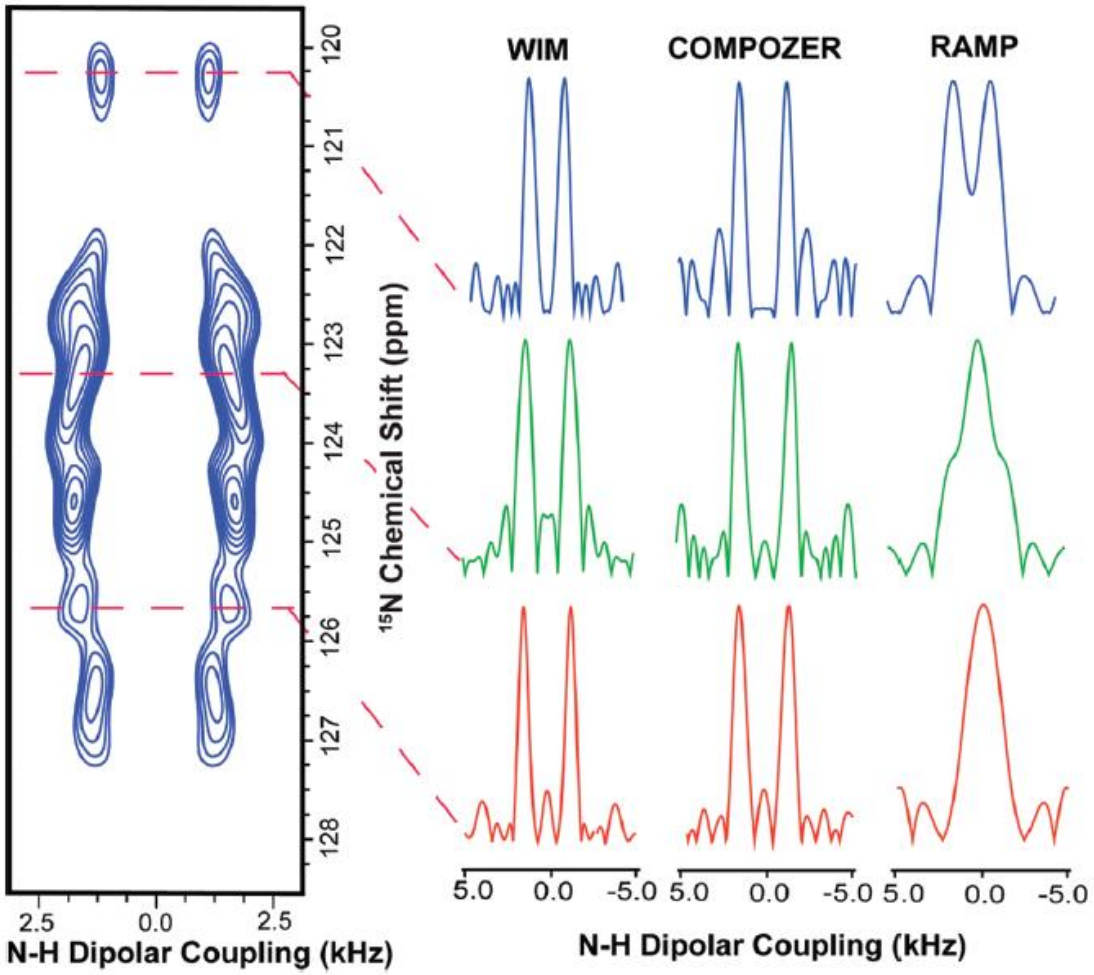

Figure IV-13. **A two-dimensional (2D) PELF-WIM spectrum of aligned bicelles containing a mutant of cytochrome b_5 uniformly labeled with ^{15}N isotope to compare the efficiencies of different PELF sequences.** Sample N-H dipolar coupling slices extracted from 2D PELF spectra, that were obtained using PELF sequences constituted with different magnetization transfer schemes, are included on the right side for a comparison of the efficiency of PELF sequences. In all of these cases, PELF with WIM or COMPOZER-CP offers a significant improvement in resolution, particularly in the dipolar coupling dimension. The *S*/*N* (signal-to-noise) ratios in the dipolar dimension of WIM, COMPOZER-CP, and CP are 7.1, 7.5, and 8, respectively. The line-widths taken at half height in the dipolar dimension for WIM, COMPOZER-CP, and CP are approximately 150, 140, 400 Hz, respectively.

literature, which provides further evidence that the observed helix of mutant-Cyt b_5 spans the membrane bilayer in bicelles.[25,42,52] However, we were unable to resolve all of the resonances in the transmembrane region due to the broadening of resonances in the indirect dimension. The resonances with small N-H dipolar couplings, as shown in green in Figure IV-14B, are probably from the portion of the soluble domain that lies near the membrane surface due to the absence of the eight-residue-linker; however, no satisfactory helical wheel fit can be obtained even though they are dispersed in an apparent circular pattern. Therefore, more experiments using selectively labeled protein samples need to be carried out in order to accurately assign all resonances in the spectrum.

The influence of the whole-body motions of the helix can be extracted from careful analysis of the helical wheel even in the absence of spectral assignments.[27] In a lipid bilayer system, an α-helix often exhibits a wide range of motions ranging from long-axis rotation to the wobbling of the whole helix. The amplitude of these motions often influences the magnitude of NMR parameters, particularly CSA and dipolar couplings.[27,53] Recently, it was suggested that dynamical information could be extracted from careful analysis of the helical wheel with an appropriate dynamic model.[27,54,55] Therefore, this will be the focus of the analysis presented in this paper. To model the motion of the whole helix, we invoke the diffusion in a cone model. In this model, the director axis of the helix wobbles freely within a cone described by the semiangle (β), and the wobble is axially symmetric with respect to the azimuthal angle (α). The resulting wobbling motion of the whole protein is shown in Figure IV-15B, and the best fit of our experimental data to our model is shown in Figure IV-15A. Notably, the angle β is defined by the tilt angle (τ) of the helix.[56] Also, we assumed that this wobbling motion and other collective local fluctuations is fast relative to the measurement time. The order parameter S_{cone} for the diffusion in a cone model is given in eq 2.[56]

$$S_{\text{cone}} = \frac{1}{2}\cos\beta(1 + \cos\beta) \quad (2)$$

To model the fluctuations in the helical director axis, a normal distribution function, given in eq 3, will be used, and the degree of fluctuation is estimated from the spread about the mean. In eq 3, β_0 is the average tilt angle of the helix, σ is the standard

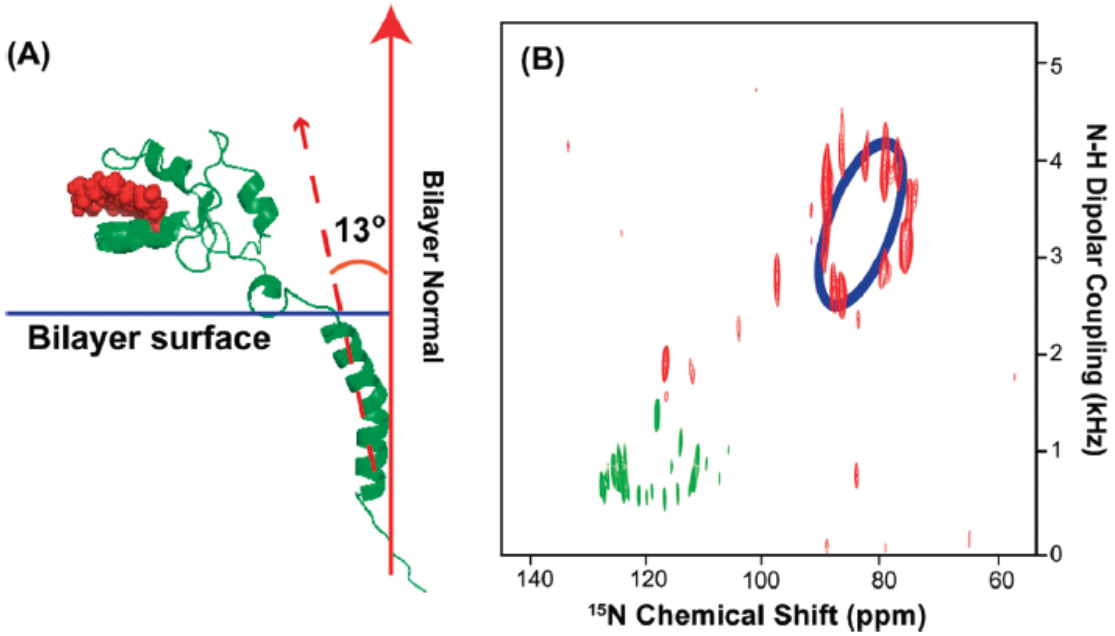

Figure IV-14. (A) **Illustration of the proposed orientation of a mutant-Cyt b_5 in magnetically aligned bicelles.** (B) Two-dimensional SLF spectrum of a mutant-Cyt b_5 embedded in aligned bicelles. Blue color represents the best fit for the helical wheel pattern of resonances from the transmembrane domain of the protein. The resonances in green represent the residues located near the membrane surface.

deviation, and β is the angle that varies between 0 to 90° with respect to the bilayer normal.[27]

$$G(\beta,\sigma) = \frac{1}{\sigma\sqrt{2\pi}} \exp\left(-\frac{(\beta - \beta_0)^2}{2\sigma^2}\right) \quad (3)$$

Importantly, the observed helical wheel will be the weighted average of all the probable orientations defined by the degree of fluctuation in the director axis of the helix.

A series of helical wheels, shown in Figure IV-16, was generated using the proposed model. Our simulations show the position of the helical wheel is sensitive to the degree of helical tilt fluctuation, particularly when the degree of helical tilt is small. In this case, small helical tilt fluctuations result in a significant change in the position of the helical wheel as shown in Figure IV-16A. On the other hand, for helix with a large tilt angle, a sizable amplitude of tilt fluctuation is required to change the position of the helical wheel as shown in Figure IV-16C. Furthermore, ambiguity can arise when dealing with helical wheels with small dipolar couplings and these cases are illustrated in panels D-F of Figure IV-16. As the amplitude of fluctuations increases, helical wheels of different tilt angles will eventually overlap as shown in Figure IV-16F. However, if the degree of fluctuation (σ) is much greater than the average tilt angle of the helix (β_0), this represents an unrealistic situation and should be ignored. Therefore, from these simulations, our model has shown to be appropriate in extracting dynamical information regarding small amplitude in helical tilt fluctuations ($\beta_0 \geq \sigma$) for helices with tilt angles in the range of 10-30°. This range of tilt angles is commonly observed in many transmembrane helices reported in the literature, which makes this model applicable to other helical membrane protein systems.[14,21,23,25,42]

When our model is incorporated into the fitting of the helical wheel as shown in Figure IV-15A, a detailed information regarding the dynamics of the membrane anchor emerges. If the fluctuation of the helical director axis, relative to the bilayer normal, is faster than its diffusion inside the cone, then we will observe only an average cone semiangle, which equals to the average tilt angle of the helix. On the other hand, if the fluctuation of the helical director axis is slow relative to its diffusion inside the cone, then the helix can

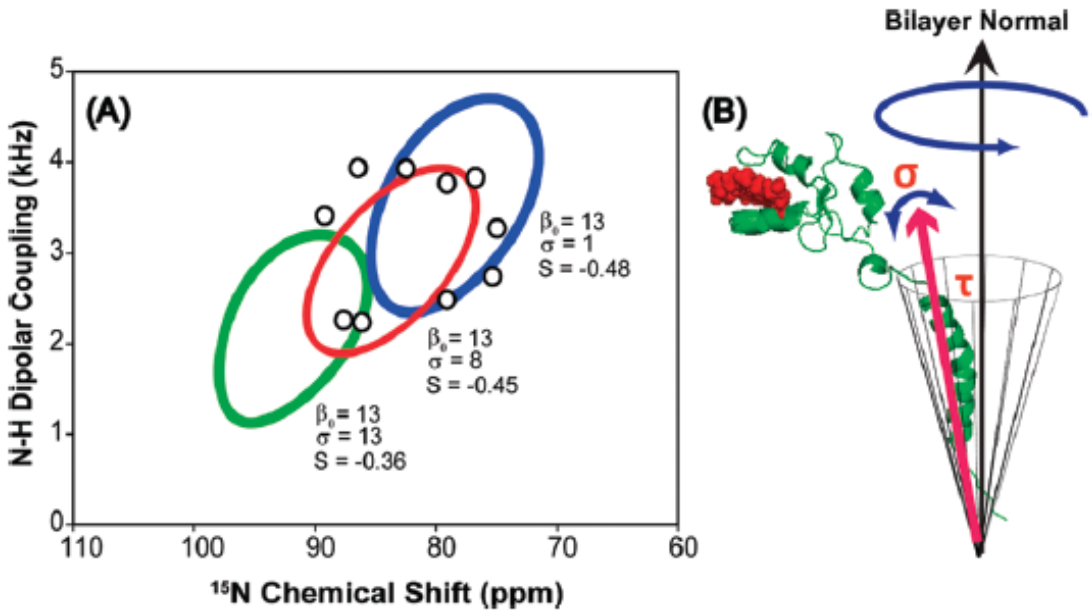

Figure IV-15. (A) **Fitting of the helical wheel pattern of resonances using the diffusion in a cone model.** The open circles (O) denote the position of the observed resonances. The three PISA wheel fits were obtained using an average tilt angle of τ = 13° and a chosen value of σ. In this case, the chosen values of σ are 1°, 8°, and 13° as indicated in the figure. (B) Diagram showing the wobbling motion of the helix in a lipid bilayer; where τ represents the tilt angle and σ represents the degree of fluctuation in the director axis.

sample a range of cone semiangles, resulting in a spread about the average helical tilt. These situations are illustrated in Figure IV-17.

The helical wheel that corroborates our experimental data, as illustrated in Figure IV-15A, requires a spread of approximately 8° about the average tilt angle of the helix, which indicates the diffusion of the helix inside the cone is faster than the fluctuation in the helical tilt. In our proposed model, the helix is wobbling in a cone defined by an average 13° tilt angle of the helix with an approximately 8° fluctuation in the helical tilt (σ). Also, from the magnitude of dipolar couplings, the collective motions of the helix are estimated to be on the order of milliseconds. This 8° fluctuation in the helical tilt defines an upper limit since the collective motions of the bicellar assemblies are incorporated into the current analysis as well. When we extend our current model to the mobile region, no satisfactory helical wheel fit can be obtained. This result demonstrates the dynamics in the mobile region is significantly different from the transmembrane domain. Due to the motional freedom in the mobile region, a greater range of motions can be afforded at various time scales, which dramatically increases the complexity required in our model for a proper description of this region. Thus, despite this shortcoming, our proposed model corroborates well with experimental results for the membrane-spanning domain, providing meaningful insights regarding helical motions in a bilayer environment, which showed the possibility of extracting both structural and dynamical information from the helical wheel. Our current dynamical analysis can be extended, with modifications, to include motions of two tightly bound helices in a lipid bilayer. These systems are commonly observed in nature with profound biological implications. For instance, the association of helices is commonly observed in macromolecular assembly such as viropins or between two cytochrome redox partners.[5,20,21,42] Therefore, understanding the dynamics that takes place in these complexes will allow us to gain a better insight into the role of molecular dynamics in facilitating their biological functions.

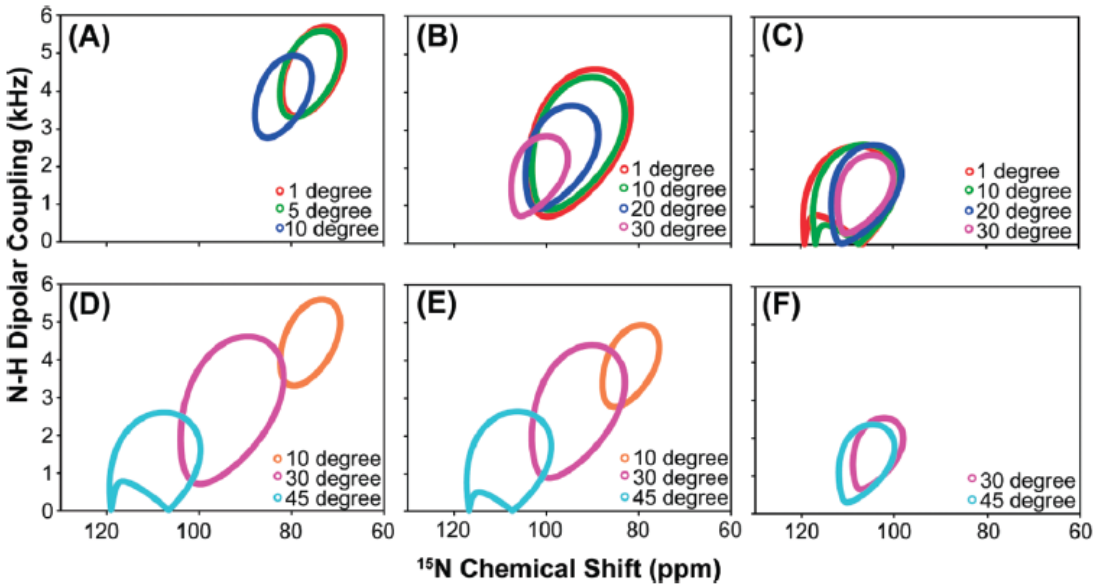

Figure IV-16. **A series of helical wheels simulated using the proposed model for cytochrome b_5 associated with bicelles.** (A-C) A series of helical wheels simulated with different degree of helical tilt angle fluctuations (σ), while keeping the average tilt (β_0) of the helix constant. The average tilt angles (β_0) used in the helical wheel simulations in A-C are 10°, 30°, and 45°. (D-F) A series of helical wheels simulated with different degree of helical tilt angles (β_0), while keeping the helical fluctuation (σ) constant. The constant helical fluctuation (σ) used in the helical wheel simulations in D-F are 5°, 10°, and 30°, and the helical tilt angle (β_0) varies from 10°, 30°, and 45° in each of the panels D-F. (Note: If the helical fluctuation is greater than the average helical tilt, it represents an unrealistic situation and was excluded from simulations.)

IV-3-6. Further Application of PELF Technique to Other Systems and To Study Molecular Dynamics.

The resolution afforded using the PELF techniques described here can be extended to other spin systems, particularly the methyl groups. Recently, ^{13}C-labeled methyl groups have been demonstrated to be an exquisite NMR probe for investigating dynamics and structure and biological functions of large protein complexes. The fact that Val, Ile, Leu, Ala, Met, and Thr constitute 30-45% of all the amino acids in membrane proteins means that the methyl group is becoming an important molecular probe for interrogating membrane protein structures and dynamics.[57-59] However, the use of methyl ^{13}C-^{1}H dipolar couplings in SLF studies of membrane proteins remains a challenge due to the lack of dispersion in the methyl ^{13}C chemical shifts as well as the complicated multiplet line shape in the indirect dimension due to the use of SLF sequences such as PISEMA, HIMSELF, and SAMMY.[57,60] Therefore, the PELF methods implemented in the current studies can be used to simplify the complicated line shape in the indirect dimension, allowing for the accurate measurement of methyl's ^{13}C-^{1}H dipolar couplings. The methyl ^{13}C-^{1}H dipolar couplings can provide dynamical information on a variety of biological systems. For example, the association of two different helices of a membrane protein often restricts the methyl group rotation at the binding interface, resulting in an increase in the magnitude of methyl's ^{13}C-^{1}H dipolar couplings. Therefore, through measuring the changes in the ^{13}C-^{1}H dipolar couplings, both the binding interface between two helices and the strength of their interactions at each methyl site can be deduced by comparing the order parameters of methyl groups as long as their resonances are resolvable. Furthermore, methyl ^{13}C-^{1}H dipolar couplings can provide structural constraints regarding the helical tilt similar to the recently proposed geometric analysis of labeled alanines (GALA) method that exploits the deuterium quadrupolar coupling of a CD_3 system.[61,62] While the GALA method is successful in providing the tilt angle of a helix in both oriented and unoriented samples, it requires numerous selectively deuterated methyl samples for different Ala residues, which is not practical.[62] The advantage of using the CH_3 group is that multiple Ala methyl sites can be ^{13}C-labeled and their ^{13}C-^{1}H dipolar couplings can be simultaneously measured using the PELF protocols, provided their resonances are resolvable. Therefore, the PELF sequence can be extended to CH_3 spin

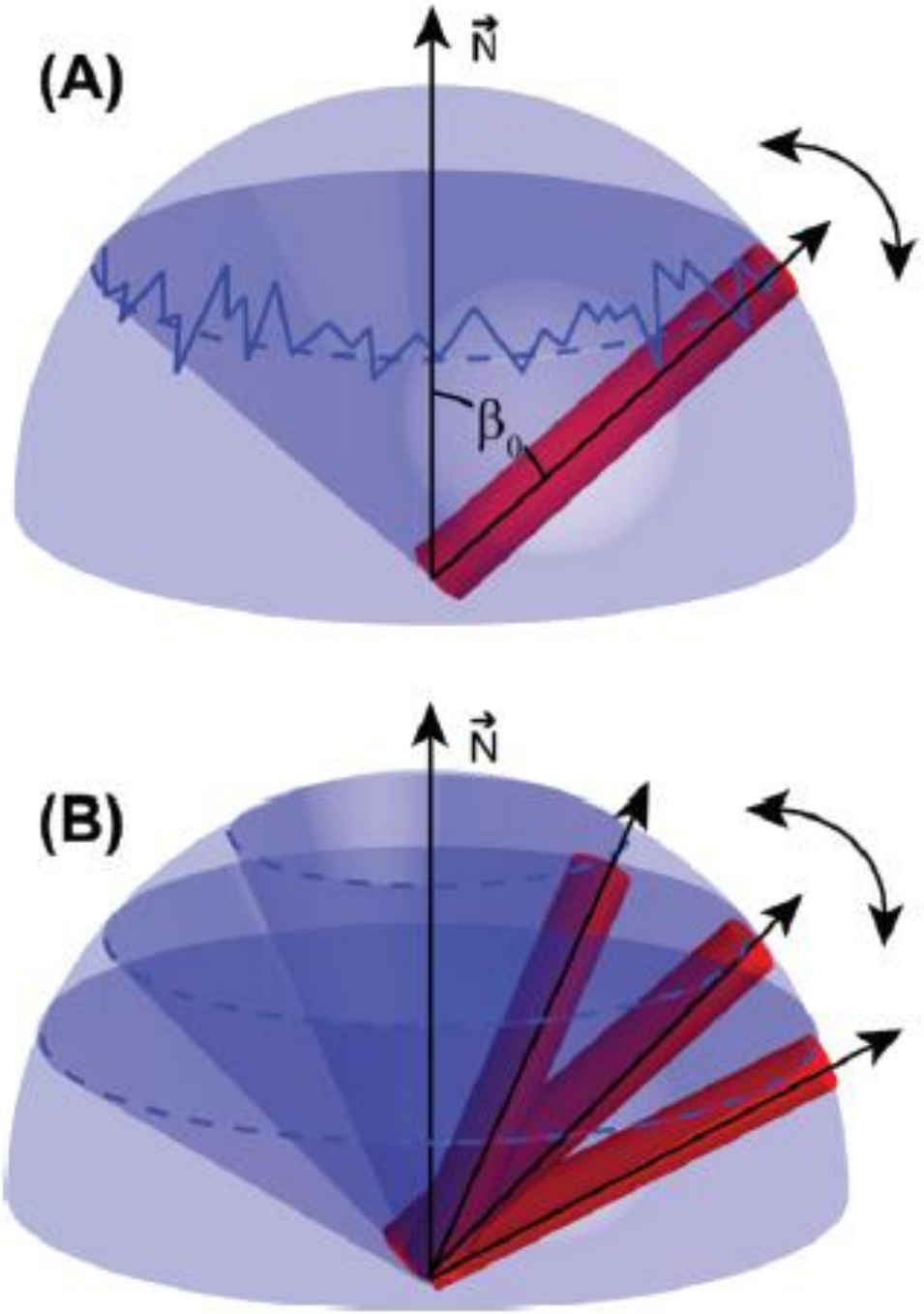

Figure IV-17. **Illustration of the importance of relative time scales in producing a motionally averaged PISA wheel spectrum.** (A) When fluctuations of the helical tilt occur on a faster time scales than diffusion in a cone, only one cone semiangle (β_0) has to be considered in the calculation of the motionally averaged helical wheel. (B) When fluctuations of the helical tilt occur on slower time scales than diffusion in the cone, several cone semiangles have to be considered in the calculation of the motionally averaged helical wheel.

systems, providing both side-chain dynamics and structural constraints for refining protein secondary structures.[57]

The ability to measure a broad range of dipolar couplings allows not only for the determination of structures but also the understanding of protein dynamics at various time scales as illustrated in our studies. Dipolar couplings can provide information on both the orientation of bond vectors and the amplitude of motions up to the millisecond time scale.[63-65] Under the commonly used rotating-frame SLF pulse sequences, only motions in the range of 10^{-4}-10^{-5} s are observed, which reflects the rotational diffusion of a transmembrane α-helix.[53] However, under the PELF approach, motions up to 10^{-3} s are revealed, thus, opening up a new avenue for probing protein dynamics via solid-state NMR experiments on aligned samples. In fact, a complete mapping of protein dynamics is now possible, using a combination of relaxation and dipolar coupling measurements.[65] Currently, applications of SLF spectroscopy mainly focus on the determination of the transmembrane domain structures of membrane proteins. Yet, in many cases, particularly for the case of membrane-associated receptors, a significant portion of the protein is in the cytoplasmic domain and conformational changes in one region of a protein can be propagated to another region through changes in protein motions such as those observed in dynamically driven allosteric interactions.[66] Despite many advances in solid-state NMR methodology, the synergy of these conformational changes has so far not been well characterized. Thus, the ability to produce a complete mapping of protein dynamics and their correlation with each other will allow for a better understanding of the intricate and enigmatic relationships between the structure of a protein and its biological functions.

IV-4. The Dynamical Structure of a 73 kDa Membrane-associated Cytochrome b_5-Cytochrome P450 Complex

The vast majority of pharmaceutical compounds in use today are hydrophobic compounds that are broken down in the body to water soluble, excretable compounds by a superfamily of enzymes known as the Cyt P450.[3,4] A single member of this family, Cyt P450 3A4, was found to metabolize more than 50% of current-day drugs.[3] Other members metabolize a broad range of xeno- as well as endobiotic substrates. Cyt b_5 is a membrane-bound protein which modifies the metabolism of selected drugs by Cyt P450.[3]

The molecular model shows the binding of Cyt P450 and Cyt b_5, which changes the efficiency of Cyt P450's enzymatic activity (Figure IV-18A).[6] A model constructed from the solution NMR structure of the soluble domain of rabbit Cyt b_5 is given in Figure IV-18B.[7] Remarkably, Cyt b_5 enhances (or is even essential) for some catalytic reactions, but does not affect or even inhibits others. Its suggested functions include direct donation of an electron to Cyt P450, fine-tuning of kinetic parameters by relaying electrons, or an allosteric effector function on Cyt P450.[1,2] In order to understand the molecular mechanism by which Cyt b_5 influences the oxidation by Cyt P450 *in vivo*, one must understand the structural details of how Cyt b_5 and Cyt P450 interact.

The 16.7kDa Cyt b_5 contains 3 structurally distinct domains (Figures IV-18B and IV-7): an ~95 amino acid amino-terminal catalytic heme-containing domain, a ~25 amino acid carboxyl-terminal membrane-anchor domain and a ~14 residue 'hinge' or 'linker' region which connects the two. The carboxyl domain is assumed to be a helix which spans the membrane. When Cyt b_5 is treated with proteases, the heme domain is released as a soluble protein which can no longer interact with Cyt P450, but which can react with the soluble protein, Cyt c.[7] Our interest is in trying to understand why the membrane-spanning domain is required for the interaction between Cyt b_5 and Cyt P450.

Since the full-length Cyt b_5 and Cyt P450 are not amenable for structural studies using most commonly used biophysical techniques, only the structures of the soluble domains these proteins have been solved using X-ray and solution NMR techniques. However, Cyt b_5 lacking the TM domain neither interacts with nor influence the function of Cyt P450. Therefore, while solving the high-resolution structure of the Cyt b_5 - Cyt P450 complex is very important, it has been proven to be challenging and not possible using commonly used biophysical approaches. On the other hand, it could be a suitable problem that can be investigated using solid-state NMR spectroscopy as it has no fundamental restriction on the molecular size and phase of the sample. Here, for the first time, we report the solid-state NMR investigation of membrane topology and dynamics of a Cyt b_5-Cyt P450 complex in lipid bilayers. Magnetically aligned bicelles are used in solid-state NMR experiments under static experimental conditions. Magnetically aligned bicelles have been previously used as model membranes in solid-state NMR studies and also been utilized as an alignment medium to measure residual dipolar couplings in the

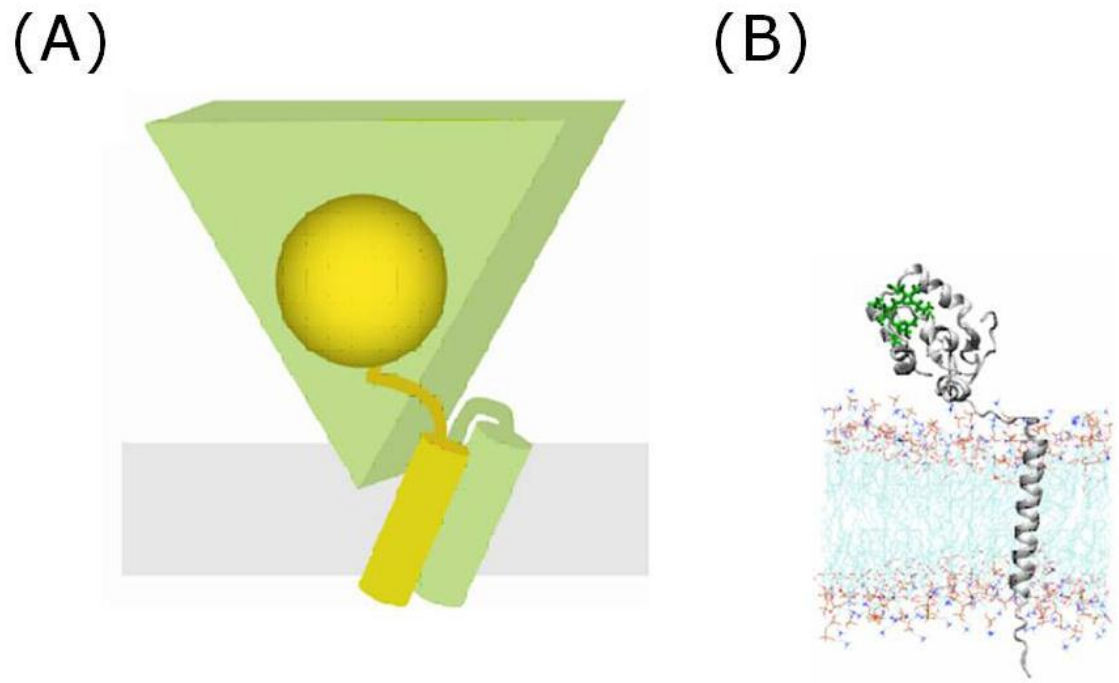

Figure IV-18. **Structural models of Cyt b_5 - Cyt P450 complex (A) and Cyt b_5 (B) in membranes** reconstructed from the original papers to give readers a graphical illustration of the protein-protein interaction and the predicted topology of Cyt b_5.

structural studies of water-soluble proteins using solution NMR techniques. Bicelles, composed of different types of combinations of lipids and a detergent, have been well characterized using ^{31}P, ^{2}H, ^{13}C and 2D SLF experiments. 2D HIMSELF and 2D SAMY spectra correlating the ^{13}C chemical shifts and ^{1}H-^{13}C dipolar couplings of the components of bicelles demonstrated the feasibility of high-resolution experiments at a physiologically-relevant temperature without having to enrich with ^{13}C isotopes. This remarkable advantage was later utilized to study the drug-membrane interactions using solid-state NMR spectroscopy. The physicochemical properties and the size of bicelles have also been well documented in the literature. Magic angle spinning solid-state NMR experiments have also utilized bilcelles, even high-resolution spectra of uniformly labeled proteins have been obtained. Recent solid-state NMR studies have shown that it is possible to obtain high-resolution spectra from peptides and proteins labeled with ^{15}N isotope under static experimental conditions. In this study, we have used bicelles to align a complex of two different membrane proteins to study the structural interactions between them. ^{31}P NMR data suggest that bicelles containing a complex of cyt b5 and Cyt P450 can be magnetically aligned at 30°C and even at higher temperatures. But the stability of Cyt P450 is a concern for experiments at temperatures above 30°C. In this study, using 15N NMR experiments, we have demonstrated that bicelles containing the Cyt b_5-Cyt P450 protein complex are stable for solid-state NMR studies and provide remarkable resolution and sensitivity even for bicelles containing as low as a concentration of 1:536 protein:lipid molar ratio. Most importantly, we have determined the tilt angle of the transmembrane domain of Cyt b_5 from bicelles containing the protein complex. The change in the mobility of Cyt b_5 due to its interaction with Cyt P450 is presented using results from 2D HIMSELF, CP and RINEPT solid-state NMR experiments and simulations of experimental data.

IV-4-1. Experimental Procedure.

Expression and purification of Cyt b_5.

^{15}N labeled full length rabbit cytochrome b_5 was over expressed in *E.coli* C41 cells using a pLW01 plasmid.[1] After adapation of the cells in ^{15}N-enriched Celtone medium

(Spectra stable Isotopes), the cells were transferred into a large volume of the ^{15}N-Celtone culture (called Celtone-N). The ^{15}N-Celtone culture contained 880 mL of Celtone-N solution, 112 mL of M9 solution, 2 mL of glycerol, 2g of [^{15}N] ammonium sulfate, 0.24 mM carbenicillin, 1 mM $CaCl_2$, 10 mM $MgSO_4$, 10 μM $FeCl_3$, 25 μM $ZnSO_4$, 20 μM $MnCl_2$, 250 μM δ-aminolaevulinic acid and vitamin mix (25 μg of biotin, choline chloride, folic acid, niacinamide, D-panthenate, pyridoxal-HCl, riboflavin and 250 μg of thiamine). Optimal expression was achieved with a 100 mL culture volume in a 500 mL Erlenmeyer flask. The flask was incubated at 35 ^{o}C and spun at 250 rpm until OD at 600 nm reached 1.2. Isoprppyl β-D-thiogalactopyranoside (IPTG) was added to the final concentration of 10 μM, and incubation was continued for 20 h at which the cells were harvested. Purification of the ^{15}N cytochrome b_5 (Cyt b_5) was performed as described previously. Expression and purification of the cytochrome P450 2B4 (Cyt P450) were performed as described previously.

Preparation of bicelles.

40 mg DMPC and 7.6 mg DHPC corresponding to a molar ratio of q = [DMPC]/[DHPC] = 3.5 were cosolubilized in chloroform. Solvent was removed under a stream of N_2 gas to produce a lipid film on the walls of a glass vessel, which was kept in vacuum overnight to remove all residual solvent. 65 ml of 50 mM HEPES buffer, pH 7.4, with 10% glycerol content was added to the lipids film and transferred to the 5 mm NMR tube that was used for the experiments. The resulting mixture of extreme viscosity was homogenized by vortexing, 30 min sonication in an ice bath, and 4 freeze/heat cycles between liquid nitrogen and 50°C. The resulting turbid gel is still extremely viscous, but its viscosity was slightly reduced at 0°C, as is common in all bicellar preparations. Protein was added in the final step of the preparation. Adding 55 ml of 2.0 mM cyt b_5 (or Cyt b_5-CytP450 complex) solution corresponding to 1.76 mg or 110 nmol protein resulted in a protein : DMPC ratio of 1:536. And 35 ml of 50 mM HEPES buffer, pH 7.4, with 10% glycerol content was added further to the sample. Once the components were satisfactorily mixed, the sample tube was sealed and the sample was transferred to the

magnet for subsequent NMR experiments. Quality of orientation was measured using ^{31}P NMR and was found to be stable after 1 h of equilibration. Since Cyt P450 is heat sensitive and unstable at higher temperatures, we performed all our solid-state NMR experiments at 30°C even though the bicelles containing the protein complex aligns at higher temperatures.

Solid-state NMR experiments.

NMR experiments were carried using a Varian/Chemagnetics 400 MHz and a 5mm double-resonance MAS probe (at the University of Michigan), a Bruker 900 MHz and a **5** mm double-resonance EFree static probe (at the Michigan State University, East Lansing), and a 900 MHz with a 5mm low-E double-resonance static probe (at National High Magnetic Field Laboratory (NHMFL) at Tallahasse). ^{31}P NMR spectra were obtained using a spin-echo sequence from all of the above-mentioned NMR spectrometers before and after each ^{15}N NMR experiment to confirm the lamellar nature of the sample. All 1D ^{15}N chemical shift spectra were obtained using a 400 MHz spectrometer. A 62.5 kHz RF field was used for all pulses in the ramp-CP and RINEPT sequences except that an 80 kHz RF field was used for the TPPM sequence to decouple protons. 1D ^{15}N chemical shift spectra were also obtained from all spectrometers to optimize the signal/noise and resolution before setting-up a 2D experiment. 2D HIMSELF experiments were performed in all the spectrometers.

Since Cyt P450 is unstable at ambient temperatures and both proteins are sensitive to different conditions, samples were checked after each solid-state NMR experiment to make sure that the proteins were not denatured during experiments. Indeed we observed that Cyt P450 in bicelles was unstable for temperatures higher than 37 ^{o}C, and therefore, we performed all our measurements at a lower temperature (30 ^{o}C) where the sample is still in the liquid crystalline phase and also quite stable for solid-state NMR experiments.

IV-4-2. ^{31}P Chemical Shift Spectra of Magnetically Aligned Bicelles.

Proton-decoupled ^{31}P chemical shift spectra of 3.5:1 DMPC/DHPC bicelles containing different concentrations of Cyt b_5 are given in Figure IV-19. Bicelles with Cyt b_5-Cyt P450 complex show a high degree of alignment as suggested by the narrow lines for DMPC (a peak observed in the high field region), DHPC (a peak observed in the low field region) and a strong signal at 0 ppm from the phosphate buffer. These results suggest that the presence of Cyt P450 does neither significantly alters the membrane environment nor the magnetic alignment of bicelles. Therefore, the bicelles containing a complex of Cyt b_5 and Cyt P450 is suitable for structural studies using solid-state NMR experiments.

IV-4-3. ^{15}N NMR of Bicelles Containing Cyt P450 and Uniformly-^{15}N-Labeled Cyt b_5.

Even though the high-resolution ^{31}P chemical shift spectra suggest that the bicelles are magnetically aligned, it is important to examine the suitability of the sample for the structural studies of proteins using ^{15}N NMR experiments. For example, ^{15}N experiments need to be performed to determine the alignment of proteins in bicelles, signal/noise ratio, and spectral resolution. Two types of solid-state NMR experiments, namely CP (cross polarization) and RINEPT (refocused insensitive nuclei enhanced by polarization transfer), were performed to measure the chemical shifts of U-^{15}N-Cyt-b_5 from bicelles. ^{15}N chemical shift spectra of uniformly-^{15}N-labeled Cyt b_5 in the absence (black) and the presence (red) of unlabeled Cyt P450 in bicelles are presented in Figure IV-20 (C-F). Narrow spectra lines, the signal/noise ratio, and the absence of a powder pattern in all ^{15}N chemical shift spectra suggest that the Cyt b_5 in both presence and absence of Cyt P450 is well aligned in bicelles and the sample is stable for long multidimensional experiments. Since bicelles are aligned with the lipid bilayer normal perpendicular to the external magnetic field direction, the ^{15}N spectral lines appearing in ~40-90 ppm region can be attributed to the transmembrane region while the lines in ~100-130 ppm range arise from the soluble domain of Cyt b_5. As mentioned in our previous study on bicelles containing Cyt b_5, the soluble domain of the protein is more mobile than the transmembrane domain of the protein. Therefore, spectral editing is achieved via the RINEPT and the CP

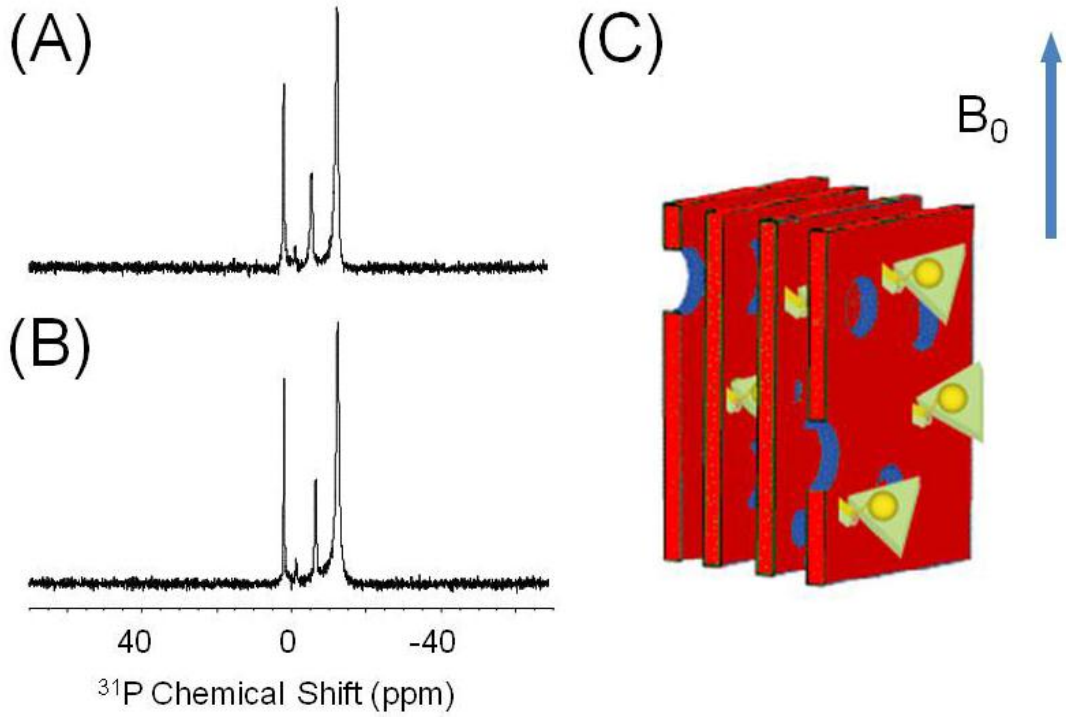

Figure IV-19. **Proton-decoupled ^{31}P-chemical shift spectra of 3.5:1 DMPC:DHPC bicelles containing a complex of 1:1 Cyt b_5 and Cyt P450** show a high degree of alignment as suggested by the narrow lines for DMPC (a peak observed in the high field region), DHPC (a peak observed in the low field region) and a strong signal at 0 ppm is from the phosphate buffer: (A) bicelles with a ratio of 1 : 536 Cyt b_5 : DMPC at 30°C; (B) bicelles with a ratio of 1 : 536 Cyt b_5 : DMPC at 37°C.

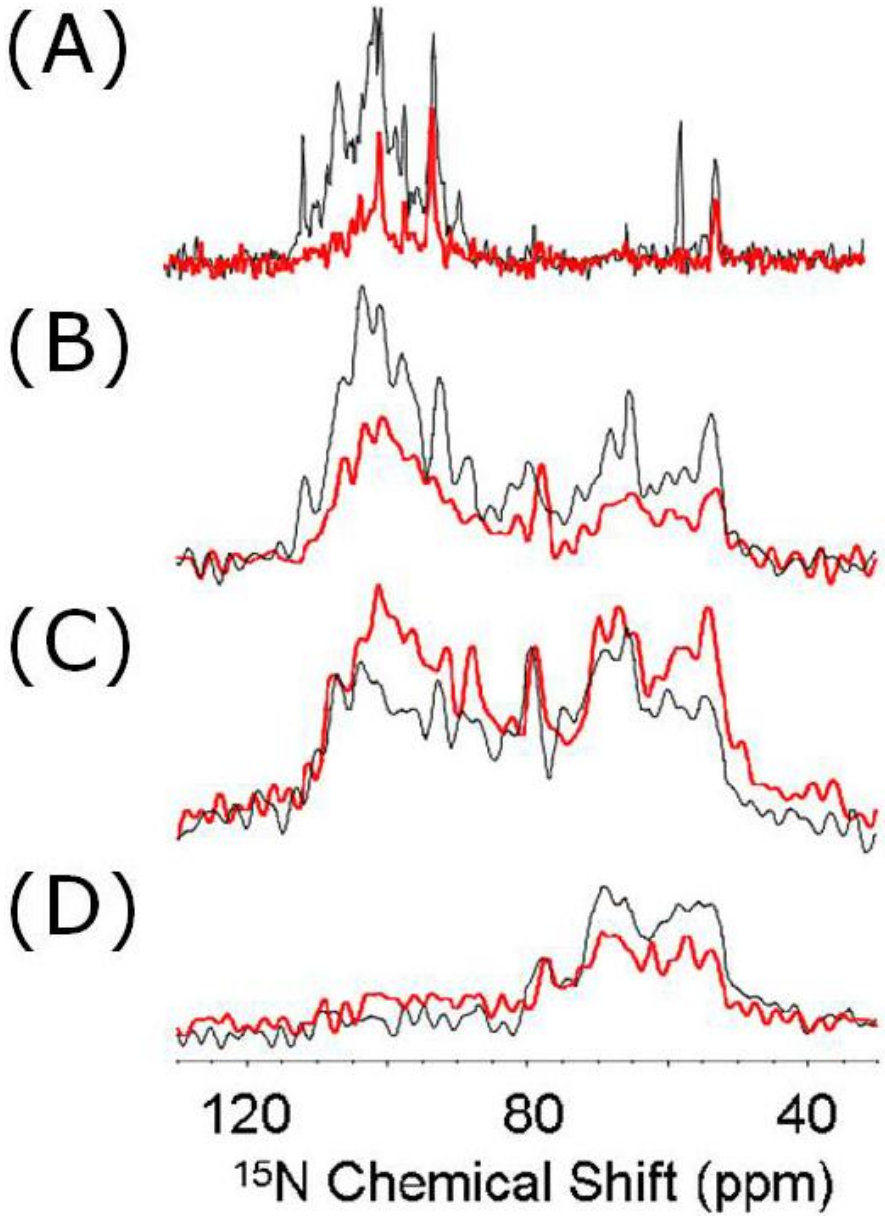

Figure IV-20. **^{15}N chemical shift spectra (A-D) of uniformly aligned DMPC/DHPC bicelles containing a U-^{15}N-Cyt b_5 without (black) and with Cyt P450 complex (red) at 30°C.** Spectra were obtained using RINEPT (A) and ramped cross-polarization (B-D) experiments with a contact time of (B) 3.0 ms, (D) 0.8 ms, and (E) 0.1 ms. The difference in the spectra not only reports on the variation in the mobilities of the three domains of the free Cyt b_5 (black) but also on the Cyt b_5 in the b_5-P450 complex (red). The ^{15}N RINEPT spectra show spectral intensity only in the 100-130 ppm region, consistent with a high mobility of the soluble domain of Cyt b_5. In the RINEPT sequence, 2.6 and 1.3 ms were used in the first (before the pair of 90^o pulses) and second (after the pair of 90^o pulses) delays, respectively.

sequences by varying the contact time. Relatively mobile regions of the protein contribute to the RINEPT spectrum while relatively immobile regions of the protein contribute to the CP spectrum. The presence of Cyt P450 significantly changed the observed spectral line shapes due to dynamical changes of Cyt b_5, indicating that the protein-protein interaction is actually taking place. In particular, the signal observed from the soluble domain (100-130 ppm) of Cyt b_5-Cyt P450 complex is weaker than that from the free Cyt b_5 in the RINEPT spectra (Figure IV-20C) and CP experiments at a longer contact time (Figure IV-20D). On the other hand, for a shorter contact time the soluble domain signal is stronger (Figure IV-20E).

IV-4-4. Two Dimensional HIMSELF spectra of Bicelles Containing Cyt P450 and Uniformly-^{15}N-Labeled Cyt b_5.

Two-dimensional HIMSELF[9] (heteronuclear isotropic mixing leading to spin exchange via the local field) spectra, which correlate ^{15}N chemical shift with ^{1}H-^{15}N dipolar coupling, were recorded on well-oriented bicelle samples containing Cyt b_5 with and without Cyt P450 (Figure IV-21A). The complete assignment of resonances in these spectra needs more experimental studies on bicelles containing Cyt b_5 that are labeled with ^{13}C & ^{15}N isotopes and may be the use of deuteration. While such studies are presently being carried out in our laboratory, there are some key features of the spectra that reveal the interaction of these two proteins and also on the structure and dynamics of Cyt b_5. Firstly, as demonstrated using spectral editing experiments on bicelles containing Cyt b_5 alone, the circular helical pattern of resonances seen in the 2D spectra (see the expanded version in Figure IV-21B) arise from the transmembrane region of Cyt b_5 even in the presence of Cyt P450. Secondly, the observation of PISA (polarity index slant angle)-wheel pattern of resonances suggests that the α-helical geometry of the transmembrane region of Cyt b_5 is not significantly altered by its interaction with Cyt P450. Thirdly, signals observed in the 100-130 ppm ^{15}N chemical shift region with reduced ^{1}H-^{15}N dipolar couplings in Figure IV-A can be attributed to the soluble domain of Cyt b_5 and suggest that the soluble domain has a relatively weak alignment as compared to the transmembrane domain of the protein. Interestingly, these reduced dipolar couplings become larger in the presence of Cyt P450. This observation indicates that the interaction of Cyt b_5 with Cyt P450 reduces the motion of the soluble domain of

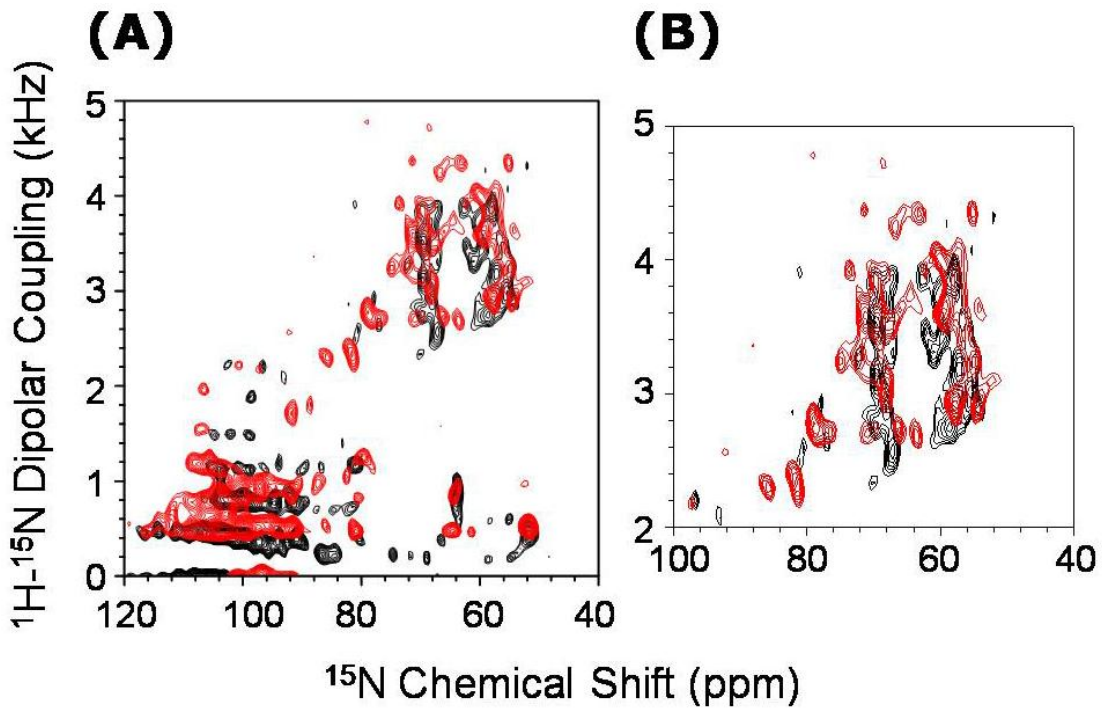

Figure IV-21. **A 2D ^{15}N-HIMSELF spectra (A), and resonances corresponding to the transmembrane region of Cyt b_5 (B), of magnetically aligned bicelles containing a U-^{15}N-Cyt b_5 (black) and the complex of U-^{15}N-Cyt b_5 with Cyt P450 (red) at 30°C.** Experimental parameters used were: an RF field of 30 kHz, 0.5 ms cross polarization contact time, 48 t_1 experiments with a dwell of 60 μs, 10.24 ms acquisition time, 25 kHz SPINAL16 decoupling, 1k scans, and 2 s recycle delay.

Cyt b_5. Fourthly, the observation of a high-resolution spectrum from bicelles containing a ~73 kDa size membrane protein complex of Cyt b_5-Cyt P450 is remarkable, which enables the development and applications of multidimensional solid-state NMR experiments to probe protein-protein interactions and structural studies without the need for freezing the model membrane samples.

IV-4-5. Simulations of HIMSELF Spectra.

Spectral simulations were performed in order to determine the tilt of the transmembrane α-helix from the observed PISA wheel in Figure IV-22. Molecular order parameter could change the PISA wheel patterns. Figure IV-22 shows the PISA wheels at three different tilt angles with various molecular order parameters. Our simulations suggest that the molecular order parameter has less effect on the shape of the wheel pattern of resonances in a 2D PISEMA or HIMSELF spectrum of aligned bicelles containing a membrane protein. In addition, calculations show that for larger tilt angles respected to the membrane normal, the order parameter does not change the position of the PISA wheel much in the 2D HIMSELF spectra. However, for a helix which has a small order parameter changes the size and frequency position of the PISA wheel in the spectra significantly, while for a helix which has a larger order parameter changes the size and frequency position of the PISA wheel in the spectra relatively less. Therefore, we have taken the influence of the order parameter into account in the PISA wheel analysis of our experimental data.

Based on the simulations, the smaller dipolar couplings observed from Cyt b_5 and Cyt b_5 - Cyt P450 complex (in the 80–110 ppm region) suggest that the partial alignment of the soluble domain of Cyt b_5 and its high mobility with an order parameter less than about 0.5 and a tilt angle of ~80°. On the other hand, due to the Cyt b_5-Cyt P450 complex formation, the soluble domain of Cyt b_5 is relatively immobilized with an order parameter of 0.55. Therefore, the small dipolar couplings in ~80-110 ppm region for Cyt b_5 become larger for the complex because of the direct interaction between soluble domains of Cyt b_5 and Cyt P450. The PISA wheel analysis for Cyt b_5 in bicelles at 30°C estimates a 14.0 (±3)° tilt of the TM helix relative to the membrane normal with a molecular order parameter of S_{mol}=0.70. On the other hand, 16.0 (±3)° tilt with a

molecular order parameter of S_{mol}= 0.8 are determined for Cyt b_5-Cyt P450 complex in bicelles at 30°C. The α-helix is may be distorted due to the kink at Pro-116 in the middle of the TM region.[11] Further experimental studies are in progress to assign the peaks in the 2D spectra and to determine the three-dimensional structure of the protein. Therefore, the difference in the PISA wheel pattern of resonances in Figure IV-21 between Cyt b_5 and Cyt b_5-Cyt P450 samples could be attributed to the structural changes due to Pro-116 as well as due to the difference in the order parameter of the protein. Interestingly, the increase in the molecular order parameter for the TM region of the Cyt b_5-Cyt P450 complex suggests the direct interaction of the TM domains of both proteins.

IV-4-6. Discussion.

Protein science in the post-genomic era is beginning to direct its course towards the elucidation of protein-protein interactions. Many biologically important protein-protein interactions, such as signal transduction, electron transport chain and photosynthesis, take place at the membrane interface of living cells. Despite their importance and ongoing investigative efforts, there are very few reports on the protein structure determination of the combinatorial complexes composed of the protein-protein interactions and lipid bilayers. The lack of success in this area of research is mainly because of the challenges imposed by membrane proteins to the most commonly used biophysical techniques such as X-ray crystallography and NMR spectroscopy. While obtaining well-behaved biologically relevant samples of these systems is a main major bottle-neck for high-resolution structural studies, recent solid-state NMR studies have demonstrated the feasibility of obtaining high quality structural information that could be used to understand the function of membrane proteins. However, structural studies of a membrane protein complex using solid-state NMR techniques have been considered to be highly risky. In this study, we have demonstrated that solid-state NMR is capable of characterizing protein-protein interactions in lipid bilayers at a very high-resolution. For the first time in the literature, we report structural and dynamical interactions in an intact mamalian membrane protein complex, rabbit cytochrome b_5 and cytochrome P450 2B4, in a membrane bilayer.

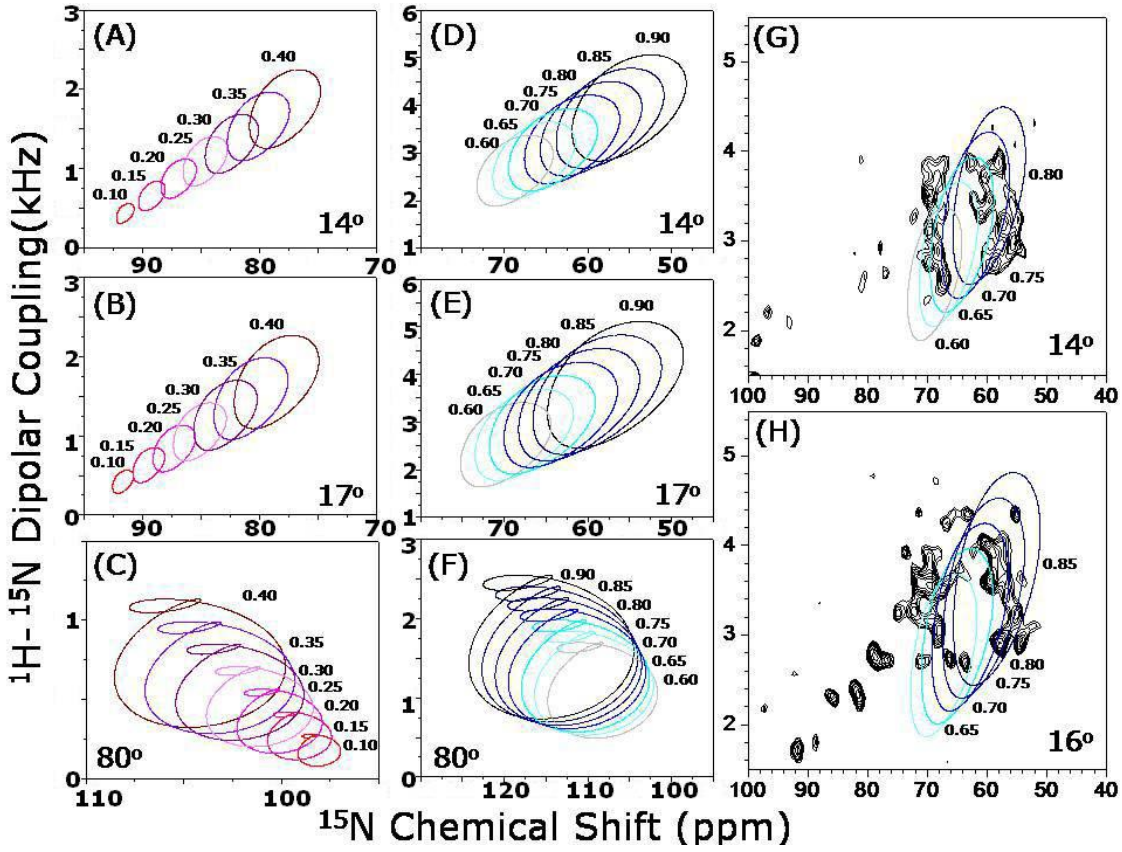

Figure IV-22. **Sensitivity of PISA wheel patterns to the order parameter of the sample.** Simulated PISA wheel patterns are shown for different helical tilts from the membrane normal: 14.0° (A & D), 17.0° (B & E) and 80.0° (C & F). The TM region of 2D ^{15}N-HIMSELF spectra of (G) U-^{15}N-cyt b_5 and (H) the membrane protein-protein complex U-^{15}N-Cyt b_5 with Cyt P450.

Our experimental results reported in this study demonstrate that not only Cyt b_5 but also a complex of Cyt b_5 and Cyt P450 can be prepared in bicelles, aligned in magnetic field for NMR studies, and high-resolution spectra and meaningful structural and dynamical information can be obtained. While it is known that Cyt P450 is unstable at ambient temperatures and both proteins are sensitive to impurities and heat, it is remarkable that the bicelles containing the complex was quite stable under our experimental conditions even up to temperatures 30^{o}C for more than two weeks. The differences in the spectra obtained using CP and RINEPT pulse sequences, and with and without Cyt P450, provide a wealth of dynamical information about Cyt b_5 as discussed below. For example, the difference in the ^{15}N chemical shift spectra (Figure IV-20) of aligned bicelles containing Cyt b_5 with and without Cyt P450 suggests the interaction between these two proteins, which reduces the mobility of Cyt b_5 in the presence of Cyt P450. This further confirmed by the 2D HIMSELF data in Figure IV-21. The 2D experimental data in combination with simulations reveal the changes in the mobilities of the soluble and TM domains. The measured order parameter for the soluble domain of Cyt b_5 slightly increases (by 0.05) due to its interaction with Cyt P450, whereas the order parameter of the TM domain is significantly increased (by 0.10). These results suggest that the interaction between the TM regions is stronger than that between the soluble domains in the bicelles sample used for NMR experiments. This explains why Cyt b_5 lacking the TM region does not influence the function of Cyt P450. Here, Cyt b_5 has a C-terminal α-helix TM domain, on the other hand, Cyt P450 has a N-terminal TM domain (data not shown). The electric dipole moments of α-helix might have an important role for the interaction of these two TM domains. Structural models of Cyt b_5 - Cyt P450 complex based on biological assays and Solid-state NMR experiments are shown in Figure IV-23. Interestingly, the interaction between the proteins neither significantly alter the helical structure of the TM domain of Cyt b_5 nor does it significantly alter the geometry of TM helix. This observation considerably simplifies our understanding on the interaction between the TM domains of the proteins. Since the soluble domains of both the proteins are highly mobile in NMR time scale, the interaction between these two domains only slightly reduces the mobility of Cyt b_5 in the presence of Cyt P450. One possible role of the membrane anchor is that it restricts the motion of the Cyt b_5 soluble

domain to those orientations that will result in a productive complex with Cyt P450. Cyt P450 is believed to be rigidly anchored to the membrane and may, therefore, be limited in its ability to form a productive complex unless its binding partner is appropriately orientated. More experiments are needed to completely characterize the structural changes and the changes in the dynamics of the proteins in the complex form at a higher resolution. We expect the results reported here to open a valuable approach to structural and dynamical studies of membrane protein complexes using solid-state NMR techniques.

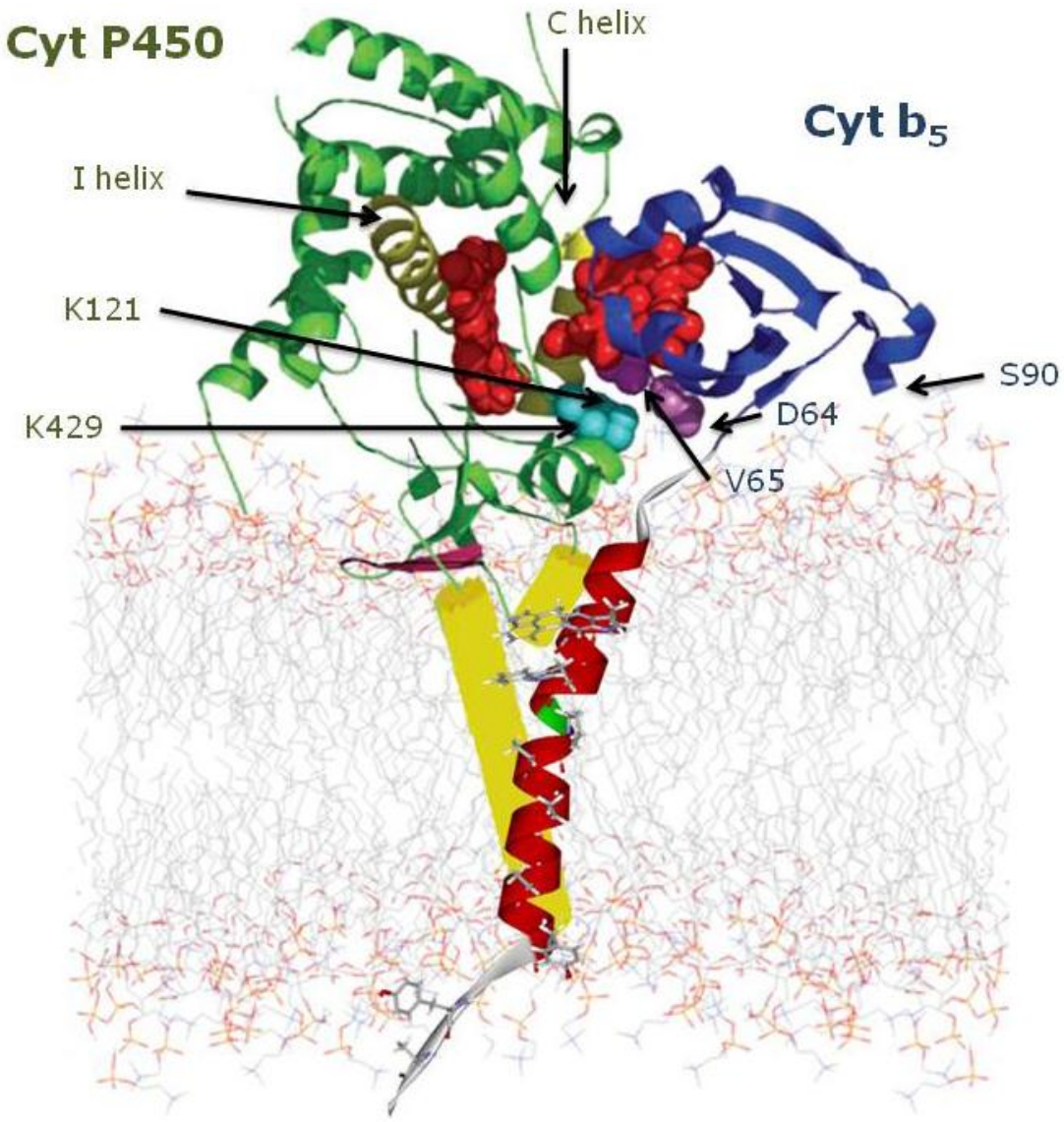

Figure IV-23. **Structural models of Cyt b_5 - Cyt P450 complex based on biological assays and Solid-state NMR experiments.**

IV-5. References

IV-2.

1 (a) Denisov, I.G.; Makris, T.M.; Sligar, S.G.; Schlichting, I. *Chem. Rev.* **2005**, *105*, 2253. (b) Guengerich, F.P. *Mechanism and Biochemistry*, 3rd ed.; de Montellano, P.O., Ed.; Plenum Publishers: New York, 2005.

2 Zhang, H.; Myshkin, E.; Waskell, L. *Biochem. Biophys. Res. Commun.* **2005**, *338*, 499.

3 (a) Vergères, G.; Waskell, L. *Biochimie* **1995**, *77*, 604. (b) Schenkman, J.B.; Jansson, I. *Pharmacol. Ther.* **2003**, *97*, 139.

4 Mulrooney, S.B.; Waskell, L. *Protein Expr. Purif.* **2000**, *19*, 173.

5 Banci, L.; Bertini, I.; Rosato, A.; Scacchieri, S. *Eur. J. Biochem.* **2000**, *267*, 755.

6 Durley, R.C.E.; Mathews, F.S. *Acta Crystallogr.* **1996**, *D52*, 65.

7 (a) Guiles, R.D.; Basus, V.J.; Kuntz, I.D.; Waskell, L. *Biochemistry* **1992**, *31*, 11365. (b) Muskett, F.W.; Kelly, G.P.; Whitford, D. *J. Mol. Biol.* **1996**, *258*, 172.

8 Clarke, T.A.; Im, S.-C.; Bidwai, A.; Waskell, L. *J. Biol. Chem.* **2004**, *279*, 36809.

9 (a) Sanders, C.R.; Prestegard, J.H. *Biophys. J.* **1990**, *58*, 447. (b) Sanders, C.R.; Hare, B.J.; Howard, K.P.; Prestegard, J.H. *Prog. Nucl. Magn. Reson. Spectrosc.* **1994**, *26*, 421. (c) Prosser, R.S.; Evanics, F.; Kitevski, J.L.; Al-Abdul-Wahid, M.S. *Biochemistry* **2006**, *45*, 8453. (d) Lu, J.X.; Damodaran, K.; Lorigan, G.A. *J. Magn. Reson.* **2006**, *178*, 283-287.

10 Burum, D.P.; Ernst, R.R. *J. Magn. Reson.* **1980**, *39*, 163.

11 Li, R.; Woodward, C. *Protein Sci.* **1999**, *8*, 1571.

12 (a) Wu, C.H.; Ramamoorthy, A.; Opella, S.J. *J. Magn. Reson., Ser. A* **1994**, *109*, 270. (b) Ramamoorthy, A.; Wei, Y.; Lee, D.K. *Annu. Rep. NMR Spectrosc.* **2004**, *52*, 1-52. (c) Yamamoto, K.; Lee, D.K.; Ramamoorthy, A. *Chem. Phys. Lett.* **2005**, *407*, 289-293.

13 (a) Dvinskikh, S.V.; Yamamoto, K.; Ramamoorthy, A. *J. Chem. Phys.* **2006**, *125*, 34507. (b) Dvinskikh, S.; Dürr, U.H.N.; Yamamoto, K.; Ramamoorthy, A. *J. Am. Chem. Soc*. **2006**, *128*, 6326-6327.

14 (a) Marassi, F.M.; Opella, S.J. *J. Magn. Reson.* **2000**, *144*, 150. (b) Denny, J.K.; Wang, J.; Cross, T.A.; Quine, J.R. *J. Magn. Reson.* **2001**, *152*, 217.

IV-3.

1 Loria, J.P.; Berlow, R.B.; Watt, E.D. *Acc. Chem. Res.* **2008**, *41*, 214–221.

2 Korzhnev, D.M.; Kloiber, K.; Kanelis, V.; Tugarinov, V.; Kay, L.E. *J. Am. Chem. Soc.* **2004**, *126*, 3964–3973.

3 Skrynnikov, N.R.; Mulder, F.A.; Hon, B.; Dahlquist, F.W.; Kay, L.E. *J. Am. Chem. Soc.* **2001**, *123*, 4556–4566.

4 Zintsmaster, J.S.; Wilson, B.D.; Peng, J.W. *J. Am. Chem. Soc.* **2008**, *130*, 14060–14061.

5 Dürr, U.H.N.; Waskell, L.; Ramamoorthy, A. *Biochim. Biophys. Acta* **2007**, *1768*, 3235–3259.
6 Ellis, J.; Gutierrez, A.; Barsukov, I.L.; Huang, W.C.; Grossmann, J.G.; Roberts, G.C. *J. Biol. Chem.* **2009**, *284*, 36628–36637.
7 Liang, B.; Tamm, L.K. *Proc. Natl. Acad. Sci. U.S.A.* **2007**, *104*, 16140–16145.
8 Arora, A.; Abildgaard, F.; Bushweller, J.H.; Tamm, L.K. *Nat. Struct. Biol.* **2001**, *8*, 334–338.
9 Hwang, P.M.; Bishop, R.E.; Kay, L.E. *Proc. Natl. Acad. Sci. U.S.A.* **2004**, *101*, 9618–9623.
10 Hwang, P.M.; Choy, W.Y.; Lo, E.I.; Chen, L.; Forman-Kay, J.D.; Raetz, C.R.; Prive, G.G.; Bishop, R.E.; Kay, L.E. *Proc. Natl. Acad. Sci. U.S.A.* **2002**, *99*, 13560–13565.
11 Porcelli, F.; Verardi, R.; Shi, L.; Henzler-Wildman, K.A.; Ramamoorthy, A.; Veglia, G. *Biochemistry* **2008**, *47*, 5565–5572.
12 Porcelli, F.; Buck-Koehntop, B.A.; Thennarasu, S.; Ramamoorthy, A.; Veglia, G. *Biochemistry* **2006**, *45*, 5793–5799.
13 Traaseth, N.J.; Buffy, J.J.; Zamoon, J.; Veglia, G. *Biochemistry* **2006**, *45*, 13827–13834.
14 Traaseth, N.J.; Shi, L.; Verardi, R.; Mullen, D.G.; Barany, G.; Veglia, G. *Proc. Natl. Acad. Sci. U.S.A.* **2009**, *106*, 10165–10170.
15 Van Horn, W.D.; Kim, H.J.; Ellis, C.D.; Hadziselimovic, A.; Sulistijo, E.S.; Karra, M.D.; Tian, C.; Sonnichsen, F.D.; Sanders, C.R. *Science* **2009**, *324*, 1726–179.
16 Ravindranathan, K.P.; Gallicchio, E.; McDermott, A.E.; Levy, R.M. *J. Am. Chem. Soc.* **2007**, *129*, 474–475.
17 Goldbourt, A.; Gross, B.J.; Day, L.A.; McDermott, A.E. *J. Am. Chem. Soc.* **2007**, *129*, 2338–2344.
18 Zhou, D.H.; Shah, G.; Mullen, C.; Sandoz, D.; Rienstra, C.M. *Angew. Chem., Int. Ed.* **2009**, *48*, 1253–1256.
19 Ader, C.; Schneider, R.; Hornig, S.; Velisetty, P.; Wilson, E.M.; Lange, A.; Giller, K.; Ohmert, I.; Martin-Eauclaire, M.F.; Trauner, D.; Becker, S.; Pongs, O.; Baldus, M. *Nat. Struct. Mol. Biol.* **2008**, *15*, 605–612.
20 Traaseth, N.J.; Verardi, R.; Torgersen, K.D.; Karim, C.B.; Thomas, D.D.; Veglia, G. *Proc. Natl. Acad. Sci. U.S.A.* **2007**, *104*, 14676–14681.
21 Ramamoorthy, A.; Kandasamy, S.K.; Lee, D.K.; Kidambi, S.; Larson, R.G. *Biochemistry* **2007**, *46*, 965–975.
22 Lambotte, S.; Jasperse, P.; Bechinger, B. *Biochemistry* **1998**, *37*, 16–22.
23 Dürr, U.H.N.; Yamamoto, K.; Im, S.C.; Waskell, L.; Ramamoorthy, A. *J. Am. Chem. Soc.* **2007**, *129*, 6670–6671.
24 Diller, A.; Loudet, C.; Aussenac, F.; Raffard, G.; Fournier, S.; Laguerre, M.; Grelard, A.; Opella, S.J.; Marassi, F.M.; Dufourc, E.J. *Biochimie* **2009**, *91*, 744–751.
25 De Angelis, A.A.; Howell, S.C.; Nevzorov, A.A.; Opella, S.J. *J. Am. Chem. Soc.* **2006**, *128*, 12256–12267.
26 Buffy, J.J.; Traaseth, N.J.; Mascioni, A.; Gor'kov, P.L.; Chekmenev, E.Y.; Brey, W.W.; Veglia, G. *Biochemistry* **2006**, *45*, 10939–10946.

27 Esteban-Martin, S.; Strandberg, E.; Fuertes, G.; Ulrich, A.S.; Salgado, J. *Biophys. J.* **2009**, *96*, 3233–3241.
28 Traaseth, N.J.; Ha, K.N.; Verardi, R.; Shi, L.; Buffy, J.J.; Masterson, L.R.; Veglia, G. *Biochemistry* **2008**, *47*, 3–13.
29 Page, R.C.; Kim, S.; Cross, T.A. *Structure* **2008**, *16*, 787–797.
30 Ramamoorthy, A.; Wu, C.H.; Opella, S.J. *J. Magn. Reson. B* **1995**, *107*, 88–90.
31 Dvinskikh, S.V.; Yamamoto, K.; Ramamoorthy, A. *J. Chem. Phys.* **2006**, *125*, 34507.
32 Dvinskikh, S.V.; Dürr, U.H.N.; Yamamoto, K.; Ramamoorthy, A. *J. Am. Chem. Soc.* **2006**, *128*, 6326–6327.
33 Clarke, T.A.; Im, S.C.; Bidwai, A.; Waskell, L. *J. Biol. Chem.* **2004**, *279*, 36809–36818.
34 Hong, M.; Pines, A.; Caldarelli, S. *J. Phys. Chem.* **1996**, *100*, 14815–14822.
35 Hong, M.; Schmidt-Rohr, K.; Zimmermann, H. *Biochemistry* **1996**, *35*, 8335–8341.
36 Fukuchi, M.; Ramamoorthy, A.; Takegoshi, K. *J. Magn. Reson.* **2009**, *196*, 105–109.
37 Burum, D.; Linder, M.; Ernst, R.R. *J. Magn. Reson.* **1981**, *44*, 173–188.
38 Fung, B. M.; Ermolaev, Y.; Yu, Y. *J. Magn. Reson.* **1999**, *138*, 28–35.
39 Veshtort, M.; Griffin, R.G. *J. Magn. Reson.* **2006**, *178*, 248–282.
40 Yamamoto, K.; Soong, R.; Ramamoorthy, A. *Langmuir* **2009**, *25*, 7010–7018.
41 De Angelis, A.A.; Nevzorov, A.A.; Park, S.H.; Howell, S.C.; Mrse, A.A. *J. Am. Chem. Soc.* **2004**, *126*, 15340–15341.
42 Park, S.H.; De Angelis, A.A.; Nevzorov, A.A.; Wu, C.H.; Opella, S.J. *Biophys. J.* **2006**, *91*, 3032–3042.
43 Smith, P.E.S.; Brender, J.R.; Ramamoorthy, A. *J. Am. Chem. Soc.* **2009**, *131*, 4470–4478.
44 Canlas, C.G.; Ma, D.; Tang, P.; Xu, Y. *J. Am. Chem. Soc.* **2008**, *130*, 13294–13300.
45 Cui, T.; Canlas, C.G.; Xu, Y.; Tang, P. *Biochim. Biophys. Acta* **2009**, *1798*, 161–166.
46 Wang, J.; Denny, J.; Tian, C.; Kim, S.; Mo, Y.; Kovacs, F.; Song, Z.; Nishimura, K.; Gan, Z.; Fu, R.; Quine, J.R.; Cross, T.A. *J. Magn. Reson.* **2000**, *144*, 162–167.
47 Ramamoorthy, A.; Wei, Y.F.; Lee, D.K. *Annu. Rep. NMR Spectrosc.* **2004**, *52*, 1–52.
48 Denny, J.K.; Wang, J.; Cross, T.A.; Quine, J.R. *J. Magn. Reson.* **2001**, *152*, 217–226.
49 Everett, J.; Zlotnick, A.; Tennyson, J.; Holloway, P.W. *J. Biol. Chem.* **1986**, *261*, 6725–6729.
50 Vergeres, G.; Ramsden, J.; Waskell, L. *J. Biol. Chem.* **1995**, *270*, 3414–3422.
51 Ladokhin, A.S.; Wang, L.; Steggles, A.W.; Malak, H.; Holloway, P.W. *Biochemistry* **1993**, *32*, 6951–6956.
52 Muller, S.D.; De Angelis, A.A.; Walther, T.H.; Grage, S.L.; Lange, C.; Opella, S.J.; Ulrich, A.S. *Biochim. Biophys. Acta* **2007**, *1768*, 3071–3079.

53 Park, S.H.; Mrse, A.A.; Nevzorov, A.A.; De Angelis, A.A.; Opella, S.J. *J. Magn. Reson.* **2006**, *178*, 162–165.
54 Shi, L.; Cembran, A.; Gao, J.; Veglia, G. *Biophys. J.* **2009**, *96*, 3648–3662.
55 Straus, S.K.; Scott, W.R.; Watts, A. *J. Biomol. NMR.* **2003**, *26*, 283–295.
56 Brainard, J.R.; Szabo, A. *Biochemistry* **1981 20**, *16*, 4618–4628.
57 Wu, C.H.; Das, B.B.; Opella, S.J. *J. Magn. Reson.* **2009**, *202*, 127–134.
58 Sprangers, R.; Kay, L.E. *Nature* **2007**, *445*, 618–622.
59 Tugarinov, V.; Sprangers, R.; Kay, L.E. *J. Am. Chem. Soc.* **2004**, *126*, 4921–4925.
60 Dvinskikh, S.V.; Dürr, U.H.N.; Yamamoto, K.; Ramamoorthy, A. *J. Am. Chem. Soc.* **2007**, *129*, 794–802.
61 Strandberg, E.; Ozdirekcan, S.; Rijkers, D.T.; van der Wel, P.C.; Koeppe, R.E.; Liskamp, R.M.; Killian, J.A. *Biophys. J.* **2004**, *86*, 3709–3721.
62 van der Wel, P.C.; Strandberg, E.; Killian, J.A.; Koeppe, R.E. *Biophys. J.* **2002**, *83*, 1479–1488.
63 Tolman, J.R.; Ruan, K. *Chem. Rev.* **2006**, *106*, 1720–1736.
64 Zhuang, T.; Leffler, H.; Prestegard, J.H. *Protein Sci.* **2006**, *15*, 1780–1790.
65 Zhang, Q.; Stelzer, A.C.; Fisher, C.K.; Al-Hashimi, H.M. *Nature* **2007**, *450*, 1263–1267.
66 Kalodimos, C.G.; Boelens, R.; Kaptein, R. *Nat. Struct. Biol.* **2002**, *9*, 193–197.

IV-4.

1 (a) Arakawa, T.; Shimono, K.; Yamaguchi, S.; Tuzi, S.; Sudo, Y.; Kamo, N.; Saitô, H. *FEBS Lett*. **2003**, 536, 237. (b) Luca, S.; White, J.F.; Sohal, A.K.; Filippov, D.V.; van Boom, J.H.; Grisshammer, R.; Baldus, M. *Proc. Natl. Acad. Sci. USA*. **2003**, 100, 10706. (c)Sato, T.; Pallavi, P.; Golebiewska, U.; McLaughlin, S.; Smith, S.O. *Biochemistry*, **2006**, 45, 12704.
2 Dürr, U.H.N.; Waskell, L.; Ramamoorthy, A. *Biochim. Biophys. Acta* **2007**, *1768*, 3235–3259.
3 Zhang, H.; Myshkin, E.; Waskell, L. *Biochem. Biophys. Res. Commun.* **2005**, *338*, 499.
4 (a) Vergéres G.; Waskell, L. *Biochimie* **1995**, *77*, 604. (b) Schenkman, J.B.; Jansson, I. *Pharmacol. Ther.* **2003**, *97*, 139.
5 Mulrooney, S.B.; Waskell, L. *Protein Expr. Purif.* **2000**, *19*, 173.
6 Clarke, T.A.; Im, S.-C.; Bidwai, A.; Waskell, L. *J. Biol. Chem.* **2004**, *279*, 36809.
7 Banci, L.; Bertini, I.; Rosato, A.; Scacchieri, S. *Eur. J. Biochem.* **2000**, 267, 755.
8 Burum, D.P.; Ernst, R.R. *J. Magn. Reson.* **1980**, *39*, 163.
9 (a) Dvinskikh, S.V.; Yamamoto, K.; Ramamoorthy, A. *Chem. Phys. Lett.* **2006**, 419, 168. (b) Yamamoto, K.; Dvinskikh, S.V.; Ramamoorthy, A. *Chem. Phys. Lett.* **2006**, 419, 533. (c) Dvinskikh, S.V.; Yamamoto, K.; Ramamoorthy, A. *J. Chem. Phys.* **2006**, *125*, 34507.

10 (a) Marassi, F.M.; Opella, S.J. *J. Magn. Reson.* **2000**, *144*, 150. (b) Denny, J.K.; Wang, J.; Cross, T.A.; Quine, J.R. *J. Magn. Reson.* **2001**, *152*, 217. (c) Ramamoorthy, A.; Wei, Y.; Lee, D.K. *Annu. Rep. NMR Spectrosc*. **2004**, *52*, 1-52.

11 Dürr, U.H.N.; Yamamoto, K.; Im, S.C.; Waskell, L.; Ramamoorthy, A. *J. Am. Chem. Soc.* **2007**, 129, 6670.

12 Gor'kov, P.L.; Chekmenev, E.Y.; Li, C.; Cotten M.; Buffy, J.J.; Traaseth, N.J.; Veglia, G.; Brey, W.W. *J. Magn Reson.* **2007**, 185, 77-93.

Chapter V

Conclusions

V-1. Conclusions

The goal of this project was to develop new Nuclear Magnetic Resonance spectroscopy methodologies to investigate structures, dynamics and functions of membrane bilayers, membrane-associated proteins, membrane-protein interactions and membrane protein-protein interactions. In order to accomplish this development following three novel concepts were discussed in this dissertation. (1) The first element is to gain atomic-level structure and dynamics determination of biologically important systems by developing new solid-state and solution NMR approaches that enhance resolution and the sensitivity of spectra, allowing for the achievement of robust NMR experiments for complex biomolecules and samples that have higher molecular weight (Chapter II). (2) The second component pertains to the preparation of stable and well-behaved biologically relevant samples of lipid bilayers (Chapter III). (3) The third is to retain the biological functions of membrane complex systems during experiments in order to investigate dynamical structure of membrane complexes in a biologically relevant form (Chapter IV). The combination of these three approaches has already led, for the first time, to the determination of structural and dynamical interactions in an intact mammalian membrane protein complex, rabbit Cytochrome b_5, and Cytochrome P450, which metabolizes more than 50% of the pharmaceuticals in clinical use today and is an extremely challenging system for NMR spectroscopy because of its huge overall molecular weight (more than 200 kDa).

The work described in Chapter II investigated the new developments of NMR spectroscopy methods for the structural and dynamical studies of membrane bilayers and membrane proteins. I have highlighted the advantages and disadvantages of the commonly used PISEMA pulse sequence. Recently developed (i) BB-PISEMA and HIMSELF to compensate the offset effects, (ii) PITANSEMA to overcome the high R.F. power effects and (iii) PELF to detect remote/smaller dipolar couplings are also discussed. I believe that these new sequences further widen the applications of PISEMA. Some of the areas that benefit from these applications are the structural studies of weakly aligned molecules, bicelles, and liquid crystalline materials. It is also possible to develop a variety of PISEMA-type pulse sequences by combining these new developments with indirect ^{1}H detection, MAS, and gradients for various studies on both rigid and mobile biological solids. Needless to mention that the optimization of phase, frequency, and width of R.F. pulses of SEMA for better performance could also provide fruitful results.

For dipolar recouplings under the solid-state Magic Angle Spinning conditions, I have demonstrated a low R.F. power pulse sequence, known as PITANSEMA-MAS, in which a combination of TAN and SEMA was used to recover the heteronuclear dipole–dipole interactions. This sequence requires an order of magnitude less power than the PISEMA-MAS sequence, while the spectral resolution and line shape are similar in both the cases. This sequence would be highly valuable for systems where the spin-locking of the transverse magnetization for heteronuclear coherence transfer is difficult.[1,2] The experimental results suggest that the performance of the sequence is independent of the spinning speed and R.F. power whereas it depends on the offset frequency of protons. Since the efficiency of the sequence is not limited by the rotor synchronization, the sensitivity and resolution enhancements, rendered by the fast MAS can be retained in various multidimensional experiments. In addition, our results indicate that the method can be used to measure heteronuclear distances even without the need for isotope enrichment. The measured dipolar couplings can also be used to determine the structure and characterize the dynamics of rigid solids and mobile systems such as membrane bilayers and liquid crystalline materials.[3-6]

In order to compensate the offset effects I have demonstrated that the high performance 2D Separated-Local-Field experiments for accurate measurements of the

heteronuclear dipolar couplings can be designed by implementing the windowless isotropic mixing. WIM24 sequence efficiently suppresses the chemical shift and frequency offset effects irrespective of the heteronuclear dipolar coupling value and therefore provides the uniform dipolar resolution in the broad dipolar coupling range. The experimental design is very flexible in terms of choosing the initial conditions and coherence transfer pathways. In particular, high dipolar resolution and essentially artifact-free spectra are obtained with PIWIM-z sequence employing the coherent polarization transfer between z-component of the spin magnetizations. The results of the new approach are comparable to other existing techniques in terms of dipolar resolution of large dipolar couplings but is superior for measurements of the motionally reduced dipolar couplings in the complex systems with a wide range of chemical shifts. The method can be further extended and used as a building block in advanced multi-dimensional NMR experiments. It is anticipated that WIM based local field spectroscopy will find widespread use for the structural studies of liquid crystalline and biological samples. Also, our results suggest that the isotropic nature of the effective Hamiltonian will be useful to transfer any component of the magnetization via heteronuclear dipolar couplings. Like PISEMA, the main limitation of this technique is that it cannot be used to measure a smaller dipolar coupling in the presence of a larger dipolar coupling as the effective Hamiltonians do not commute. Nevertheless, we expect that this sequence will be useful in the structural, geometrical and dynamical studies of aligned molecules such as lipid bilayers, bicelles and liquid crystalline materials

In this Chapter II, I also discussed various practical aspects of ^{13}C and ^{14}N NMR experiments in magnetically oriented bicelles. We have demonstrated that R.F. heating effects in bicellar samples can easily be calibrated and taken into account by monitoring the water proton chemical shift. This approach can be used for studies on other samples like mechanically aligned bilayers and multilamellar vesicles as well. We have also demonstrated that by applying advanced broadband decoupling sequences the required decoupling RF power can be considerably reduced and thus RF heating can be minimized. A comparison of various methods to enhance the sensitivity of experiments to detect less sensitive nuclei and to enhance the resolution of the chemical shift spectrum of less sensitive nuclei in bicelles is presented. Our results infer that ^{14}N NMR experiments on

bicelles are easy to carry out with a standard commercial set-up. The detection of ^{14}N nuclei could be used as a 'voltmeter' to study ligand–membrane interactions. We believe that the results presented in this paper can be utilized in performing advanced multidimensional solid-state NMR experiments[7-9] on bicelles containing peptides, proteins, drugs or other types of molecules.

The work described in Chapter III-2 investigated Carbon-13 NMR spectroscopy of lipid bilayers, when applied as a 2D SLF experiment, provides a number of important advantages over the traditional ^{2}H NMR approach. Advantages include a more straightforward signal assignment, accessibility of remote couplings and couplings to heterospins other than protons, and resolving the ambiguous splitting within the methylene groups. Thus, the information content in the 2D spectrum that is useful for structural studies is increased dramatically. Our results suggest that the 2D PDLF is the most efficient experiment on bicelles as compared to other separated local field techniques in terms of the resolution of the dipolar couplings. However, BB-PISEMA or HIMSELF sequences provided the best resolution in rigid solids. Since the spectral splitting in a spin cluster with multiple spin dipolar couplings behave distinctly in PDLF and PISEMA-type techniques, some ambiguity issues in assigning the dipolar doublets are resolved by comparing the data of these two experiments. Therefore, a combination of PDLF with one of the rotating-frame experiments like BB-PISEMA or HIMSELF is highly recommended. Our results also suggest that the 2D experiment can be used to measure the membrane interaction of ligands. Interestingly, this approach does not depend on the molecular size, and therefore it should be useful in studying the interaction of membrane proteins with the lipid bilayer environment. This approach will also be applicable to study the structure of ^{13}C- or ^{15}N-labeled proteins in bicelles. In particular, the laboratory-frame SLF experiment like PDLF and its variants will be valuable in determining the structure and dynamics of soluble domains, loop regions, and mobile parts of membrane proteins.

The work described in Chapter III-3 investigated knowledge on the variation of lipid dynamics in bicelles is essential in the investigation of ligand-induced structural and dynamical disorders in membranes. For example, bicelles are valuable in probing the mechanism of membrane disruption by antimicrobial peptides, toxins, amyloid peptides,

fusion peptides, dendrimers, and pharmaceutical compounds.[10-14] In such studies, changes in the order at each carbon site have been shown to provide valuable insights into various important aspects of ligand-membrane interactions. The depth of insertion, disorder/order induced by ligands near the lipid head-group or hydrophobic core regions of lipid bilayers, tilt of the lipid head-group, phase changes, and toroidal-pore formation are commonly characterized using order parameters measured from NMR experiments on bicelles. In such analysis, caution must be exercised because dehydration effects and detergent-like behavior of peptides can be misinterpreted for a change in the size of the bicellar aggregates. The unique way of preparing well-defined toroidal pores in bicelles is highly valuable to understand the mechanism of membrane disruption by a variety of systems, such as antimicrobial and amyloidogenic peptides.

The increasing popularity of bicelles in NMR studies of membrane proteins necessitates a better understanding of lipid dynamics in bicelles. It is now possible to obtain a high-resolution solid-state NMR spectrum of a membrane protein embedded in magnetically aligned bicelles. SLF experiments, such as PISEMA or HIMSELF, require a fine balance between motions of a protein in the membrane and the various anisotropic nuclear interactions. Therefore, one of the avenues to fine tune this delicate balance is through manipulating the experimental conditions of bicelles. Our series of comprehensive experiments shows that the q ratio greatly influences the overall ordering of bicelles and the motions of lipids relative to other experimental parameters, such as temperature and hydration. As such, increasing the q ratio as a mean to exemplify dipolar couplings is a reasonable approach to improve spectral resolutions of a SLF spectrum. Unfortunately, this approach may compromise the alignment of bicelles; however, bicelles have been shown to exhibit macroscopic alignment over a wide range of q ratios from 2.5 to 5.5.[15] Therefore, there must exist a q ratio where experimental conditions, bicelles alignment, and spectral resolutions can be satisfied for a specific membrane protein. Nevertheless, the use of bicelles in solid-state NMR studies of membrane proteins is a continuing endeavor that requires constant optimization of sample conditions.

The work described in Chapter IV-2 investigated a first structural study on holo Cyt b_5 in a membrane environment. We found an α-helical structure for the rigid

transmembrane region, with atypical geometrical imperfection due to the Pro residue, and very fast dynamics for the soluble domain. We believe that the presented results point out a versatile way to investigate numerous structural and dynamic properties of Cyt b_5 and its physiologically important interaction with Cyt P450. The successful demonstration of spectral editing approaches will significantly reduce the difficulties in the resonance assignment of Cyt b_5. Moreover, the combination of these unique NMR spectral editing methods will be applicable in the structural and dynamical studies of a large number of other membrane proteins, as well.

The work described in Chapter IV-3 demonstrated the practicality of using PELF pulse sequence to generate a complete mapping of dynamics by measuring dipolar couplings of directly bonded ^{15}N-^{1}H spin pairs of a membrane-anchored cytochrome b_5 in magnetically aligned bicelles. The superiority in resolution of a PELF spectrum under WIM-CP or COMPOZER-CP sequence rivals that of conventional rotating frame SLF techniques such as SAMMY, BB-PISEMA, and HIMSELF. Importantly, under our approach, an SLF spectrum of both transmembrane and mobile regions is recorded in a single experiment, allowing for a complete correlation of protein dynamics between the two regions. The observed PISA wheel was fit using a dynamical model, which includes the whole-body motions of the helix. Using this approach, the helix is modeled as wobbling in a cone with an approximate 8° fluctuation in the tilt of the helix, which is estimated to be 13°. Importantly, this approach represents the first step in extracting the motions of a membrane protein from an aligned sample, allowing for a better understanding of the dynamics of a protein in a bilayer environment. Although this method is demonstrated successfully on a membrane protein, it can also be used for other aligned liquid crystalline materials. Finally, while this method of extracting dynamical information can be extended to the system of two binding helixes, MD simulations will be needed to include all the motions pertaining to such a complex in order to provide a proper and insightful description regarding its motions in membranes.

The work described in Chapter IV-4 demonstrated that solid-state NMR is capable of characterizing protein-protein interactions in lipid bilayers at a very high-resolution. For the first time in literature, we report structural and dynamical interactions in an intact

mamalian membrane protein complex, rabbit cytochrome b_5 and cytochrome P450 2B4, in a membrane bilayer.

Our experimental results demonstrate that not only Cyt b_5 but also a complex of Cyt b_5 and Cyt P450 can be prepared in bicelles, aligned in magnetic field for NMR studies, and high-resolution spectra and meaningful structural and dynamical information can be obtained. While it is known that Cyt P450 is unstable at ambient temperatures and both proteins are sensitive to impurities and heat, it is remarkable that the bicelles containing the complex was quite stable under our experimental conditions even up to temperatures 30^oC for more than two weeks. This observation considerably simplifies our understanding on the interaction between the TM domains of the proteins. Since the soluble domains of both the proteins are highly mobile in NMR time scale, the interaction between these two domains only slightly reduces the mobility of Cyt b_5 in the presence of Cyt P450. One possible role of the membrane anchor is that it restricts the motion of the Cyt b_5 soluble domain to those orientations that will result in a productive complex with Cyt P450. Cyt P450 is believed to be rigidly anchored to the membrane and may, therefore, be limited in its ability to form a productive complex, unless its binding partner is appropriately orientated. More experiments are needed to completely characterize the structural changes and the changes in the dynamics of the proteins in the complex form at a higher resolution. We expect the results reported here to open a valuable approach to structural and dynamical studies of membrane protein complexes using solid-state NMR techniques.

V-2. References

1 Zhao, X.; Hoffbauer, W.; Schmedt auf der Gunne, J.; Levitt, M.H. *Solid State NMR Spectrosc.* **2004**, 26, 57.

2 Wei, Y.F.; Lee, D.K.; Hallock, K.J.; Ramamoorthy, A. *Chem. Phys. Lett.* **2002**, 351, 42.

3 Lee, D.K.; Santos, J.S.; Ramamoorthy, A. *J. Phys. Chem. B* **1999**, 103, 8383.

4 Hallock, K.J.; Lee, D.K.; Ramamoorthy, A. *J. Chem. Phys.* **2000**, 113, 11187.

5 Hallock, K.J.; Lee, D.K.; Ramamoorthy, A. *Chem. Phys. Lett.* **1999**, 302, 175.

6 Hong, M.; Yao, X.; Jakes, K.; Huster, D. *J. Phys. Chem. B* **2002**, 106, 7355.

7 Lu, J.X.; Damodaran, K.; Lorigan, G.A. *J. Magn. Reson.* **2006**, 178, 283–287.

8 Dvinskikh, S.V.; Dürr, U.H.N.; Yamamoto, K.; Ramamoorthy, A. *J. Am. Chem. Soc.* **2006**, 128, 6326.

9 Park, S.H.; Prytulla, S.; De Angelis, A.A.; Brown, J.M.; Kiefer, H.; Opella, S.J. *J. Am. Chem. Soc.* **2006**, 128, 7402–7403.

10 (a) Dvinskikh, S.V.; Dürr, U.H.N.; Yamamoto, K.; Ramamoorthy, A. *J. Am. Chem. Soc.* **2006**, 128, 6326–6327. (b) Dvinskikh, S. V.; Yamamoto, K.; Scanu, D.; Deschenaux, R.; Ramamoorthy, *A. J. Phys. Chem.* **2008**, 112, 12347–12353.

11 Dvinskikh, S.V.; Dürr, U.H.N.; Yamamoto, K.; Ramamoorthy, A. *J. Am. Chem. Soc.* **2007**, 129, 794–802.

12 (a) Ramamoorthy, A.; Lee, D.K.; Santos, J.S.; Henzler-Wildman, K.A. *J. Am. Chem. Soc.* **2008**, 130, 11023–11029. (b) Ramamoorthy, A. *Solid State Nucl. Magn. Reson.* **2009**, in press.

13 Smith, P.E.S.; Brender, J.R.; Ramamoorthy, A. *J. Am. Chem. Soc.* **2009**, 131, 4470–4478.

14 Barry, J.; Fritz, M.; Brender, J.R.; Smith, P.E.S.; Lee, D.K.; Ramamoorthy, A. *J. Am. Chem. Soc.* **2009**, 131, 4490–4498.

15 Cardon, T.B.; Dave, P.C.; Lorigan, G.A. *Langmuir* **2005**, 21, 4291–4298.

APPENDIX
A. SIMPSON Simulation Input Files for Separate-Local-Field Spectroscopy

A-1. SIMPSON Input File Examples

(i) PISEMA (single crystal)

```
spinsys {
  channels 1H 15N
  nuclei 1H 15N
  dipole 1 2 10000.0 0 0 0
}

par {
  method           direct
  spin_rate        0.0
  gamma_angles     1
  crystal_file     alpha0beta0
  start_operator   -I1y + I2x
  detect_operator  I2p
  proton_frequency 400e6
  verbose          1101
  np               4096

  variable rf_H     75000.0

  variable eff_H    sqrt(3.0/2.0)*rf_H
  variable t_delay  0.0
  variable rf_15N_1 eff_H
  variable rf_15N_2 eff_H
  variable tau1     1000000.0/eff_H
  variable tau2     1000000.0/eff_H
  variable Offset_1 (-rf_H/sqrt(2.0))+0
  variable Offset_2 (+rf_H/sqrt(2.0))+0
  variable X_Offset 10000
  variable X_Offset_2 -(X_Offset)

  variable Cycle    2
  sw 1000000.0/((tau1+tau2)*Cycle)
```

```
  variable theta_m  (1000000.0/rf_H)*(90-54.73561032)/360.0

}
proc pulseq {} {
  global par
#maxdt 1

reset
pulse $par(theta_m) $par(rf_H) -x 0 x
acq x

for {set i 2} {$i <= $par(np)} {incr i} {
offset $par(Offset_1)    $par(X_Offset)
 pulse  $par(tau1) $par(rf_H)  y $par(eff_H)  x
offset $par(Offset_2)    $par(X_Offset_2)
 pulse  $par(tau2) $par(rf_H) -y $par(eff_H) -x

offset $par(Offset_1)    $par(X_Offset)
 pulse  $par(tau1) $par(rf_H)  y $par(eff_H)  x
offset $par(Offset_2)    $par(X_Offset_2)
 pulse  $par(tau2) $par(rf_H) -y $par(eff_H) -x
acq x
}
}

proc main {} {
  global par

puts "============================================================="
puts " PISEMA April, 2011"
puts "============================================================="
set f [fsimpson]; faddlb $f 100 0; fsave $f $par(name).fid -binary;
fft $f;
fsave $f $par(name).spe -binary;
}
```

(ii) BBPISEMA (powder)

```
spinsys {
  channels 1H 15N
  nuclei 1H 15N
  dipole 1 2 10000.0 0 0 0
}

par {
  method           direct
  spin_rate        0.0
  gamma_angles     1
  crystal_file     zcw986              #for the powder pattern
simulation
  start_operator   -I1y + I2x
```

```
  detect_operator  I2p
  proton_frequency 400e6
  verbose          1101
  np               4096

  variable rf_H     50000.0
  variable pi_rf_B  rf_H                #RF power of refocusing
pulses

  variable eff_H    sqrt(3.0/2.0)*rf_H  #Effective field
  variable t_delay  0.0
  variable pi       (1000000/pi_rf_B)/2 #refocusing pulse length
  variable rf_15N_1 eff_H
  variable rf_15N_2 eff_H
  variable tau1     1000000.0/eff_H
  variable tau2     1000000.0/eff_H
  variable Offset_1 (-rf_H/sqrt(2.0))+0 # for the offset dependence
  variable Offset_2 (+rf_H/sqrt(2.0))+0 # evaluations
  variable Cycle    2
  sw 1000000.0/((tau1+tau2+pi)*Cycle)

  variable theta_m  (1000000.0/rf_H)*(90-54.73561032)/360.0

}
proc pulseq {} {
  global par
#maxdt 1

reset
pulse $par(theta_m) $par(rf_H) -x 0 x
acq x

for {set i 2} {$i <= $par(np)} {incr i} {
offset $par(Offset_1)    0
 pulse  $par(tau1) $par(rf_H)  y $par(eff_H)  x
offset $par(Offset_2)    0
 pulse  $par(tau2) $par(rf_H) -y $par(eff_H) -x
offset 0  0
pulse  $par(pi)  $par(pi_rf_B)  x $par(pi_rf_B)  y

offset $par(Offset_1)    0
 pulse  $par(tau1) $par(rf_H)  y $par(eff_H)  x
offset $par(Offset_2)    0
 pulse  $par(tau2) $par(rf_H) -y $par(eff_H) -x
offset 0  0
pulse  $par(pi)   $par(pi_rf_B)  -x $par(pi_rf_B)  -y
acq x
}
}

proc main {} {
  global par

puts "============================================================"
```

```
puts " BBPISEMA April, 2011"
puts "============================================================="
set f [fsimpson]; faddlb $f 100 0; fsave $f $par(name).fid -binary;
fft $f;
fsave $f $par(name).spe -binary;
}
```

(iii) PISEMA MAS at 14 kHz

```
############################################################
# SPIN SYSTEM
############################################################
spinsys {
  channels 1H 13C
  nuclei   1H 13C
  dipole   1 2 -22000.0 0 0 0
}
############################################################
# end of SPIN SYSTEM
############################################################

############################################################
# PARAMETERS
############################################################
par {
  method           direct
  gamma_angles     1
# crystal_file     alpha0beta0 zcw 4180
  crystal_file     zcw376
  spin_rate        14000.0
  start_operator   0.577350269189*I1z - 0.816496580928*I1y + I2x
  detect_operator  I2p
  proton_frequency 400e6
  verbose          1101
  np               4096*2

  variable X_Offset 0
  variable I_Offset 0
  variable eff_X_Mismatch 0
  variable eff_I_Mismatch 0

  variable rf_H          62500
  variable rf_H_pract    rf_H + eff_I_Mismatch
  variable Offset_H_1    -rf_H/sqrt(2.0)+I_Offset
  variable Offset_H_2    +rf_H/sqrt(2.0)+I_Offset
  variable rf_H_1_eff    sqrt(1.5)*rf_H
  variable rf_H_2_eff    sqrt(1.5)*rf_H
  variable tau1          (1000000/rf_H_1_eff)
  variable tau2          (1000000/rf_H_1_eff)

  variable taf           (tau1-tau2)/(tau1+tau2)
  variable tauC_tauLG    (tau1+tau2)/(1000000/rf_H_1_eff)
```

```
  variable rf_15N_1      (rf_H_1_eff) + spin_rate + eff_X_Mismatch
  variable rf_15N_2      (rf_H_2_eff) - spin_rate + eff_X_Mismatch
  variable angle1        rf_H_1_eff*0.000001*tau1*360.0
  variable angle2        rf_H_2_eff*0.000001*tau2*360.0
  variable Cycle         1
  sw                     1000000.0/((tau1 + tau2)*Cycle)
}
##############################################################
# end of PARAMETERS
##############################################################

##############################################################
# PULSE SEQUENCE
##############################################################
proc pulseq {} {
global par
maxdt 1.0
reset
acq x
for {set i 2} {$i <= $par(np)} {incr i} {
offset $par(Offset_H_1)                $par(X_Offset)
pulse  $par(tau1) $par(rf_H_pract)  y   $par(rf_15N_1)  x
offset $par(Offset_H_2)                $par(X_Offset)
pulse  $par(tau2) $par(rf_H_pract) -y   $par(rf_15N_2) -x
offset 0 0
acq x }}
##############################################################
# end of PULSE SEQUENCE
##############################################################

##############################################################
# MAIN PROCEDURE
##############################################################
proc main {} {
global par
puts "===== Start Main Procedure ================================="
set f [fsimpson]; faddlb $f 100 0; fsave $f $par(name).fid -binary;
fft $f;
fsave $f $par(name).spe;
puts "===== End Main Procedure ==================================="
}
##############################################################
# end of MAIN PROCEDURE
##############################################################
```

(iv) HIMSELF (PIWIMz)

```
spinsys {
  channels 1H 15N
  nuclei 1H 15N
  dipole 1 2 10000.0 0 0 0
}
```

```
par {
  method           direct
  spin_rate        0.0
  gamma_angles     1
  crystal_file     alpha0beta0
  start_operator   I1x + I2x
  detect_operator  I2p
  proton_frequency 400e6
  verbose          1101
  np               4096*2

  variable X_Offset 0
  variable I_Offset 0
  variable eff_X_Mismatch 0
  variable eff_I_Mismatch 0

  variable rf_H        100000.0
  variable rf_H_pract  rf_H + eff_I_Mismatch
  variable rf_X_pract  rf_H + eff_X_Mismatch

  variable I_pulse     (1000000.0/rf_H)/4

  variable Num_pulse   24
  sw 1000000.0/(I_pulse*Num_pulse)

#  variable theta_m     (1000000.0/rf_H)*(180-(90.0-63.1))/360.0

}
proc pulseq {} {
  global par
#maxdt 1

reset
#offset $par(I_Offset) $par(X_Offset)
#pulse $par(theta_m) $par(rf_H_pract) -y 0 -y
#acq x

for {set i 2} {$i <= $par(np)} {incr i} {
offset $par(I_Offset)  $par(X_Offset)
pulse  $par(I_pulse)   $par(rf_H_pract)  -y  $par(rf_X_pract) -y
offset $par(I_Offset)  $par(X_Offset)
pulse  $par(I_pulse)   $par(rf_H_pract)   x  $par(rf_X_pract)  x
offset $par(I_Offset)  $par(X_Offset)
pulse  $par(I_pulse)   $par(rf_H_pract)  -y  $par(rf_X_pract) -y
offset $par(I_Offset)  $par(X_Offset)
pulse  $par(I_pulse)   $par(rf_H_pract)  -y  $par(rf_X_pract) -y
offset $par(I_Offset)  $par(X_Offset)
pulse  $par(I_pulse)   $par(rf_H_pract)   x  $par(rf_X_pract)  x
offset $par(I_Offset)  $par(X_Offset)
pulse  $par(I_pulse)   $par(rf_H_pract)  -y  $par(rf_X_pract) -y
offset $par(I_Offset)  $par(X_Offset)
pulse  $par(I_pulse)   $par(rf_H_pract)   y  $par(rf_X_pract)  y
offset $par(I_Offset)  $par(X_Offset)
```

```
pulse  $par(I_pulse)   $par(rf_H_pract)   x  $par(rf_X_pract)  x
offset $par(I_Offset)  $par(X_Offset)
pulse  $par(I_pulse)   $par(rf_H_pract)   y  $par(rf_X_pract)  y
offset $par(I_Offset)  $par(X_Offset)
pulse  $par(I_pulse)   $par(rf_H_pract)   y  $par(rf_X_pract)  y
offset $par(I_Offset)  $par(X_Offset)
pulse  $par(I_pulse)   $par(rf_H_pract)   x  $par(rf_X_pract)  x
offset $par(I_Offset)  $par(X_Offset)
pulse  $par(I_pulse)   $par(rf_H_pract)   y  $par(rf_X_pract)  y

offset 0  0

acq x


offset $par(I_Offset)  $par(X_Offset)
pulse  $par(I_pulse)   $par(rf_H_pract)  -y  $par(rf_X_pract) -y
offset $par(I_Offset)  $par(X_Offset)
pulse  $par(I_pulse)   $par(rf_H_pract)  -x  $par(rf_X_pract) -x
offset $par(I_Offset)  $par(X_Offset)
pulse  $par(I_pulse)   $par(rf_H_pract)  -y  $par(rf_X_pract) -y
offset $par(I_Offset)  $par(X_Offset)
pulse  $par(I_pulse)   $par(rf_H_pract)  -y  $par(rf_X_pract) -y
offset $par(I_Offset)  $par(X_Offset)
pulse  $par(I_pulse)   $par(rf_H_pract)  -x  $par(rf_X_pract) -x
offset $par(I_Offset)  $par(X_Offset)
pulse  $par(I_pulse)   $par(rf_H_pract)  -y  $par(rf_X_pract) -y
offset $par(I_Offset)  $par(X_Offset)
pulse  $par(I_pulse)   $par(rf_H_pract)   y  $par(rf_X_pract)  y
offset $par(I_Offset)  $par(X_Offset)
pulse  $par(I_pulse)   $par(rf_H_pract)  -x  $par(rf_X_pract) -x
offset $par(I_Offset)  $par(X_Offset)
pulse  $par(I_pulse)   $par(rf_H_pract)   y  $par(rf_X_pract)  y
offset $par(I_Offset)  $par(X_Offset)
pulse  $par(I_pulse)   $par(rf_H_pract)   y  $par(rf_X_pract)  y
offset $par(I_Offset)  $par(X_Offset)
pulse  $par(I_pulse)   $par(rf_H_pract)  -x  $par(rf_X_pract) -x
offset $par(I_Offset)  $par(X_Offset)
pulse  $par(I_pulse)   $par(rf_H_pract)   y  $par(rf_X_pract)  y

offset 0  0

acq x
}
}

proc main {} {
  global par

puts "============================================================="
puts " HIMSELF (PIWIMz) April, 2011"
puts "============================================================="
set f [fsimpson]; faddlb $f 100 0; fsave $f $par(name).fid -binary;
fft $f;
```

```
fsave $f $par(name).spe;
}
```

A-2. References

1. Bak, M.; Rasmussen, J.T.; Nielsen, N.C. *J. Magn. Reson.* **2000**, 147, 296.